

Surface-atmosphere exchange of ammonia

**Measurements and modeling over non-fertilized
grassland in the Netherlands**

R.J. Wichink Kruit

Thesis committee

Thesis supervisors

Prof. dr. A.A.M. Holtslag
Professor of Meteorology
Wageningen University

Prof. dr. M.C. Krol
Professor of Air Quality and Atmospheric Chemistry
Wageningen University

Thesis co-supervisor

Dr. ir. W.A.J. van Pul
National Institute for Public Health and the Environment, Bilthoven, the Netherlands

Other members

Prof. D. Fowler, Centre for Ecology and Hydrology, Edinburgh, United Kingdom
Dr. ir. F. Dentener, Joint Research Centre, Ispra, Italy
Prof. ir. N.D. van Egmond, Utrecht University
Prof. dr. T.W.M. Kuyper, Wageningen University

This research was conducted under the auspices of the C.T. de Wit Graduate School
Production Ecology & Resource Conservation (PE&RC)

Surface-atmosphere exchange of ammonia

Measurements and modeling over non-fertilized grassland in the Netherlands

R.J. Wichink Kruit

Thesis

submitted in fulfilment of the requirements for the degree of doctor
at Wageningen University

by the authority of the Rector Magnificus,

Prof. dr. M.J. Kropff,

in the presence of the

Thesis Committee appointed by the Academic Board

to be defended in public

on Wednesday 26 May 2010

at 1.30 p.m. in the Aula

R.J. Wichink Kruit

Surface-atmosphere exchange of ammonia. Measurements and modeling over non-fertilized grassland in the Netherlands. 175 pages.

Thesis, Wageningen University, Wageningen, the Netherlands (2010)

With references, with summaries in Dutch and English

ISBN number: 978-90-8585-642-9

Voorwoord

Het onderzoek, waar ik hier verslag van doe, is tot stand gekomen door een samenwerking tussen Wageningen Universiteit en het Centrum voor MilieuMonitoring van het Rijksinstituut voor Volksgezondheid en Milieu (RIVM) in Bilthoven en is mede gefinancierd door het ministerie van Volkshuisvesting, Ruimtelijke Ordening en Milieu (VROM).

I am very grateful to the European Commission for NitroEurope Integrated Project, the ACCENT joint research programme and the iLEAPS project of the IGBP for the financial support for the visits to their conferences and workshops, which gave me the opportunity to meet many scientists in this field of research.

Heel veel mensen hebben (bewust en onbewust) een bijdrage geleverd aan de totstandkoming van dit proefschrift. Het is dan ook bijna ondoenlijk om iedereen persoonlijk te bedanken. Ik bied dan ook bij voorbaat mijn excuses aan voor degenen die ik hierna vergeet te vermelden. Ik ga toch een poging wagen.....

Allereerst wil ik Addo van Pul graag bedanken als co-promotor en initiator van het onderzoek. Addo, jij hebt mij de mogelijkheid geboden om mij op wetenschappelijk vlak te kunnen ontwikkelen. Dat is van onschatbare waarde en heeft me naast enorm veel kennis en ervaring, ook de nodige internationale contacten opgeleverd.

Ook wil ik mijn promotoren Bert Holtslag en Maarten Krol bedanken voor hun vele waardevolle adviezen en commentaren die hebben bijgedragen aan de totstandkoming van dit proefschrift.

Verder wil ik Adrie Jacobs bedanken als enthousiaste dagelijks begeleider aan de universiteit gedurende een groot deel van mijn promotietraject.

Willy Hillen en Frits Antonysen wil ik bedanken voor de vele uurtjes die we samen in het veld hebben doorgebracht. Vakmensen zoals jullie zijn vandaag de dag schaars, maar o zo onmisbaar! Peter Hofschreuder en Bert van Hove wil ik bedanken voor de vele waardevolle discussies over ammoniak, die bijzonder hebben bijgedragen aan het begrijpen van de relevante processen. Naast degenen die ik hierboven al heb genoemd wil ik verder natuurlijk alle andere (ex-)collega's van de vakgroep Meteorologie en Luchtkwaliteit (in willekeurige volgorde): Leo, Arnold, Jordi, Henk, Oscar, Bas, Wouter P., Gert-Jan, Kees, Bert Heu., Gerrie, Wouter M., Dirk, Alessandro, Sarah, Pete, Monica, Krijn, Olaf, Peter B., Chiel en Joel (ik hoop dat ik iedereen heb.....) bedanken voor de gezellige tijd die ik met jullie heb beleefd. Ook de vakgroepsuitjes, die ik samen met Adrie, Sarah, Krijn, Monica en Chiel in de feestcommissie heb georganiseerd waren onvergetelijk.

Ariën Stolk (RIVM) en Geert van Uden (ENVITEC) wil ik bedanken voor hun technische ondersteuning bij het verrichten van de ammoniakmetingen. Daarnaast wil ik Ariën bedanken voor het vele jaren kamergenoot zijn op het RIVM, net als Hans Verboom (ex-kamergenoot) en Willem Uiterwijk. We hebben heel wat vakantie verhalen uitgewisseld en weerkaartjes bekeken (om toch nog een klein beetje meteoroloog te kunnen spelen). Ik heb altijd met veel plezier en met minder of meer ruimte bij jullie op de kamer gezeten. Margreet van Zanten en Miranda van den Broek wil ik bedanken voor de prettige samenwerking en hun adviezen over het schrijven van een proefschrift en promoveren.

Ferd Sauter wil ik bedanken voor zijn assistentie in het leren van een nieuwe programmeertaal en de vele brainstormsessies. Verder wil ik Daan Swart, Marty Haaima, Hester Volten, Dorien Lolkema en Hans Bergwerff bedanken voor de goede samenwerking in de ontwikkeling van een nieuwe ammoniakflux opstelling. Het belooft een superieur apparaat te worden! Nou maar hopen dat de economische crisis geen roet in het eten gooit. Verder wil ik natuurlijk al mijn andere collega's van het Centrum voor MilieuMonitoring op het RIVM bedanken voor de gezellige labuitjes, borrels, lunches en koffiegesprekken. Aangezien dit er ondertussen meer dan 100 zijn, ga ik geen poging wagen om hen hier allemaal te vermelden.

Van het Plan Bureau voor de Leefomgeving (PBL) wil ik Jan Aben bedanken voor het maken van een aantal mooie plaatjes, Hans van Jaarsveld voor de vele tests die heeft gedaan met het OPS model om de effecten van het nieuwe model te testen en Erik Noordijk voor het bewerken van de metingen in het Meetnet Ammoniak in Natuurgebieden, die in dit proefschrift zijn gebruikt.

Eiko Nemitz and Mark Sutton are gratefully acknowledged for their hospitality during my working visit in Edinburgh and for sharing their incredible knowledge on this topic. It was a great pleasure to work with you.

Verder wil ik graag de ECN-ers René Otjes, Arnoud Frumau en Jan-Willem Erisman uit het mooie, maar verre Petten bedanken voor de gedachtewisselingen over het meetinstrument en de meetopstelling.

Ook veel dank ben ik verschuldigd aan mijn vrienden en teamgenoten, die ondanks dat ze me regelmatig hebben gestalkt met de vraag: "Is je werkstuk al af?", me toch de nodige afleiding en ontspanning hebben bezorgd. Allen bedankt!

Verder ben ik natuurlijk ontzettend veel dank verschuldigd aan mijn ouders, die vroeger zelf de kans niet hebben gekregen, maar er alles aan hebben gedaan om mij die kans wel te geven. Onwijs bedankt! Ook wil ik mijn zus, Inge, bedanken voor eigenlijk te veel om op te noemen, dus dan maar in 't kort alles!

Dan zijn er nog twee mensen die ik de afgelopen jaren alles heb proberen uit te leggen en die met engelengeduld al mijn overpeinzingen hebben aangehoord. Allereerst, Marieke, met jou heb ik een ontzettend goede tijd beleefd en we hebben fantastische reizen gemaakt. Je bent zonder enige twijfel mijn allerbeste vriendin! Last but not least, Remco, ik beloof je dat ik mijn oude levensmotto's weer ga oppakken en dat we nog veel van de wereld zullen gaan zien. Je bent mijn allerbeste maatje!

Het zit erop!

Abstract

In this thesis the surface-atmosphere exchange of ammonia over agricultural grassland in the Netherlands is studied. The main objectives of this thesis are to achieve a better understanding of the surface-atmosphere exchange process of ammonia, especially over agricultural grassland in the Netherlands, and to improve the model description of the surface-atmosphere exchange process of ammonia.

To achieve these objectives, flux measurements of ammonia over a non-fertilized agricultural grassland site in the Netherlands have been carried out with a new instrument in the period 2004-2006. These flux measurements revealed that deposition on wet surfaces is an important mechanism in the surface-atmosphere exchange process, because ammonia is well soluble in water. Analysis of the measurements indicated that absorption at the surface mainly occurs during nighttime when the surface is usually wet by dew. In the Netherlands, the average number of dew nights is 250 per year. Leaf wetness measurements showed that grassland is generally wet at relative humidities higher than 71%. In this thesis, we have shown that in a polluted area leaf surface water saturates with ammonium due to relatively high ammonia concentrations in the air. The saturated water layers reduce the uptake of ammonia from the atmosphere at the surface.

Another important mechanism in the surface-atmosphere exchange process is the emission of ammonia from vegetation due to a concentration within the canopy. The measurements showed that the canopy emits ammonia especially in warm and dry daytime conditions. The emissions from the canopy are caused by a relatively high concentration within the canopy compared to the ambient ammonia concentration. The equilibrium concentration at the vegetated surface for which the net ammonia flux is zero is generally called canopy compensation point. Canopy compensation points were derived from flux direction changes during non-stable dry daytime conditions. In these conditions, the canopy compensation point is equal to the air concentration. For the non-fertilized agricultural grassland site, the derived canopy compensation points range from 0.5 to 29.7 $\mu\text{g m}^{-3}$ with associated leaf temperatures between 7 and 29°C. The average canopy compensation point was $7.0 \pm 5.1 \mu\text{g m}^{-3}$. The canopy compensation point is a function of the leaf temperature and the ratio between NH_4^+ and H^+ concentration in the canopy, Γ_c . The average value for Γ_c derived from our micrometeorological flux measurements was 2200 ± 1600 .

The model description of the surface-atmosphere exchange process in atmospheric transport models is generally based on resistance modeling, in which the different pathways for surface-atmosphere exchange are represented by resistances and concentrations. In general, the two mechanisms described above are currently not explicitly included in the models. In this thesis, a new model description of the surface-atmosphere exchange process of ammonia has been developed that does account for the saturation of water layers on the leaf surface and the concentration within the canopy. These processes are especially important in more polluted areas, like in the Netherlands.

All together, the flux measurements resulted in a better understanding of the surface-atmosphere exchange process of ammonia over agricultural grassland in the Netherlands and over vegetated surfaces in general. The new insights resulted in a new model description of the surface-atmosphere exchange process of ammonia that is expected to be generally applicable in atmospheric transport models, because it accounts for local pollution levels.

Table of Contents

Voorwoord	5
Abstract	7
Table of Contents	9
1 Introduction and research questions	13
1.1 The nitrogen cycle	15
1.1.1 Nitrogen in the atmosphere	15
1.1.2 Reactive N formation	15
1.1.3 Fate of reactive N	17
1.1.4 Environmental impacts of the increased fertilizer use	17
1.2 Ammonia in the atmosphere.....	18
1.2.1 Emission	18
1.2.2 Transport and dispersion	19
1.2.3 Removal.....	19
1.3 Surface-atmosphere exchange of ammonia	20
1.3.1 Stomatal exchange	21
1.3.2 External leaf surface exchange	22
1.3.3 Soil exchange	23
1.3.4 Water exchange	24
1.3.5 Ammonia exchange within the canopy.....	24
1.4 Resistance modeling of the surface-atmosphere exchange of ammonia	25
1.4.1 Aerodynamic resistance, R_a	27
1.4.2 Quasi-laminar boundary layer resistance, R_b	28
1.4.3 Canopy resistance models	28
1.4.4 Canopy compensation point models	30
1.5 Ammonia in the Netherlands.....	31
1.5.1 Ammonia concentration measurements in the Netherlands	31
1.5.2 Ammonia concentration modeling in the Netherlands	32
1.5.3 Uncertainties in the current concentration modeling.....	36
1.5.4 Measurements of the surface-atmosphere exchange in the Netherlands	38
1.6 Objectives and outline of the thesis.....	38
2 Theory and overview of the NH_3 flux measurements at the micrometeorological Haarweg station, Wageningen, the Netherlands	41
2.1 Derivation of the flux	43
2.1.1 Basic theory	43
2.1.2 Gradient or flux-profile technique	46
2.1.3 Footprint analysis	48
2.2 Site description and instrumentation	50
2.2.1 Site description	50
2.2.2 Instrumentation.....	51
2.3 Error analysis	53
2.3.1 Systematic and random errors in the concentration	53
2.3.2 Random error in the flux	59
2.3.3 Effects of systematic errors in concentration measurements on the flux.....	63
2.3.4 Summary uncertainties and concluding remarks.....	64
2.4 Overview of NH_3 flux measurements and derived variables.....	65
2.5 Discussion and Conclusion.....	75
3 Ammonia fluxes and derived canopy compensation points over non-fertilized agricultural grassland in the Netherlands using the new GRAdient Ammonia - High Accuracy - Monitor (GRAHAM).....	79
Abstract	81
3.1 Introduction.....	82

3.2 Materials and Methods	82
3.2.1 Site description	82
3.2.2 Micrometeorological theory.....	83
3.2.3 GRAdient Ammonia - High Accuracy - Monitor (GRAHAM)	83
3.2.4 Precision improvement of the GRAHAM in relation to earlier AMANDA systems	84
3.2.5 Canopy and stomatal compensation point	85
3.2.6 Leaf temperature and leaf wetness.....	86
3.3 Results.....	86
3.3.1 Meteorological conditions.....	86
3.3.2 Observations.....	87
3.4 Discussion and Conclusions	93
4 Observations and estimates of leaf wetness duration over agricultural grassland.....	97
Abstract	99
4.1 Introduction.....	100
4.2 Materials and Methods	101
4.2.1 Site description	101
4.2.2 Measurement devices	101
4.2.3 Statistical data analysis	102
4.2.4 Physical dew models.....	103
4.2.5 Empirical leaf wetness models.....	104
4.3 Results.....	105
4.3.1 Meteorological conditions.....	105
4.3.2 Measurements and model results	106
4.4 Discussion and conclusions.....	113
5 Modeling the surface-atmosphere exchange of ammonia.....	117
Abstract	119
5.1 Introduction.....	120
5.2 Observations	121
5.3 Model parameterizations for NH ₃ exchange with vegetation.....	122
5.3.1 Derivation of new model parameterizations of R _w and χ_w	125
5.3.2 Existing model parameterizations of R _w	127
5.3.3 Derivation of new model parameterizations of χ_s and Γ_s	128
5.4 Results.....	129
5.4.1 New model parameterizations of R _w and χ_w	129
5.4.2 Seasonal variability of Γ_s	134
5.4.3 Comparison of the new method with the DEPAC and EMEP schemes	135
5.5 Discussion	137
5.6 Conclusion	143
6 Summary and Recommendations	145
6.1 Summary	147
6.2 Recommendations.....	150
6.2.1 Improving the measurement device.....	150
6.2.2 Application of the χ_s - χ_w model.....	150
References	155
Appendix A. Ammonium-ammonia equilibrium	166
Appendix B. Micrometeorological variables and instrumentation at the micro meteorological observatory 'Haarweg' in Wageningen, the Netherlands.....	167
Appendix C. Cuticular resistance (R _w) parameterization in the DEPAC module	168
Samenvatting.....	169
Curriculum vitae.....	173
Scientific publications and contributions.....	174
PE&RC PhD Education Certificate	175

1 Introduction and research questions

1.1 The nitrogen cycle

1.1.1 Nitrogen in the atmosphere

This thesis deals with ammonia, NH_3 . Ammonia is one of the most abundant nitrogen-containing compounds in the earth's atmosphere together with nitrogen gas (N_2), nitrous oxide (N_2O), nitrogen oxides (NO_x) and nitric acid (HNO_3) (Seinfeld and Pandis, 2006).

The earth's atmosphere consists for 78% of nitrogen. Almost all nitrogen in the atmosphere is present in the non-reactive molecular form (N_2), i.e., 99.9999%. Nitrous oxide (N_2O) makes up more than 99% of the remaining atmospheric nitrogen. Although the amount of N_2O is small (in the order of 320 ppb in 2005; IPCC, 2007), with an estimated lifetime of 114 years, nitrous oxide is one of the most important greenhouse gases (together with H_2O , CO_2 , CH_4 and O_3) and is therefore important for climate change issues (Jacob, 1999). Despite their even smaller amounts, the remaining nitrogen gases in the atmosphere, e.g., ammonia (NH_3), nitrogen oxides (NO_x), nitric acid (HNO_3), are important for local and regional scale environmental issues. These environmental issues concern air quality, like particulate matter formation and photochemical smog, but also impacts on water and soil quality resulting from increased nitrogen deposition, like eutrophication and acidification that can lead to reduced biodiversity (Bobbink et al., 1998; Erisman et al., 2008).

N_2 is non-reactive, because of its strong triple bond that binds the two nitrogen atoms. Only a limited number of nitrogen fixing bacteria are able to reduce N_2 and incorporate it directly into the living cell, e.g., cyanobacteria in natural waters, *Rhizobia* in root nodules of legumes. However, most living organisms can only use reactive or 'fixed' forms of nitrogen to form organic nitrogen compounds for their maintenance and growth (Warneck, 2000). Reactive N that can be used by living organisms can be divided into three types (Jacob, 1999):

- (inorganic) reduced nitrogen, e.g., ammonia (NH_3), ammonium (NH_4^+),
- (inorganic) oxidized nitrogen, e.g., nitrite (NO_2^-), nitrate (NO_3^-), nitrous oxide (N_2O), nitrogen oxides ($\text{NO}_x = \text{NO} + \text{NO}_2$), and
- organic nitrogen, e.g., urea, amines, proteins.

1.1.2 Reactive N formation

In Figure 1.1, the global annual production of reactive nitrogen is shown. Non-reactive nitrogen can be fixed naturally (thin solid horizontal line) or by human activities (thick lines). The natural N fixation remained rather constant during the 20th century, while the human induced N fixation (long dashed line) dramatically increased (Galloway et al., 2004).

Natural formation of reactive N occurs through lightning and by nitrogen fixing bacteria in natural ecosystems (thin solid horizontal line). The formation of reactive N through lightning mainly consists of NO, which is oxidized to NO_2 and HNO_3 in the atmosphere. The oxidized nitrogen that is produced by lightning contributes about 5 Tg N yr^{-1} to the total annual reactive N formation (Lelieveld and Dentener, 2000). Nitrogen fixation by nitrogen fixing bacteria in natural ecosystems mainly consists of NH_3 , NH_4^+ and organic nitrogen (Seinfeld and Pandis, 2006). Biological nitrogen fixation (BNF) by terrestrial ecosystems contributes about 107 Tg N yr^{-1} , while BNF by marine ecosystems contributes about 121 Tg N yr^{-1} in 1990 (Cleveland et al., 1999; Galloway et al., 2004).

BNF also occurs in agricultural crops, but this is considered as human induced. N fixation in cropland (light gray solid line) contributes about 33 Tg N yr⁻¹ (Smil, 1999a). The emission of nitrogen oxides by fossil fuel combustion (short dashed line) is also human induced and is shown to increase steadily after the Second World War to about 25 Tg N yr⁻¹ in the early 90s (Galloway et al., 2004). However, the large increase in the total reactive N production by human activities in the 20th century is caused by industrial formation of reactive N through the Haber-Bosch process (dark gray solid line), which nowadays accounts for more than 100 Tg N yr⁻¹ (Galloway et al., 2004). Most of this industrial N is in the form of NH₃ and NH₄⁺. The Haber-Bosch process is called after two Nobel price winning German scientists, i.e., Fritz Haber and Carl Bosch, who developed a process to produce ammonia (NH₃) from nitrogen gas (N₂) and hydrogen gas (H₂). After the Second World War, commercialization of the production process led to the global use of artificial fertilizers, which strongly increased crop and food production. This increased crop and food production supplies in the growing demand of the rapidly growing human population in the 20th century.

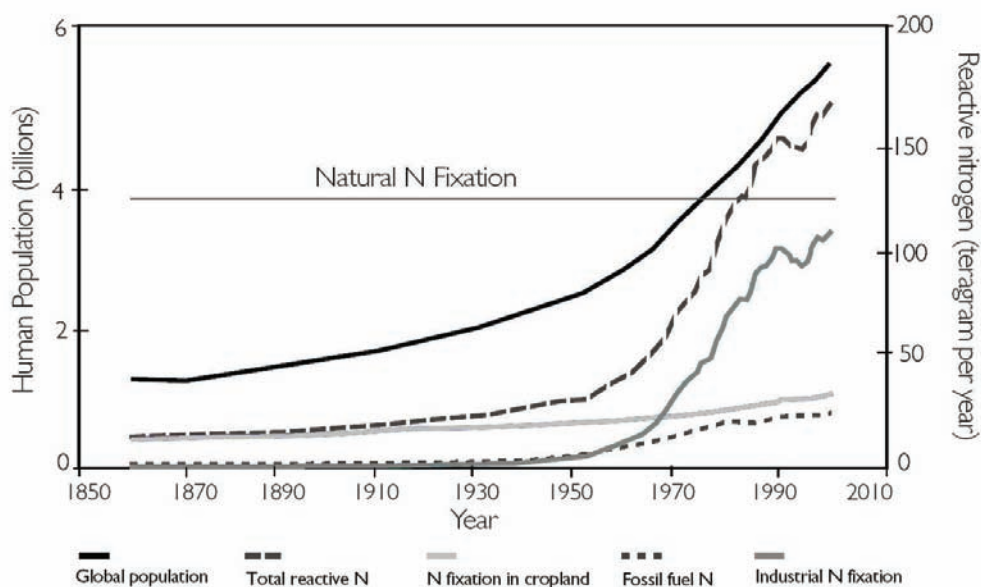


Figure 1.1. Historical trends of the formation of terrestrial reactive N by: natural N fixation (thin solid horizontal line) and human induced N fixation (long dashed line). Human induced N fixation includes N fixation in cropland (light gray solid line), emissions of N from fossil fuel combustion (short dashed line), and the industrial N fixation (Haber-Bosch process; dark gray solid line). The thick black solid line represents the growth of the human population (Source: Driscoll et al., 2003 after Galloway et al., 2003, 2004).

1.1.3 Fate of reactive N

There are several processes that transform reactive N into other forms of reactive or non-reactive nitrogen (Seinfeld and Pandis, 2006):

- nitrification is the oxidation of NH_4^+ to NO_2^- and NO_3^- by microbes.
- assimilation is the use of NH_4^+ or NO_3^- by plants to form organic nitrogen.
- mineralization is the conversion of dead plant material (organic nitrogen) into NH_4^+ .
- denitrification is the reduction of NO_3^- to NO_2^- , NO, N_2O and finally N_2 .

The latter process is the only process that converts reactive N back to non-reactive N. The magnitudes of the removal processes of the natural and anthropogenic terrestrial reactive N are rather uncertain. However, Galloway et al (2004) estimated that about 30% of the reactive N is transferred towards the marine environment through the atmosphere and by rivers, 5% is emitted to the atmosphere as N_2O (which is a strong greenhouse gas), 43% is denitrified to N_2 and 22% is accumulated in terrestrial ecosystems. Galloway et al. (2004) remark that especially the storage (in biomass and soils) and the denitrification amounts are highly uncertain.

1.1.4 Environmental impacts of the increased fertilizer use

The use of artificial fertilizer has significantly increased the quantity and quality of food. However, because of inefficient use of artificial fertilizers, much of the reactive N is lost to the environment before it is consumed by humans. It is estimated that only about ten percent of the applied N is finally consumed by humans. A vegetarian diet is more efficient (14% of the applied N is consumed) than a carnivorous diet (4% of the applied N is consumed). The rest is recycled to agricultural ecosystems, e.g., manure, or lost to the environment, e.g., stored in soils, transported by rivers, emitted to the atmosphere (Galloway and Cowling, 2002). This is especially the case in large regions of Europe, North America and Asia. Here, the abundance of reactive N led to a growing number of environmental problems, like photochemical smog, fine particulate pollution, ecosystem acidification and fertilization, coastal eutrophication and global warming (Sutton et al., 2009b).

The invention of the Haber-Bosch process is therefore arguably one of the most influential discoveries of the 20th century (Smil, 1999b) supporting the growth of human population from 1.6 billion to over 6 billion people at the beginning of the 21st century and as such contributing to climate change and environmental pollution.

1.2 Ammonia in the atmosphere

In the previous section, the importance of the invention of the Haber-Bosch process in the global nitrogen cycle has been discussed. Especially due to the inefficient use of fertilizer, environmental problems occur in regions with large N surpluses in Europe, North America and Asia. In this section, we will therefore focus on the ammonia budget in the atmosphere. Several processes determine and influence the ammonia budget in the atmosphere (Figure 1.2). Ammonia is 'lost' or emitted to the atmosphere from sources that are generally close to the ground, represented by the dotted arrow. Once emitted, ammonia is transported and dispersed in the atmosphere, represented by the dashed arrows. During this transport, ammonia can react with other gases to form ammonium aerosols (upper left solid arrow) that can be transported over long distances (upper right solid arrow). Ammonia and ammonium aerosols can be absorbed at the surface by soil, vegetation or water again either through dry deposition (solid arrows on the left) or wet deposition (solid arrows on the right). The processes are described in more detail in the following subsections.

1.2.1 Emission

The emission of ammonia is indicated by the dotted arrow in Figure 1.2. On a global scale, the estimates for the total ammonia emission range from about 45 to about 75 Tg N yr⁻¹ (Schlesinger et al., 1992; Dentener and Crutzen, 1994; Bouwman et al., 1997). More recently, Galloway et al. (2004) estimated the total global ammonia emission at 58 Tg N yr⁻¹. The emissions mainly consist of ammonia from the decomposition and volatilization of animal waste (about 40% of the total global NH₃ emission) and artificial fertilizers (about 20%). The process that is responsible for the release of ammonia to the atmosphere is the hydrolysis of urea, which is present in large quantities in animal waste and in artificial fertilizers. This process is strongly dependent on temperature and pH, and can be catalyzed by the enzyme urease. Urease is abundantly present in leaf litter and soils with high organic matter content. Other terrestrial sources of ammonia include natural emissions from soils and vegetation, emissions from crops, emissions from humans, pets and waste water, emissions from biofuel combustion, emissions from savannah and agricultural waste burning, emissions from combustion as part of deforestation, emissions from natural forest fires, emissions from fossil fuel burning and emissions from industrial processes (Galloway et al., 2004).

Ammonia is also produced in the upper layers of the ocean, mainly from the degradation of organic nitrogen compounds and excreta of zooplankton into dissolved ammonium which is in equilibrium with the air concentration above (Quinn, 1996). The emissions from the oceans are estimated to be about 10-15% of the global NH₃ emission and were calculated using a compensation point approach (Asman et al, 1994), which will be discussed later on.

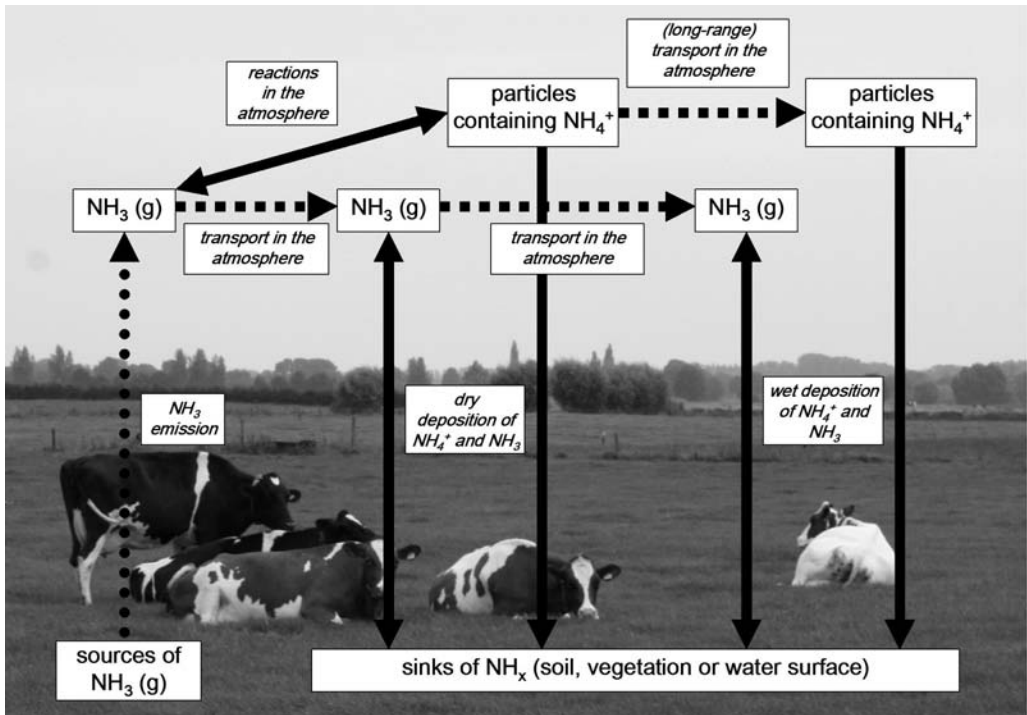


Figure 1.2. Processes that determine the atmospheric ammonia budget. See text for explanation of the figure.

1.2.2 Transport and dispersion

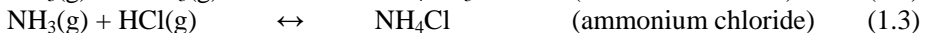
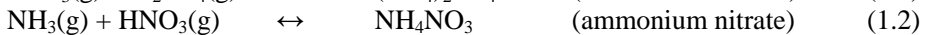
The emission of NH₃ is followed by atmospheric transport and dispersion, which is indicated by the dashed arrows in Figure 1.2. Transport and dispersion of ammonia and ammonium aerosols (see next section) in the air occurs by the mean wind and turbulence. Due to much longer lifetimes, ammonium aerosols are generally transported over much larger distances than ammonia. In the following section, three removal mechanisms will be discussed that can either transform or deposit ammonia during atmospheric transport.

1.2.3 Removal

The three removal mechanisms for ammonia from the atmosphere are indicated by the solid arrows in Figure 1.2: chemical transformation (reactions in the atmosphere), dry deposition and wet deposition.

1. Chemical transformation of NH₃.

Ammonia reacts with a few acid gases, by which it is transformed from gas into particles that contain ammonium, i.e. secondary aerosol. The partitioning between the gas and particulate phase is regulated by chemical reactions with sulphuric, nitric and hydrochloric acid as follows (Walker et al., 2004):



The reaction of NH_3 with sulphuric acid into ammonium sulfate aerosol is considered as irreversible, because the vapor pressure of ammonium sulphate is small. However, the reactions with nitric acid and hydrochloric acid are reversible, due to the significant vapor pressures of ammonium nitrate and ammonium chloride.

2. Dry deposition of NH_3 and NH_4^+ .

NH_3 and NH_4^+ are exchanged with soil, vegetation and water surfaces. In the next section, we will discuss this 'removal' mechanism in more detail.

3. Wet deposition of NH_3 and NH_4^+ .

Wet deposition is the transfer of NH_3 and NH_4^+ to the ground via precipitation, e.g., rain and snow. Wet deposition measurements are directly estimated from ammonium concentration measurements in precipitation and precipitation amounts.

The dry and wet deposition of NH_3 and NH_4^+ contribute to a total global deposition of $56.7 \text{ Tg N yr}^{-1}$, of which 32% deposits on oceans and 68% deposits on continents (Galloway et al., 2004). Oceans receive much more ammonia from deposition of NH_3 and NH_4^+ from continental origin than they do naturally produce. Especially in coastal areas, algal blooming may result from this nitrogen excess.

1.3 Surface-atmosphere exchange of ammonia

The dry and wet deposition fluxes of NH_3 in Figure 1.2 are bi-directional, i.e. the surface may act either as a sink for or as a source of atmospheric ammonia. The term 'deposition' actually only describes the ammonia transport towards the surface. A better description for this process is therefore: 'surface-atmosphere exchange'.

For a better understanding of the surface-atmosphere exchange of ammonia, it is necessary to understand the different pathways involved in the exchange process and the factors that control these pathways. A schematic overview of the main pathways involved in surface-atmosphere exchange of ammonia is shown in Figure 1.3. Each of the pathways is affected by the degree of turbulence of the atmosphere and the roughness of the surface. The straight arrows represent the direct pathways of ammonia exchange with the surface; the circular arrows represent exchange pathways within the canopy. The direct exchange pathways are through the stomata, with the external leaf surface, with the soil surface and with the water surface. Some of these pathways can act simultaneously, but exchange pathways within the canopy are also possible. It is the net effect of all these pathways acting in parallel, which controls the flux above the canopy. The individual exchange pathways of Figure 1.3 are described in more detail in the following sections.

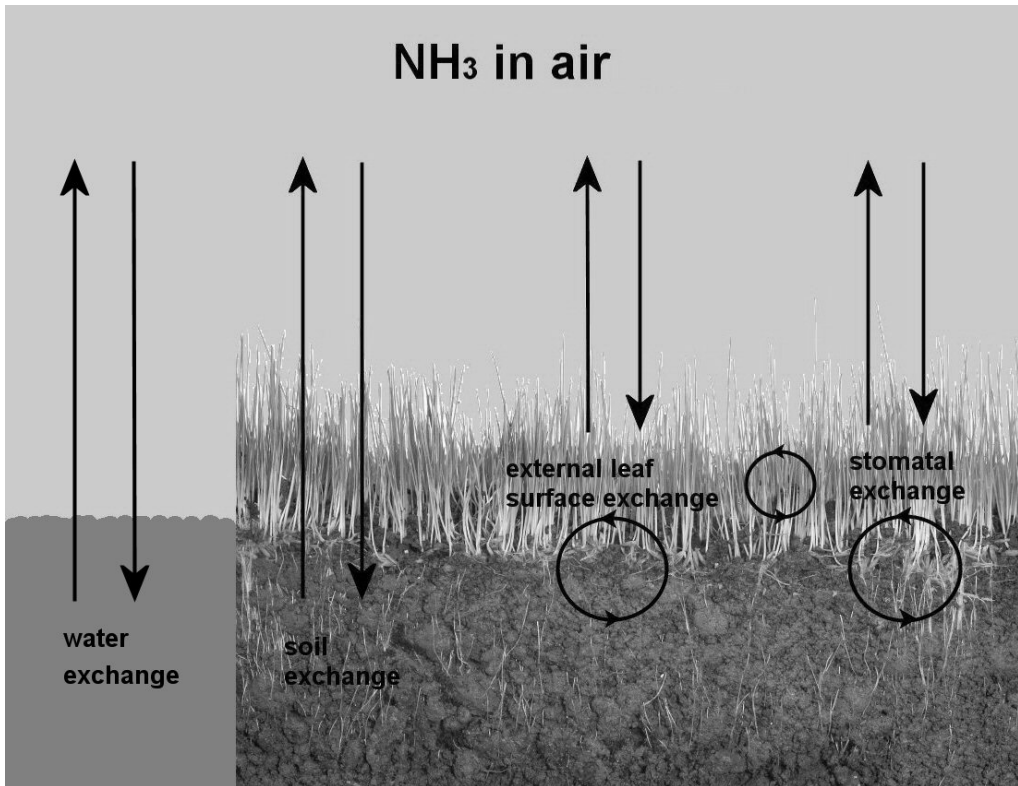


Figure 1.3. Schematic overview of the surface-atmosphere exchange processes over water and vegetated surface.

1.3.1 Stomatal exchange

Ammonia can diffuse through the stomata into the substomatal cavities in leaves in which it can be absorbed in the intercellular or apoplastic fluid. The ammonia concentration in the substomatal cavities is in chemical equilibrium with the ammonium concentration in the apoplastic fluid. The equilibrium concentration that is present in the substomatal cavities in leaves is called the "compensation point" (Farquhar et al., 1980). The compensation point is defined as the concentration at which the net NH_3 flux towards the stomata is zero (Farquhar et al., 1980). The compensation point is often called the stomatal compensation point (χ_s), because it represents the air concentration in the stomata that is in equilibrium with the ammonium concentration and pH in the *intercellular* or *apoplastic* fluid, i.e., $[\text{NH}_4^+]_{\text{apo}}$ and $[\text{H}^+]_{\text{apo}}$. In this thesis, we use stomatal compensation point and stomatal concentration interchangeably.

A general relationship between the gaseous ammonia concentration and the NH_4^+ concentration and pH in a solution, is derived from the temperature response of the Henry equilibrium and the ammonium-ammonia dissociation equilibrium (see Appendix A). By applying this general relationship (Equation A1.4) to the gas-liquid interface in the stomata, the theoretical stomatal compensation point (χ_s) is written as:

$$\chi_s = \frac{a}{T_{leaf}} \exp\left(\frac{-b}{T_{leaf}}\right) \cdot \Gamma_s \quad (1.4)$$

where χ_s is the stomatal compensation point ($\mu\text{g m}^{-3}$), a and b are constants ($a = 2.75 \cdot 10^{15} \mu\text{g m}^{-3} \text{ K}$ and $b = 1.04 \cdot 10^4 \text{ K}$), T_{leaf} is the leaf temperature (K) and Γ_s is the molar ratio between the NH_4^+ and H^+ concentration in the apoplastic fluid (dimensionless).

Figure 1.4 shows the stomatal compensation point as a function of the leaf temperature for three different values for Γ_s . An increase in leaf temperature of about 6 degrees doubles the stomatal concentration. Furthermore, a doubling of Γ_s also doubles the stomatal concentration. Leaf temperature, NH_4^+ and H^+ concentrations in the apoplastic fluid are therefore very important and sensitive variables in the calculation of the stomatal compensation point.

The actual exchange of ammonia with the stomata depends on two factors, namely the concentration difference between the concentration in the stomata and the concentration in the atmosphere, and the diffusion resistance in the stomatal pores.

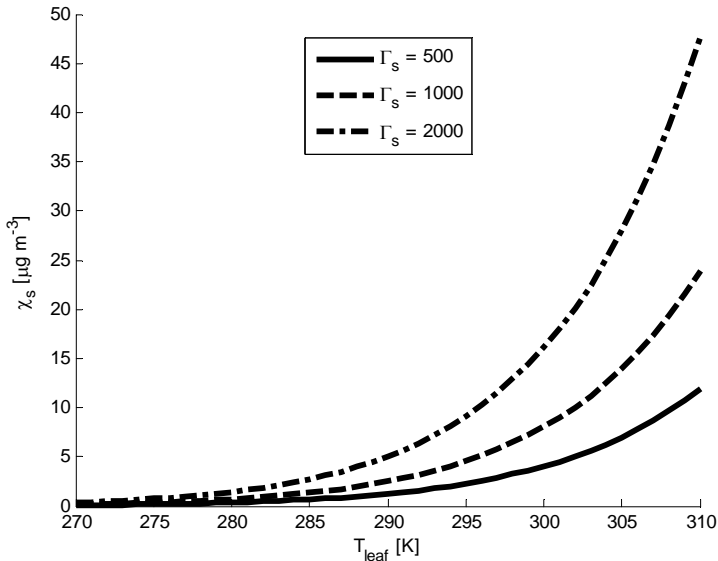


Figure 1.4. The stomatal compensation point as a function of leaf temperature for three different values of Γ_s .

1.3.2 External leaf surface exchange

The mechanism of uptake of ammonia by the external leaf surface is either by dissolution in water films present on the leaf surface or by physical adsorption to leaf surface waxes (Van Hove et al., 1989). Water films form on the leaf surface either by dew or by precipitation. Dew occurs when in the evening radiative cooling allows water vapor in the atmosphere to condense on a surface (Garratt and Segal, 1988). As soon as the surface starts to cool down, dew starts to accumulate on the surface, and when the surface starts to heat up again, the accumulated dew starts to evaporate until no dew is left. In addition to this, dew forms when soil water evaporates during the night and is intercepted by the canopy (Monteith,

1957; Garratt, 1992). Under rainy circumstances, the leaf surface intercepts part of the precipitation. Van Hove and Adema (1996) found that the water film thickness varies from 10 μm at low relative humidity to about 100 μm at high relative humidity. Flechard et al. (1999) found a much larger range of water film thicknesses for a moorland canopy, ranging from about 0.1 μm in dry circumstances to a maximum value of 1-2 mm. For their model calculations, however, they use a maximum value of 100 μm for the water film thickness.

Because of the high solubility of ammonia in water, ammonia will easily deposit to wet surfaces. With a solubility of about 56 mol l^{-1} at 25 $^{\circ}\text{C}$, the amount of NH_3 that can dissolve in the water layer ranges from 5.6 mmol m^{-2} leaf surface in dry circumstances (for a water layer thickness of 0.1 μm) to 5.6 mol m^{-2} leaf surface at wet circumstances (for a water layer thickness of 100 μm). Interactions between NH_3 and other acid gases may enhance the leaf surface uptake, such as co-deposition with SO_2 as discussed by Van Breemen et al. (1982) and Van Hove et al. (1989).

Periods of desorption of previously deposited NH_3 from evaporating leaf water films have been observed, particularly in the early morning as shown and modeled by Sutton et al. (1998), Flechard et al. (1999) and Burkhardt et al. (2009).

In dry conditions, Van Hove et al. (1988, 1989) have shown that the surface adsorption of ammonia increases with relative humidity. Burkhardt and Eiden (1994) ascribe this behavior to hygroscopic particles/salts on the leaf that act as condensation nuclei in which ammonia can dissolve. Especially ammonium sulphate, which cannot dissociate to the precursor gases because of its low vapor pressure, accumulates at the leaf surface (until it is washed off by precipitation).

Van Hove et al. (1987) showed that the transfer of ammonia *through* the cuticle is very slow and can be neglected. Therefore, we consider the process *at* the surface as dominant.

1.3.3 Soil exchange

For the exchange of ammonia with the soil surface, the presence of ammonia in equilibrium with ammonium dissolved in soil moisture is important. An analogous equation to Equation 1.4 can be used to determine the gaseous soil surface ammonia concentration (χ_{soil}) in equilibrium with the ammonium concentration $[\text{NH}_4^+]_{\text{soil}}$ and the pH in soil moisture:

$$\chi_{\text{soil}} = \frac{a}{T_{\text{soil}}} \exp\left(\frac{-b}{T_{\text{soil}}}\right) \cdot \Gamma_{\text{soil}} \quad (1.5)$$

where χ_{soil} is the soil surface concentration ($\mu\text{g m}^{-3}$), T_{soil} is the soil surface temperature (K), a and b are constants ($a = 2.75 \cdot 10^{15} \mu\text{g m}^{-3} \text{K}$ and $b = 1.04 \cdot 10^4 \text{K}$) and Γ_{soil} is the molar ratio between NH_4^+ and H^+ concentration in the soil moisture (dimensionless). Besides the strong dependency of the NH_4^+ and H^+ concentration in soil moisture, the rate and amount of absorption or desorption at the soil surface depends strongly on the soil surface temperature and the availability of soil moisture at the surface. These variables have a high spatial and temporal variability, which makes the exchange with the soil very uncertain, especially, when the soil is covered with vegetation. In order to interact with the soil surface, ammonia has to be transported from the air above the vegetation to the soil. This transport depends on the height and density of the vegetation and the turbulent transport within the canopy.

At the soil surface, decomposing plant material or leaf litter may be present, which increases the concentration of ammonia at the soil surface. The process of decomposition of

plant material or leaf litter is very complex and depends on the N content, temperature and humidity of the plant material or leaf litter (Whitehead et al., 1988, 1989; Nemitz et al., 2000a, 2001; Mattsson and Schjoerring, 2003; David et al., 2009).

1.3.4 Water exchange

As mentioned before the oceans can naturally produce NH_4^+ from the degradation of organic nitrogen compounds and excreta of zooplankton (Quinn, 1996). However, in coastal areas, the amount of NH_4^+ in sea water might be considerably higher due to the deposition of NH_3 and NH_4^+ from continental origin and riverine inputs of NH_4^+ .

The ammonia concentration at the water surface - atmosphere interface can be calculated in analogy with Equation 1.4 again:

$$\chi_{\text{water}} = \frac{a}{T_{\text{water}}} \exp\left(\frac{-b}{T_{\text{water}}}\right) \cdot \Gamma_{\text{water}} \quad (1.6)$$

where χ_{water} is the ammonia concentration at the water surface - atmosphere interface ($\mu\text{g m}^{-3}$), T_{water} is the water temperature (K), a and b are constants ($a = 2.75 \cdot 10^{15} \mu\text{g m}^{-3} \text{ K}$ and $b = 1.04 \cdot 10^4 \text{ K}$) and Γ_{water} is the molar ratio between the NH_4^+ and H^+ concentration in the water (dimensionless). The equation is similar to the equation presented by Asman et al. (1994), in which activity coefficients for NH_3 and NH_4^+ in sea water are included. These activity coefficients account for the larger ionic strength of sea water that influence the Henry's law and the dissociation constants.

1.3.5 Ammonia exchange within the canopy

As shown in Figure 1.3, several exchange pathways within the canopy are possible. In the previous sections, we already discussed that ammonia can deposit on the leaf surface and dissolve in leaf surface water as ammonium. Ammonia can also form ammonium-containing particles that remain on the leaf surface after evaporation of the leaf surface water. In both cases, the deposited ammonia can be washed off by precipitation to the soil. Contrary, a wet leaf surface can recapture emissions of ammonia from the soil, preventing it from being emitted from the vegetation. Another exchange pathway within the canopy is the absorption of desorbed ammonia from the external leaf surface by the plant through the stomata. Contrary, recapturing of emitted ammonia from the stomata by the external leaf surface can occur. Similarly, emitted ammonia from the soil can be absorbed by the plant through the stomata, while emitted ammonia from the plant can deposit on a wet soil surface.

These exchange pathways within the canopy have not been studied explicitly and are therefore highly uncertain. Only a few studies suggest that the exchange pathways within the canopy can be significant in size, however, these in-canopy fluxes have not shown to significantly influence the net flux above the canopy (Denmead, 1976; Sutton et al., 1995b; Nemitz et al., 2000a). Therefore, these processes can be considered of minor importance for the net flux.

1.4 Resistance modeling of the surface-atmosphere exchange of ammonia

Several models of varying complexity have been developed to describe the surface-atmosphere exchange of ammonia, i.e., the different exchange processes described in the previous section. These models are all based on the same concept: resistance modeling using electrical circuit analogue (Monteith and Unsworth, 1990). In this modeling approach, the flux or current is modeled as the concentration difference or potential difference divided by the resistance, i.e., $F = \Delta C/R$ equivalent to $I = V/R$. The deposition pathways described in the previous section are represented by resistances that may act in series and/or in parallel. The exchange fluxes of many trace gases vary in sign as well as in magnitude, with emission and deposition both being observed. Emission can only be obtained if the concentration at the surface is larger than the concentration above, independent of the magnitude of the resistance. The best known example of bi-directional exchange of a trace gas is probably the bi-directional exchange of CO_2 . CO_2 is taken up due to photosynthesis in the daytime and emitted due to respiration at night. The concept of bi-directional surface-atmosphere exchange is now widely recognized for a number of trace gases (NH_3 , NO , CO_2). However, the processes that control this bi-directional exchange can differ for the different trace gases. The recognition of bi-directional exchange requires modeling approaches that are appropriate for the trace gas considered (Fowler et al., 2009). In this section, the different modeling approaches for the surface-atmosphere exchange of NH_3 are discussed. In some model approaches, the concentration at the surface is assumed to be zero and all exchange processes are represented by the surface resistance. In other model approaches, a surface concentration is taken into account. The existing resistance models, used for the description of the surface-atmosphere exchange process of NH_3 over vegetated surfaces, have been reviewed by Sutton et al. (1998) and Nemitz et al. (2001). In this thesis, we will present a brief overview of these resistance models.

For short, dense vegetation, like grassland, the single-layer or 'big-leaf' approach is considered to be adequate. This approach is based on the assumption that all exchange processes happen in one part of the canopy. In general, this is assumed to be the top of the canopy, because this is where the dominant exchange processes take place. The most important processes to be modeled are therefore the external leaf surface exchange and the stomatal exchange.

These so-called single-layer models can be divided into two categories (see Figure 1.5):

1. Canopy resistance models (Figure 1.5a and 1.5b) that assume zero surface concentrations, often applied to model dry deposition of NH_3 over natural and semi-natural ecosystems (Sutton et al., 1992; Erisman and Wyers, 1993; Sutton et al., 1993a; Duyzer et al., 1994).
2. Canopy compensation point models (Figure 1.5c and 1.5d) that allow for bi-directional fluxes and are generally required to model plant/atmosphere exchange of NH_3 over agricultural crops and intensively managed grasslands (Sutton et al., 1998; Nemitz et al., 2001).

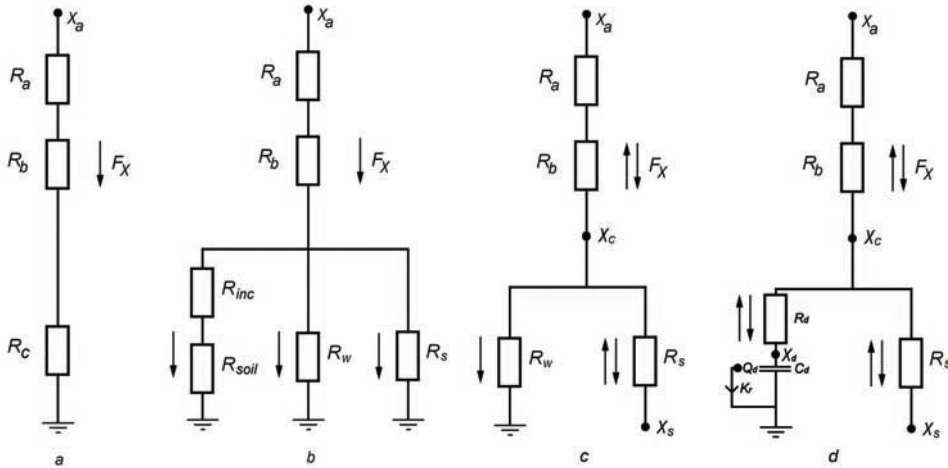


Figure 1.5. Examples of single-layer models of plant-atmosphere exchange of NH₃: (a) simple canopy resistance (R_c) model. (b) simple canopy resistance (R_c) model with the canopy resistance subdivided into a soil, a stomatal and a non-stomatal (or external leaf surface) pathway. (c) 'traditional' canopy compensation point (χ_s-R_w) model, with a bi-directional pathway with the stomata and a deposition pathway towards the external leaf surface (or cuticle). (d) 'dynamic' canopy compensation point (χ_s-C_d) model with ad-/desorption from leaf-water layers parameterized through a capacitor with capacitance (Q_d) and surface charge (χ_d). χ_a is the air concentration; χ_c is the canopy compensation point; χ_s is the stomatal compensation point; χ_d is the adsorption (or leaf water layer) concentration; R_a is the aerodynamic resistance; R_b is the quasi-laminar boundary layer resistance; R_w is the external leaf surface resistance; R_s is the stomatal resistance; R_c is the canopy resistance; C_d is the adsorption capacitance; Q_d is the ammonia adsorption charge; K_r is the reaction rate. In Section 1.4.3 and 1.4.4 these models will be discussed in more detail (after Sutton et al., 1998).

The single-layer approach is, however, less suited to situations where the net NH₃ exchange is dominated by exchange mechanisms that take place at different heights in the canopy, and are controlled by different responses to meteorological or physiological conditions. After the application of fertilizer or for sparse tall canopies, for example, the soil exchange is likely to be dominant. For these situations, a multi-layer model, which accounts for the soil and/or the leaf litter exchange pathway (e.g., Figure 1.6; Nemitz et al., 2001), might be more appropriate. This approach contains a bi-directional pathway to the soil/leaf litter through the canopy. Several studies have shown that the ammonia concentrations at the soil surface can be very large (Denmead et al., 1976; Nemitz et al., 2000a), especially in the presence of leaf litter. However, it has to be mentioned that it is very difficult to derive parameterizations for the individual exchange processes in the multi-layer model, especially for the soil exchange pathway, which is influenced by the transport of ammonia through the canopy and several soil variables (e.g., N-content, soil moisture availability, pH, soil temperature). The two-layer canopy compensation point model has shown, however, that it can be useful in the modeling of surface-atmosphere exchange of ammonia in canopies with leaf litter as an important source of ammonia (Personne et al., 2009). An important condition that needs to be satisfied in this model is that detailed information about the different variables is available.

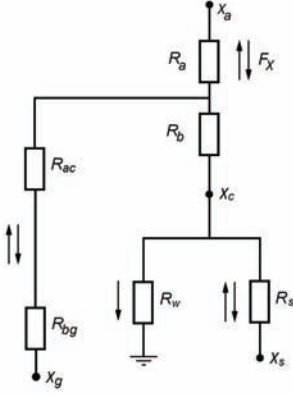


Figure 1.6. A two-layer canopy compensation point model. In addition to the single-layer canopy compensation point (x_c - R_w) model (Figure 1.5c), this approach contains a soil concentration (x_s) and the diffusion through the canopy is described by the sum of the in-canopy aerodynamic resistance (R_{ac}) and the soil boundary-layer resistance (R_{bg}) (after Nemitz et al., 2001).

As mentioned before, emissions from the soil and decomposing leaf litter are often completely recaptured by the overlying canopy and do hardly contribute to the net exchange as shown by Denmead (1976) and Nemitz et al. (2000a). Therefore, the single-layer or 'big-leaf' approach generally seems to be appropriate.

In the following sections, we will give a detailed description of the resistances and concentrations that are used in the single-layer models. As we can see in Figure 1.5, two resistances always contribute to the transport of ammonia through the atmosphere, i.e., the aerodynamic resistance (R_a) and the quasi-laminar boundary layer resistance (R_b). These resistances, which are independent of the model approach chosen, are discussed below. Besides, the different model approaches and the related model parameters are discussed.

1.4.1 Aerodynamic resistance, R_a

The aerodynamic or atmospheric resistance (R_a) is the only resistance that is always in series with the other resistances. The aerodynamic resistance describes the transport through the turbulent part of the atmosphere and is assumed to be similar to that of heat (e.g., Hicks et al., 1987). $R_a(z-d)$ is determined by integrating the inverse of the eddy diffusivity for heat (K_H) over the height range between $z-d$ and z_0 (Thom, 1975; Garland, 1977, 1978):

$$R_a = \frac{1}{k u_*} \left[\ln \left(\frac{z-d}{z_0} \right) - \Psi_H \left(\frac{z-d}{L} \right) + \Psi_H \left(\frac{z_0}{L} \right) \right] \quad (1.7)$$

where k is the Von Karman constant (~ 0.4), u_* is the friction velocity (m s^{-1}), z is the height above the surface (m), d is the displacement height (m; ~ 0.75 times the canopy height), z_0 is the roughness length (m), Ψ_H is the integrated stability function for heat, L is the Obukhov length (m).

Here, we use the integrated stability function of Paulson (1970) and Dyer (1974) for unstable conditions (i.e., $L < 0$):

$$\Psi_{\chi}(\zeta) \approx \Psi_{\text{H}}(\zeta) = 2 \ln \left[\frac{1+x^2}{2} \right] \quad (1.8a)$$

where $x = (1-16\zeta)^{1/4}$ with $\zeta = (z-d)/L$

and the integrated stability function of Beljaars and Holtslag (1991) for stable conditions (i.e., $L > 0$):

$$\Psi_{\chi}(\zeta) \approx \Psi_{\text{H}}(\zeta) = - \left(1 + \frac{2}{3} a \zeta \right)^{3/2} - b \left(\zeta - \frac{c}{d} \right) \exp(-d\zeta) - \frac{bc}{d} + 1 \quad (1.8b)$$

where $a = 1$, $b = 0.667$, $c = 5$, $d = 0.35$ and $\zeta = (z-d)/L$.

From Equation 1.7, it can be seen that the aerodynamic resistance (R_a) decreases with friction velocity (u_*) and increases with height ($z-d$), which physically means that NH_3 is more efficiently exchanged in turbulent conditions and over small heights.

1.4.2 Quasi-laminar boundary layer resistance, R_b

R_b is associated with the transfer of ammonia through the quasi-laminar boundary layer in contact with the surface. R_b quantifies the way in which a pollutant transfer differs from momentum transfer in the immediate vicinity of the surface (Hicks et al., 1987). In this study, the quasi-laminar layer resistance R_b is approximated following Hicks et al. (1987):

$$R_b = \frac{2}{k \cdot u_*} \left(\frac{Sc}{Pr} \right)^{2/3} \quad (1.9)$$

where k is the Von Karman constant (~ 0.4), u_* is the friction velocity (m s^{-1}), Sc is the Schmidt number ($= \nu/D_{\text{NH}_3}$ with ν being the kinetic viscosity of air ($\sim 0.15 \text{ cm}^2 \text{ s}^{-1}$ at 20°C) and D_{NH_3} being the molecular diffusivity of ammonia ($\sim 0.20 \text{ cm}^2 \text{ s}^{-1}$; Massman, 1998)) and Pr is the Prandtl number (~ 0.72). For NH_3 , we normally use a simplified relation for R_b : $R_{b,\text{NH}_3} = 5.1 / u_*$.

From Equation 1.9 (and its simplification), it can be seen that also the quasi-laminar boundary layer resistance (R_b) decreases with the friction velocity (u_*).

1.4.3 Canopy resistance models

The canopy resistance (R_c in Figure 1.5a) in the single-layer canopy resistance models can be divided into three (parallel) pathways: the external leaf surface pathway, the stomatal pathway and the soil pathway (represented by R_w , R_s , $R_{\text{inc}}+R_{\text{soil}}$ respectively in Figure 1.5b). The subscript 'w' stands for waxes (cuticular waxes) or water layer, and was chosen to stay consistent with literature, subscript 's' stands for stomatal and subscript 'inc' stands for 'in-canopy'. The canopy resistance models assume that the surface concentration is zero. The resistances associated with these pathways are described below.

External leaf surface resistance

Many studies have shown that the external leaf surface can act as an effective sink, especially for soluble gases like ammonia at wet surfaces (Van Hove et al., 1988; Benner et al., 1992; Wyers and Erisman, 1993; Sutton and Fowler, 1993; Erisman et al., 1994; Sutton et al., 1995b). However, in more polluted areas, the external leaf surface seems to be a less effective sink (Sutton et al., 1997; Wyers and Erisman, 1998; Flechard et al., 1999). This has resulted in many different parameterizations describing this process. Most of the parameterizations have (or can be transformed into) the following form:

$$R_w = \alpha \cdot \exp\left(\frac{100 - RH}{\beta}\right) \quad (1.10)$$

where α is often called $R_{w,\min}$ and β is the steepness of the relative humidity response (high values of β correspond to a weak relative humidity response).

Erisman and Wyers (1993), Flechard (1998) and Nemitz et al. (2001) also presented a response of NH_3 adsorption at the external leaf surface to SO_2 concentration. Fowler et al. (1998a) and Jones et al. (2007a,b) showed a direct response of the NH_3 adsorption at the leaf surface with the ambient NH_3 concentration. It is not clear if this effect is present in the functions presented by Erisman and Wyers (1993), Flechard (1998) and Nemitz et al. (2001).

Stomatal resistance

The diffusion resistance by the stomatal pores is generally called the stomatal resistance. The stomatal resistance is regulated by the plant and mainly depends on photosynthetic active radiation (PAR), leaf temperature, vapor pressure deficit and the water balance of the plant. This resistance is generally modeled in analogy with transpiration of water vapor from the plant. Ammonia from the stomata can only escape to the atmosphere and ammonia from the atmosphere can only be absorbed in the stomata, if the stomata are open, i.e. if the stomatal resistance is small. Therefore, the actual stomatal NH_3 exchange flux is determined by the size of the stomatal compensation point and the factors that control stomatal opening.

Based on the work of Jarvis (1976), many authors have developed models to calculate the stomatal resistance (e.g., Baldocchi et al., 1987; Wesely et al., 1989; Emberson, 2000a). In this study, we chose to use the multiplicative model of Emberson et al. (2000a,b):

$$g_s = g_{\max} f_{\text{phen}} \max\{f_{\min}, f_{\text{light}} \times f_T \times f_{\text{VPD}} \times f_{\text{SWP}}\} \quad (1.11)$$

where g_s is the stomatal conductance (i.e., the inverse of the stomatal resistance), g_{\max} is the maximum stomatal conductance (m s^{-1}), and f_x are factors (from 0-1) accounting for time of year (leaf phenology; f_{phen}), the minimum observed stomatal conductance (f_{\min}), light (f_{light}), leaf temperature (f_T), vapor pressure deficit (f_{VPD}) and soil water potential (f_{SWP}).

Soil resistance

R_{inc} and R_{soil} are resistances that represent the in-canopy vertical transport to the soil and the resistance of the soil itself, respectively. R_{inc} represents the resistance against turbulent transport within the canopy and can be calculated according to Van Pul and Jacobs (1994):

$$R_{\text{inc}} = \frac{b \cdot \text{LAI} \cdot h}{u_*} \quad (1.12)$$

where b is an empirical constant ($=13.9 \text{ m}^{-1}$), h is the height of the vegetation (m) and LAI is the leaf area index (dimensionless).

R_{soil} is often modeled as a constant empirical value for certain conditions, e.g., 10 s m^{-1} for wet soil conditions, 100 s m^{-1} for dry soil conditions in the OPS model (Van Jaarsveld, 2004).

1.4.4 Canopy compensation point models

The canopy resistance models are not able to describe bi-directional fluxes. As shown in Figure 1.5, the canopy compensation point models do account for bi-directional fluxes. There are two types of canopy compensation point models, i.e., the 'traditional' canopy compensation point model with a bi-directional pathway to the stomata (Figure 1.5c) and the 'dynamic' canopy compensation point model with two bi-directional pathways to the external leaf surface and to the stomata (Figure 1.5d). Both will be described briefly below.

'traditional' canopy compensation point model

In the 'traditional' canopy compensation point model, a bi-directional pathway with the stomata is defined. The external leaf surface pathway is identical to the description in Section 1.4.3.1. The stomatal pathway, however, is made bi-directional by introducing the stomatal concentration or stomatal compensation point, χ_s . The transfer through the stomata is still limited by the stomatal resistance as described in Section 1.4.3.2. With the introduction of this bi-directional pathway, daytime emissions from vegetation can be modeled. χ_s is modeled according to Equation 1.4 and is mainly determined by the leaf temperature and Γ_s , which is the molar ratio between the NH_4^+ and H^+ concentration in the apoplastic fluid.

Many values for Γ_s have been reported in the range between 20 and 5000 (Husted et al., 1996; Mattsson et al., 1997; Husted et al., 2000; Van Hove et al., 2002; Loubet et al., 2002; Flechard and Fowler, 1998; Plantaz, 1998; Milford et al., 2001a; Milford et al., 2001b; Spindler et al., 2001; Nemitz et al., 2004; Horvath et al., 2005; Walker et al., 2006; Wichink Kruit et al., 2007; Neiryck et al., 2008; Burkhardt et al., 2009). The lower values are found in areas with low ambient ammonia concentrations/low pollution levels; the higher values are mostly found in agricultural areas/high pollution levels. With an average temperature of 15°C the corresponding stomatal compensation points range between 0.04 and $10 \mu\text{g m}^{-3}$. Several techniques were used to derive these values, e.g., micrometeorological flux measurements, controlled gas-exchange measurements in cuvettes and direct measurements of extracted leaf apoplastic fluid (latter two are often called together as bioassay estimates).

'dynamical' canopy compensation point model

The 'traditional' canopy compensation point model is generally giving reasonable agreement with the measurement data. However, cases have been observed where the model underestimates emissions in the morning and overestimates emissions in the evening. This hysteresis effect can be explained by the fact that the external leaf surface resistance is not represented correctly, and that NH_3 both adsorbs and desorbs from the cuticle, dependent on humidity and wetness. If the deposited NH_3 is not fixed by the

reaction with SO_2 to form low vapor pressure salts (e.g., $(\text{NH}_4)_2\text{SO}_4$), it may be released to the atmosphere (Sutton et al., 1998). To model this adsorption/desorption process from the leaf water layer, Sutton et al. (1998) build in a capacitance (C_d), with an adsorption charge (Q_d) and an adsorption concentration (χ_d). By treating the leaf surface exchange as a capacitance, the flux calculation is made time dependent (or dynamical) on the previous fluxes. The flux in or out the adsorption capacitor is restricted by the charging resistance (R_d) of the capacitor. The amount of NH_4^+ that is removed from the capacitor by chemical reactions (to form low vapor pressure salts) can be accounted for by adding a reaction (or leaf uptake) flux with a rate constant (K_r). A disadvantage of this model approach is that the leaf surface water pH needs to be defined as input. This input parameter strongly depends on other soluble gases that are present in the leaf surface water.

Flechar et al. (1999) therefore extended this model with a complete aqueous chemistry model for the leaf surface. In this model, the leaf surface water pH is solved by calculation of the chemical composition in the leaf surface water based on previous fluxes. Advantage of this model is that it is able to simulate the exchange of SO_2 and other gases at the same time.

Although the 'dynamical' canopy compensation point model is physically most realistic, it needs several highly uncertain input parameters, which are generally not available at the required time and spatial scales in atmospheric transport models. Furthermore, short-term influences, like for example wash off of ammonium salts by precipitation, are not included in this model approach either. In addition, the dynamical canopy compensation point model approach would increase the calculation time considerably for calculations over larger areas with the required high temporal resolution. Because of all these limitations, the dynamical canopy compensation point model is currently not used in atmospheric transport models.

1.5 Ammonia in the Netherlands

1.5.1 Ammonia concentration measurements in the Netherlands

During the last 3 decades, ammonia is increasingly being recognized as an important atmospheric pollutant in the Netherlands and internationally. This is the result of the acidifying and eutrophying effects of ammonia deposition onto terrestrial and aquatic ecosystems (Van Breemen et al., 1982, 1988; Derwent et al., 1989; Bobbink et al., 1998) and the influence of ammonia on regional scale tropospheric chemistry and related public health (Schlesinger and Cassee, 2003; Buijsman et al., 2005; Sutton et al., 2009b). Especially, eutrophication and acidification of soils induce shifts in the nutrient balance of plant species that can result in a loss of biodiversity. Therefore, one of the main items in the national air pollution policy of the Netherlands is to reduce agricultural ammonia emissions (as the main source of ammonia in the Netherlands). The European Parliament and the Council of the European Union have set national emission ceilings (NEC) for acidifying and eutrophying pollutants, including ammonia, and for ozone precursors in order to provide fuller protection for the environment and human health against their adverse effects (EU, 2001). The NEC for NH_3 in the Netherlands to be attained by 2010 is 128 million kg NH_3 . The ammonia emissions in the Netherlands in 2008 are estimated to be about 135 million kg NH_3 .

To monitor the effectiveness of the measures taken by the government, The National Institute for Public Health and the Environment (RIVM) measures NH_3 concentrations at 8 locations in the Netherlands (black dots in Figure 1.7). RIVM also measures aerosol

concentrations at 7 locations (gray dots) and precipitation composition at 11 locations (white dots) in the Netherlands. The measuring stations are located around the country in areas with high as well as low NH_3 emissions. Because of the spatial variability in the ammonia emissions, it is not possible to get a representative map of the ammonia concentrations with the 8 measuring stations of NH_3 alone. Therefore, country-wide calculations of the ammonia concentrations are made with the atmospheric transport model OPS, i.e., the Operational Priority Substances model (Van Jaarsveld, 2004).



Figure 1.7. National monitoring network for ammoniacal components in the Netherlands (Source: Van Pul et al., 2008).

1.5.2 Ammonia concentration modeling in the Netherlands

The OPS model uses NH_3 emissions and meteorological data as input and calculates the NH_3 and NH_4^+ concentrations as well as the dry and wet deposition of NH_3 and NH_4^+ , accounting for the transport and the three removal mechanisms of ammonia from the

atmosphere. The modeled concentrations of all ammoniacal components are validated with the concentration measurements at the different measuring stations (Van Pul et al., 2008).

Emissions in the Netherlands

For a better understanding of the atmospheric ammonia budget in the Netherlands, we will first present estimates for the magnitude of the processes that are currently used to calculate this budget, i.e., the NH_3 emission (source), the chemical transformation of NH_3 into NH_4^+ (sink), the dry deposition of NH_3 and NH_4^+ (sink) and the wet deposition of NH_3 and NH_4^+ (sink).

The total anthropogenic emissions of ammonia in the Netherlands are estimated at a total of 135 million kg (or 135 ktonnes) in 2005, of which 91% was of agricultural origin (Milieubalans, 2008). Figure 1.8 shows the partitioning of the anthropogenic emissions of NH_3 in the Netherlands in the year 2005. Cattle and pigs contributed the largest fraction of the Dutch NH_3 emission, 44% and 25%, respectively. Poultry and artificial fertilizer were responsible for 13% and 9% of the emission, respectively. The remaining 9% was emitted by humans (through breathing and transpiration), traffic, domestic animals and other small sources.

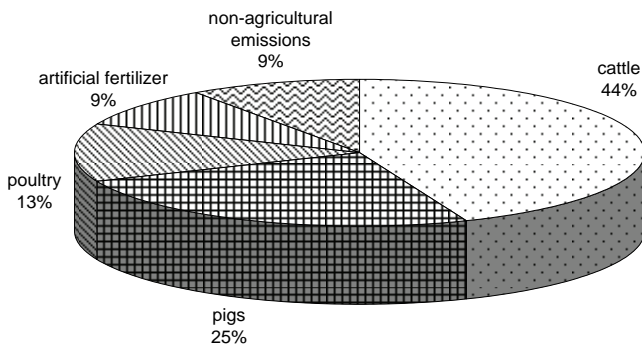


Figure 1.8. Anthropogenic NH_3 emissions in the Netherlands in the year 2005. (source: Pollutant Release and Transfer Register; web: <http://www.emissieregistratie.nl>)

The agricultural emission of ammonia (91% of the total anthropogenic ammonia emission) occurred primarily during the storage of slurry and manure in or near livestock houses (50%) and during the land spreading of slurries (33%). About 10% was emitted from artificial fertilizer application and the remaining 7% was emitted during grazing of cattle (Milieu- en Natuurcompendium, 2008).

Figure 1.9 shows the spatial distribution of ammonia emissions by agriculture estimated for 2005 over the Netherlands on a 5x5 km scale. The average agricultural ammonia emission in the Netherlands in 2005 is estimated to be about $30 \text{ kg ha}^{-1} \text{ yr}^{-1}$.

Especially the emission 'hot spots' with an emission of more than $100 \text{ kg ha}^{-1} \text{ yr}^{-1}$ ($\sim 6000 \text{ mol ha}^{-1} \text{ yr}^{-1}$) in the center of the Netherlands due to poultry housing and in the southeastern part of the Netherlands due to pig housing are conspicuous. However, there are also large areas with less intense animal housing (cattle, pigs and poultry) in the western, eastern and northern part of the Netherlands.

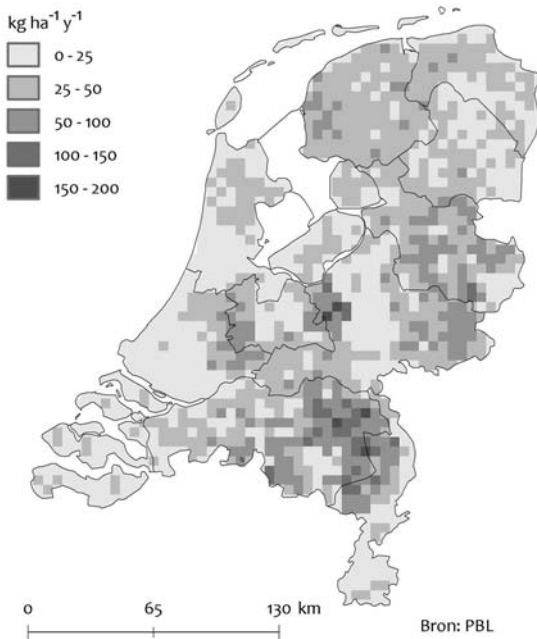


Figure 1.9. Spatial distribution of the emission of NH_3 by agricultural sources in the Netherlands in 2005. Source: LEI/PBL, courtesy to J. Aben, PBL.

Concentration and removal mechanisms in the Netherlands

Figure 1.10 gives an impression of the magnitude and the spatial distribution of the concentration (upper left panel) and the three removal mechanisms in the Netherlands in 2005, i.e., the chemical transformation of NH_3 into NH_4^+ (upper right panel), the dry deposition of NH_3 and NH_4^+ (lower left panel) and the wet deposition of NH_3 and NH_4^+ (lower right panel) as calculated with the OPS model (Van Jaarsveld, 2004).

The upper left panel shows that the concentration is closely related to the distribution of the emissions of NH_3 . The highest concentrations are calculated in the center and the southeastern part of the country with values exceeding $10 \mu\text{g m}^{-3}$. The upper right panel shows that the chemical transformation of ammonia into ammonium aerosol primarily occurs in the western part of the country, although most of the ammonia is emitted in the center and southeastern part of the country. This is likely because the acid gases that react with ammonia are mainly produced in regions with abundant industry and traffic, which are concentrated in the western part of the country. In other parts of the country, the sources of these acid gases are more evenly distributed and consequently, the ammonium concentrations are rather constant here. The NH_4^+ concentrations are in the order of $1\text{-}2 \mu\text{g m}^{-3}$ in the Netherlands in 2005. The lower left panel in Figure 1.10 shows that the distribution of the dry deposition of NH_3 and NH_4^+ is closely related to the distribution of the concentration, which in turn is closely related to the distribution of the emissions of NH_3 (Figure 1.9). Therefore, the highest dry deposition can be found in the center and the southeastern part of the country with values exceeding $30 \text{ kg } (\text{NH}_3 + \text{NH}_4^+) \text{ ha}^{-1} \text{ yr}^{-1}$. The average dry deposition of NH_3 and NH_4^+ in the Netherlands is calculated to be about 12 kg

$(\text{NH}_3 + \text{NH}_4^+) \text{ ha}^{-1} \text{ yr}^{-1}$ in 2005. The lower right panel of Figure 1.10 shows that the spatial distribution of the wet deposition of NH_3 and NH_4^+ is closer related to the spatial distribution of the NH_3 concentration than that of the NH_4^+ concentration. This suggests that the wet deposition is closer related to the washout of NH_3 during precipitation than to the usage of NH_4^+ -aerosol as condensation nuclei in cloud formation, i.e. rainout. The average wet deposition is about $5 \text{ kg } (\text{NH}_3 + \text{NH}_4^+) \text{ ha}^{-1} \text{ yr}^{-1}$ in the Netherlands in 2005. From this analysis, it follows that the dry deposition mechanism is the most important removal mechanism in the Netherlands.

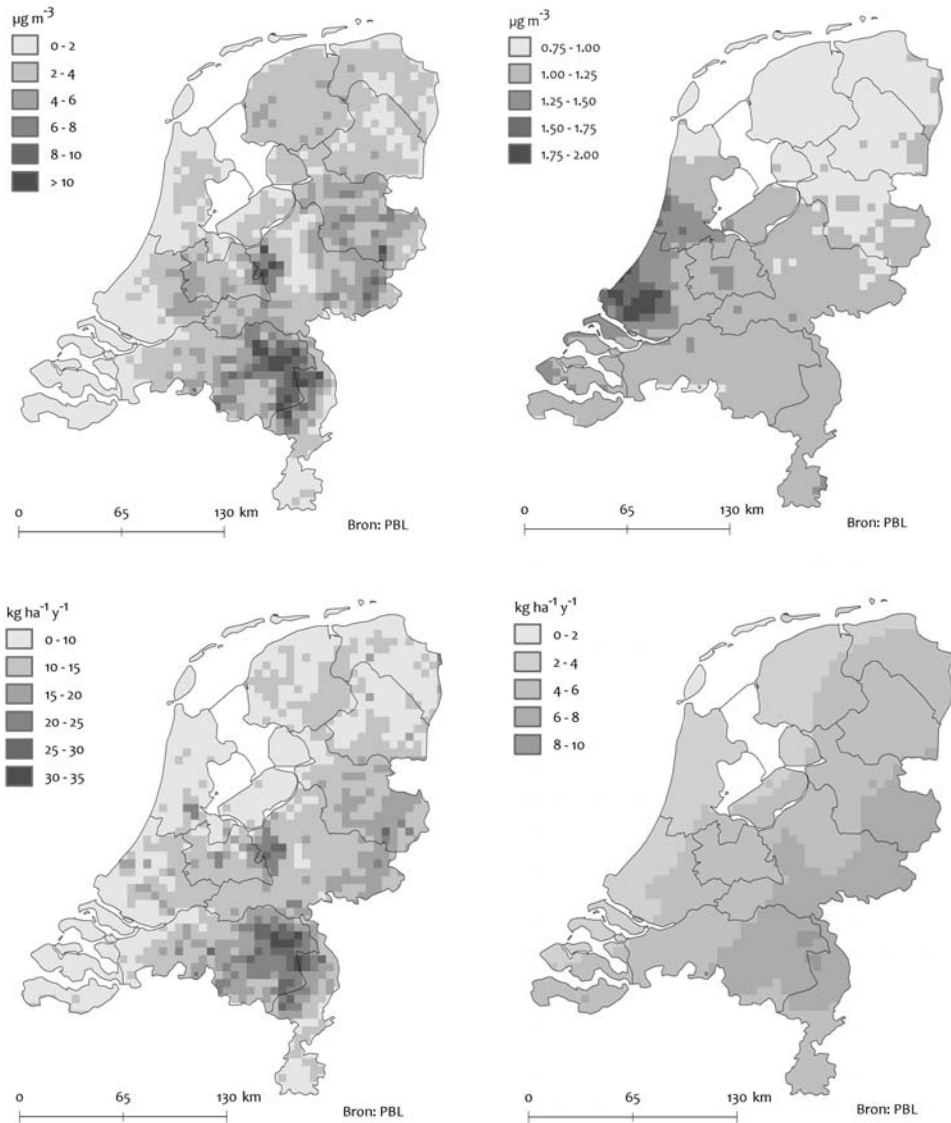


Figure 1.10. NH_3 concentration (upper left), chemical transformation into NH_4^+ -aerosol (upper right), dry deposition of NH_3 and NH_4^+ (lower left) and wet deposition of NH_3 and NH_4^+ (lower right) in the Netherlands in 2005 as calculated with the OPS model. Courtesy to J. Aben, PBL.

The 'ammonia gap'

The modeled annual average ammonia concentration, for the locations in the National Monitoring Network where ammonia is measured, is plotted in Figure 1.11 (gray dashed line with triangles). The figure also shows the measured annual average ammonia concentration (black solid line with squares) and the estimated total anthropogenic ammonia emissions by agricultural and other sources (bars). A significant reduction in the estimated emissions of ammonia is observed between 1995 and 2002 (from about 195 million kg yr⁻¹ to about 140 million kg yr⁻¹). Since 2002, the anthropogenic ammonia emissions only slightly decreased to about 135 million kg NH₃ in 2008 (Milieubalans, 2009). The measured ammonia concentrations follow the decrease in ammonia emissions from 10.5 µg m⁻³ in 1995 to 7.2 µg m⁻³ in 2002. Since 2002, the ammonia concentrations have stabilized around 8 µg m⁻³. The higher concentrations in 2003 and 2006 are attributed to the relatively warm conditions in these years.

In general, the modeled concentrations (gray dashed line with triangles) are lower than the measured concentrations (black solid line with squares). This difference between the measured and modeled ammonia concentrations is about 25% and is called the 'ammonia gap'.

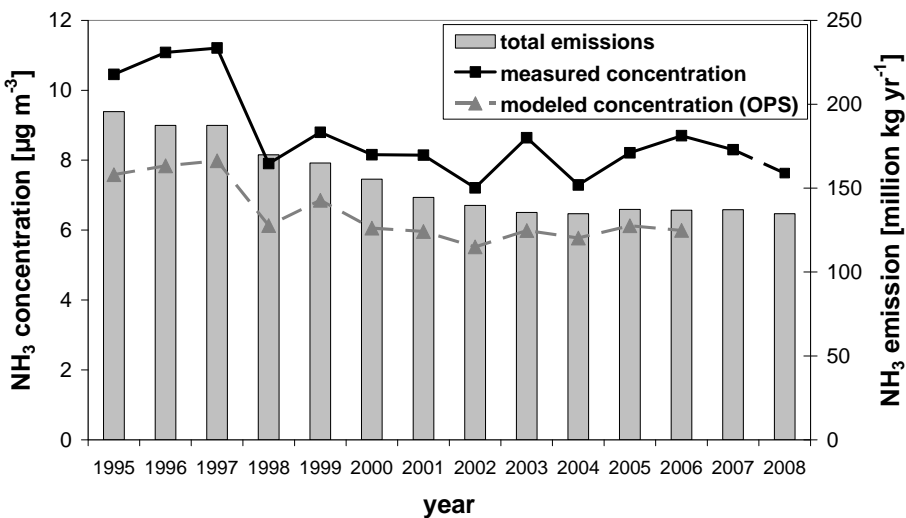


Figure 1.11. Emissions, measured and modeled ammonia concentrations from 1995 till 2008 (based on Milieu- en Natuurcompendium, 2008, Van Pul et al., 2008 and Milieubalans, 2009).

1.5.3 Uncertainties in the current concentration modeling

Uncertainty in the concentration measurements

The random uncertainty in the measured ammonia concentrations is estimated to be approximately 10% for the individual hourly measurements and 7% for the annual average concentration (Wyers et al., 1993; Van Pul et al., 2008). However, Figure 1.11 showed that the systematic difference of about 25% between the modeled and measured concentration is much larger than the random uncertainty in the measurements. Therefore, this difference can be considered as significant. An analysis showed that the used ammonia emissions as

well as the model calculations include large uncertainties that can be responsible for this difference (Steenvoorden et al., 1999, Van Jaarsveld et al., 2000). Higher ammonia emissions to the atmosphere or reduced removal from the atmosphere will both lead to higher concentrations in the model. Research on the 'ammonia gap' therefore focuses on improving the *emission factors* from manure application and animal housings (Mol, 2004; Berkhout et al., 2008; Velthof et al., 2009) and improving the description of the *dry deposition removal process* of ammonia (this thesis).

Uncertainties in the emissions

The emissions of ammonia are difficult to estimate, because there are many different ways of agricultural practice. Based on the known uncertainties in the emission factors that are used to calculate the total yearly ammonia emission in the Netherlands, the uncertainty in the total emission is estimated to be about 17% (Van Gijlswijk et al., 2004). This is a random uncertainty, which results in a random uncertainty in the modeled concentration, but it will not explain the ammonia gap.

Van Jaarsveld and Van Pul (2002) and Van Pul et al. (2004) found that the spatial resolution of the emissions is very important for the agreement between the modeled and the measured concentrations. They showed that the calculated concentrations provided much better agreement with the measurements using the emissions at a resolution of 500 by 500 meters instead of a resolution of 5000 by 5000 meters. Both the regression and the absolute values of the modeled concentrations improved. This is because the ammonia concentration at a location is closely related to the local emissions. However, these improvements were already included in the model calculations in Figure 1.11.

More recently, Velthof et al. (2009) developed a new methodology to calculate NH₃ emissions from animal housing systems and manure storage. This method also includes the emission from grazing and from the application of manure and fertilizers on farmland. The total emission from agricultural sources increased with about 1% compared to the values reported before. We can conclude that these higher emissions only explain a very small part of the ammonia gap.

Uncertainties in the dry deposition

The dry deposition flux is generally estimated as the product of the ammonia concentration and a modeled deposition velocity. The modeled deposition velocities at the ecosystem scale depend on process-based surface-atmosphere exchange models. The mechanistic understanding of the processes regulating the surface-atmosphere exchange of ammonia has increased considerably during the past few decades (Sutton et al., 1995a, 1998; Nemitz et al., 2001). However, large uncertainties in the modeled surface-atmosphere exchange of ammonia over different ecosystems still exist due to a lack of validation by both laboratory and field flux measurements. An overview of the uncertainties in the modeled concentration by Van Jaarsveld (2004) indicated that especially the dry deposition velocity is highly uncertain. A simple sensitivity analysis showed that the uncertainty in the dry deposition velocity over grassland also has a large impact on the uncertainties in the concentration and flux over other land-use types like arable land, forest, heathland and small water bodies. Many recent studies have shown that especially agricultural vegetation can be a source of ammonia in warm and dry circumstances due to the stomatal compensation point. Besides, leaf surface water layers can saturate in polluted areas, which leads to high external leaf surface resistances or even short periods of desorption of ammonia. The current description of the dry deposition process in the OPS model does not account for either of these

processes. Because grassland is the dominating land-use type in the Netherlands and uncertainties in the deposition process over grassland can possibly explain the ammonia gap, Van Jaarsveld et al. (2000) recommended carrying out flux measurements of ammonia over grassland.

1.5.4 Measurements of the surface-atmosphere exchange in the Netherlands

The surface-atmosphere exchange of ammonia, i.e., the ammonia flux, is usually not measured directly, despite of its importance for the mass balance and the uncertainties in the model parameterizations. Reason for this is that these measurements are expensive. To study the exchange of ammonia over agricultural grassland, accurate long-term ammonia flux measurements are essential. During the 90s, the AMANDA (Ammonia Measurement by Annular Denuder Sampler with online Analysis) rotating wet denuder was developed (Wyers et al., 1993), which made it possible to measure accurate concentration gradients, which are needed to calculate reliable fluxes. Although this technique is labor intensive and expensive, several datasets have been collected over the past 15 years (e.g. Erisman and Wyers, 1993; Sutton et al., 1995a; Fowler et al., 1998b; Flechard and Fowler, 1998; Plantaz, 1998; Milford et al., 2001a,b; Neiryneck and Ceulemans, 2008, Sutton et al., 2009a). First, the measurements were mainly focused on (semi-)natural ecosystems, e.g., heathland, moorland, mixed coniferous forest, because of their sensitivity for acidification and eutrophication. But later on, large European campaigns focused on agricultural vegetation in the EXAMINE and the GRAMINAE projects. However, measurements over agricultural grassland in severely polluted areas are still sparse. Therefore, new long-term flux measurements were carried out with an improved version of the AMANDA system, i.e., the GRAdient Ammonia - High Accuracy - Monitor (GRAHAM), over an agricultural grassland site in the Netherlands between 2004 and 2006. Agricultural grassland was chosen because it covers about 25% of the total land surface in the Netherlands and is therefore expected to be important for the mass balance of ammonia in the Netherlands.

1.6 Objectives and outline of the thesis

On basis of the above, we define the main objectives of this thesis as:

1. to achieve a better understanding of the surface-atmosphere exchange process of ammonia, i.e., the dry deposition process, especially over agricultural grassland in the Netherlands
2. to improve the model description of the surface-atmosphere exchange process of ammonia

To reach these objectives, long-term flux measurements with a new measurement device, i.e., GRAHAM, have been carried out and analyzed. In Chapter 2, the methodology to calculate ammonia fluxes from concentration measurements at several heights is described. We continue with a consideration of the conditions that should be met for this methodology and a description of the measurement site and the instrumentation. Then, the quality of the measurements is discussed and an overview of the NH_3 concentration and flux measurements is given.

In Chapter 3, two contrasting periods in 2004 are highlighted, i.e., a dry and warm summer period and a wet and cool autumn period, to illustrate the important mechanisms in the

surface-atmosphere exchange process. In this chapter, canopy compensation points are derived for the grassland site using the new flux measurements and the effect of leaf wetness on the ammonia fluxes is shown.

Chapter 4 deals with the modeling of leaf wetness over grassland. In this chapter, seven leaf wetness models are evaluated with measurements from two different measurement devices. To compare the leaf wetness models with the measurements, we used a statistical data analysis method, i.e., the contingency table, which is normally used for the verification of precipitation forecasts.

In Chapter 5, a new model description of the surface-atmosphere exchange of ammonia is presented for application in atmospheric transport models. The surface-atmosphere exchange calculated with the new model description is also compared with the surface-atmosphere exchange calculated with model descriptions from literature in this chapter.

Finally, in Chapter 6 a summary, reflections and recommendations are presented.

2 Theory and overview of the NH₃ flux measurements at the micrometeorological Haarweg station, Wageningen, the Netherlands

Parts of this chapter have been published as Wichink Kruit R.J., Stolk A.P., Volten H., Van Pul W.A.J., 2009. Flux measurements of ammonia at the micrometeorological weather station in Wageningen, the Netherlands. Bilthoven, RIVM Letter report 680150004/2009, 56 pp.

2.1 Derivation of the flux

This section describes how the flux can be derived from concentration gradient and micrometeorological measurements. The gradient (or flux-profile) technique is commonly used in dry deposition studies and is based on the theory of turbulent flow of the atmospheric boundary layer. In applying this technique one should keep in mind that it is based on theory, which is only valid under certain conditions. If these conditions are not met this will lead to serious errors in the estimated flux.

2.1.1 Basic theory

Starting with the basic conservation equation of ammonia and expanding into mean ($\bar{\chi}$) and turbulent (χ') parts, the following equation is obtained (e.g., Stull, 1988):

$$\frac{\partial \bar{\chi}}{\partial t} + \frac{\partial \chi'}{\partial t} + \frac{\bar{U}_j \partial \bar{\chi}}{\partial x_j} + \frac{\bar{U}_j \partial \chi'}{\partial x_j} + \frac{u_j' \partial \bar{\chi}}{\partial x_j} + \frac{u_j' \partial \chi'}{\partial x_j} = \frac{D \partial^2 \bar{\chi}}{\partial x_j^2} + \frac{D \partial^2 \chi'}{\partial x_j^2} + S \quad (2.1)$$

where χ is the ammonia concentration, t is time, U is wind speed, x is the direction, u' is wind speed fluctuation, D is the molecular diffusivity of ammonia, S is the net remaining source/sink term and j indicates the three spatial dimensions (x , y and z). Reynolds averaging and using the turbulent continuity equation (which puts the turbulent advection term into flux form (term III)) gives:

$$\underbrace{\frac{\partial \bar{\chi}}{\partial t}}_I + \underbrace{\frac{\bar{U} \partial \bar{\chi}}{\partial x} + \frac{\bar{V} \partial \bar{\chi}}{\partial y} + \frac{\bar{W} \partial \bar{\chi}}{\partial z}}_{II} + \underbrace{\frac{\partial (\bar{u}' \chi')}{\partial x} + \frac{\partial (\bar{v}' \chi')}{\partial y} + \frac{\partial (\bar{w}' \chi')}{\partial z}}_{III} = \underbrace{\frac{D \partial^2 \bar{\chi}}{\partial x^2} + \frac{D \partial^2 \bar{\chi}}{\partial y^2} + \frac{D \partial^2 \bar{\chi}}{\partial z^2}}_{IV} + \underbrace{S}_V \quad (2.2)$$

Term *I* represents the mean storage of ammonia (i.e., concentration change in time).

Term *II* describes the advection of ammonia by the mean wind.

Term *III* represents the divergence of the ammonia flux.

Term *IV* represents the mean molecular diffusion of ammonia.

Term *V* is the mean net body source (or sink) term for additional ammonia processes.

where U , V and W (and u , v and w) are the wind speed (fluctuations) in the x , y and z direction respectively.

To investigate the relative importance of each term in Equation 2.2 in the atmospheric surface layer, we scale all variables (a) with a typical scale (A) to make them dimensionless (\hat{a}) similar to Van Pul (1992). We replace all variables according to $\hat{a} = a / A$ and Equation 2.2 is then rewritten as:

$$\begin{aligned}
& \underbrace{\frac{C}{t} \left[\frac{\partial \bar{\chi}}{\partial t} \right]}_I + \underbrace{\frac{V_x \Delta c_x}{L} \left[\frac{\bar{U} \partial \bar{\chi}}{\partial \hat{x}} \right]}_{IIA} + \underbrace{\frac{V_y \Delta c_y}{B} \left[\frac{\bar{V} \partial \bar{\chi}}{\partial \hat{y}} \right]}_{IIB} + \underbrace{\frac{V_z \Delta c_z}{Z} \left[\frac{\bar{W} \partial \bar{\chi}}{\partial \hat{z}} \right]}_{IIC} + \\
& \underbrace{\frac{v_x c}{L} \left[\frac{\partial (\hat{u}' \bar{\chi}')}{\partial \hat{x}} \right]}_{IIIA} + \underbrace{\frac{v_y c}{B} \left[\frac{\partial (\hat{v}' \bar{\chi}')}{\partial \hat{y}} \right]}_{IIIB} + \underbrace{\frac{v_z c}{Z} \left[\frac{\partial (\hat{w}' \bar{\chi}')}{\partial \hat{z}} \right]}_{IIIC} = \quad (2.3) \\
& \underbrace{\frac{DC}{L^2} \left[\frac{D \partial^2 \bar{\chi}}{\partial \hat{x}^2} \right]}_{IVA} + \underbrace{\frac{DC}{B^2} \left[\frac{D \partial^2 \bar{\chi}}{\partial \hat{y}^2} \right]}_{IVB} + \underbrace{\frac{DC}{Z^2} \left[\frac{D \partial^2 \bar{\chi}}{\partial \hat{z}^2} \right]}_{IVC} + \underbrace{S \left[\hat{S}_x \right]}_V
\end{aligned}$$

Note that all factors between brackets are dimensionless and have values in the order of unity. The factors before the brackets are the scale variables needed to make the variables dimensionless. In Table 2.1 characteristic scales for all scale variables in Equation 2.3 are defined to investigate the relative importance of the individual terms.

Table 2.1. Characteristic scales and typical values used in scaling of the conservation equation of ammonia in the atmospheric surface layer.

Characteristic scale	Symbol	Typical value
concentration scale for NH ₃	C	10 $\mu\text{g m}^{-3}$
concentration fluctuation scale for NH ₃	c	1 $\mu\text{g m}^{-3}$
concentration difference scales for NH ₃ in the x , y and z direction	$\Delta c_x, \Delta c_y, \Delta c_z$	1, 1, 10 $\mu\text{g m}^{-3}$
time scale of the mean concentration changes of NH ₃	t	1000 s
mean wind speed scales of U , V and W	V_x, V_y, V_z	5, 5, 0.001 m s^{-1}
wind fluctuation scales in x , y and z direction	v_x, v_y, v_z	2, 2, 1 m s^{-1}
length scales in the x , y and z direction	L, B, Z	200, 200, 4 m
molecular diffusion coefficients for NH ₃	D	1.8 $10^{-5} \text{m}^2 \text{s}^{-1}$

If we fill in the typical values for the scales in the atmospheric surface layer from Table 2.1 in Equation 2.3, we are able to make an estimation of the importance of each term:

I local time derivative:

$$\frac{C}{t} = \frac{10}{1000} = 0.01$$

IIA and IIB horizontal transport/advection by mean flow:

$$\frac{V_x \Delta c_x}{L} = \frac{5 \cdot 1}{200} = 0.025$$

IIC vertical transport by mean flow:

$$\frac{V_z \Delta c_z}{Z} = \frac{0.001 \cdot 10}{4} = 0.0025$$

IIIA and *IIIB* horizontal transport/advection by turbulence:

$$\frac{v_x c}{L} = \frac{2 \cdot 1}{200} = 0.01$$

IIIC vertical transport by turbulence:

$$\frac{v_z c}{Z} = \frac{1 \cdot 1}{4} = 0.25$$

IVA and *IVB* horizontal molecular diffusion:

$$\frac{DC}{L^2} = \frac{10 \cdot 1.8 \times 10^{-5}}{200^2} = 4.5 \times 10^{-9}$$

IVC vertical molecular diffusion:

$$\frac{DC}{Z^2} = \frac{10 \cdot 1.8 \times 10^{-5}}{4^2} = 1.125 \times 10^{-5}$$

As we do not have any information about the source/sink term (*V*), this term is ignored. However, it seems unlikely that sources and sinks are very strong within the surface layer and therefore this term is assumed to be relatively small compared to the other terms. We have to keep in mind that ignoring term *V* does not mean that there is no source or sink at the surface itself. We only ignore sources or sinks within the surface layer (e.g., chemical conversions within the surface layer).

We see that the largest term in Equation 2.3 is the vertical transport by turbulence term (*IIIC*) and that all other terms are at least one order of magnitude smaller. Therefore, as an

approximation, Equation 2.2 is reduced to $\frac{\partial(\overline{w' \chi'})}{\partial z} \approx 0$, which means that the flux is

approximately constant with height. In other words, a flux that is measured at height *z* within the surface layer is approximately equal to the flux at the surface. The second largest term in Equation 2.3 is the advection by mean flow term (*IIA* and *IIB*). To be sure that the derived fluxes are not influenced by advection, we will use footprint analysis (Section 2.1.3) to exclude situations in which advection might have influenced the flux measurements.

2.1.2 Gradient or flux-profile technique

At present, there exists no operational fast response sensor for ammonia. As a consequence, the ammonia fluctuations, χ' , cannot be measured and the ammonia flux, $F_\chi = -\overline{w'\chi'}$, can not be derived with the eddy covariance technique.

Therefore, we have to rely on another method to derive the ammonia flux: the aerodynamic gradient or flux-profile technique. This method relates the flux of ammonia to the vertical gradient of ammonia analogous to the description of molecular diffusion by Fick's law:

$$F_\chi = -K_\chi \frac{\partial \chi}{\partial z} \quad (2.4)$$

where $\partial\chi/\partial z$ is the concentration gradient, i.e., the concentration difference, $\partial\chi$, over a height difference, ∂z , and K_χ is the eddy diffusion coefficient for ammonia. K_χ is a property of the flow and depends largely on turbulence in that flow.

Characteristic turbulence scales for the different scalar quantities are defined: a turbulence velocity scale, the so-called friction velocity:

$$u_* = \left(\overline{u'w'^2} + \overline{v'w'^2} \right)^{1/4} \quad (2.5a)$$

and a turbulence scale for the quantity of interest such as temperature, absolute humidity or in our case ammonia (χ), generally written as:

$$\chi_* = -\frac{\overline{w'\chi'}}{u_*} \quad (2.5b)$$

By combining Equation 2.5a and 2.5b, the ammonia flux is written as:

$$F_\chi = -u_* \chi_* \quad (2.6)$$

In the surface layer, i.e., the lowest 10% of the boundary layer, Monin-Obukhov similarity theory has allowed us to describe the vertical profiles of several variables (e.g. wind speed, temperature, ammonia) as a function of the height above the displacement height ($z-d$) and a key parameter describing atmospheric stability, the Obukhov length L (Monin and Obukhov, 1954; Businger et al., 1971).

The gradient in Equation 2.4 is made dimensionless through the flux-profile relationships (or stability/similarity functions) for ammonia (Φ_χ). Ammonia is assumed to be transported in the same way as heat (H) and moisture (Q), e.g., $\Phi_\chi(\zeta) \approx \Phi_H(\zeta) \approx \Phi_Q(\zeta)$ (Dyer and Hicks, 1970; Businger et al., 1971; Webb, 1980):

$$\frac{k z}{u_*} \frac{\partial \overline{\chi}}{\partial z} = \Phi_m(\zeta) \quad (2.7a)$$

$$\frac{k z}{\chi_*} \frac{\partial \bar{\chi}}{\partial z} = \Phi_\chi(\zeta) \approx \Phi_H(\zeta) \quad (2.7b)$$

where k is the von Karman constant ($=0.4$). The dimensionless flux-profile relationships Φ_m and Φ_χ are functions of the atmospheric stability parameter $\zeta = (z-d)/L$, where L is the Obukhov length scale defined by:

$$L = -\frac{T}{kg} \frac{u_*^3}{w' \chi'} \quad (2.8)$$

Using Equation 2.4, 2.6 and 2.7, the eddy diffusion coefficient for ammonia is written as:

$$K_\chi = \frac{k u_* z}{\Phi_\chi(\zeta)} \quad (2.9)$$

If we integrate Equation 2.7a over a height difference, $(z-d) - z_{0,m}$, we obtain:

$$\int_{z_{0,m}}^{z-d} \bar{I} \frac{\partial \bar{U}}{\partial z} = \int_{z_{0,m}}^{z-d} \frac{u_* \Phi_m(\zeta)}{k z} \partial z \equiv \bar{U}(z-d) - \bar{U}(z_{0,m}) = \frac{u_*}{k} \left(\ln \left(\frac{z-d}{z_{0,m}} \right) - \Psi_m \left(\frac{z-d}{L} \right) + \Psi_m \left(\frac{z_{0,m}}{L} \right) \right) \quad (2.10a)$$

In a similar way Equation 2.7b is integrated over a height difference, $(z-d) - z_{0,\chi}$:

$$\bar{\chi}(z-d) - \bar{\chi}(z_{0,\chi}) = \frac{\chi_*}{k} \left[\ln \left(\frac{z-d}{z_{0,\chi}} \right) - \Psi_\chi \left(\frac{z-d}{L} \right) + \Psi_\chi \left(\frac{z_{0,\chi}}{L} \right) \right] \quad (2.10b)$$

where $\Psi_m(\zeta)$ and $\Psi_\chi(\zeta)$ are the integrated stability functions, $z_{0,m}$ and $z_{0,\chi}$ are the characteristic length scales of the underlying surface for wind speed, U , and ammonia, χ , respectively. They indicate the height above a virtual zero level at which the centre is located where the quantity is transmitted, absorbed or released. The $z_{0,m}$, called the roughness length, is dependent on the roughness of the surface. The $z_{0,\chi}$ is mainly dependent on the vertical distribution of the sources or sinks of ammonia at the surface. Here, we use the integrated stability functions of Paulson (1970) and Dyer (1974) for unstable conditions (i.e., $L < 0$):

$$\Psi_m(\zeta) = 2 \ln \left[\frac{1+x}{2} \right] + \ln \left[\frac{1+x^2}{2} \right] - 2 \tan^{-1}(x) + \frac{\pi}{2} \quad (2.11a)$$

$$\Psi_\chi(\zeta) \approx \Psi_H(\zeta) = 2 \ln \left[\frac{1+x^2}{2} \right] \quad (2.11b)$$

where $x = (1 - 16\zeta)^{1/4}$ with $\zeta = (z-d)/L$

and the integrated stability functions of Beljaars and Holtslag (1991) for stable conditions (i.e., $L > 0$):

$$\Psi_m(\zeta) = -a\zeta - b\left(\zeta - \frac{c}{d}\right)\exp(-d\zeta) - \frac{bc}{d} \quad (2.12a)$$

$$\Psi_\chi(\zeta) \approx \Psi_H(\zeta) = -\left(1 + \frac{2}{3}a\zeta\right)^{3/2} - b\left(\zeta - \frac{c}{d}\right)\exp(-d\zeta) - \frac{bc}{d} + 1 \quad (2.12b)$$

where $a = 1$, $b = 0.667$, $c = 5$, $d = 0.35$ and $\zeta = (z - d)/L$.

Substituting Equation 2.10a and 2.10b into Equation 2.6 provides an expression for the ammonia flux as:

$$F_\chi = -\frac{k\left[\bar{U}(z-d) - \bar{U}(z_{0,m})\right]}{\left[\ln\left(\frac{z-d}{z_{0,m}}\right) - \Psi_m\left(\frac{z-d}{L}\right) + \Psi_m\left(\frac{z_{0,m}}{L}\right)\right]} \frac{k\left[\bar{\chi}(z-d) - \bar{\chi}(z_{0,\chi})\right]}{\left[\ln\left(\frac{z-d}{z_{0,\chi}}\right) - \Psi_\chi\left(\frac{z-d}{L}\right) + \Psi_\chi\left(\frac{z_{0,\chi}}{L}\right)\right]} \quad (2.13)$$

For the flux measurements presented in this thesis, u_* was obtained directly from eddy covariance measurements using a sonic anemometer rather than from wind speed profiles. The vertical concentration gradients are measured by the GRADIENT Ammonia – High Accuracy – Monitor (GRAHAM, described elsewhere). Consequently, the ammonia flux was calculated from the following expression:

$$F_\chi = -ku_* \frac{\left[\bar{\chi}(z-d) - \bar{\chi}(z_{0,\chi})\right]}{\left[\ln\left(\frac{z-d}{z_{0,\chi}}\right) - \Psi_\chi\left(\frac{z-d}{L}\right) + \Psi_\chi\left(\frac{z_{0,\chi}}{L}\right)\right]} \quad (2.14)$$

NH₃ concentrations were measured at several heights. Therefore, the quotient in Eq. 2.14 is calculated from linear regression through the concentration differences (numerator) and the stability corrected heights (denominator).

2.1.3 Footprint analysis

The validity of the above flux measurement method relies on the principle of the flux being constant with height. However, this is only true for the surface layer in equilibrium with a homogeneous surface. Changes in the roughness of a surface or in the vegetative properties will lead to changes in the vertical flux. To ensure that the flux measurement is representative for a particular surface, the measurement height must be within the new internal boundary layer which forms after a surface inhomogeneity (which might be a local source or sink). The height of this layer (δ) depends on the upwind distance (x_L) or “fetch” to the inhomogeneity. Empirical evidence suggests that the ratio of x_L to δ is approximately

100 (Monteith and Unsworth, 1990). However, the extent of an upwind area affecting a flux measurement changes with wind direction, wind speed, surface roughness and stability. Therefore, a more thorough analysis has been developed to assess the contribution to the flux measurement from a particular upwind source area. This is called “footprint” analysis. The footprint is defined as “the upwind area most likely to affect a downwind flux measurement at a given height z ” (Schuepp et al., 1990). Schuepp et al. (1990) provided analytical solutions of the diffusion equation based on Gash (1986) and defined the Cumulative Normalized contribution to the Flux measurement (CNF) at height $(z-d)$ and upwind distance x_L . To account for non-neutrality Schuepp et al. (1990) also proposed an approximate adjustment by multiplying by the momentum stability correction function (Φ_m) resulting in:

$$CNF(x_L) = \exp\left(-\frac{U(z-d)}{k u_* x_L} \Phi_m\left(\frac{z-d}{L}\right)\right) \quad (2.15)$$

where U is defined as the average wind speed between the surface and the measurement height $(z-d)$, assuming a logarithmic wind speed profile for neutral stability:

$$U = \frac{\int_{z_0}^{z-d} u(z-d) dz}{\int_{z_0}^{z-d} dz} = \frac{u_* \left[\ln\left(\frac{z-d}{z_0}\right) - I + \left(\frac{z_0}{z-d}\right) \right]}{k \left(I - \left(\frac{z_0}{z-d}\right) \right)} \quad (2.16)$$

If this equation is substituted in Equation 2.15, the following equation for the CNF is obtained:

$$CNF(x_L) = \exp\left(-\frac{\left[\ln\left(\frac{z-d}{z_0}\right) - I + \left(\frac{z_0}{z-d}\right) \right] (z-d)}{k^2 \left(I - \left(\frac{z_0}{z-d}\right) \right) x_L} \cdot \Phi_m\left(\frac{z-d}{L}\right)\right) \quad (2.17)$$

Figure 2.1 shows the CNF as a function of x_L for different measuring heights $(z-d)$ and different stabilities (very stable ($L = 5$), very unstable ($L = -5$) and neutral ($L = \pm \infty$)). The CNF was calculated with Eq. 2.17 assuming a roughness length, z_0 , of 0.01m. The figure shows that as long as the measurements are carried out close to the ground, even in very stable situations, the measurements are mainly influenced by their direct environment. However, especially in very stable situations, a high measuring height leads to low CNF values. Or in other words, especially in very stable situations a high measuring height is influenced by a large surrounding.

Monteith and Unsworth (1990) proposed a typical ratio between measurement height and fetch of 1:100 for short vegetation. In neutral conditions, the fetch for a measurement height of 4 meters should be more than 400 meters. This means that the footprint of the measurement should be homogeneous for at least 400 meters in the upwind direction of the

measurement. This corresponds to a CNF threshold of 0.75 (the black dashed line in Figure 2.1). We will also apply this CNF threshold to stable and unstable conditions, which means that the footprint should be homogeneous for at least 2100 m in the upwind direction in very stable conditions ($L = 5$ m) and for at least 225 m in very unstable condition ($L = -5$ m).

At the measurement site, a small farm is located to the west-northwest at about 400 m (See Figure 2.2). To meet the criterion for a minimum *CNF* of 0.75 in this wind direction, only measurements during unstable and neutral conditions can be used. Similar limitations are found in the easterly wind directions due to buildings at the northwestern part of Wageningen.

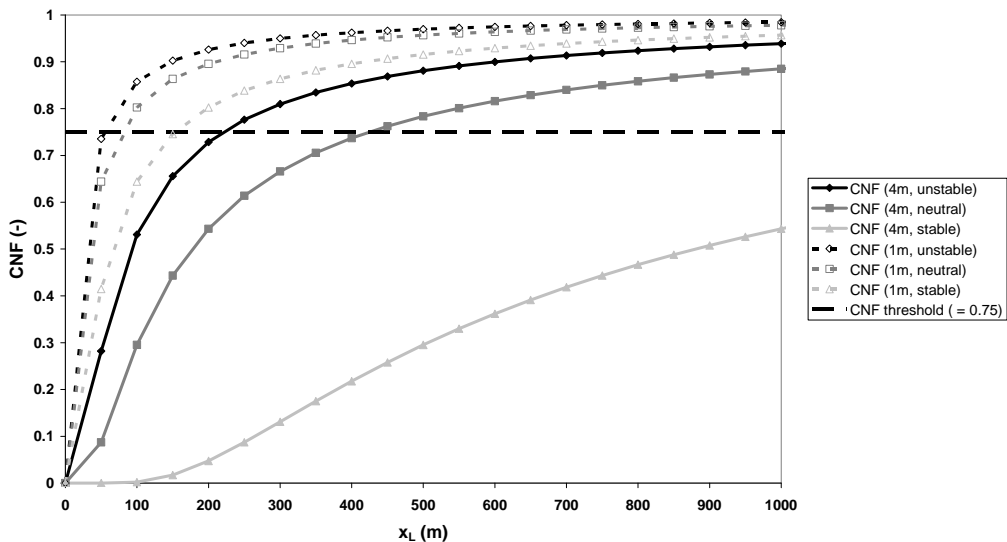


Figure 2.1. CNF for various values of measurement height and stability as a function of x_L .

2.2 Site description and instrumentation

2.2.1 Site description

All reported NH_3 flux measurements are calculated from concentration profiles measured at a meteorological observatory, where continuous measurements of air and soil temperature, air humidity, radiation, wind direction and wind speed are available. The measurement site is located west of Wageningen in the Netherlands ($51^\circ 58' 18'' \text{ N}$; $5^\circ 38' 30'' \text{ E}$) on a heavy clay soil with a temperate humid perennial ryegrass pasture (*Lolium perenne*) (Van Hove, 1989). Figure 2.2 shows an aerial overview of the meteorological observatory and its surroundings. The black dot represents the location of the ammonia gradient set-up. There is no application of manure at the site and grass is cut on average 3-4 times a year. The average elevation of the measurement site is 6.80m above mean sea level. (Webpage of observatory: <http://www.maq.wur.nl>).



Figure 2.2. Aerial view of the micrometeorological site 'Haarweg' in Wageningen, the Netherlands. (courtesy: Google Earth)

2.2.2 Instrumentation

2.2.2.1 Meteorological instrumentation

The micrometeorological weather station at the Haarweg in Wageningen is a Special Agro-Meteorological Station. Appendix B gives an overview of the standard (micro)meteorological variables that are measured at this observatory. Besides these standard meteorological variables, measurements of horizontal wind speed (U), wind direction, friction velocity (u_*) and sensible heat flux (H) are provided by a CSAT3 3-D sonic anemometer (Campbell Scientific) mounted at 3.5 m.

Meteorological variables are logged with a frequency of once every 10 minutes. The micrometeorological flux measurements, however, are averaged over a 30-minute time period. Since these data are required for the eventual ammonia flux calculations, all measurements are converted to 30-minute averages.

2.2.2.2 Ammonia instrumentation

The NH_3 -concentration profiles (needed in Equation 2.14) are measured using the new GRAdient Ammonia – High Accuracy – Monitor (GRAHAM), a more advanced version of the AMANDA (a continuous rotating wet denuder analyzer; Wyers et al., 1993; Wichink

Kruit et al., 2007). The GRAHAM (shown in Figure 2.3) is an instrument that measures the NH_3 -concentration at 1 m, 2.5 m (2.0 m from 30 May 2005 onwards) and 4 m height with a frequency of once every 10 minutes. The GRAHAM is well suited for micrometeorological measurements because of its low detection limit, high precision and accuracy and high time resolution. The measurement principle of the GRAHAM denuder is basically the same as the existing AMANDA denuder as described by Wyers et al. (1993, 1998).

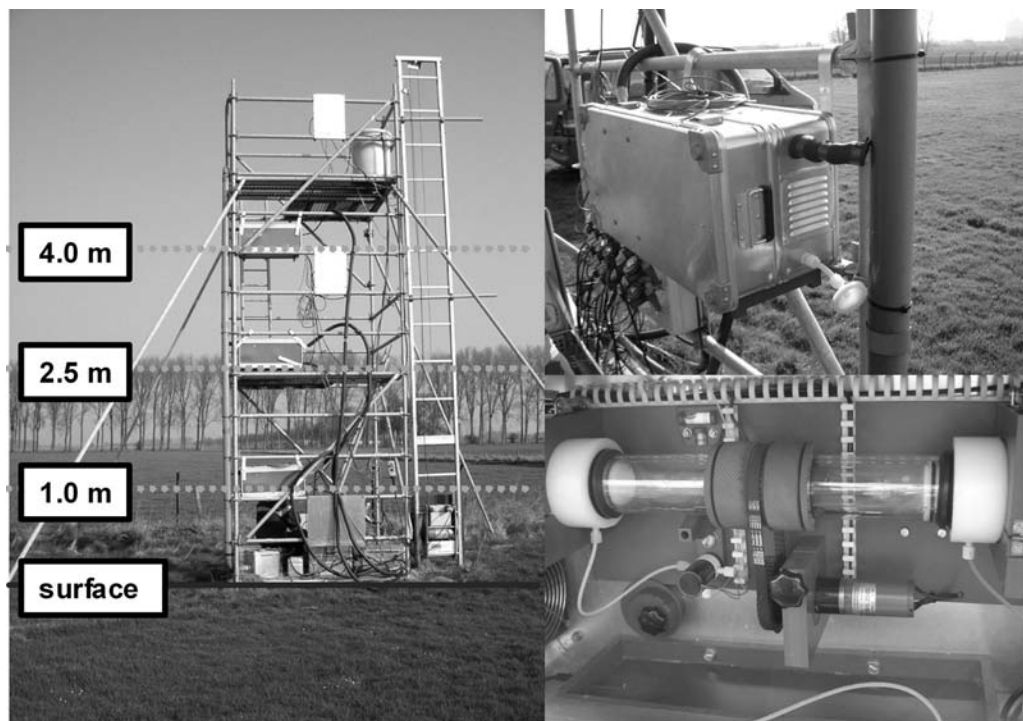


Figure 2.3. GRAHAM measurement system (left), close up of one of the three denuder boxes (upper right) and close up of an annular denuder inside the box (lower right).

The GRAHAM uses horizontally-positioned rotating annular denuder tubes. A denuder tube consists of two concentric glass tubes of 30 cm in length and up to 50 mm in diameter. The walls of the annular denuder are coated with a slightly acidic absorption fluid (3.6 mM NaHSO_4). Air is pumped through the space between the two glass tubes at a rate of approximately 23 l min^{-1} . Any gaseous ammonia present in the air diffuses to the walls of the denuder, where it is captured by the absorption fluid. Ammonium aerosol (NH_4^+) passes through the denuder almost unimpeded (only 1-2% absorption) as the diffusion rate of aerosols is much smaller than that of the gaseous NH_3 .

The absorption fluid is continuously pumped through the denuders at a rate of 1 ml min^{-1} and flows in opposite direction to the air flow. The absorption fluid containing the dissolved NH_3 (as NH_4^+) is now analyzed by a common detector. Once in the detector, the absorption fluid containing NH_4^+ is mixed with a solution of 0.5 M NaOH , so that molecular ammonia is formed again. This molecular ammonia diffuses through a semi-permeable PTFE membrane and is dissolved in de-ionized water present on the other side of the membrane. At pH lower than 7, it is mostly present in the form of NH_4^+ and the NH_4^+ concentration in this water flow is determined by conductivity. The analyzer is calibrated

with aqueous standards of typically 0, 50 and 500 $\mu\text{g l}^{-1}$ NH_4^+ . The detection limit of NH_3 in air is approximately $0.02 \mu\text{g m}^{-3}$.

Several modifications have been carried out with respect to the AMANDA to improve the accuracy as well as the precision of the instrument. In the old AMANDA system flow rates were determined manually at service visits. In the current GRAHAM system continuous in-line airflow measurements are implemented, which is an obvious improvement with respect to the precision and accuracy. The flow rates are determined by measurements of temperature and the pressure drop over a restriction. To minimize systematic errors the restrictions have been brought together in an aluminum body.

Second, two 3-channel syringe pumps (type Mechatronics) replaced the multi channel peristaltic pump allowing a well-defined sample flow from the denuders. With two coupled 10 ml syringes per denuder and a 1 ml min^{-1} sample flow a cycle time of ten minutes is obtained. During a cycle the three samples are sequentially led through the detector allowing two minutes of flushing in between.

Third, the conical structure in the inlet is now also applied on the outlet of the wet rotating denuder. This optimized aerosol conducting system prevents ammonium particles (aerosols) from impaction on wetted surfaces and from being a potential source of interfering ammonium.

Average concentration values for all three denuders were determined during a 10 minute cycle. The 3 denuders were sampled sequentially with a stabilizing time of 2 minutes and an averaging time of 1 minute. After this cycle of 9 minutes, the detector is flushed for 1 minute and a new cycle starts. The tube length for transporting the solution to the detector is equal for all three heights to ensure that the concentrations measured in the analyzer refer to identical air sampling periods.

A vertical PVC pipe of diameter 0.1 m was attached to the three denuders to be able to mutually compare the three denuders in the field. A high volume of ambient air is blown through the pipe (about $200 \text{ m}^3 \text{ hr}^{-1}$) to ensure that the concentration at all three denuder heights is the same during comparison. Each denuder samples the same air from this PVC pipe and should consequently measure the same concentration. Observed differences between the individual denuders can be considered as systematic differences. With this vertical PVC pipe, we are able to correct for the systematic differences between the denuders under field conditions. The procedure for systematic error correction is described in the following section.

2.3 Error analysis

2.3.1 Systematic and random errors in the concentration

2.3.1.1 Laboratory comparison

Data on the performance of the earlier version of this instrument (AMANDA) were reported by Wyers et al. (1993, 1998) and Mennen et al. (1996). Wyers et al. (1993) positioned three instruments in the field at the same height and averaged the measurements every 30 min. They corrected the obtained concentrations for systematic differences, and reported the between-instrument standard deviation based upon 22 simultaneous triplicates to be 2.6% relative over the entire time spanned by the concentrations. The correction method and the concentrations themselves were not reported. The current GRAHAM system was tested in a similar way. The three instruments were placed on a lab bench. They

were simultaneously fed with the same sample, which was alternately clean air and $8 \mu\text{g m}^{-3}$ NH_3 , each period lasting about 5 hours on 14 and 15 November 2002 (see Figure 2.4). Readouts were obtained every 10 minutes. The used triplicates are indicated with black dots in Figure 2.4 (1 = high concentration (about $8 \mu\text{g m}^{-3}$); 0 = transition period (between 0 and $8 \mu\text{g m}^{-3}$); -1 = low concentration (about $0 \mu\text{g m}^{-3}$)).

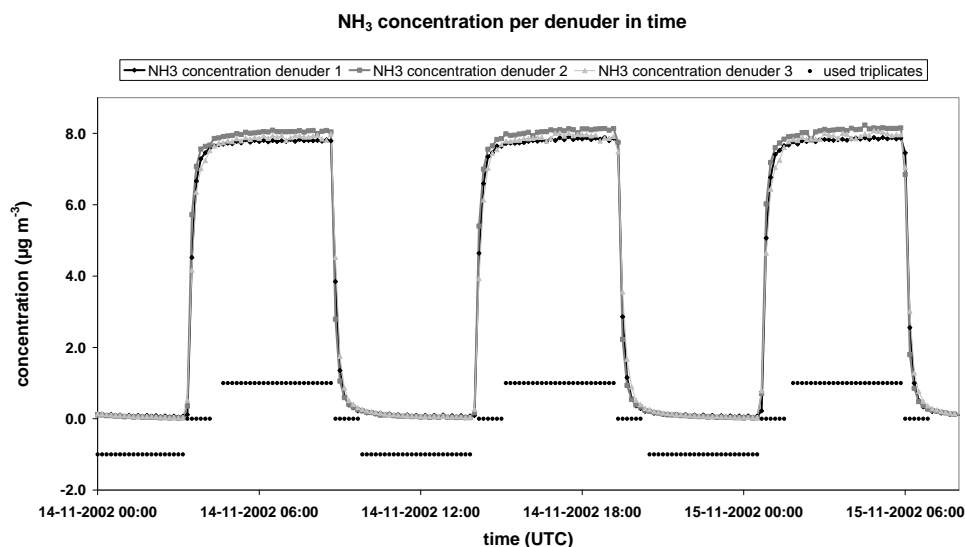


Figure 2.4. Laboratory concentration measurements for precision determination. The black diamonds represent the different situations during the concentration comparison test (1 = high concentration (about $8 \mu\text{g m}^{-3}$); 0 = transition period (between 0 and $8 \mu\text{g m}^{-3}$); -1 = low concentration (about $0 \mu\text{g m}^{-3}$)).

If we assume that the average of the three concentrations in Figure 2.4 is the 'real' concentration, we can distinguish two types of systematic errors. The first type is the difference in delay times between the three individual denuders. Figure 2.5 shows the absolute difference between the individual denuders and the real concentration, versus the change of the real concentration in time. An increase in the real concentration will lead to a larger increase for denuder 2 than the average increase in concentration, i.e., denuder 2 is faster than the average. Denuder 3 gives a smaller increase than the average and can therefore be considered as 'too slow'.

absolute error in the concentration per denuder vs. average NH₃ concentration

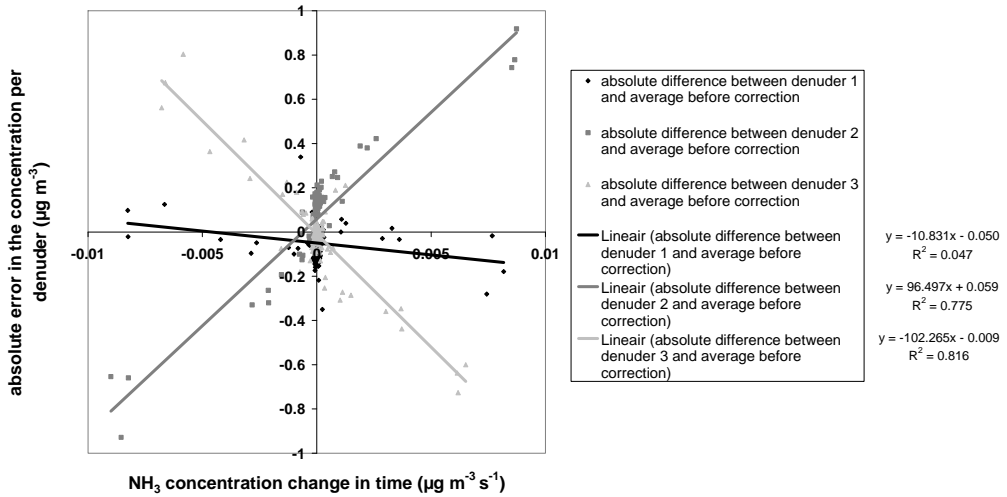


Figure 2.5. The absolute difference between each denuder and the average concentration versus the concentration change in time ($\mu\text{g m}^{-3} \text{ s}^{-1}$)

The second type of systematic error that was corrected is the regression of the measured concentrations per denuder (slope and offset) relative to the average concentration (Figure 2.6).

NH₃ concentration per denuder vs. average NH₃ concentration

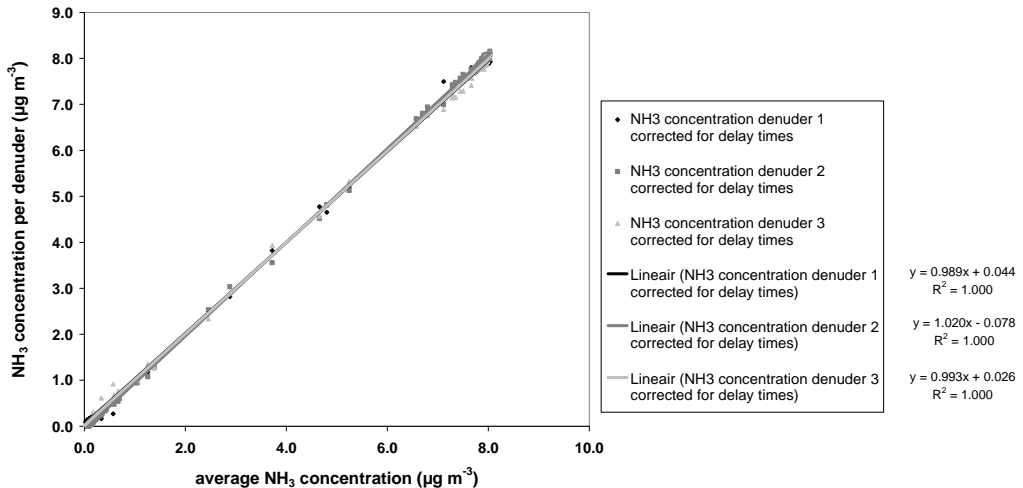


Figure 2.6. Linear regression through the measured concentrations per denuder relative to the average concentration after correction for the different delay times.

The figures below show the absolute difference between the measured concentrations per denuder and the average concentration before (Figure 2.7) and after (Figure 2.8) systematic error correction. The systematic error correction for the differences in delay times reduces

the large peaks just after concentration change, while the systematic error correction for the linear regression reduces the differences between the individual denuders and the average. The resulting absolute difference (between the measured concentration per denuder and the average concentration) after systematic error correction represents the random error (Figure 2.8). The figure shows that the random error is a little bit higher (and variable) in periods of quickly changing concentrations (transition periods), while it is rather low (and constant) in stationary conditions (around 0 and $8 \mu\text{g m}^{-3}$).

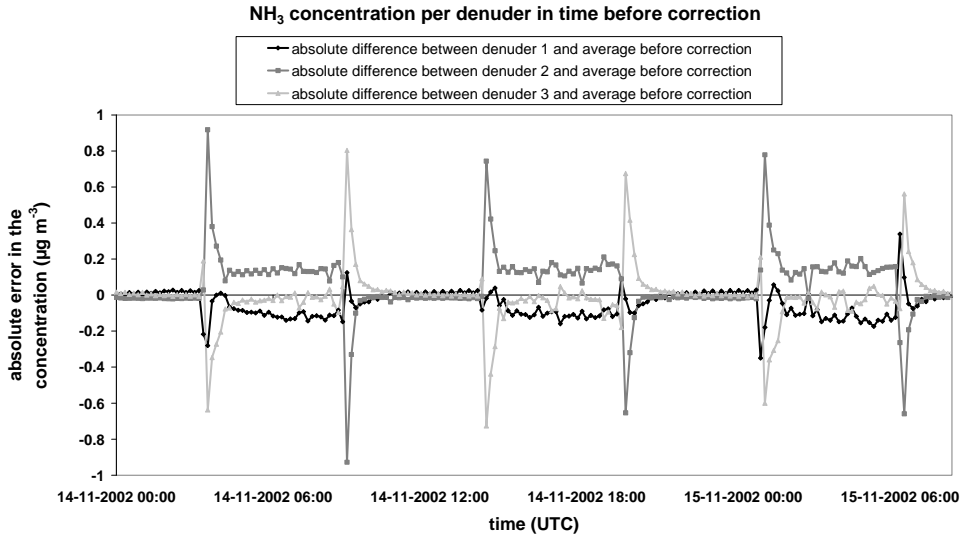


Figure 2.7. Absolute difference between the measured concentrations per denuder and the average concentration before systematic error correction.

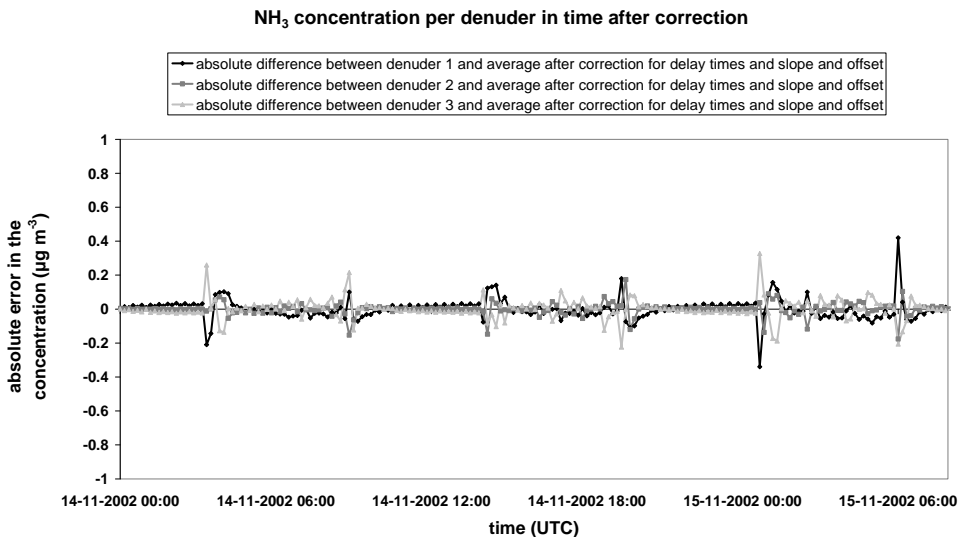


Figure 2.8. Absolute difference between the measured concentrations per denuder and the average concentration after systematic error correction.

In order to be able to compare the performance of the GRAHAM with the performance of AMANDA, every three subsequent results of each denuder were averaged in order to obtain one triplicate every 30 min. The results of the error analysis in the concentration measurements corrected for systematic errors are shown in Table 2.2. The table shows the random errors for two different averaging times, e.g., 10 and 30 minutes. We also distinguished three different regimes, e.g., $0 \mu\text{g m}^{-3}$, between 0 and $8 \mu\text{g m}^{-3}$, and $8 \mu\text{g m}^{-3}$.

Table 2.2. Random errors in the concentration measurements corrected for systematic errors for two averaging times (10 and 30 minutes) and three periods ($0 \mu\text{g m}^{-3}$, $0-8 \mu\text{g m}^{-3}$ and $8 \mu\text{g m}^{-3}$)

	10-minute average		30-minute average	
	absolute random error	Relative random error	Absolute random error	Relative random error
average deviation of the mean concentration at $0 \mu\text{g m}^{-3}$	$0.012 \mu\text{g m}^{-3}$	-	$0.012 \mu\text{g m}^{-3}$	-
number of triplicates	48	48	16	16
average deviation of the mean concentration between 0 and $8 \mu\text{g m}^{-3}$	$0.080 \mu\text{g m}^{-3}$	2%	$0.058 \mu\text{g m}^{-3}$	1.45%
number of triplicates	36	36	12	12
average deviation of the mean concentration at $8 \mu\text{g m}^{-3}$	$0.027 \mu\text{g m}^{-3}$	0.34%	$0.018 \mu\text{g m}^{-3}$	0.23%
number of triplicates	75	75	24	24

The random error in the 10-minute average data in this laboratory test is $0.027 \mu\text{g m}^{-3}$ at $8 \mu\text{g m}^{-3}$, which corresponds to a relative random error of about 0.34%. The random error is even smaller at $0 \mu\text{g m}^{-3}$ ($0.012 \mu\text{g m}^{-3}$), but much higher in the transition periods, $0.080 \mu\text{g m}^{-3}$. The relative random error in the transition periods (assuming an average concentration of $4 \mu\text{g m}^{-3}$) is about 2% and can mainly be ascribed to the differences in delay times between the individual denuders. The random error in the 30-minute average data is $0.018 \mu\text{g m}^{-3}$ at $8 \mu\text{g m}^{-3}$, which corresponds to a relative error of about 0.23%. The random error at $0 \mu\text{g m}^{-3}$ is $0.012 \mu\text{g m}^{-3}$ again and the random error in the transition period is $0.058 \mu\text{g m}^{-3}$ (or about 1.45%).

2.3.1.2 Field comparison

During a field comparison 'campaign' of 10 days in June 2004, a precision test was done with the attached PVC pipe (described in Section 3.2.2). Concentrations roughly varied between 4 and $50 \mu\text{g m}^{-3}$ during this period and all three denuders showed a similar pattern. To estimate random errors in the concentration measurements, data are corrected for systematic errors following the procedure described before. We only considered concentration measurements between 0 and $20 \mu\text{g m}^{-3}$ to have a homogeneous distribution of concentrations and to be sure that possible saturation effects were excluded. Before the systematic error correction, the average difference between each denuder and the average of the three denuders was $0.05 \mu\text{g m}^{-3}$ at an average concentration of $8.77 \mu\text{g m}^{-3}$ (about 0.6 %). After systematic error correction, this difference is reduced to zero by definition. Figure 2.9 shows the absolute difference between the individual denuders and the average of the three denuders versus the concentration change in time. This yields a systematic error correction due to differences in delay times between the individual denuders. Figure 2.10 shows the regression of the measured concentrations per denuder (corrected for differences

in delay times) relative to the average concentration, i.e., the second systematic error correction.

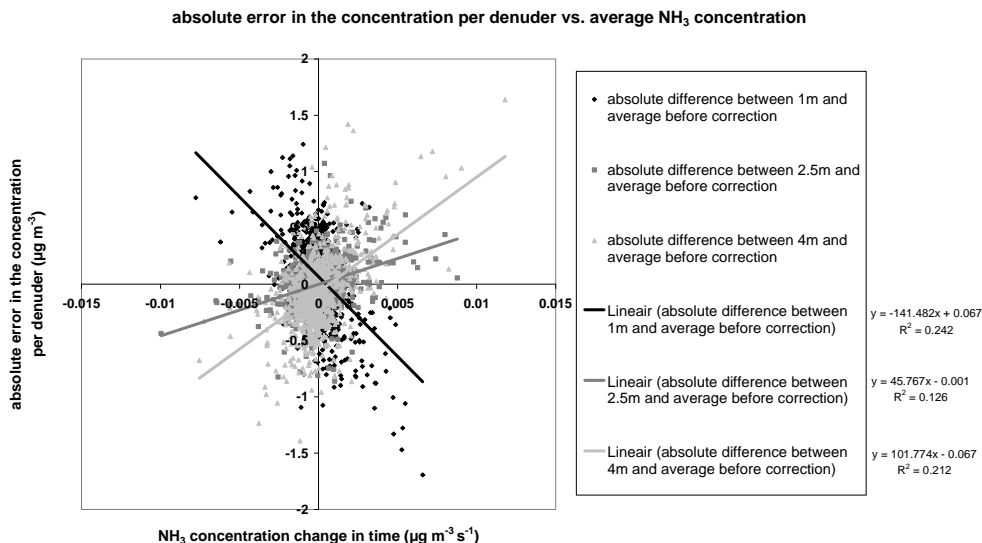


Figure 2.9. Absolute difference between each denuder and the average concentration versus the concentration change in time (µg m⁻³ s⁻¹)

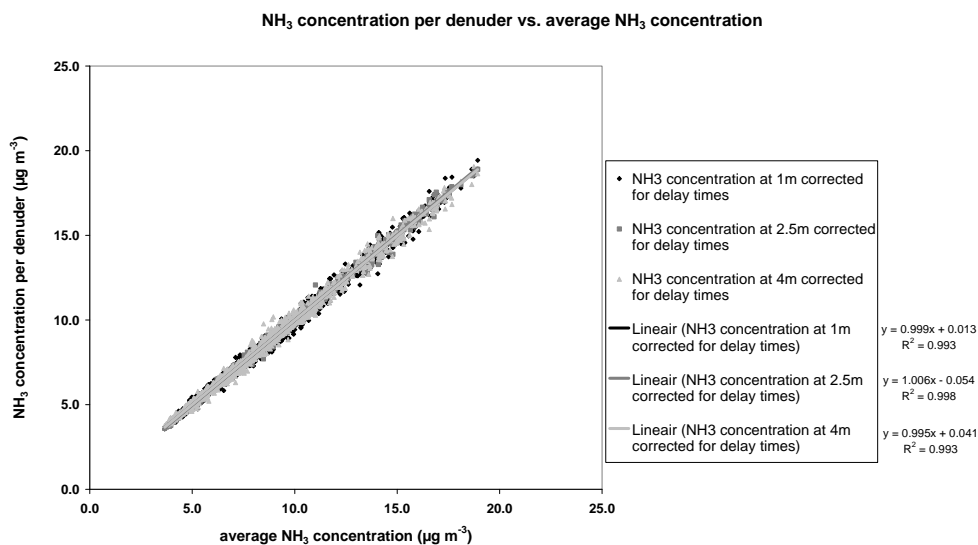


Figure 2.10. Linear regression through the measured concentrations per denuder relative to the average concentration after correction for the different delay times.

To compare the results from this field comparison with the results in the laboratory, the absolute between-instrument differences are calculated. Figure 2.11 shows the random error as a function of the average NH₃ concentration. The random error in the measurements increases with an increasing NH₃ concentration. The average slope of the random error is about 1.9%. This means that the random error for an average concentration of about 8 µg m⁻³ is 0.16 µg m⁻³.

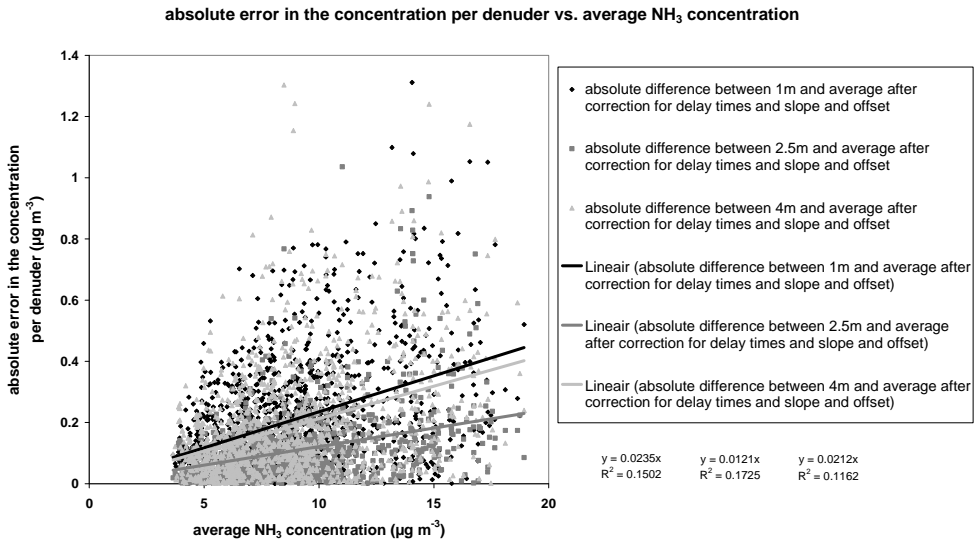


Figure 2.11. Random error as a function of the average NH₃ concentration for the three measurement heights.

We conclude that the precision of the instrument in the field (1.9%) is comparable to the precision of the instrument in the laboratory in transition periods (about 2%). Although the average concentration changes in the field are generally smaller than the concentration changes (8 µg m⁻³) in the transition periods in the laboratory, weather influences such as substantial temperature and humidity changes are likely to affect the precision. In the presented results, a random error of 1.9% (based on the field comparison) is applied on the concentration measurements. The systematic error of 0.6% in the concentration measurements was corrected for and is not propagated in the flux calculation. In Section 2.3.3, we will investigate how large the effect of this systematic error correction would be on our flux calculation in the hypothetical case that we would not correct our concentration measurements for the known systematic errors.

2.3.2 Random error in the flux

For quantities that are a function of several parameters, a combined random error is calculated. The relative random error in our flux calculation, $F_\chi = -u_*\chi_*$ (Equation 2.6), is given as:

$$\frac{\delta F_\chi}{|F_\chi|} = \sqrt{\left(\frac{\delta u_*}{|u_*|}\right)^2 + \left(\frac{\delta \chi_*}{|\chi_*|}\right)^2} \quad (2.18)$$

The random error in the friction velocity (δu_*) is calculated with the ECpack software developed by Wageningen University (Van Dijk et al., 2004; freely available at <http://www.maq.wur.nl>). Figure 2.12 shows that the relative random error in the friction velocity is about 4-5%. The relative random error in u_* is rather constant during the day,

whereas relative random errors higher than 5% mainly occur during very stable and calm nighttime situations.

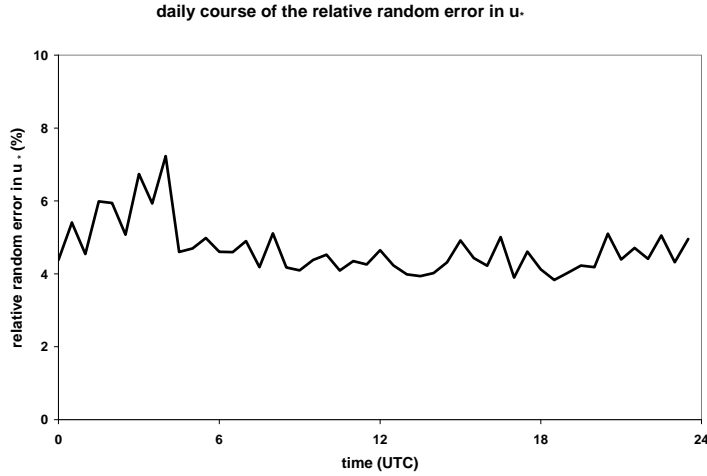


Figure 2.12. Diurnal cycle of relative random error in u_* for the entire data set.

The random error in χ_* is more difficult to determine. We start with rewriting Equation 2.10b into:

$$\chi_* = k \frac{\chi(z_2) - \chi(z_1)}{\ln\left(\frac{z_2}{z_1}\right) - \Psi_\chi\left(\frac{z_2}{L}\right) + \Psi_\chi\left(\frac{z_1}{L}\right)} \quad (2.19)$$

The relative random error in χ_* is described as:

$$\frac{\delta\chi_*}{|\chi_*|} = \sqrt{\left(\frac{\delta[\chi(z_2) - \chi(z_1)]}{|\chi(z_2) - \chi(z_1)|}\right)^2 + \left(\frac{\delta f(z, \Psi)}{|f(z, \Psi)|}\right)^2} \quad (2.20)$$

where:

- $\delta[\chi(z_2) - \chi(z_1)] = \sqrt{(\delta\chi(z_2))^2 + (\delta\chi(z_1))^2}$ represents the random error in the concentration difference (the numerator in Equation 2.19, shown as error bars in Figure 2.13 together with the diurnal cycle of the concentration difference).
- $\delta f(z, \Psi)$ represents the random error in the stability corrected height (the denominator in Equation 2.19; abbreviated as $f(z, \Psi)$ in Equation 2.20).

Assuming that the errors in the heights of the measurements (z_1 and z_2) are negligible, the error in the stability corrected height in Equation 2.20 is only determined by errors in the stability corrections. However, the errors in the stability corrections are difficult to determine as they are complex functions of the Obukhov length. In this study we assume a relative random error in the stability correction functions of 5% (Nieuwstadt, 1978; Holtslag and Van Ulden, 1983). Figure 2.14 shows the diurnal cycle of the relative random error in χ_* (Equation 2.20).

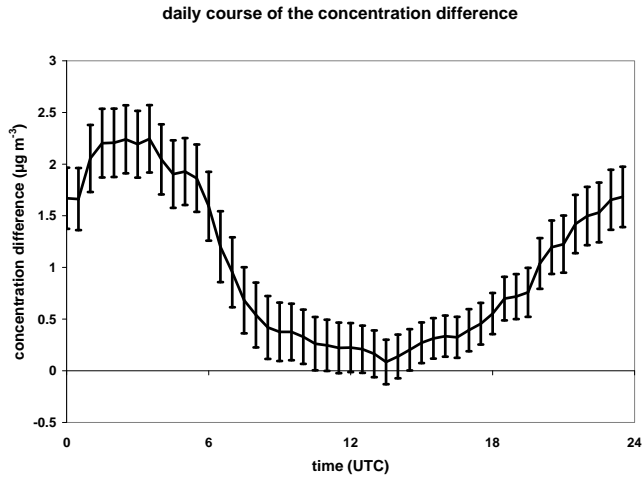


Figure 2.13. Diurnal cycle of the concentration difference for the entire data set.

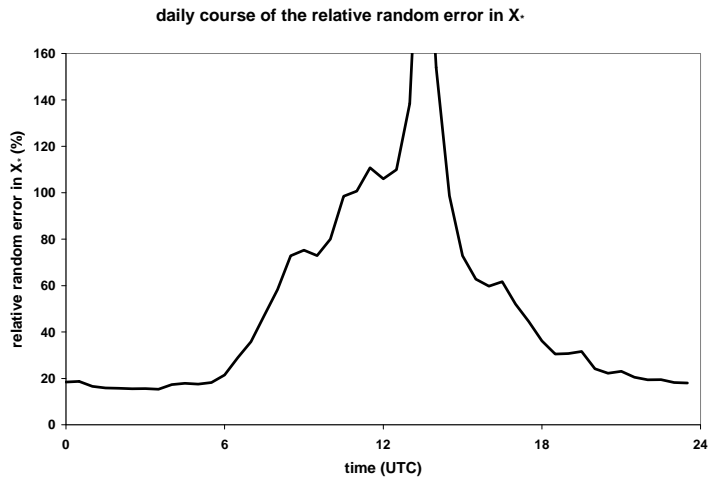


Figure 2.14. Average diurnal cycle of the relative random error in χ_* for the entire data set. (peak value is 255%)

The random error in the flux estimate is calculated by multiplying the relative error in the flux by the absolute value of the flux, according to:

$$\delta F_\chi = |F_\chi| \cdot \sqrt{\left(\frac{\delta u_*}{|u_*|}\right)^2 + \left(\frac{\delta \chi_*}{|\chi_*|}\right)^2} \quad (2.21)$$

Figure 2.15 shows the random error in the flux estimate for the entire data set. The random error in the flux estimate is largest (about $0.06 \mu\text{g m}^{-2} \text{s}^{-1}$) in the early morning and during daytime mainly due to small concentration differences, whereas it is relatively small (about $0.01 \mu\text{g m}^{-2} \text{s}^{-1}$) during night time, when concentration differences are relatively large. On average the random error in the flux estimate is about $0.03 \mu\text{g m}^{-2} \text{s}^{-1}$.

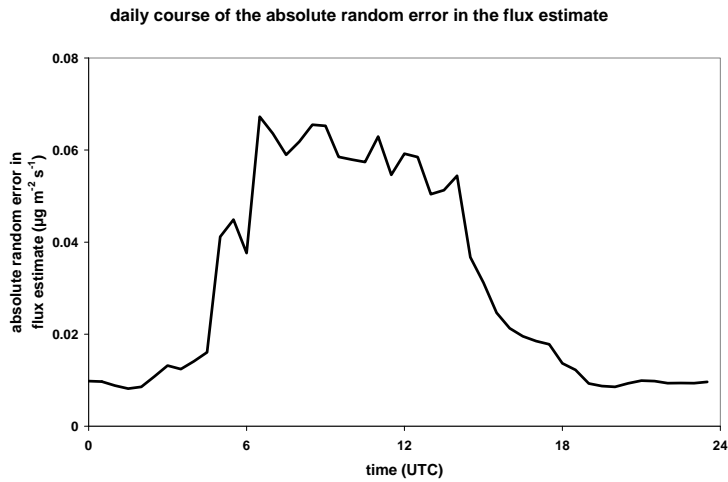


Figure 2.15. The diurnal cycle of random error in the flux estimate for the entire data set.

If we look at the relative random error in the flux measurement (Figure 2.16), i.e., the (absolute) random error in the flux divided by the flux, we see that the relative random error is rather small (in the order of about 20%) during night time, when the gradient is well defined, and becomes very large (over 100%) during daytime, when the concentration differences and consequently the fluxes approach zero.

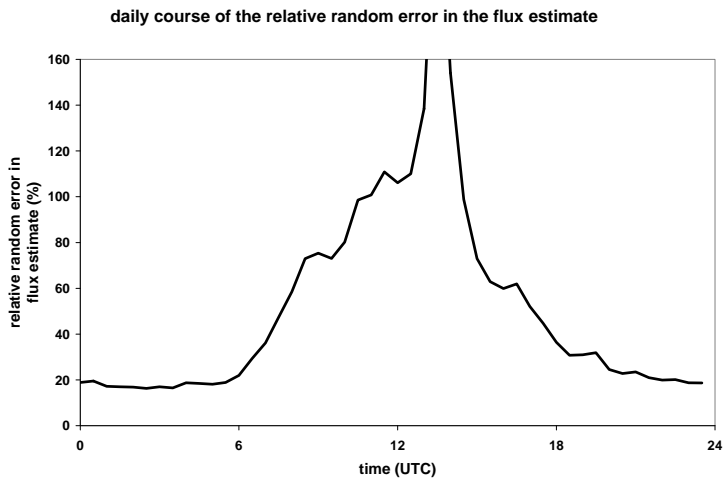


Figure 2.16. The diurnal cycle of relative random error in the flux estimate for the entire data set. (peak value is 255%)

Table 2.3 gives an overview of the observed ranges for the diurnal cycle of the different parameters in the flux calculation. It also shows the ranges for the absolute and relative random error in the different parameters in the flux calculation.

Table 2.3. Overview of ranges for the absolute and relative random error in the flux calculation parameters.

parameter	mean	Absolute random error	Relative random error
χ	10.0 $\mu\text{g m}^{-3}$ (7.3 - 12.7)	0.19 $\mu\text{g m}^{-3}$ (0.14 - 0.24)	1.9%
u_s	0.18 m s^{-1} (0.13 - 0.25)	0.008 m s^{-1} (0.006 - 0.011)	5% (4 - 7)
$\chi(z_2) - \chi(z_1)$	1.01 $\mu\text{g m}^{-3}$ (0.08 - 2.24)	0.27 $\mu\text{g m}^{-3}$ (0.20 - 0.34)	52% (15 - 255)
χ_s	0.41 $\mu\text{g m}^{-3}$ (0.08 - 1.53)	0.16 $\mu\text{g m}^{-3}$ (0.05 - 0.39)	52% (15 - 255)
F_χ	-0.07 $\mu\text{g m}^{-2} \text{s}^{-1}$ (-0.02 - -0.24)	0.03 $\mu\text{g m}^{-2} \text{s}^{-1}$ (0.01 - 0.07)	52% (15 - 255)

The relative random error in the flux calculation varies between 15% during night time and 255% during daytime. The average relative random error in the flux estimate is about 52% (the median value is 31%). Note that these large relative random errors are mainly caused by the (relatively small) random errors in the concentration measurements in combination with the small concentration differences.

2.3.3 Effects of systematic errors in concentration measurements on the flux

To investigate the effect of the systematic errors in the concentration measurements on the flux estimates (e.g., to see if systematic errors can lead to a different sign for the flux), we compared the flux measurements without correction for systematic errors with the flux measurements with corrections for systematic errors (like described in the previous Sections). Figure 2.17 shows the diurnal cycle of the calculated systematic error in the flux estimate (flux without systematic error correction - flux with systematic error correction). The systematic error in the flux estimate is about 2 times smaller than the random error in the flux estimate (solid line compared to the dashed line). The systematic error in the flux estimate is largest in the morning (i.e., about $0.03 \mu\text{g m}^{-2} \text{s}^{-1}$) mainly due to large concentration changes in time, while it is relatively small during night time (i.e., about $0.005 \mu\text{g m}^{-2} \text{s}^{-1}$), when there might be large concentration changes, but there is minimum exchange.

Figure 2.18 shows the average diurnal cycle of the 'best' flux estimate (black solid line) with the random errors (error bars). The flux calculated without the systematic error corrections (black dashed line) does not significantly affect the pattern of the diurnal cycle of the flux and only seem to influence the size of the mean (annual) flux.

Several short comparison tests (of about 1 day) in 2004 indicate that the systematic error corrections obtained from the 10-day comparison period are representative for the whole period, although the slopes and the offsets might sometimes change sign (opposite systematic error correction) or are larger (larger systematic error correction) than the slopes and offsets used in this study. Since these short comparison tests only concern few measurements and a very limited concentration range, they are considered to be highly uncertain and inadequate for intermediate data correction. Therefore, we decided to use the systematic error corrections from the 10-day comparison period to correct all our data.

daily course of the absolute systematic and random error in the flux estimate

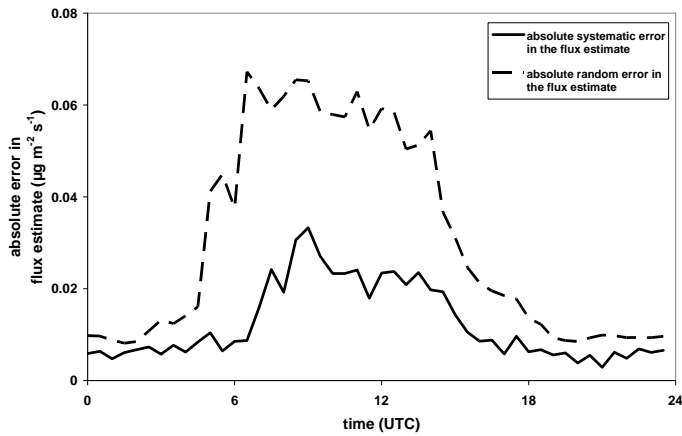


Figure 2.17. The diurnal cycle of the absolute systematic (solid line) and random (dashed line) error in the flux estimate for the entire data set.

Effect of systematic error correction on flux estimate

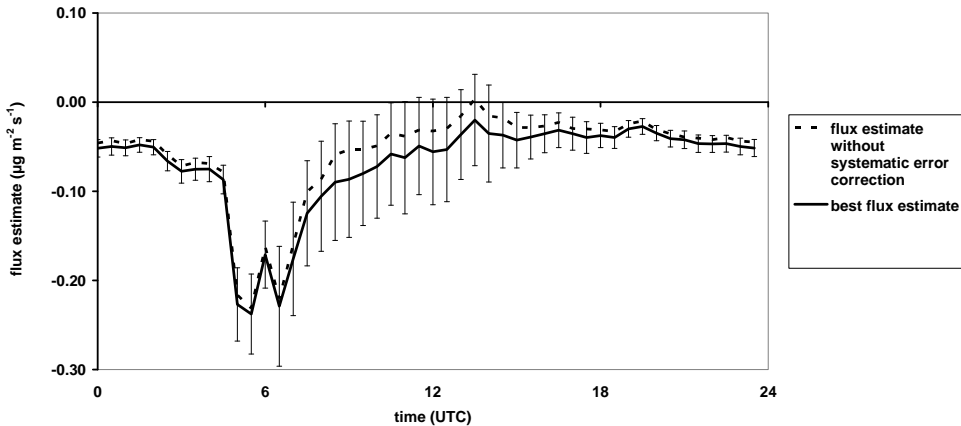


Figure 2.18. Average diurnal cycle of the flux estimate (solid black line) and the random errors (error bars) for the entire data set. The dashed line represents the flux estimate without systematic error corrections to show the sensitivity for systematic error corrections in the flux estimate.

2.3.4 Summary uncertainties and concluding remarks

2.3.4.1 Errors in the concentration

In a *laboratory comparison* test, a random error of $0.027 \mu\text{g m}^{-3}$ at $8 \mu\text{g m}^{-3}$ is found in the 10-minute average data after systematic error correction, which corresponds to a random error of about 0.34%. The random error at a provided concentration of $0 \mu\text{g m}^{-3}$ is even smaller, i.e., $0.012 \mu\text{g m}^{-3}$. On the other hand, the random error in the transition periods (between 0 and $8 \mu\text{g m}^{-3}$ and vice versa) is much larger, i.e., $0.080 \mu\text{g m}^{-3}$, which

corresponds to a **random error** of about 2% (assuming an average concentration of $4 \mu\text{g m}^{-3}$).

In a *field comparison* test of 10 consecutive days, we obtained that the average **systematic error** in the concentration between the three denuders is about 0.6% at an average concentration of $8.7 \mu\text{g m}^{-3}$. After systematic error correction, this systematic difference reduced to zero by definition. The random error in the concentration that remained after this systematic error correction was $0.17 \mu\text{g m}^{-3}$ at an average concentration of $8.7 \mu\text{g m}^{-3}$, which corresponds to a **random error** of 1.9%.

So, the random error in a concentration measurement under field conditions (1.9%) is much larger than the random error in a concentration measurement under stable laboratory conditions (0.34%). This difference is mainly caused by a continuously changing concentration in the field, while in the laboratory the concentration was kept constant until it stabilized. The random error in the transition periods in the laboratory comparison of 2%, however, compares well with the random error found in the field comparison.

2.3.4.2 Errors in the flux

After correcting our concentration measurements for systematic errors, the flux can be calculated as described in Section 2.1.2. However, the random errors in the concentration measurements (1.9%) propagate in the flux calculations and result in an average **random error** in the calculated fluxes of 52% (median value is 31%). Large differences are observed between the random error in the flux calculation during nighttime (15%) and during daytime (255%). The large random errors during daytime are mainly caused by small concentration differences in combination with the random errors in the concentrations at the different heights. During nighttime, these concentration differences are considerably larger and consequently, the random error in the flux calculation is smaller.

If we would not correct our concentration measurements for systematic errors, an average **systematic error** in the flux calculation of 18% would be made. However, because we assume that the systematic error corrections are justified and correct, there is no systematic error present in our final flux calculation. However, if the systematic error correction in the concentration measurements is applied unjustified, the error that we make in the flux calculation as a consequence of the systematic error correction is relatively small (18%) compared to the random error in the flux calculation (52%) on an hourly basis.

2.4 Overview of NH_3 flux measurements and derived variables

In this section an overview of the available concentration measurements, flux measurements and derived variables is given. For practical reasons, hourly values are derived from the half-hourly measurements in this overview. The total number of hourly measurements (for which two half-hourly measurements were available) in 2004, 2005 and 2006 is 8593, which is about 33% of this three year period. In order to select the reliable ammonia profiles, a selection from these 8593 hours was made based on several quality criteria. The reasons for applying the criteria for data acceptance were discussed in the

previous sections and will only be mentioned briefly here. The percentage of rejected data is given per criteria in parenthesis.

- Concentration larger than detection limit, i.e., $0.02 \mu\text{g m}^{-3}$; here a lower limit of $1 \mu\text{g m}^{-3}$ was used (1.0%)
- Stationary conditions, i.e., concentration change $< 20 \mu\text{g m}^{-3} \text{ hr}^{-1}$ and flux change $< 0.5 \mu\text{g m}^{-2} \text{ s}^{-1} \text{ hr}^{-1}$ (5.2% respectively 2.4%)
- No extremely stable or unstable meteorological conditions, i.e., $|L| > 5 \text{ m}$ (15.0%)
- Profile determined by its direct environment, e.g., no external influence of farms or neighboring fields, i.e., $\text{CNF} > 0.75$ (32.3%)

Some of the criteria have an overlap with one or more of the other criteria, e.g., the criteria for the CNF and L (as L is included in the formulation for CNF). The total reduction of the number of hourly measurements as a consequence of the criteria is 41.9%. This means that from the available 8593 hours, 4994 are used for further analysis.

Table 2.4 gives an overview of the percentage and number of hourly measurements available per month after application of the quality criteria in the years 2004, 2005 and 2006. In the months November, December, January, February and March relatively few data are available due to (yearly) maintenance of the instrument and cold weather conditions during which the instrument is switched off to prevent it from freezing. Exception is the warm winter of 2006/2007. In the summer of 2006 extremely high temperatures (>35 degrees Celsius) and a technical failure have reduced the data coverage.

Table 2.4. Availability of flux measurements per month accounting for quality criteria (between brackets availability without quality criteria). Months with a data coverage of more than 30% are marked in gray.

month	2004		2005		2006	
	%	hours	%	hours	%	hours
January	0%(0%)	0(0)	0%(0%)	1(2)	0%(0%)	0(0)
February	0%(0%)	0(0)	10%(21%)	64(141)	0%(0%)	0(0)
March	0%(0%)	0(0)	24%(36%)	177(265)	0%(0%)	0(0)
April	0%(0%)	0(0)	33%(62%)	239(443)	31%(58%)	223(416)
May	0%(0%)	0(0)	26%(46%)	196(340)	60%(84%)	446(623)
June	14%(27%)	99(191)	0%(0%)	0(0)	19%(37%)	135(268)
July	34%(54%)	250(404)	16%(24%)	119(175)	16%(32%)	117(236)
August	33%(68%)	243(509)	35%(63%)	259(469)	9%(13%)	70(97)
September	14%(20%)	99(141)	33%(63%)	239(451)	19%(51%)	137(364)
October	46%(74%)	342(547)	37%(76%)	275(564)	51%(82%)	383(609)
November	1%(3%)	6(23)	20%(28%)	142(201)	36%(67%)	259(481)
December	0%(0%)	0(0)	0%(0%)	0(0)	64%(85%)	474(633)
yearly average	12%(21%)	1039(1815)	20%(35%)	1711(3051)	26%(43%)	2244(3727)

The figures below give an overview of the measured concentrations and fluxes and the derived deposition velocity and surface resistance in the years 2004, 2005 and 2006. The dashed lines are the different years (2004 = long dashes, diamonds; 2005 = short dashes, squares; 2006 = dash dot, triangles), the solid black line (with the closed circles) represents the average diurnal cycle of all measurement data (or the sum, for the frequency

distributions) and the 'error' bars give the 25-percentile and the 75-percentile values of all measurement data.

The figures give a picture of the measured data in each year and do not have to be representative for a whole year. Based on the measurements only, which are not equally distributed in each year, it is not possible to draw any conclusions from the differences between years. As such the data can only be used to study processes underlying the surface/atmosphere exchange of ammonia. Despite this restriction, we give an indicative overview of the results per year and try to explain the differences.

In Figure 2.19, the average diurnal cycle (average of all measurement data at a single time) of the concentration is shown. The concentration for each year is highest in the early morning. In 2004 and 2005 the average concentrations are a little higher than in 2006, which is possibly caused by the large content of winter data in 2006.

The average concentrations are 7.5, 8.4 en 6.1 $\mu\text{g m}^{-3}$ in 2004, 2005 en 2006. The average concentration for all measurement data is 7.2 $\mu\text{g m}^{-3}$. The yearly spread of the data is shown by the error bars, which represent the 25-percentile and 75-percentile values (in between 50% of the data are present). 50% of the concentration measurements are between 3.3 and 9.1 $\mu\text{g m}^{-3}$.

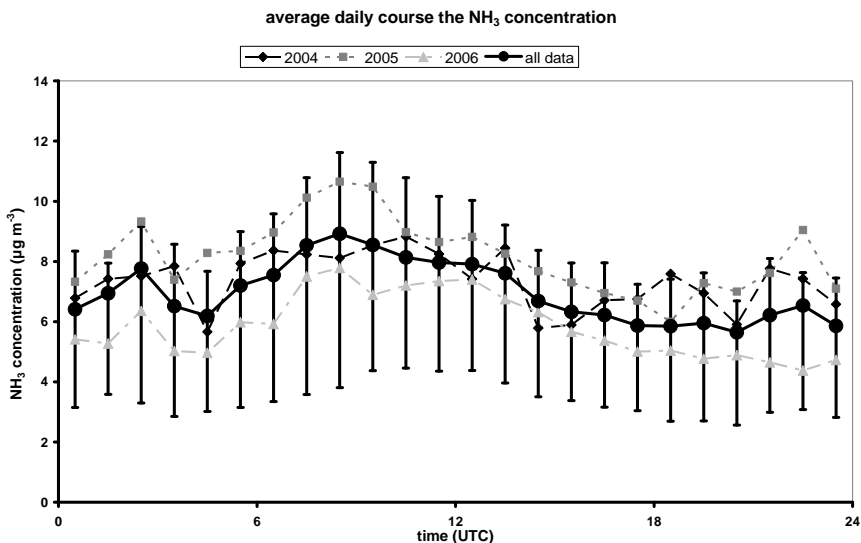


Figure 2.19. Average diurnal cycle of the ammonia concentration.

In Figure 2.20 the frequency distributions of the concentrations in the years 2004, 2005 and 2006 are shown. The figure clearly shows that 2006 has a higher measurement density, especially in the low concentration range. The measurements in 2006 are mainly done in the autumn and winter periods in which the concentrations are relatively low. In contrast, the frequency distributions in the years 2004 and 2005 are mainly caused by measurements in summer and autumn. This is one of the reasons for the difference in average concentration between these years.

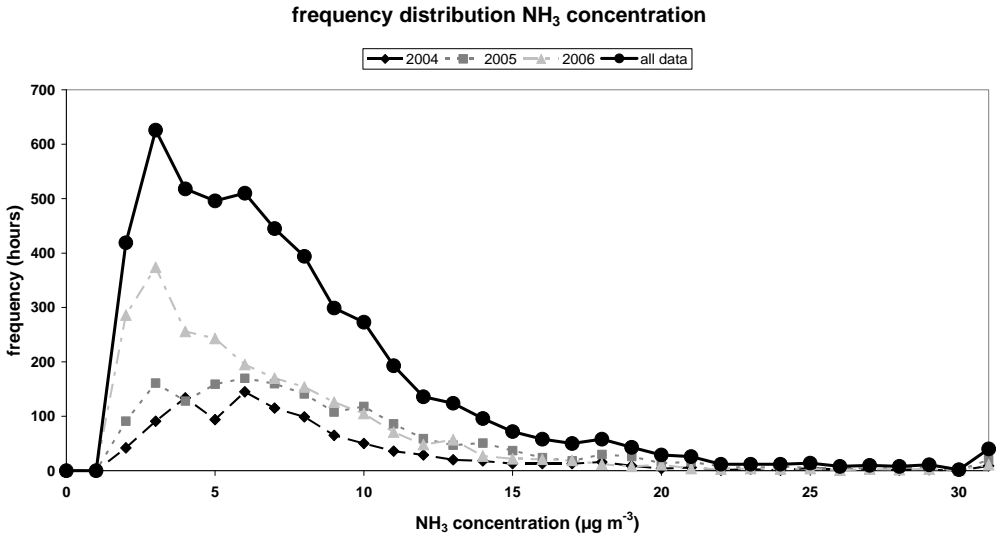


Figure 2.20. Frequency distribution of the concentration.

In Figure 2.21 the average diurnal cycle of the ammonia flux is shown. It is remarkable that the average diurnal cycle of the flux differs so strongly from year to year. Like the average diurnal cycle of the concentration, the diurnal cycle of the flux is strongly influenced by the season and the weather conditions during the measurements. The spread of the data is shown by the error bars again, which represent the 25-percentile and 75-percentile values (in between 50% of the data are present). These error bars show that there are mainly deposition (negative) fluxes. The average fluxes are -0.018 , -0.043 and $-0.083 \mu\text{g m}^{-2} \text{s}^{-1}$ in 2004, 2005 and 2006. The average flux of all data is $-0.056 \mu\text{g m}^{-2} \text{s}^{-1}$. The spread of all data is $0.064 \mu\text{g m}^{-2} \text{s}^{-1}$, which means that 50% of all data are between -0.083 and $-0.019 \mu\text{g m}^{-2} \text{s}^{-1}$. Emission fluxes were particularly present in 2004 as shown in Figure 2.21.

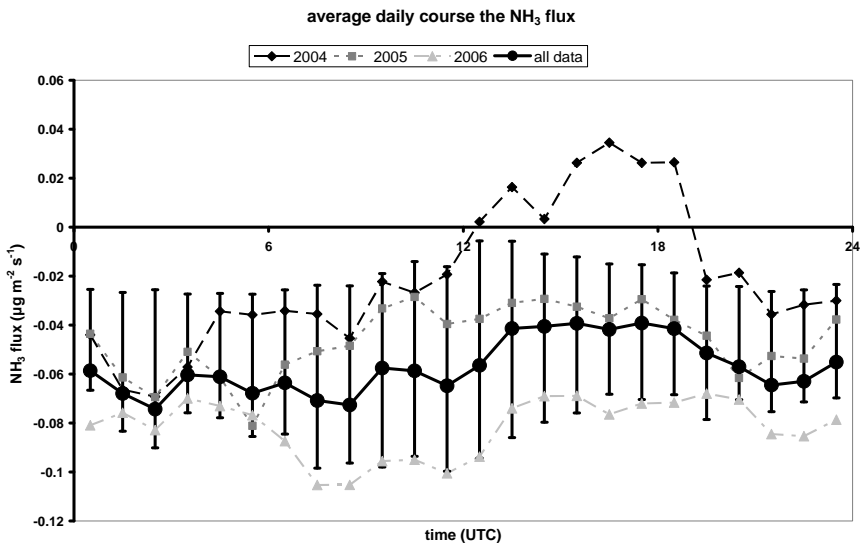


Figure 2.21. Average diurnal cycle of the ammonia flux, positive = emission and negative = deposition.

The frequency distributions of the surface-atmosphere exchange flux of ammonia in Figure 2.22 show that in all years the (negative) deposition fluxes dominate, but also that there is a substantial number of emission cases in each year.

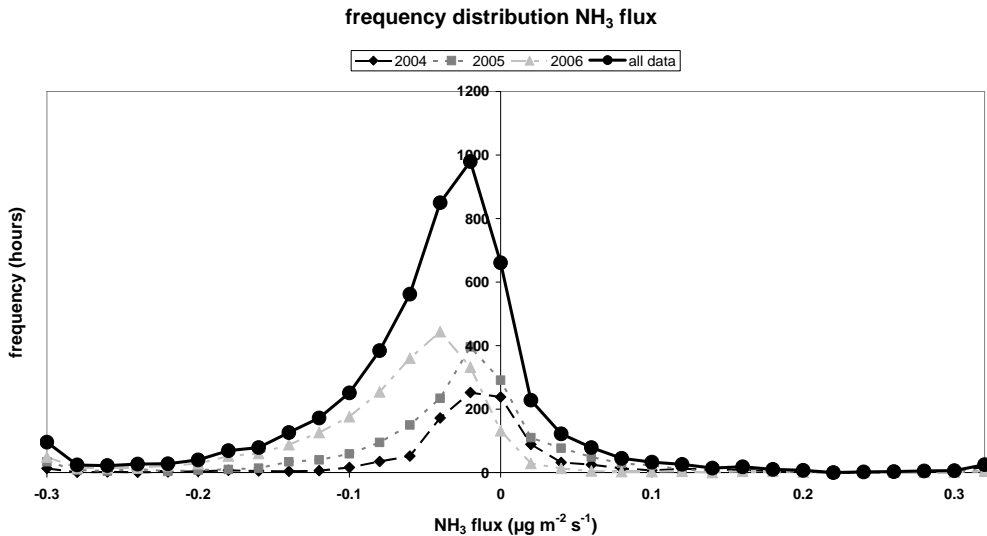


Figure 2.22. Frequency distribution of the ammonia flux, positive = emission and negative = deposition.

In Figure 2.23, we tried to explain the differences between the different years that we observed in Figure 2.19 till Figure 2.22 with the average diurnal cycles of surface temperature (upper panel), global radiation (middle panel) and relative humidity (lower panel). Note that only the hours for which NH₃ flux (and/or concentration) measurements were available, are considered here. Figure 2.23 nicely illustrates why it is difficult to mutually compare the different years.

The upper panel clearly shows that the surface temperature during the NH₃ flux measurements in 2004 was about 2 degrees Celsius higher compared to the other two years. A higher temperature will lead to higher internal plant concentrations (compensation points) and consequently less deposition or even emission.

The middle panel shows that in 2006 the measurements were carried out during less sunny conditions than in 2004 and 2005. Radiation is a driving force in the photosynthetic activity of plants and therefore the stomatal opening. Less radiation will lead to less stomatal opening and likely also to less emission events.

The lower panel shows the average diurnal cycle of the relative humidity in the measurement period. The relative humidity was relatively high during daytime in 2006 compared to 2004 and 2005 (about 5% higher). A high relative humidity will lead to a relatively wet external leaf surface and consequently a preference for deposition of ammonia towards the leaf surface.

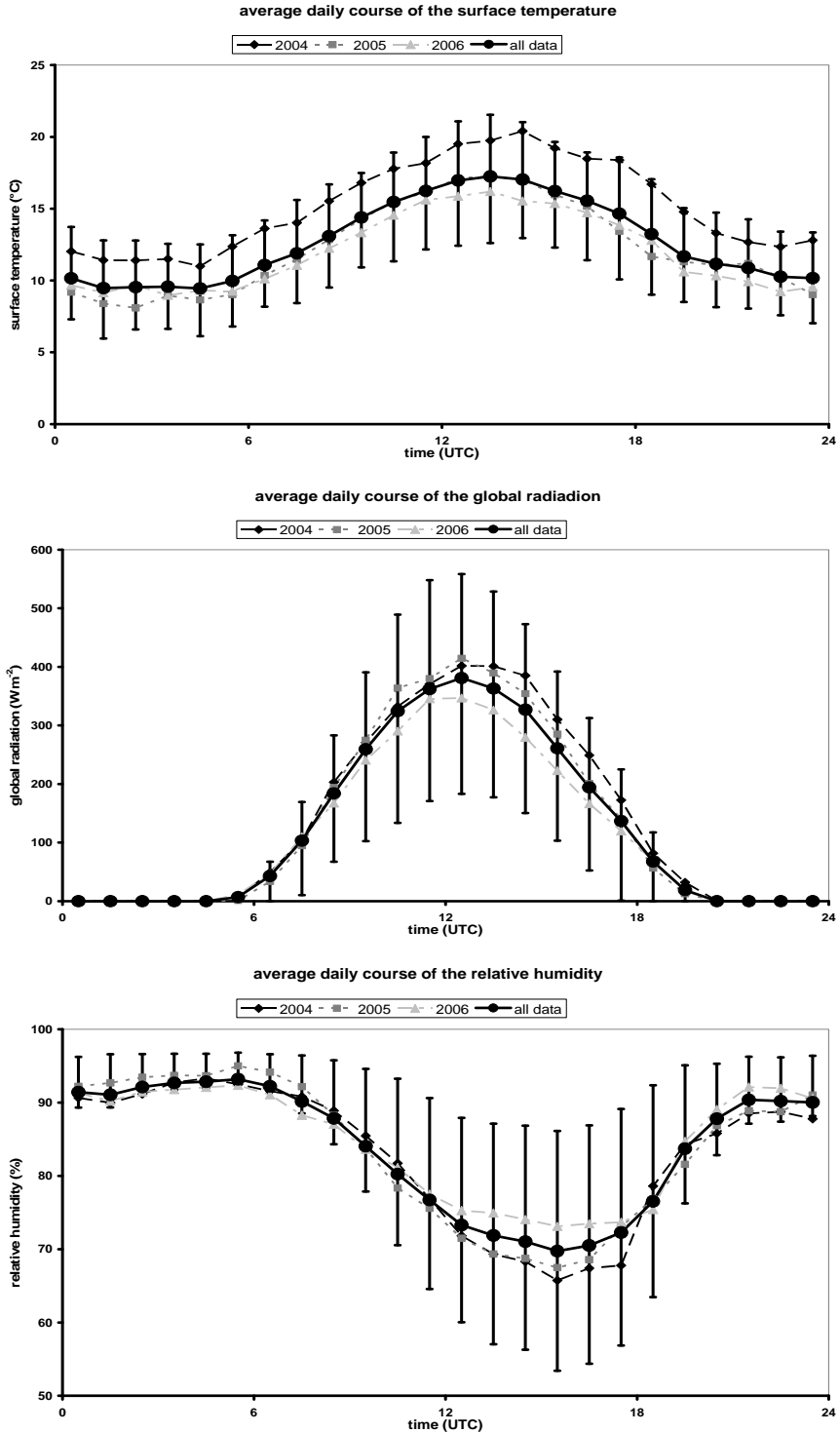


Figure 2.23. Average diurnal cycle of the surface temperature (upper panel), global radiation (middle panel) and relative humidity (lower panel) during the NH_3 flux measurement and flux estimate period.

In the atmospheric transport model OPS that is used at RIVM, the ammonia concentration is calculated as the product of a deposition velocity and the ambient concentration. The deposition velocity is an important quantity to characterize the deposition process. The deposition velocity at a certain height is defined as the quotient of the flux and the concentration at that height:

$$v_{d,1m} = -\frac{F_{\text{NH}_3}}{C_{\text{NH}_3,1m}} \quad (2.22)$$

The relative random error in the deposition velocity is dominated by the relative random error in the flux, because the relative error in the concentration (about 1.9%) is very small compared to the relatively error in the flux (more than 20%) as shown in Figure 2.16.

Figure 2.24 shows the average diurnal cycle of the deposition velocity at 1 meter height. A negative deposition velocity means emission of ammonia. The figure shows that especially in 2004 reduced deposition or even emission occurred between 6 and 18 UTC, while 2006 hardly shows any diurnal cycle and much higher deposition velocities. The negative deposition velocities in 2004 can be explained by the higher temperature in that year. These higher temperatures lead to higher surface concentrations and therefore reduced deposition or emission. The higher (positive) deposition velocities in 2006 can be explained by the lower global radiation and higher relative humidity in that year. Lower global radiation reduces emission from the stomata; higher relative humidity enhances surface wetness, which is favorable for deposition (as ammonia dissolves well in water layers on the leaf surface). On average, the deposition velocity at 1m for 2004, 2005 and 2006 amounts to 0.005, 0.007 and 0.017 m s⁻¹ respectively. For all measurement data the average deposition velocity is about 0.011 m s⁻¹. The spread of the data (shown by the error bars, which represent the 25-percentile and 75-percentile values) is 0.014 m s⁻¹, which means that 50% of the data are within the range between 0.003 and 0.017 m s⁻¹ (deposition). The frequency distributions of the deposition velocity in Figure 2.25 confirm the picture that is outlined above. Note again that the distribution of the measurements over the year is not the same in 2004, 2005 and 2006.

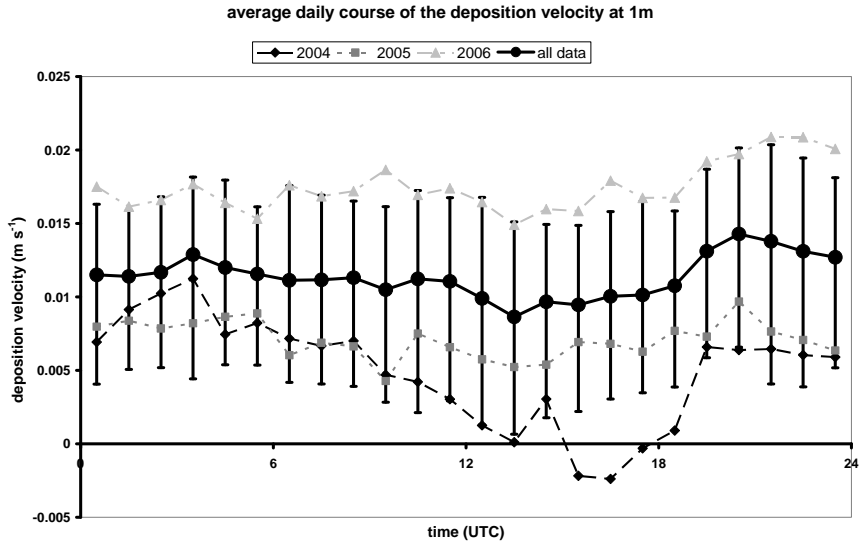


Figure 2.24. Average diurnal cycle of the deposition velocity at 1m height, positive = deposition and negative = emission.

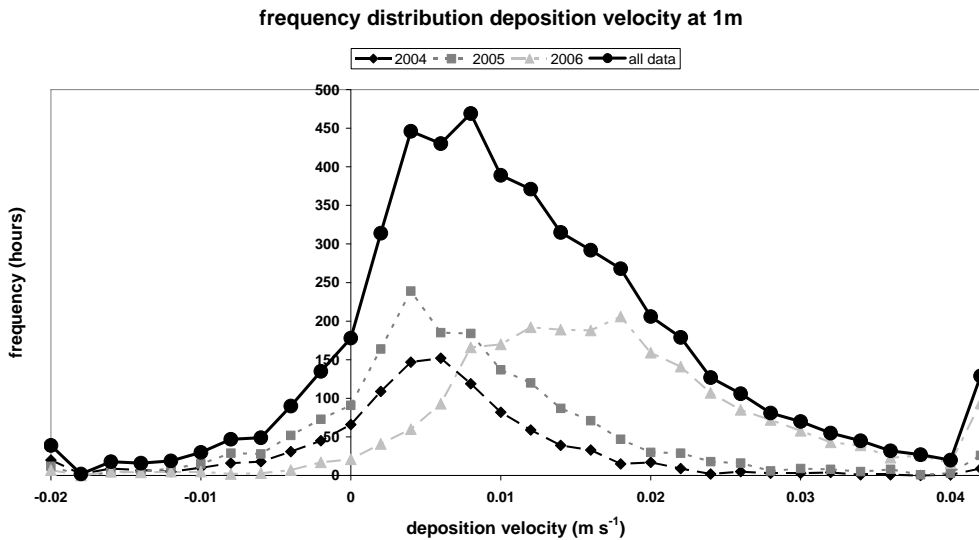


Figure 2.25. Frequency distribution of the deposition velocity at 1m, positive = deposition and negative = emission.

The different deposition pathways, along which ammonia deposits, are represented with resistances. The most simple form of this resistance approach assumes that the concentration at the surface is zero or in other words, the potential difference (concentration in the air minus the concentration at the surface (= 0)) is only determined by the concentration of ammonia in the air. The actual ammonia flux towards the surface is determined by the air concentration and the total resistance that ammonia experiences on its way towards the surface. This total resistance consists of an atmospheric resistance ($R_{a,1m}$), a quasi-laminar leaf boundary layer resistance (R_{b,NH_3}) and a surface resistance (R_c). For

ammonia, the surface resistance (R_c) is especially important because this resistance determines how much ammonia deposits on the surface. The atmospheric and the leaf boundary layer resistance can be determined rather well from meteorological measurements and therefore the surface resistance can be calculated from the concentration and the flux estimate according to:

$$R_c = -\frac{C_{\text{NH}_3,1\text{m}}}{F_{\text{NH}_3}} - R_{a,1\text{m}} - R_{b,\text{NH}_3} \quad (2.23)$$

However, as can be seen in Figure 2.21 and Figure 2.22, the assumption that the surface concentration is zero is not always correct since emission fluxes are regularly observed. These emission fluxes only occur if the concentration at the surface is higher than the concentration in the air. In principle, this resistance approach is too simple for ammonia and a more complex compensation point model is needed to model the bi-directional fluxes. However, many atmospheric transport models (like the OPS model at RIVM) still use this simple approach because of model limitations. To provide these models with input, the surface resistance, R_c , is derived from the flux measurements, even though this gives considerable problems in the derivation and interpretation of these resistances. Therefore, the surface resistance is a very uncertain factor in atmospheric transport models.

Besides the conceptual shortcomings, the derived R_c from the measurements also contains the uncertainties from the flux and concentration measurements as well as the uncertainties in $R_{a,1\text{m}}$ and R_{b,NH_3} . As we have seen in many of the previous figures, the ammonia flux is often close to zero or even positive (emission). In the surface resistance calculations from Equation 2.23, infinite or negative resistances are obtained in these situations. This generates an enormous spread in the measured R_c -values and makes it very complex to calculate a simple arithmetical average value. Therefore, a reciprocal averaging (or harmonic averaging) is used. The idea is that the arithmetical averaging may be applied to the reciprocal of the resistance i.e., the conductance. An extremely high resistance leads to a very small conductance and this very small conductance has little influence on the average.

Figure 2.26 and Figure 2.27 show the average diurnal cycle and the frequency distribution of $1/R_c$ for the different years respectively. By using this harmonic averaging method we obtain an average $1/R_c$ value of 0.009 m s^{-1} in 2004 ($\sim R_{c,\text{har}}$ of 106 s m^{-1}), 0.006 m s^{-1} ($\sim R_{c,\text{har}}$ of 178 s m^{-1}) in 2005 and 0.007 m s^{-1} ($\sim R_{c,\text{har}}$ of 148 s m^{-1}) in 2006. The average $1/R_c$ of all data is 0.007 ($\sim R_{c,\text{har}}$ of 144 s m^{-1}). However, the spread in $1/R_c$ is very large (the difference between the 25% and 75% percentile values is 0.027 m s^{-1}).

The frequency distribution of $1/R_c$ shows a clear peak around 0.005 ($R_c \sim 200$) in 2004 and 2005. In 2006 this peak is less pronounced around 0.015 ($R_c \sim 70$). The observed range of $1/R_c$ values of all data is between -0.01 and 0.05 . Consequently, R_c values correspond to two ranges of values, i.e., -100 to $-\infty$ and 20 to ∞ . The negative $1/R_c$ (and R_c) values occur in emission periods.

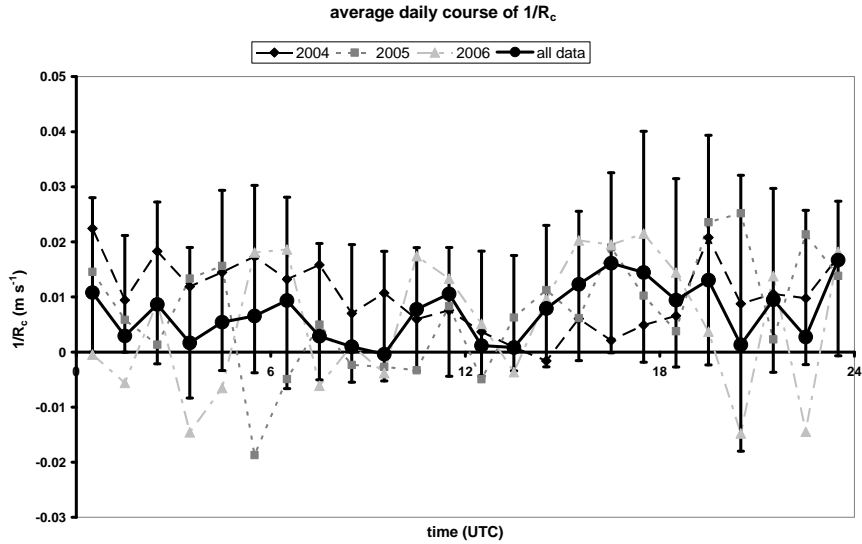


Figure 2.26. Average diurnal cycle of the reciprocal surface resistance.

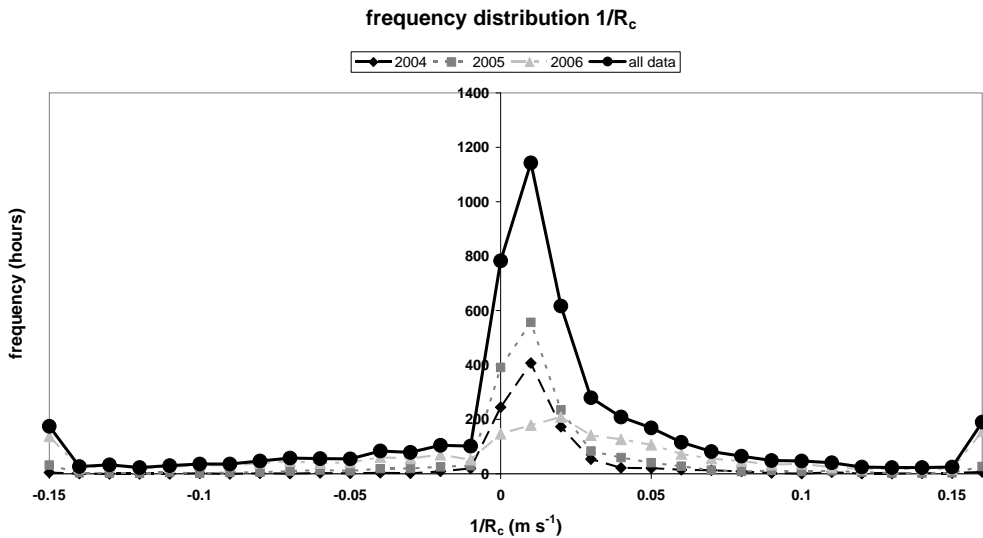


Figure 2.27. Frequency distribution of the reciprocal of the surface resistance.

Another way to calculate R_c is by using the average diurnal cycle of the concentration and the flux estimate and the average diurnal cycle of the median $R_{a,1m}$ and R_{b,NH_3} values in Equation 2.23. Figure 2.28 shows the derived average diurnal cycle of R_c . The error bars are calculated from the 25- and 75-percentile values of the flux, concentration, $R_{a,1m}$ and R_{b,NH_3} . The differences between the three years are very large (as expected), however, the average R_c value of 67 s m^{-1} for all data and its reciprocal value of 0.015 m s^{-1} are well within the same range of R_c and $1/R_c$ values obtained with the harmonic averaging method, i.e., 20 to ∞ and -0.01 to 0.05 respectively.

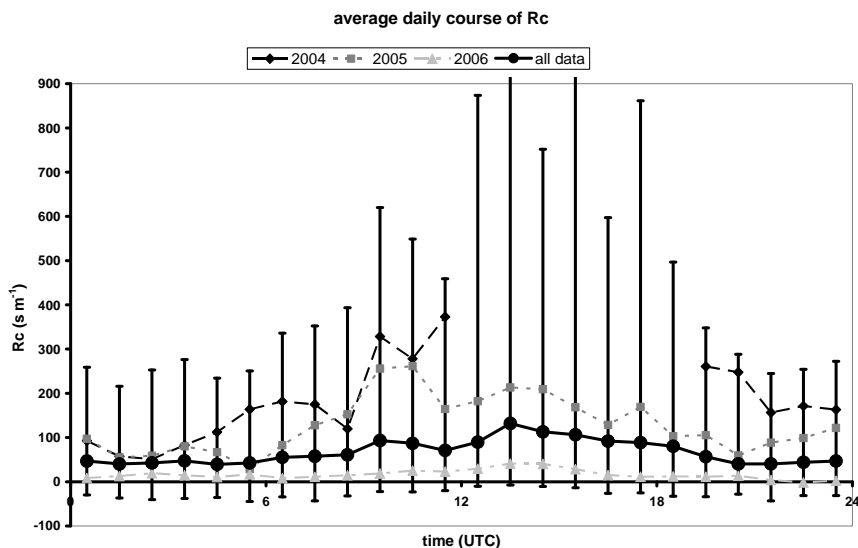


Figure 2.28. Average diurnal cycle of the surface resistance.

2.5 Discussion and Conclusion

In this chapter, the NH_3 flux measurements over agricultural grassland at the Haarweg in Wageningen were described. We also described the applied data selection procedure, the measurement site and the instrumentation. We furthermore gave an analysis of the random and systematic errors in the concentration measurements and consequently the flux measurements. After correction for the systematic errors in the concentration measurements, the relative random error in the concentration is estimated to be 1.9%. The relative random error in the NH_3 flux measurements is on average estimated to be about 50%. We showed that the relative random error in the NH_3 flux measurements is much smaller during night time (about 20%) than during daytime (more than 100%). Reason for this is that the concentration differences are generally large during night time. The random error in the concentration is then relatively small compared to the concentration difference that determines the flux. During daytime the concentration difference is generally much smaller, as a result of which the random error in the concentration is relatively large.

The surface resistance, R_c , is essential in model parameterizations that describe the surface-atmosphere exchange process of ammonia with the surface. The model parameterizations for R_c are derived from the R_c values that are deduced from the flux and concentration measurements as well as the aerodynamic resistances. The random error in the R_c parameterization therefore includes all the random errors of all these variables, of which the random error in the flux measurement is largest most of the time. For non-fertilized grassland, a harmonic averaged R_c value of about 67 s m^{-1} was found. However, we have seen that the assumption that the surface concentration is zero is not always (or probably never) met, because many emission situations were observed, mainly during daytime. Therefore, the canopy compensation point approach should be applied instead of the canopy resistance modeling approach. However, when only nighttime conditions are

considered, both approaches are equal, as the stomatal pathway is switched off and we are able to derive the external leaf surface (or cuticular) resistance, R_w .

Many studies have shown the dependency of R_w on relative humidity (RH). Reason for this is that the leaf surface is getting moister or wetter at higher humidity and that ammonia as a result dissolves easier, which reduces the resistance to uptake. The cuticular resistance, R_w , is often derived from the nocturnal surface resistance, R_c (at night), when stomata are closed and the stomatal resistance is assumed to be infinitely large. Theoretically, this nocturnal surface resistance consists of both the cuticular resistance, R_w , and the soil resistance, R_{soil} . However, especially for dense grassland vegetation, the soil pathway is assumed to be cut off (as discussed in Chapter 1).

Figure 2.29 shows the dependency of R_w on relative humidity for fifteen different field studies over different vegetations in different pollution climates. For comparison, the harmonic averaged R_w values from the measurements at the non-fertilized grassland site in Wageningen (note that only nighttime deposition fluxes are considered here) and the fertilized grassland site in Schagerbrug are included in this figure. We also included the parameterization of R_w from the DEPAC module (Appendix C) described in Van Jaarsveld (2004). This parameterization is used in the current version of the operational atmospheric transport model OPS of RIVM and PBL and the Lotos/Euros model of TNO, RIVM and PBL.

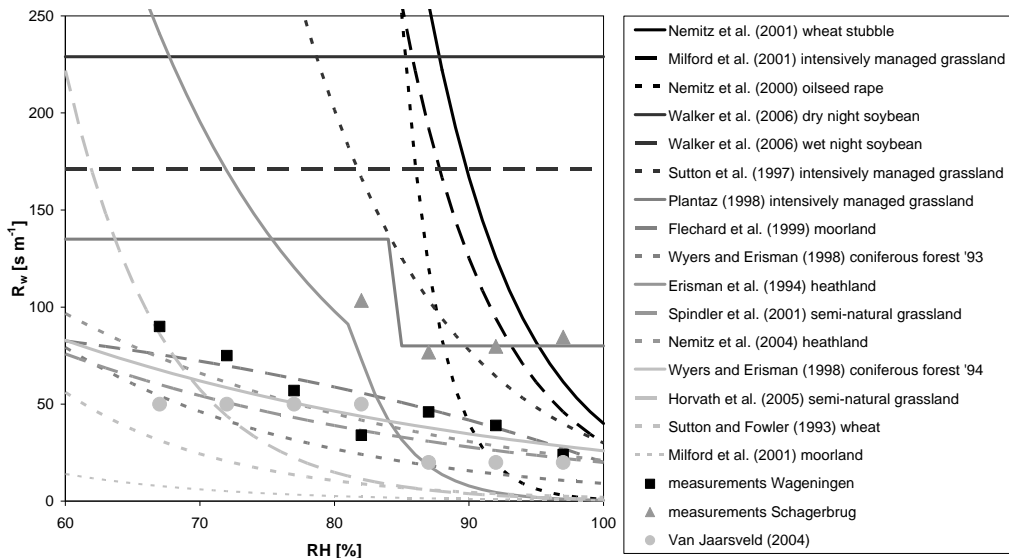


Figure 2.29. R_w versus relative humidity for 15 different flux measurement campaigns (represented by the colored lines) (following Nemitz et al., 2008). The symbols represent 2 measurement campaigns over agricultural grassland in the Netherlands in Wageningen (non-fertilized; black squares) and Schagerbrug (fertilized; red triangles) and the current model parameterization of Van Jaarsveld (2004) (blue circles).

It is clear that in all studies, a lower relative humidity leads to a higher value of R_w . The same is true for higher ambient concentrations or pollution levels (increasing with line colors going from dashed light gray to solid black). This conclusion is made based on the field studies in literature as well as on our own data. We see that R_w values for agricultural grassland (fertilized as well as non-fertilized) found in this study are predominantly larger

than the R_w values that are applied in the OPS model of RIVM for this land use class (Van Jaarsveld, 2004). An increase of R_w with increasing ambient concentration is also shown in a few other studies (Fowler et al., 1998a; Jones et al., 2007). An explanation for this behavior is that leaf water layers, which already exist at very low humidity (Van Hove et al., 1989), are getting saturated. In Chapter 5, we will discuss this topic in more detail.

3 Ammonia fluxes and derived canopy compensation points over non-fertilized agricultural grassland in the Netherlands using the new GRadiant Ammonia - High Accuracy - Monitor (GRAHAM)

This chapter has been published as Wichink Kruit R.J., Van Pul W.A.J., Otjes R.P., Hofschreuder P., Jacobs A.F.G., Holtslag A.A.M., 2007. Ammonia fluxes and derived canopy compensation points over non-fertilized agricultural grassland in the Netherlands using the new GRadiant Ammonia - High Accuracy - Monitor (GRAHAM). Atmospheric Environment 41, 1275-1287.

Abstract

During the period from June till November 2004, ammonia fluxes above non-fertilized managed grassland in the Netherlands were measured with a Gradient Ammonia – High Accuracy – Monitor (GRAHAM). Compared with earlier ammonia measurement systems, the GRAHAM has higher accuracy and a quality control system.

Flux measurements are presented for two different periods, i.e., a warm, dry summer period (from 18 July till 15 August) and a wet, cool autumn period (23 September till 23 October). From these measurements canopy compensation points were derived. The canopy compensation point is defined as the effective surface concentration of ammonia. In the summer period (negative) deposition fluxes are observed in the evening, night and early morning due to leaf surface wetness, while in the afternoon emission fluxes are observed due to high canopy compensation points. The mean NH_3 -flux in this period was $4 \text{ ng m}^{-2} \text{ s}^{-1}$, which corresponds to a net emission of $0.10 \text{ kg N ha}^{-1}$ over the 28 day sampling period. The NH_3 -flux in the autumn period mainly shows (negative) deposition fluxes due to small canopy compensation points caused by low temperatures and a generally wet surface. The mean NH_3 -flux in this period is $-24 \text{ ng m}^{-2} \text{ s}^{-1}$, which corresponds to a net deposition of $0.65 \text{ kg N ha}^{-1}$ over the 31 day sampling period.

Frequency distributions of the NH_3 -concentration and flux show that despite higher average ambient NH_3 -concentrations ($13.3 \text{ } \mu\text{g m}^{-3}$ in the summer period vs. $6.4 \text{ } \mu\text{g m}^{-3}$ in the autumn period) there are more emission events in the summer period than in the autumn period (about 50% of the time in summer vs. 20% in autumn). This is caused by the high canopy compensation points in summer due to high temperatures and a dry surface. In autumn, deposition dominates due to a generally wet surface that induces low canopy compensation points.

For our non-fertilized agricultural grassland site, the derived canopy compensation points (at temperatures between 7 and 29°C) varied from 0.5 to $29.7 \text{ } \mu\text{g m}^{-3}$ and were on average $7.0 \pm 5.1 \text{ } \mu\text{g m}^{-3}$, which is quite high for non-fertilized conditions and probably caused by high nitrogen inputs in the past or high dry deposition amounts from local sources. The average value for the ratio between NH_4^+ and H^+ concentration in the canopy, Γ_c , that was derived from our data was 2200.

3.1 Introduction

Ammonia deposition is an important eutrophying input to ecosystems. As such it may lead to a number of detrimental effects such as a loss in biodiversity (Fangmeier et al., 1994; Bobbink et al., 1998). Quantifying the ammonia deposition to ecosystems has been subject of many studies over the last two decades. However, the quantification of the exchange of ammonia above agricultural areas is also important in terms of obtaining a correct mass balance of ammonia over a regional scale. Recently, a number of studies on the ammonia exchange above agricultural surfaces (Sutton et al., 2000 (EXAMINE)) and specifically above grassland (Bussink et al., 1996; Sutton et al., 2001; Mosquera et al., 2001, Milford et al., 2001a; Spindler et al., 2001) have been carried out. To obtain a better insight into the long-term ammonia exchange above grassland in the Netherlands new measurements are carried out varying from fertilized to non-fertilized conditions. In this paper we report and discuss long-term measurements of concentrations and fluxes above a non-fertilized agricultural grassland site. With non-fertilized we mean that no fertilizer (mineral or organic) has been applied nor grazing by animals has taken place for more than at least 10 years.

The exchange of ammonia is basically induced by differences in concentration between the atmosphere and the surface. The actual exchange flux depends on the sign and magnitude of the concentration difference, as well as on the efficiency of all mechanisms involved in the transport and transfer. Only few techniques are available for high time resolution ammonia flux measurements (one value in 10 minutes). Up to now, in most cases ammonia fluxes were measured using AMANDA-systems which did have a precision of about 1%. This is adequate to derive fluxes, however, the AMANDA's didn't always operate to this precision and were not always sufficiently reliable. A system is requested that can maintain a high precision and that remains reliable under different conditions. Therefore a new device, the so-called GRAdient Ammonia – High Accuracy – Monitor (GRAHAM) system, was built. The GRAHAM has a higher precision (of about 0.4 %), which enables us to derive more accurately fluxes and deposition parameters such as canopy compensation points and canopy gamma values (ratio between NH_4^+ and H^+ concentration in the canopy). In this paper we give a description of the experimental set up and we present measurements with this new instrument above non-fertilized agricultural grassland. We show the typical daily behavior of the ammonia flux in two different periods, a summer period of 28 days and an autumn period of 31 days. We also show the typical concentration and flux distributions for these two periods. Furthermore, we present canopy compensation points obtained from flux direction changes and its dependency on temperature. We also show the apparent seasonal behavior of the derived gamma values.

3.2 Materials and Methods

3.2.1 Site description

Long-term gradient measurements of ammonia were made from June till November 2004 at the 'Haarweg' meteorological observatory in Wageningen, the Netherlands. The data contain two interesting periods on which we focus in this paper, a warm and sunny summer period (between 18 July and 15 August 2004) and a cool and cloudy autumn period

(between 23 September and 23 October 2004). At the meteorological observatory continuous measurements of air and soil temperature, air humidity, radiation, wind direction and wind speed are available.

The measurement site and its homogeneous surrounding are located west of Wageningen in the Netherlands (51°58'N, 5°38'W) on a heavy clay soil. The vegetation predominantly consists of temperate humid perennial ryegrass (*Lolium perenne* L.). There was no application of any kind of fertilizer (mineral or organic) at the measurement site for at least 10 years. However, the neighboring fields to the west and north received 30,000 kg of animal manure (from cows) and 500 kg of mineral fertilizer (KAS) per hectare during three applications this year. The last application of both animal manure and mineral fertilizer (on the northern field) was on 5 August, 9 days after a grass cut on all fields including the measurement site on 27 July. Note that these dates are within the selected summer period and might affect our flux measurements.

The grass at the measurement site was kept at a roughly fixed height of 10 cm, which means that two grass cuts are included in the summer period (20 and 27 July) and one in the autumn period (6 October). The surrounding fields were only cut three (west field) to four times (north field) this year, of which the grass cut on all fields on 27 July is included in the summer period and a grass cut on the northern field on 11 October is included in the autumn period. A small farm is located about 500 meters to the west-northwest of the measuring instrument and data collected with a wind direction from the farm were excluded from our dataset. The average elevation of the measurement site is 6.80m above mean sea level. (Webpage of observatory: www.met.wau.nl)

3.2.2 Micrometeorological theory

NH₃-fluxes are calculated using the aerodynamic flux-gradient method. This method requires the measurement of NH₃-concentrations at several heights in the surface layer to provide vertical gradients. These vertical gradients combined with eddy diffusivities then provide turbulent fluxes. The NH₃-flux (F_χ) is calculated as:

$$F_\chi = -ku_* \frac{\partial \chi}{\partial \left\{ \ln(z-d) - \psi_H \left(\frac{z-d}{L} \right) \right\}} \quad (3.1)$$

where k is the Von Karman constant (0.4), u_* is the friction velocity, χ is the concentration of gaseous ammonia, z is the height above ground, d is the zero plane displacement, L is the Obukhov length and ψ_H is the integrated stability correction function for heat (and inert tracers). In this study we used the integrated stability correction functions from Beljaars and Holtslag (1991). Turbulence parameters were obtained with measurements of a Campbell Scientific 3-D sonic anemometer (type CSAT3) mounted at 3.3 m height. Note that the flux-gradient theory assumes horizontal homogeneous conditions and no flux divergence (e.g., by chemical reactions).

3.2.3 GRadient Ammonia - High Accuracy - Monitor (GRAHAM)

NH₃-concentration profiles were obtained with the GRadient Ammonia – High Accuracy – Monitor (GRAHAM) previously referred to as AMANDA (a continuous rotating wet

denuder analyzer; Wyers et al., 1993). The GRAHAM is ideally suited for micrometeorological measurements because of its low detection limit, high precision and accuracy and high time resolution. The GRAHAM denuder is basically the same as the existing AMANDA denuder as described by Wyers et al. (1993, 1998). However, in respect to the AMANDA several modifications have been carried out.

First, the implementation of continuous in line airflow measurements is an obvious improvement in respect to the precision and accuracy. The flow rates are determined by measurement of temperature and the pressure drop over a restriction. To minimize systematic errors the restrictions were brought together in an aluminum body. In the old system flow rates were determined manually at service visits. All these modifications improved the accuracy as well as the precision of the instrument.

Second, two 3-channel syringe pumps (type Mechatronics) replaced the multi channel peristaltic pump allowing a well-defined sample flow from the denuders. With two coupled 10 ml syringes per denuder and a 1 ml min^{-1} sample flow a cycle time of ten minutes was obtained. During a cycle time the three samples were sequentially led through the detector allowing two minutes of flushing in between.

Third, the conical structure in the inlet is now also applied on the outlet of the wet rotating denuder. This optimized aerosol conducting system prevents ammonium particles (aerosols) from impaction on wetted surfaces and from being a potential source of interfering ammonium.

Concentrations of gaseous ammonia were measured at three heights, 4.0, 2.5 and 1.0 m. It has to be noted that it should be more favorable to install the denuders on a logarithmic height scale with the lowest denuder as close as possible to the surface. Average concentration values for all three denuders were determined during a 10 minute cycle. The 3 denuders were sampled sequentially with a stabilizing time of 2 minutes and an averaging time of 1 minute. After this cycle of 9 minutes, the detector is flushed for 1 minute and a new cycle starts. The tube length for transporting the solution to the detector is adapted to the time that the solution is analyzed. This is done to ensure that the concentrations measured in the analyzer for the three heights referred to the same air sampling period.

3.2.4 Precision improvement of the GRAHAM in relation to earlier AMANDA systems

Data on the performance of the earlier version of this instrument (AMANDA) were reported by Wyers et al. (1993, 1998) and Mennen et al. (1996). Wyers et al. (1993) positioned three instruments in the field at the same height and averaged the measurements every 30 min. They corrected the obtained concentration profiles for systematic differences, and reported the between-instrument standard deviation based upon 22 simultaneous triplicates to be 2.6% relative over the entire time spanned by the profiles. The correction method and the profiles themselves were not reported. The current GRAHAM system was tested in a similar but slightly different way. The three instruments were placed on a lab bench. They were simultaneously fed with the same sample, which was alternately zero air and $8 \mu\text{g m}^{-3} \text{NH}_3$, each period lasting 5 hours. Readouts were obtained every 10 minutes. The profiles were corrected for systematic differences between the instruments by multiplication of the signal of each instrument with the ratio of the average signal of that instrument to the average of the signals of all instruments at $8 \mu\text{g m}^{-3} \text{NH}_3$. This was done after a steady state was reached. In order to be able to compare the performance with the performance of AMANDA, every three subsequent results of each instrument were

averaged as to obtain one triplicate every 30 min. The relative between-instrument standard deviation between the corrected signals based on 30 minute averages was 0.34% at 8 $\mu\text{g NH}_3 \text{ m}^{-3}$ (25 triplicates, $v=50$). Based on 10 minute readouts it was 0.49% (75 triplicates, $v=150$). So, the improvement relative to AMANDA appears to be considerable, though some of it may be due to the disparate dynamic behavior of the AMANDA instruments when exposed to rapid concentration changes in the field, the concentration levels during the evaluation of AMANDA, and differences between the correction methods.

3.2.5 Canopy and stomatal compensation point

In this study, we derived canopy compensation points from flux direction changes during non-stable dry daytime conditions. The canopy compensation point, χ_c , is defined as the NH_3 concentration at z_0' , the notional height of gaseous exchange. The canopy compensation point can differ from the stomatal compensation point (χ_s), because it might be influenced by cuticular deposition (e.g., deposition on wet leaf surfaces), stomatal resistance and exchange with the soil. The emission from the soil, however, may be neglected because of low soil pH (about $\text{pH}=5$). This means that for flux direction changes (or zero net flux) in conditions where cuticular deposition may be neglected (dry surface) and stomatal exchange is dominant (daytime), the canopy compensation point is equal to the stomatal compensation point and the air concentration, $\chi_c = \chi_s = \chi_a$ (Flechard et al., 1999; Spindler et al., 2001; Nemitz et al., 2004).

Gaseous NH_3 is present in substomatal cavities within plant leaves. This NH_3 is expected to be in thermodynamic equilibrium with the apoplastic (intercellular leaf tissue) NH_4^+ -concentration. The substomatal NH_3 -concentration is known as the stomatal compensation point (χ_s) (Sutton et al., 1995) and was originally identified by Farquhar et al. (1980). The relationship between the stomatal compensation point, leaf temperature and apoplastic NH_4^+ concentration and pH is derived from the temperature response of the Henry equilibrium for ammonia, $\text{NH}_3(\text{g}) \leftrightarrow \text{NH}_3(\text{aq})$, and the ammonium-ammonia dissociation equilibrium, $\text{NH}_3(\text{aq}) + \text{H}^+ \leftrightarrow \text{NH}_4^+$. From the values found in literature for the Henry equilibrium (Dasgupta and Dong, 1986) and the dissociation equilibrium (Bates and Pinching, 1950), the partial pressure of ammonia can be calculated. The partial pressure of NH_3 is only a function of temperature and the ratio between NH_4^+ and H^+ concentration, which is often reduced to a single variable, Γ_s .

Using the ideal gas law, the NH_3 -concentration, χ_s (kg m^{-3}), in air can be calculated as:

$$\chi_s = \frac{p_{\text{NH}_3} \cdot M_{\text{NH}_3}}{R^* \cdot T} = \frac{a}{T} \exp\left(\frac{-b}{T}\right) \cdot \Gamma_s \quad (3.2)$$

where p_{NH_3} is the partial pressure of ammonia (Pa), M_{NH_3} is the molecular mass of ammonia (kg mol^{-1}), R^* is the universal gas constant ($\text{J mol}^{-1} \text{K}^{-1}$), T is the leaf temperature (K), a and b are constants ($a = 2.75 \cdot 10^6 \text{ kg m}^{-3} \text{ K}$ and $b = 1.04 \cdot 10^4 \text{ K}$), and Γ_s is the ratio between NH_4^+ and H^+ concentration (dimensionless). The complete derivation of Equation 3.2 can be found in Appendix A.

If the ambient atmospheric NH_3 -concentration (χ_a) is larger than the stomatal compensation point, absorption of NH_3 into the leaf through the stomata will occur. Emission from the leaf will occur if the opposite is true. Therefore, in dry circumstances, the stomatal compensation point is a key parameter in NH_3 exchange. The actual NH_3 exchange flux is determined by the size of the stomatal compensation point, which is dependent on leaf

temperature and Γ_s , and the factors that control stomatal opening (water potential of the leaf, temperature, vapor pressure deficiency, CO₂ concentration and light efficiency). From the derived canopy compensation points (χ_c) and the theoretical relation between stomatal compensation point, leaf temperature and ratio between NH₄⁺ and H⁺ concentration (Equation 3.2), a value for Γ_c ($\approx \Gamma_s$) can be derived:

$$\Gamma_c = \frac{\chi_c}{\frac{a}{T} \exp\left(\frac{-b}{T}\right)} \quad (3.3)$$

where χ_c is the derived canopy compensation point (kg m⁻³), a and b are constants ($a = 2.75 \cdot 10^6$ kg m⁻³ K and $b = 1.04 \cdot 10^4$ K), and T is leaf temperature (K).

Values for Γ_c ($\approx \Gamma_s$) have been derived in various other field studies (Sutton et al., 1995; Sutton et al. 1998; Nemitz et al. 2000b, Nemitz et al. 2004) and vary between less than 100 for natural vegetation to several thousands for agricultural crops.

3.2.6 Leaf temperature and leaf wetness

As mentioned before, leaf temperature is important for the canopy compensation point. In this study, leaf temperature is assumed to be equal to the surface temperature, which can be derived from the outgoing longwave radiation measured with a pyrgeometer (Kipp &

Zonen, model CG 1) according to $T_{surf} = \sqrt[4]{\frac{R_{lo}}{\varepsilon\sigma}}$, where R_{lo} is the outgoing longwave radiation, ε is the emissivity and σ is the Stefan Boltzmann constant.

Another important variable in the dry deposition process of ammonia is leaf wetness. As emission of NH₃ tends mainly to occur in dry conditions, it is important to know whether the leaf surface is dry or wet. The Campbell Scientific Model 237 Leaf Wetness Sensor was used to measure the leaf wetness. The sensor is a circuit board with interlacing gold-plated fingers. Condensation on the sensor lowers the resistance between the fingers, which is measured by the datalogger. Droplets must touch two fingers simultaneously to change the sensor resistance. For this reason, this type of sensor is coated with flat latex paint to spread the water droplets. The sensor is attached at a fixed position of 10 cm above ground level.

3.3 Results

3.3.1 Meteorological conditions

Measurements were made during a warm and sunny summer period (between 18 July and 15 August 2004) and during a cool and cloudy autumn period (between 23 September and 23 October 2004). The average temperatures at 1.8 m were 19.9°C during the summer period and 11.8°C during the autumn period. Despite the relatively large amount of rainfall in the summer period of 111 mm due to a few large thunderstorms at the end of the period, it was quite sunny with an average relative sunshine duration of 53%. The autumn period had a normal amount of rainfall of 76.5 mm and the average relative sunshine duration was much lower, 38%.

3.3.2 Observations

Figure 3.1 shows a period of 5 days in which the bi-directional nature of the NH_3 -fluxes over the non-fertilized agricultural grassland is shown together with the concentration pattern of the three individual denuders (at 4.0, 2.5 and 1.0 m height) and some important meteorological variables (wetness, net radiation, leaf temperature and relative humidity). The figure shows that the concentration profiles are (as they should be) monotonic. The concentrations can get really high (up to more than $80 \mu\text{g m}^{-3}$) during stable nighttime conditions, where the difference between the highest and lowest denuder can get as large as $30 \mu\text{g m}^{-3}$.

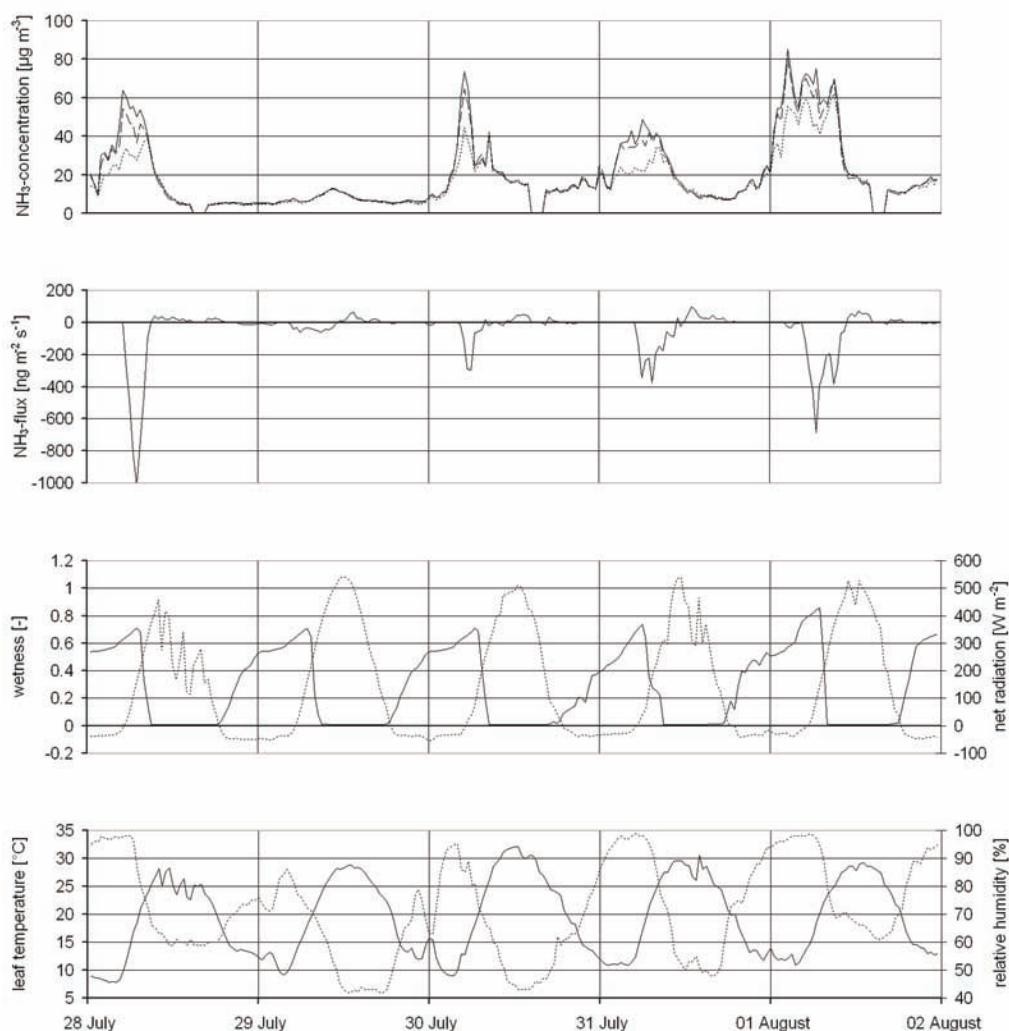


Figure 3.1. All measurements shown in this figure were made from 28 July till 2 August 2004. First panel: NH_3 -concentrations ($\mu\text{g m}^{-3}$) at the three sampling heights (4.0 m (—), 2.5 m (---) and 1.0 m (----)). Second panel: NH_3 -fluxes ($\text{ng m}^{-2} \text{s}^{-1}$). Third panel: leaf surface wetness (-) (—) and net radiation (W m^{-2}) (----). Fourth panel: leaf temperature ($^{\circ}\text{C}$) (—) and relative humidity (%) (----).

The calculated NH_3 -fluxes seem to be in good agreement with the classical daily pattern of NH_3 -fluxes. However, we have to be careful with the interpretation of early morning (deposition) fluxes, because the large concentration gradient in combination with only a small amount of turbulence (by means of u_*) can generate large fluxes. Because the surface is wet and turbulence starts up, these large deposition fluxes might be realistic and are therefore included in our data analysis. What is nicely shown in the third panel is that the onset of leaf wetness corresponds well to the drop of the net radiation below zero. The drying process only starts some time after the net radiation has risen above zero since it takes some time before the leaf surface is entirely dry again. At first sight it is remarkable is that the leaf surface gets wet during the night of 29 July, while the relative humidity remains far below 90%. Explanation for this is that the relative humidity is measured at 1.80 m, while the wetness is measured near the surface, where radiative cooling and thus condensation takes place.

Figure 3.2 shows NH_3 -concentration measurements in the upper panel and calculated NH_3 -fluxes together with the average leaf wetness in the lower panel for the summer period. The dots are the calculated values for the half-hourly NH_3 -concentration and flux; the solid line (with vertical 25 and 75 percentile bars) is the median of all half-hourly concentrations and fluxes for that time. The dotted line in the lower panel is the average leaf wetness. The median NH_3 -concentration shows a peak in the early morning when the surface layer is shallow and stable. In these conditions, ammonia can be accumulated due to advection from sources in the area or from surface emissions. The concentration drops when the surface layer grows due to turbulent mixing. If there remains some turbulence during nighttime, because of a relatively large wind speed, the concentrations remain relatively small (as can be seen in Figure 3.1 on 29 July 2004). This causes large variations in the nighttime concentration, while the daytime concentration shows much less variation.

The median NH_3 -flux in summer (lower panel) shows a clear diurnal cycle. During nighttime and in the early morning deposition fluxes are observed. These negative fluxes are a result of absorption of ammonia on the wet leaf surface due to dew formation, which results in a small surface (or cuticular) resistance. The stomatal exchange is suppressed because the stomata are closed and/or emitted ammonia is recaptured on the wet leaf surface. However, in the afternoon emission fluxes are observed because of the dry leaf surface and open stomata. These emission fluxes are caused by high canopy compensation points. As dew starts to form in the evening, NH_3 -fluxes change sign again. The mean NH_3 -flux in this summer period was $4 \text{ ng m}^{-2} \text{ s}^{-1}$, which corresponds to a net emission of $0.10 \text{ kg N ha}^{-1}$ over the 28 day sampling period.

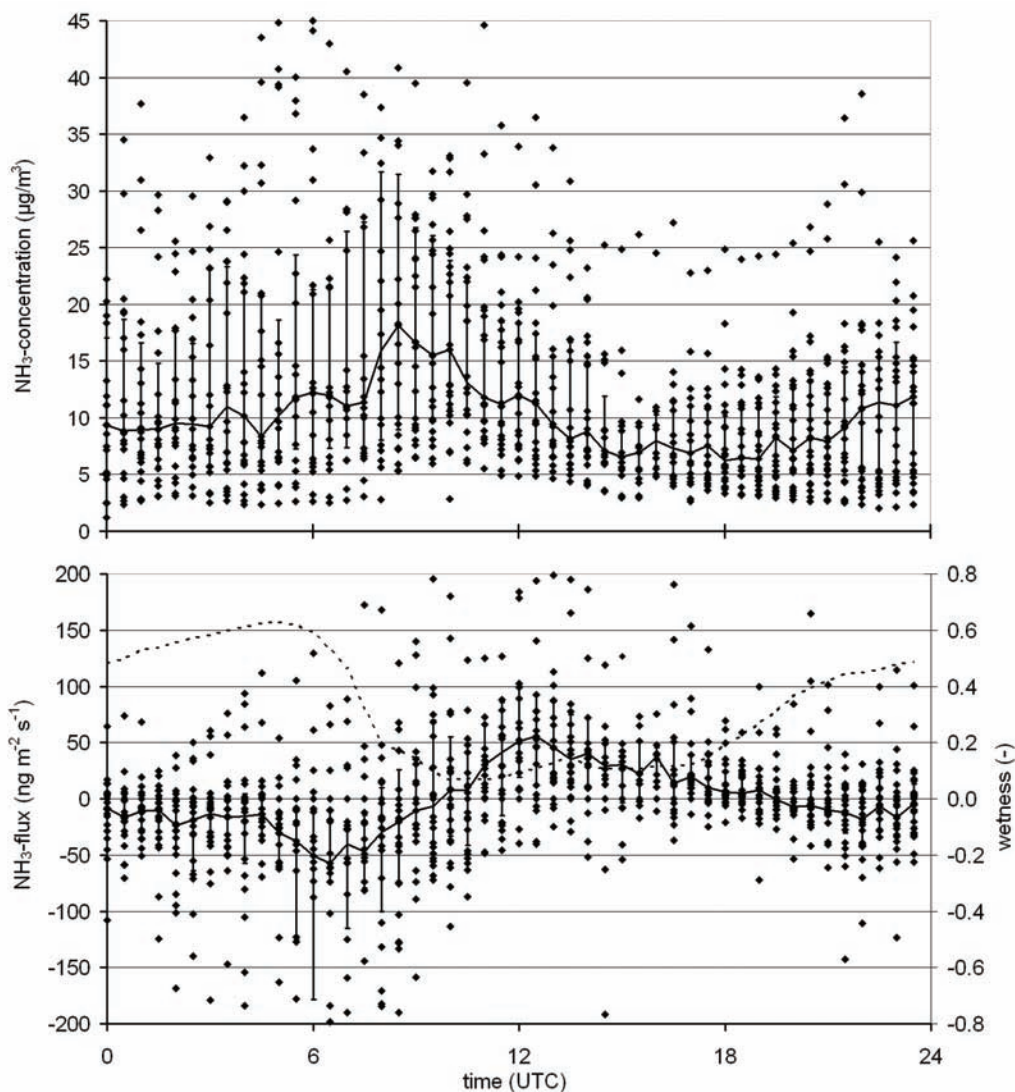


Figure 3.2. NH_3 -concentration (upper panel) and NH_3 -flux (lower panel) measurements above managed grassland in the Netherlands from 18 July until 15 August 2004 (summer period). The horizontal axis represents time of the day (UTC). Local time is UTC + 2. The vertical axis represents the NH_3 -concentration ($\mu\text{g m}^{-3}$) or NH_3 -flux ($\text{ng m}^{-2} \text{s}^{-1}$). Diamonds \blacklozenge are calculated values for the half-hourly NH_3 -concentration or NH_3 -flux; the solid line (—) (with vertical 25 and 75 percentile bars) is the median of all half-hourly fluxes for that time. The dashed line (----) in the lower panel is the mean leaf wetness signal during this period.

Figure 3.3 shows a similar plot, but now for the autumn period. The peak in the concentration (upper panel) in the early morning is not present in this period because the wind keeps the surface layer well mixed. For this reason, there is much less variation in the nighttime NH_3 -concentration in the autumn period than in the summer period. The lower panel mainly shows deposition fluxes (negative values) due to a predominantly wet surface and small canopy compensation points. In the autumn period, the mean NH_3 -flux was $-24 \text{ ng m}^{-2} \text{ s}^{-1}$, which corresponds to a net deposition of $0.65 \text{ kg N ha}^{-1}$ over the 31 day sampling period.

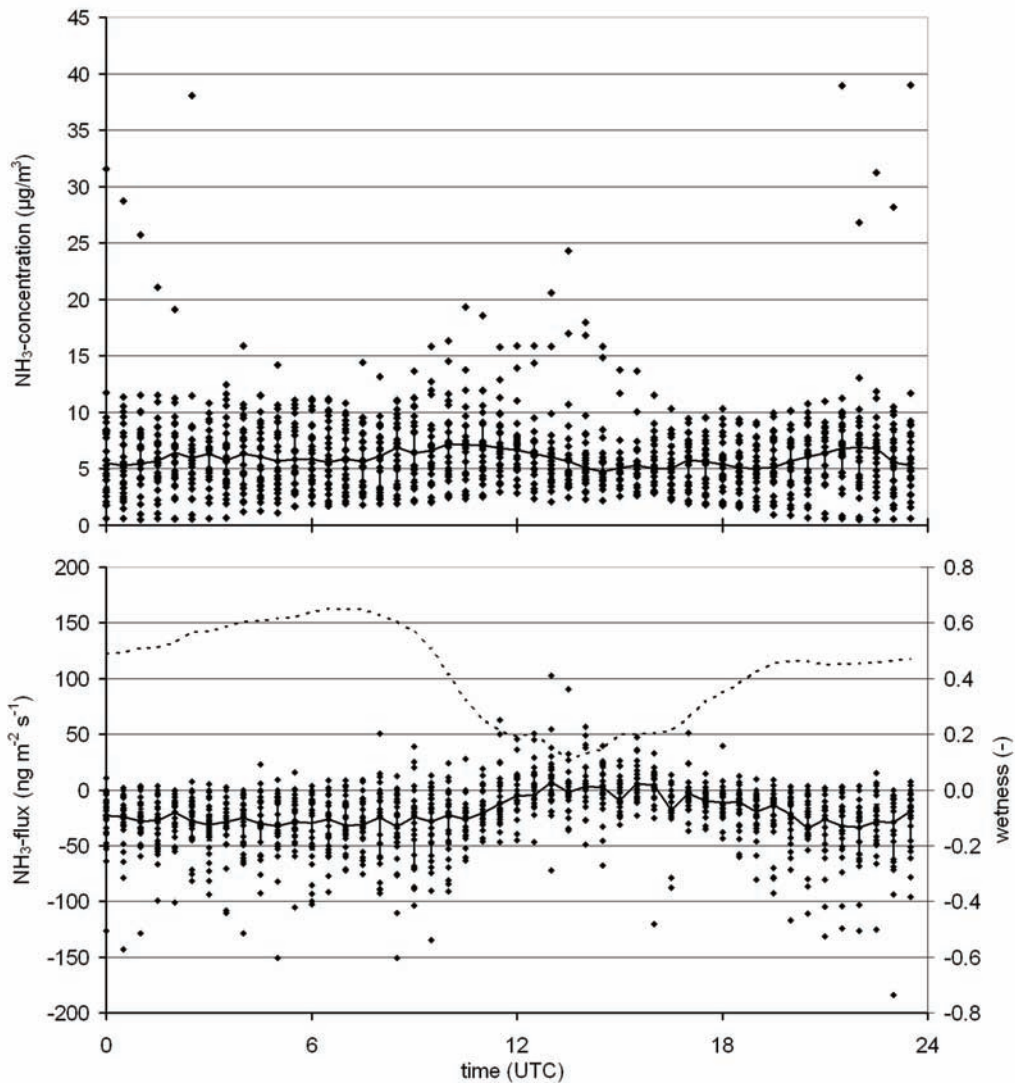


Figure 3.3. NH_3 -concentration (upper panel) and NH_3 -flux (lower panel) measurements above managed grassland in the Netherlands from 23 September until 23 October 2004 (autumn period). The horizontal axis represents time of the day (UTC). Local time is UTC + 2. The vertical axis represents the NH_3 -concentration ($\mu\text{g m}^{-3}$) or NH_3 -flux ($\text{ng m}^{-2} \text{s}^{-1}$). Diamonds \blacklozenge are calculated values for the half-hourly NH_3 -concentration or NH_3 -flux; the solid line (—) (with vertical 25 and 75 percentile bars) is the median of all half-hourly fluxes for that time. The dashed line (---) in the lower panel is the mean leaf wetness signal during this period.

In Figure 3.4, the frequency distributions of the NH_3 -concentration are shown for the summer and the autumn period. Concentration classes ($1 \mu\text{g m}^{-3}$ interval) are shown on the x-axis and the frequency (%) is shown on the y-axis. The frequency of concentrations between 0 and $10 \mu\text{g m}^{-3}$ is about 50% in summer and about 90% in autumn. This means that the variance in the concentrations is much larger in summer than in autumn. The highest frequencies are observed in the range between 5 and $7 \mu\text{g m}^{-3}$ (in both summer and autumn), only the frequency at which these concentrations are observed is much higher in

autumn (13%) than in summer (8%). This confirms that the range of concentrations is larger in summer than in autumn. The average air concentration is $13.5 \pm 10.8 \mu\text{g m}^{-3}$ in summer and $6.3 \pm 3.8 \mu\text{g m}^{-3}$ in autumn.

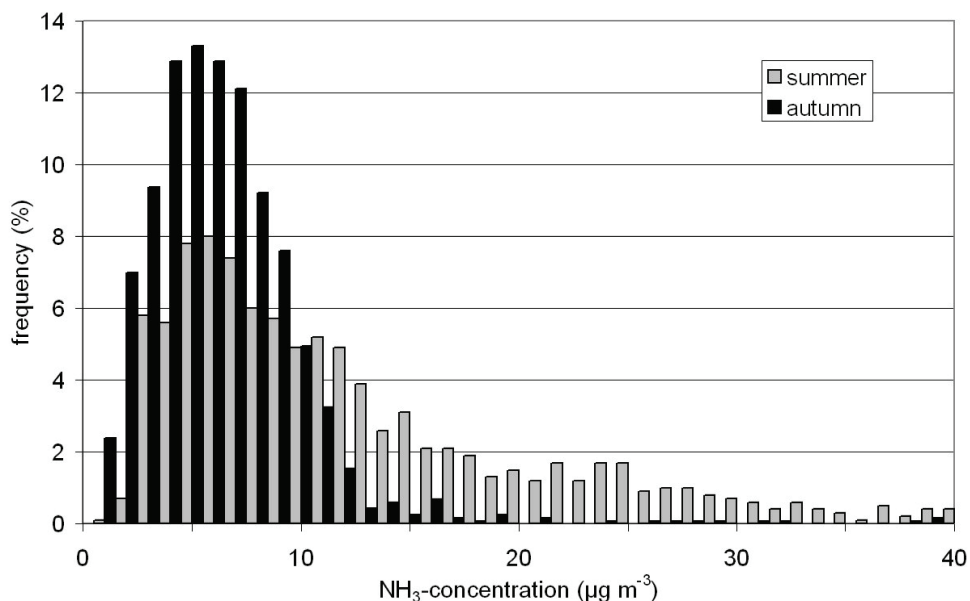


Figure 3.4. Frequency distributions of the 30-minute mean NH₃-concentration measurements in the summer and autumn period in 2004. Concentration classes ($1 \mu\text{g m}^{-3}$ interval) are shown on the x-axis and the frequency (%) is shown on the y-axis.

In Figure 3.5, the frequency distributions of the 30-minute mean NH₃-flux measurements are given for the summer and autumn period. The frequency distributions show that in the summer period, the frequency of emission fluxes is almost equal to the frequency of deposition fluxes, while in autumn, the frequency of deposition fluxes (about 80%) is much larger than that of emission fluxes (about 20%). Furthermore, the frequency of fluxes between -200 and $200 \text{ ng m}^{-2} \text{ s}^{-1}$ is 93% in summer and 99% in autumn. So, the variance in the NH₃-flux is larger in summer than in autumn, which can also be observed in Figure 3.2 and 3.3.

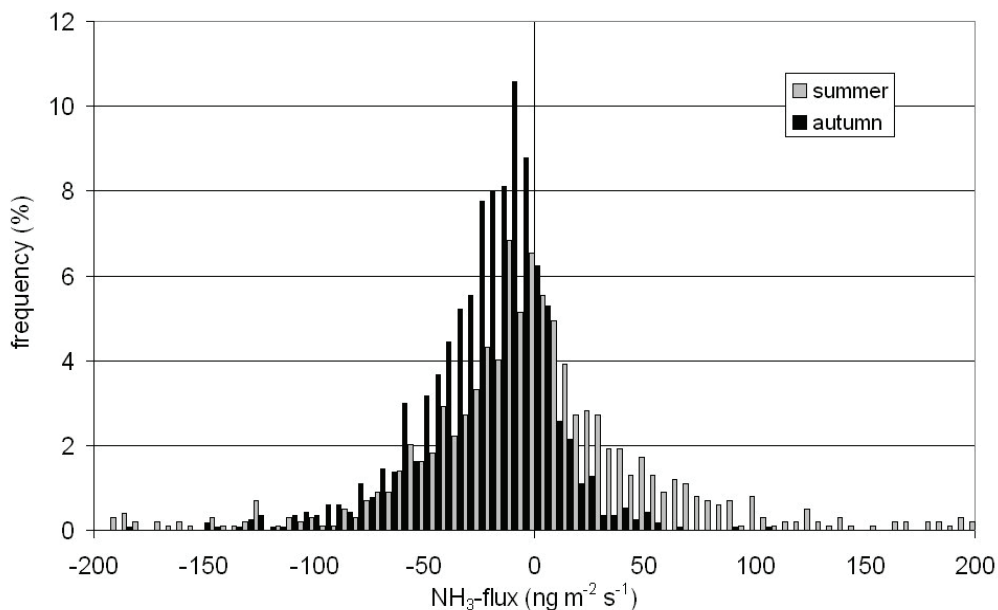


Figure 3.5. Frequency distributions of the 30-minute mean NH_3 -flux measurements in the summer and autumn period in 2004. Flux classes ($5 \text{ ng m}^{-2} \text{ s}^{-1}$ interval) are shown on the x-axis and the frequency (%) is shown on the y-axis.

Canopy compensation points were derived from flux direction changes during non-stable dry daytime conditions. In Figure 3.6, the canopy compensation points are shown as a function of the leaf surface temperature. The canopy compensation points were on average $7.0 \mu\text{g m}^{-3}$ and range from $0.5 \mu\text{g m}^{-3}$ to a maximum of $29.7 \mu\text{g m}^{-3}$. The solid line represents the theoretical relation for the stomatal compensation point (Equation 3.2), assuming a constant value of 2200 for Γ_s .

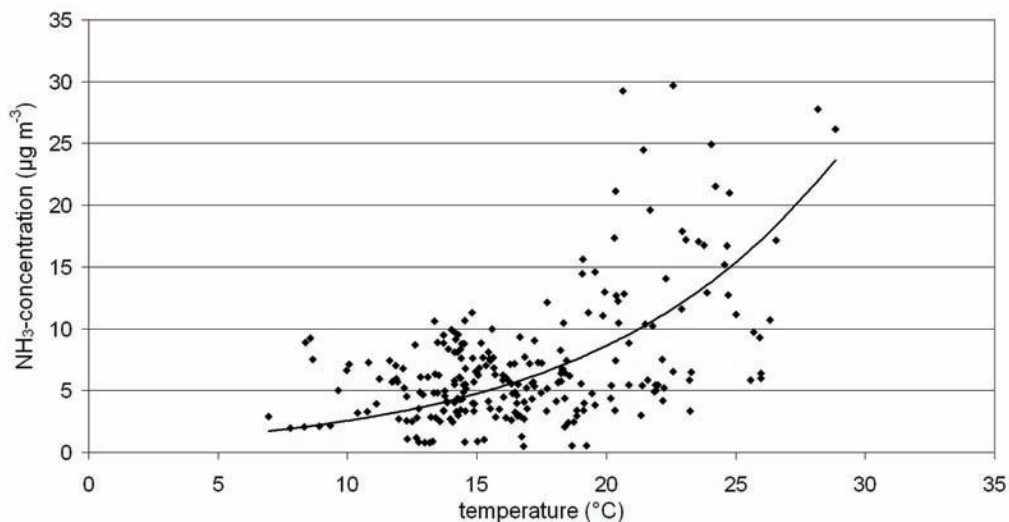


Figure 3.6. Canopy compensation points derived from micrometeorological measurements as a function of temperature (diamonds) and the theoretical compensation point according to Equation 3.2 (line) with $\Gamma_s = 2200$.

In Figure 3.7, we have depicted values for Γ_c deduced from the derived canopy compensation points and Equation 3.3. In this figure the derived values for Γ_c are plotted in time.

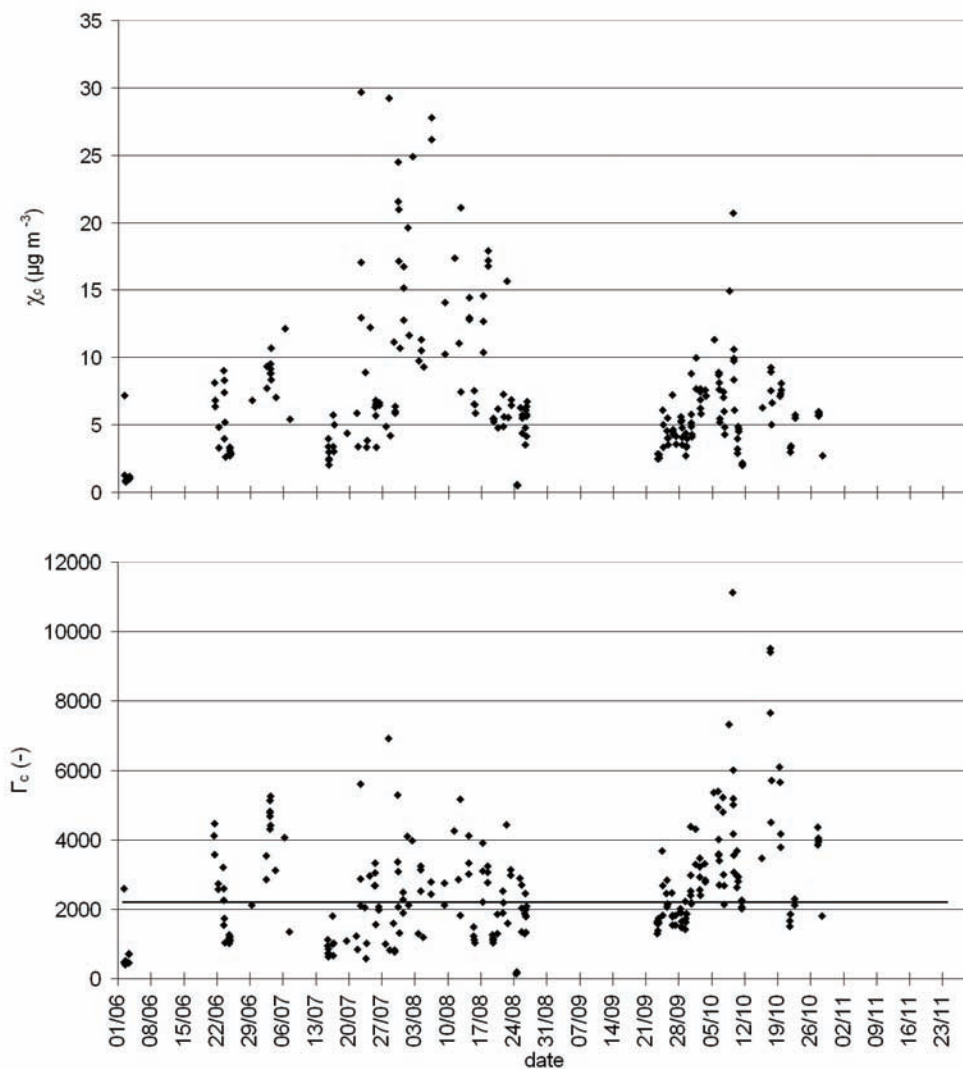


Figure 3.7. Derived canopy compensation points (= χ_c) (upper panel) and ratios between NH_4^+ and H^+ concentration (= Γ_c) (lower panel) from the end of May until the end of October 2004 (diamonds) and the constant value (2200) that is normally assumed for modeling (line).

3.4 Discussion and Conclusions

In this paper we describe and analyze observations with a novel instrument to measure ammonia (GRAHAM). Although these data were collected in different circumstances and have higher accuracy, concentration and flux patterns are consistent with earlier findings in the Netherlands (Plantaz 1998, Mosquera et al. 2001, Nemitz et al. 2004). In summer, the

frequency of emission and deposition events almost balance each other resulting in a small net emission. Emission only occurs during dry periods with high canopy compensation points. This implies that, although ambient NH_3 -concentrations are relatively high in summer, canopy compensation points need to be even higher to explain ammonia emission. In autumn, the frequency of NH_3 deposition is much larger than the frequency of NH_3 emission. This is because deposition generally occurs on wet surfaces and the canopy compensation point drops to almost zero in these cases. The frequency of wet surfaces is quite high in autumn. This is a consequence of the high number of dew nights in the Netherlands (250 ± 25 days per year, which are rather evenly distributed over the year (Jacobs et al., 2006)) in combination with a relatively short day length. Because day length is much shorter in autumn than in summer, this leads to much longer leaf wetness durations in autumn and therefore longer periods with deposition. Besides, when the surface is dry, canopy compensation points are generally low due to low temperatures and therefore low canopy compensation points. Leaf wetness will be investigated further in Chapter 4.

Derived canopy compensation points were on average $7.0 \mu\text{g m}^{-3}$ and varied between $0.5 \mu\text{g m}^{-3}$ up to $29.7 \mu\text{g m}^{-3}$ in the temperature range between 7 and 29°C . These compensation points are relatively high considering the non-fertilized nature of the grassland site. Most of the reported high canopy compensation points in the Netherlands were obtained at fertilized agricultural grassland sites. Plantaz (1998) reported a compensation point of $19 \mu\text{g m}^{-3}$ at 20°C (vs. about $9 \mu\text{g m}^{-3}$ at 20°C in this study). However, it looks like these high compensation points are reasonable, because Nemitz et al. (2004) also found relatively high stomatal compensation points of about $5 \mu\text{g m}^{-3}$ at 20°C above heathland in the Netherlands.

Van Hove et al. (2002) measured stomatal compensation points directly using the vacuum infiltration technique and found values between 0.5 and $4 \mu\text{g m}^{-3}$ for a nearby intensively managed pasture. These stomatal compensation points derived from direct measurement of apoplastic NH_4^+ and pH are typically a factor 2 to 3 lower than the canopy compensation points derived from flux measurements. Similar discrepancies are found in other studies (Mattson et al. 1997, 1999; Hill et al. 2001). Hill et al. (2001) suggests that spatial variability of pH and/or NH_4^+ concentration within the foliar apoplast appears the most promising line of further investigation.

The gamma values (Γ_c) deduced from our NH_3 measurements also seem to be higher than the values found in literature (under the same non-fertilized field conditions). We observe an increase of Γ_c values at the end of the measurement period. Husted et al. (1996) suggest that seasonal variations are coupled to plant phenology. Our observations are also in agreement with observations from Van Hove et al. (2002), who also found an increase in Γ_s at the end of the growing season. Besides, they found a decrease in Γ_s at the beginning of the growing season. It was shown that especially the NH_4^+ concentration has a seasonal trend and that H^+ concentration or pH remains rather constant during the year. They also noted that temperature not only seems to have an effect on the equilibrium between χ_s and NH_3 dissolved in the apoplast but also on the physiological processes responsible for the NH_4^+ concentration in the apoplast. Other laboratory studies (e.g., Schjoerring et al., 2000) have shown that plant development stage and soil nitrogen are important for the size of internal plant NH_3 -concentration. In field experiments this has been shown by Milford et al. (2001a) and Loubet et al. (2002) for grassland management activities as cutting and fertilization. However, more research is needed to find relations between the plant interior NH_3 -concentration and plant development stage (N_{total} , LAI, height, dry matter content) and/or soil N (N_{total} , NO_3^- or NH_4^+).

4 Observations and estimates of leaf wetness duration over agricultural grassland

This chapter has been published as Wichink Kruit R.J., Jacobs A.F.G., Holtslag A.A.M., 2008. Observations and estimates of leaf wetness duration over agricultural grassland. Atmospheric Environment 42, 5304-5316.

Abstract

Leaf wetness is an important and frequent phenomenon for the surface-atmosphere exchange of some atmospheric trace gases that are well soluble in water, such as ammonia (NH_3), as well as for plant disease epidemiology. This study shows a comparison of two different techniques to measure leaf wetness; namely a painted flat-plate grid sensor and a system of four clip sensors. Although both techniques gave comparable results, the flat-plate grid sensor was favored, because of its stable signal and its ease of use. In this technique, the measurement height turned out to be of great importance for the leaf wetness duration (LWD); the flat-plate sensor at 1.0 m systematically underestimated LWD, while the flat-plate sensor at 0.1 m better represented the actual LWD. To obtain a representative signal, leaf wetness should be measured close to the surface. Using the available leaf wetness measurements, a comparison was made between three physical and four empirical leaf wetness models. Without any optimization, the physical model that calculates the potential condensation at the leaf surface gave the best results. However, after optimizing the humidity thresholds in the empirical leaf wetness models, the optimized model based on the difference between the actual and saturated specific humidity at the surface gave best results. For practical applications in atmospheric transport models, like for the calculation of dry deposition of well soluble gases, the relative humidity (RH) threshold model might be easiest to implement. This study showed that different thresholds should be used for different vegetation types. In this study, an optimized RH threshold of 71% was derived for agricultural grassland.

4.1 Introduction

Leaf wetness is an important parameter in the deposition process of some atmospheric trace gases with high solubility in water. Van Hove et al. (1989) showed the importance of water films for the adsorption of NH_3 and SO_2 on the leaf surface. The adsorbed quantities increased strongly with increasing air humidity, indicating that water on the leaf surface plays a major role in the interaction of these gases with the leaf surface. Wichink Kruit et al. (2007) showed the bidirectional behavior of NH_3 and the importance of leaf wetness for the direction of the NH_3 flux. Emission of NH_3 mainly occurs from a dry leaf surface, when the internal plant concentration (stomatal compensation point) is higher than the ambient air concentration (Van Hove et al., 2002). Deposition occurs, when the leaf surface is wet or when the stomatal compensation point is smaller than the ambient NH_3 concentration. The resistance of a wet leaf surface to the uptake of ammonia is much lower than the resistance of a dry leaf surface. As a result, the deposition flux towards the leaf surface is much higher in wet conditions. In regional-scale deposition models, the surface resistance for SO_2 and NH_3 are usually set to zero, as long as wetting is assumed (Wesely, 1989). Therefore, it is very important to have reliable leaf wetness estimates in these models.

Leaf wetness also plays an important role in the outbreak of foliar diseases caused by pathogenic fungi (Aylor, 1986; Huber and Gillespie, 1992; Van Den Ende et al., 2000). When leaf wetness periods exceed a pathogen-specific length, spores of fungal foliar pathogens such as *Phytophthora infestans* on potato, *Botrytis elliptica* on lily and *Plasmopara viticola* (downy mildew) on grapevine are enabled to infect the crop. Such diseases are typically prevented by repeated fungicide applications. With increasing environmental awareness and the high cost of fungicides, there is a need to reduce the excessive use of chemicals. Accurate determination of environmental conditions relevant to pathogen development can help to reduce the necessary fungicide input (Jones, 1986). So reliable estimates of leaf wetness duration can also improve decision making and assist in maximizing the efficiency of fungicide input.

Jacobs et al. (2006) showed that the average number of dew nights in a mid-latitude country is 250 ± 25 per year. This emphasizes the importance of a proper description of leaf wetness in atmospheric transport models, disease simulation models and warning systems.

Leaf wetness can be defined as free liquid water that is present on the outer surface of plant leaves. Depending on the tissue hygroscopicity, it consists of individual drops or water films of thickness between a few nanometers (Burkhardt and Eiden, 1994) and a few micrometers (Van Hove and Adema, 1996). Leaf wetness is formed either through condensation of water vapor on the leaf surface or through deposition of hydrometeors such as rain or fog droplets from the atmosphere.

There are different techniques to measure leaf wetness (Davis and Hughes, 1970; Gillespie and Kidd, 1978; Wei et al., 1995; Burkhardt and Eiden, 1994; Heusinkveld et al., 2008). In this study, we compare two of these techniques over a grassland area; an electrical flat-plate grid sensor and a system of four clip sensors that are directly attached to the leaf. To investigate the effect of measurement height, we study two flat-plate grid sensors; one

attached at standard reference height (1.0 m) and the other attached at canopy height (0.1 m).

Beside measurements, there is an urgent need for models that give reliable estimates of leaf wetness. However, many different models exist that vary in complexity. They can roughly be divided into physical models (Monteith, 1981; Pedro and Gillespie, 1982a,b ; Garratt and Segal, 1988; Monteith and Unsworth, 1990; Bass et al., 1991; Luo and Goudriaan, 2000) that are mainly based on the energy budget of the leaf, and empirical models (Gleason et al., 1994; Rao et al., 1998; Kim et al., 2002; Van Jaarsveld, 2004; Wichink Kruit et al., 2004) that are mainly statistically coupled to one or more meteorological variables. In this study, three physical models and four empirical models are compared.

4.2 Materials and Methods

4.2.1 Site description

Wageningen University operates a meteorological observatory, the Haarweg station, in the center of the Netherlands (51°58'N, 5°38'E, 7 m a.s.l.; www.maq.wur.nl). The region is characterized by perennial grassland with dominant plant species consisting of *Lolium perenne* and *Poa trivialis*. The mean height of the grass vegetation is about 0.1 m and the mean leaf area index (LAI) is about 3. The soil at the site is predominantly heavy basin clay resulting from the back swamps of the Rhine River. At the observatory continuous measurements of air temperature, humidity, net radiation (short and long wave radiation), wind direction and wind speed are available at standard measurement height (1.8 m) averaged every 10 minutes. Besides, air temperature at 0.1 m height and soil temperatures at 0.5 m, 0.2 m, 0.1 m and 0.05 m depth are available, from which the soil heat flux (G) is calculated.

4.2.2 Measurement devices

To measure leaf surface wetness, we utilized the flat-plate grid sensor (model 237, Campbell Scientific, Logan, Utah) (Davis and Hughes, 1970; Gillespie and Kidd, 1978; Wei et al., 1995) and a system of four clip sensors (Burkhardt and Eiden, 1994). Both measurement devices primarily consist of gold-plated electrodes, between which the electric conductivity is measured. In the case of the grid sensor, the surface on which water deposition and condensation may occur, consists of polyamide with three coatings of off-white latex paint to increase the ability to detect small amounts of water, as was shown to be important by Sentelhas et al. (2004b). The grid sensors were heat-treated to remove or deactivate hygroscopic components of the paint. Grid sensors were chosen because of their good performance under different field conditions. The grid sensors were deployed facing north at an inclination angle of 30° at heights of 0.1 m and 1.0 m. Results of Pedro (1980) for apple, soybean, and maize, Lau et al. (2000) for tomatoes, and Sentelhas et al. (2005) for turfgrass and maize, showed that the differences between sensor measurements and visual observations of wetness were around 15–30 min, confirming the accuracy of flat-plate grid sensors for measuring LWD in different crops. Good agreement was also found between wetness measurements with the flat-plate grid sensor at 0.1 m and microlysimeter measurements during a 20 night measuring campaign in 2004 (Jacobs et al. 2006).

Therefore, the flat-plate grid sensor at 0.1 m will be used as the reference technique in this study.

The leaf wetness clip sensors (Burkhardt and Eiden, 1994) are clip electrodes that are attached to real leaves (or needles, as in the original paper). For data analysis the average signal of four clip sensors is used to account for spatial variability. Both techniques only give a qualitative indication for the occurrence of leaf surface wetness.

Flat-plate grid and clip sensor measurements of leaf wetness were available during the period from 23 March till 30 April 2005. However, because of a general failure of the data logging system, no grid sensor data were collected between 18 April 14.30 UTC and 22 April 23.40 UTC and therefore this time period is not included in the data analysis. A total of 34 days is finally used to evaluate the sensors and to test the models.

4.2.3 Statistical data analysis

To compare the measurements and models in this study, we use a statistical data analysis method, i.e., the contingency table (Wilks, 1995; Jolliffe and Stevenson, 2003). This method gives insight into whether a model correctly predicts wetness occurrence or not. Limits are assumed to distinguish the difference between wet and dry situations for the measurements (flat-plate grid sensor at 0.1 m) as well as for the model calculations. By doing this, a 2 x 2 contingency table is obtained (Table 4.1).

Table 4.1. Contingency table

	wetness observed	no wetness observed	
wetness modeled	hit (<i>a</i>)	false alarm (<i>b</i>)	$P_m = a + b$
no wetness modeled	miss (<i>c</i>)	correct rejection (<i>d</i>)	$n - P_m = c + d$
	$P_o = a + c$	$n - P_o = b + d$	$a + b + c + d = n$

P_m = modeled events; P_o = observed events; n = total number of events.

There are two cases when the forecast is correct, either a 'hit' (*a*) or a 'correct rejection' or 'correct no forecast' (*d*) and two cases when the forecast is incorrect, either a 'false alarm' (*b*) or a 'miss' (*c*). A perfect forecast system would have only hits (*a*) and correct rejections (*d*), with the other cells (*b* and *c*) being zero. By combining the four categories, different scores can be calculated, which enables us to make an objective judgement on model performance. In this study, the recommendations for the verification of precipitation forecasts (Nurmi, 2003) will also be applied for the verification of our leaf wetness estimates. The applied statistical scores are briefly outlined below.

The bias of dichotomous forecasts compares the frequency of modeled (P_m) to the frequency of observed (P_o) leaf wetness and is represented by the ratio: $B = (a + b)/(a + c) = P_m/P_o$. The range of B is zero to infinity. An unbiased score thus corresponds to $B = 1$.

The most simple and intuitive performance measure that provides information on the accuracy of a categorical forecast system is 'proportion correct': $PC = (a + d)/n$. The range of PC is 0-1, a perfect score = 1.

The measure that examines by default the (extreme) event by measuring the proportion of observed events that were correctly forecasted is 'probability of detection': $POD = a/(a + c)$. The range of POD is 0-1, a perfect score = 1.

POD is sensitive to hits but takes no account of false alarms. It can be artificially improved by producing excessive "yes" forecasts to increase the number of hits (with a consequence of numerous false alarms). While maximizing the number of hits and minimizing the number of false alarms is desirable, it is required that POD be examined together with 'false alarm ratio': $FAR = b/(a + b)$. The range of FAR is 1-0, a perfect score = 0.

The 'equitable threat score' adjusts for the number of hits associated with random chance, and is defined as: $ETS = (a - ar)/(a + b + c - ar)$, where $ar = (a + b)(a + c)/n$ is the number of hits for random forecasts. The range of ETS is -1/3 to 1, a perfect score = 1, no skill forecast = 0.

One of the most commonly used skill scores for summarizing the 2 x 2 contingency table is 'Heidke skill score'. Its reference accuracy measure is 'proportion correct' (PC), adjusted to eliminate forecasts which would be correct due to random chance. Using the cell counts it can be written in the form: $HSS = 2(ad - bc)/\{(a + c)(c + d) + (a + b)(b + d)\}$. The range of HSS is $-\infty$ to 1, a perfect score = 1, no skill forecast = 0.

4.2.4 Physical dew models

Dew can occur when in the evening radiative cooling allows water vapor in the atmosphere to condense on a given surface (Garratt and Segal, 1988; Jacobs and Nieveen, 1995). In addition, dew can form when soil water evaporates during the night and is intercepted by a canopy (Monteith, 1957; Garratt, 1992).

Monteith (1981) shows that for a natural surface, the maximum possible condensation or potential dew is given by:

$$\lambda_v E = \frac{s}{s + \gamma} (Q^* - G) \quad (4.1)$$

where λ_v is latent energy for vaporization ($J \text{ kg}^{-1}$), E is evaporation or dew formation rate ($\text{kg m}^{-2} \text{ s}^{-1}$), s is slope of the saturation curve (Pa K^{-1}), γ is the psychrometric constant (66 Pa K^{-1}), Q^* is net radiation (W m^{-2}) and G is soil heat flux (W m^{-2}). This is the first physical model that will be tested.

For the second physical model that will be tested, the energy budget equation is combined with the equation for evaporation or dew formation of free liquid water. By using Penman's substitution, the following equation is obtained (e.g., Garratt and Segal, 1988; Holtslag and De Bruin, 1988):

$$\lambda_v E = \frac{s}{s + \gamma} (Q^* - G) + \frac{\gamma}{s + \gamma} \lambda_v \rho \frac{(q_s(z) - q(z))}{R_{av}} \quad (4.2)$$

where ρ is air density (kg m^{-3}), $q_s(z)$ is saturated specific humidity at reference level (kg kg^{-1}), q is specific humidity at reference level (kg kg^{-1}) and R_{av} is atmospheric resistance to water vapor transport (s m^{-1}). This equation contains the 'potential dew' term

and a 'drying' term to correct for the unsaturated air at reference level. If the air at reference level is saturated, the drying term becomes zero and Equation 4.2 reduces to Equation 4.1.

Pedro and Gillespie (1982a,b) developed a model that is based on the energy budget equation along with heat transfer theory for flat plates. This model is developed especially for tall canopies to simulate dew duration on a single leaf, but will also be tested in this study for relatively short grass. This is the third physical model that will be tested.

From all three physical models described above, dew duration is inferred from a computation of the latent heat flux. As soon as the latent heat flux becomes negative, dew starts to accumulate. When the latent heat flux becomes positive again, the accumulated dew first has to evaporate until there is no dew left. A rain interception model (Jacobs et al., 2005) is used to account for rain events during the period.

4.2.5 Empirical leaf wetness models

Besides the physical leaf wetness models based on the energy balance technique, several empirical leaf wetness models exist. These models generally consist of threshold values for one or more relevant variables. These threshold values vary from place to place and need to be optimized for the local circumstances.

In a first approximation, leaves are assumed to be wet if the relative humidity (RH) at 1.8 m exceeds a certain threshold value. For RH below this threshold value, leaves are assumed to be totally dry. Van Jaarsveld (2004) used a threshold value of 87 % in an atmospheric transport model in the Netherlands. This value was originally derived from surface wetness measurements in the Speulder forest and later applied for all vegetation types.

The second empirical approximation is an extended version of the RH threshold approximation, hereafter RH_EXT, first described by Wichink Kruit et al. (2004). This approximation is based on the RH threshold of 87% above which leaves are supposed to be wet. Leaves are supposed to be dry when RH is below 70% and between 70% and 87%, an RH increase of more than 3% in 10 minutes is assumed to lead to wet leaves, while a RH decrease of more than 2% in 10 minutes is assumed to lead to dry leaves.

The third empirical model is the classification and regression tree/stepwise linear discriminant (CART/SLD) model described by Gleason et al. (1994). The CART/SLD model uses a dew point depression (air temperature minus dew point temperature; DPD) threshold of 3.7 °C above which no dew occurs. If the wind speed is greater than 2.5 m s⁻¹ and RH is less than 87.8%, dew neither occurs. If wind speed is less than 2.5 m s⁻¹ or RH is greater than 87.8% an equation is applied to determine if dew occurs or not.

Finally, we tested a new empirical model approach by taking a limit for the difference between the saturated specific humidity at the surface, $q_s(T_{\text{surf}})$, and the actual specific humidity at 1.8 m, $q(T_{1.8\text{ m}})$. We call this model, the 'delta q' model in the rest of this paper. The main assumption in this model approach is that water vapor condenses at the surface when the difference between the saturated specific humidity at the surface and the actual specific humidity at the surface, which is assumed to be equal to the specific humidity at 1.8 m, becomes smaller than a chosen limit (here chosen as 0 g kg⁻¹).

All the empirical models automatically include the rainfall events because they contain moisture parameters (RH or specific humidity).

4.3 Results

4.3.1 Meteorological conditions

In this study, a period of 39 days (from 23 March till 30 April 2005) is investigated. In general, the period was characterized by sunny and dry weather with clear nights, but there were also some rainfall events during this period. Figure 4.1 shows the temperature at 1.8 m (upper panel), the wind speed at 2 m (middle panel) and the global radiation at 1.8 m (lower panel). A depression brought cold, rainy and windy weather in the period between 6 and 10 April 2005. All together, these weather conditions are quite normal for the spring season in this region.

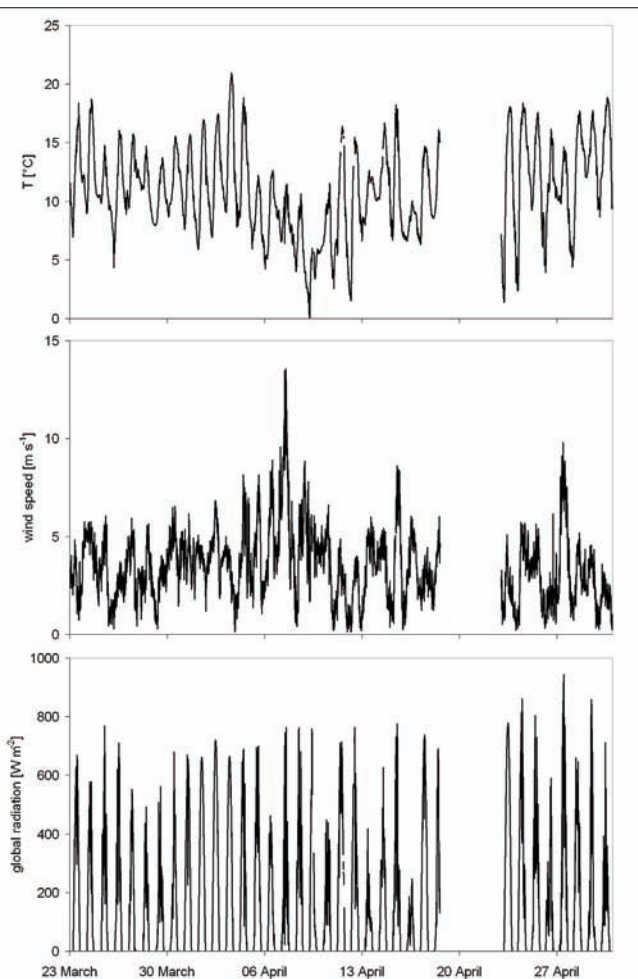


Figure 4.1. Meteorological conditions temperature at 1.8 m (upper panel), wind speed at 2 m (middle panel) and global radiation at 1.8 m (lower panel) from 23 March till 30 April 2005. No data are available for 19-22 April.

4.3.2 Measurements and model results

Figure 4.2 shows a time series of 5 successive days for the three leaf wetness measurement devices, i.e., the grid sensor at 0.1 m, the grid sensor at 1.0 m and the average of the four clip sensors. The picture shows how the sensors react on dew formation as well as on rainfall. The grid sensor at 0.1 m reacts rather quickly to dew formation, while the signal of the grid sensor at 1.0 m increases more gradually. The signal of the clip sensors is much smaller and therefore less clear in dew situations. Although the start of the dew formation is almost equal for all the measurement devices, the evaporation of the dew starts first at the grid sensor at 1.0 m, while the signal of the grid sensor at 0.1 m and the clip sensors typically start to decrease about 1.5-2 hours later. In case of a rainfall event (e.g., 13 April), all sensors react quickly with a relatively strong signal.

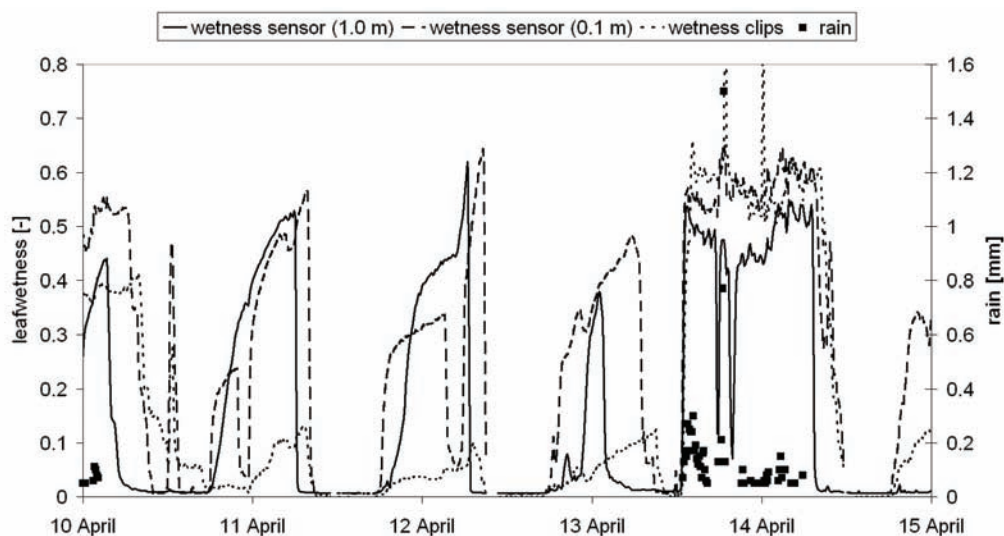


Figure 4.2. Time series (5 days) of leaf wetness by three different measurement devices: grid sensor at 1.0 m (solid line), grid sensor at 0.1 m (dashed line) and average of four clip sensors (dotted line). The squares represent the observed rain amounts per 10 minutes.

For data analysis the signals are made dichotomous, which means that they get value 1 if there is a signal and they get value 0 if there is no signal. Figure 4.3 shows the daily averaged dichotomous signal of the three devices for the period between 23 March and 30 April 2005. By averaging, a clear daily course in the leaf wetness signal is obtained which is mainly caused by dew formation, as rain events are randomly scattered over the days and therefore only contribute to the height and 'noise' of the averaged signal. Remarkable is the time difference in the dew evaporation (drying) process in the morning between the grid sensor at 1.0 m and the other two devices near the surface. There is no clear time difference in the dew formation process, although it seems that at 1.0 m height dew starts to form somewhat later than at the surface. The grid sensor at 0.1 m most clearly shows the onset of dew in the afternoon (with a strong increase in the signal) and the dew evaporation in the morning (with a strong decrease in the signal). It appears that the clip sensors remain wet for about 0.5 hour longer than the grid sensor at 0.1 m. This might be due to the position of the clip sensors within the grass canopy, since the grid sensor is attached just above the

grass canopy. However, the dichotomous signals of the clip sensors and the wetness sensor at 0.1 m generally compare well.

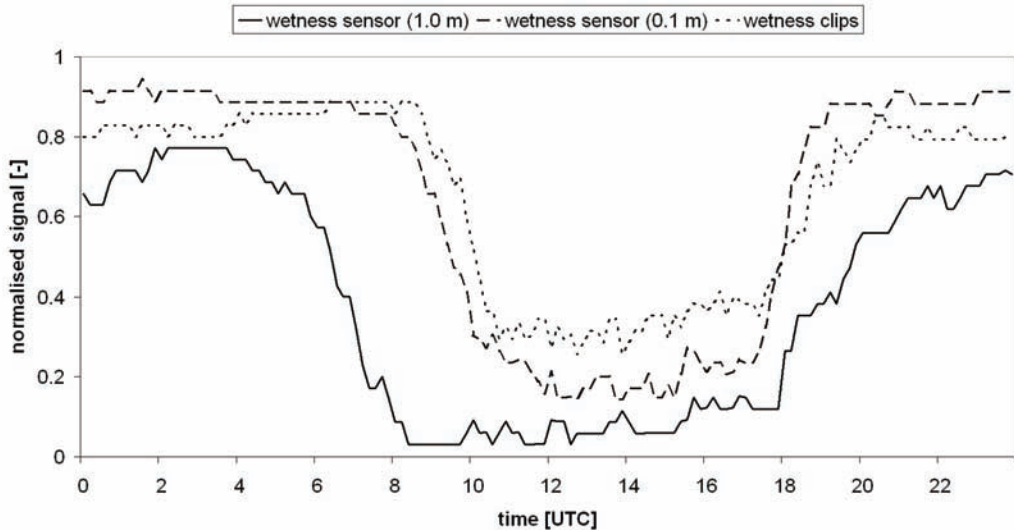


Figure 4.3. Daily averaged signal of the three wetness measurement devices for the period between 23 March till 30 April 2005 (39 days); the grid sensor at 1.0 m (solid line), grid sensor at 0.1 m (dashed line) and the average of four clip sensors (dotted line).

In Figure 4.4 the leaf wetness durations (LWD) of the dichotomous signal of the three devices is shown for each day in the period. The LWD is the sum of the wet 10-minute measurements between 16 UTC on the previous day and 16 UTC on the present day. The figure nicely shows that in general the LWD of the grid sensor at 1.0 m is shorter than the two sensors near the surface. The grid sensor at 0.1 m and the clip sensors give similar

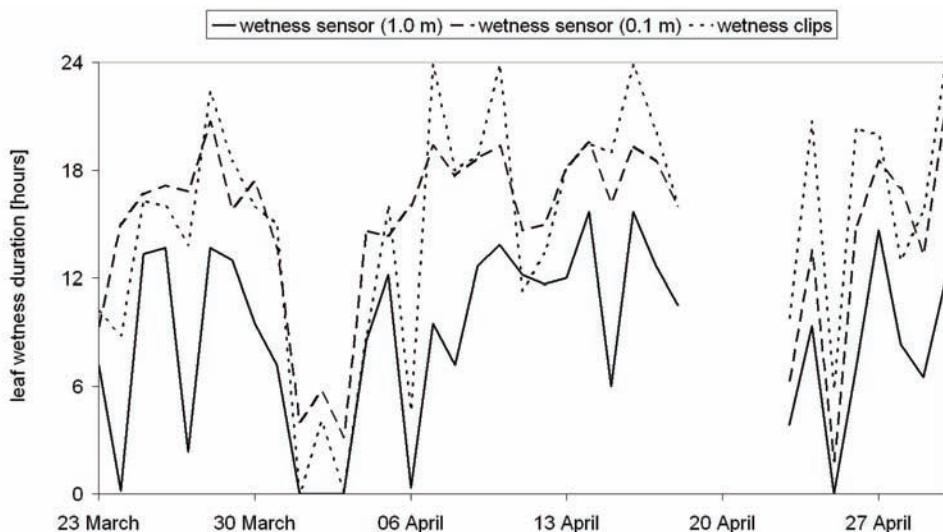


Figure 4.4. Leaf wetness duration (in hours) of the grid sensor at 1.0 m (solid line), the grid sensor at 0.1 m (dashed line) and the average of four clip sensors (dotted line) from 23 March till 30 April 2005.

results, although the LWD of the clip sensors shows more variability than the LWD of the grid sensor. The grid sensor at 0.1 m is chosen as a reference for the model intercomparison study, because of its more practical use and its stable signal.

Figure 4.5 shows the results of all leaf wetness models as well as the measured leaf wetness in a time series plot for the whole period between 23 March and 30 April 2005. It is difficult to draw any conclusions from these kinds of plots. Therefore, the objective method of contingency tables is used to validate the different models. This method was originally developed for the validation of rain forecasting, but also appears to be useful for the validation of leaf wetness prediction models (Nurmi, 2003) as will be shown hereafter.

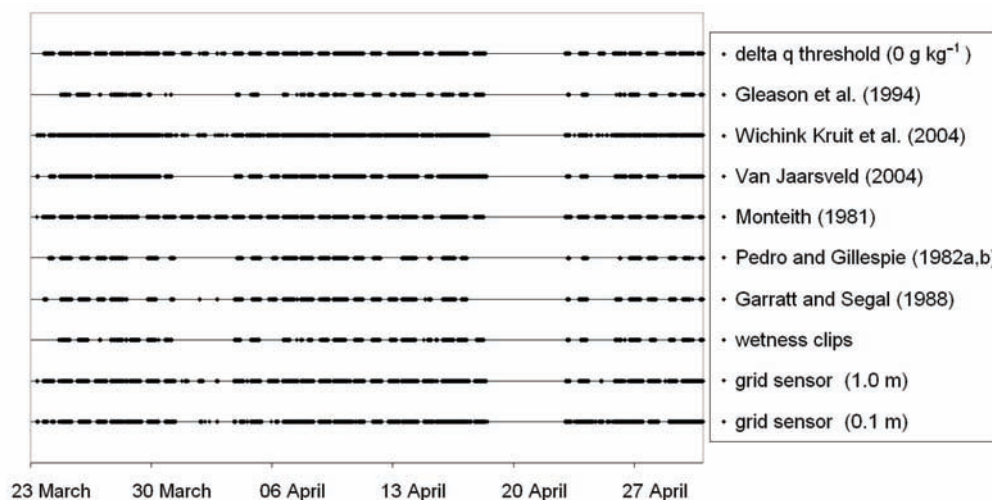


Figure 4.5. Time series of the surface wetness by three measurement devices, three physical and four empirical leaf wetness models for the period between 23 March and 30 April 2005. Each horizontal line represents the dichotomous signal of a measurement device or model (blanc means 'no signal'; black means 'signal').

A change in the threshold values in the empirical models will result in different statistical scores. By changing the RH threshold and the delta q threshold, an optimum threshold value is derived for both variables. Figure 4.6 shows the optimizing plots for the RH threshold model and the delta q model. The bias (the modeled frequency divided by the observed frequency) is displayed on the x-axis and the proportion correct is displayed on the y-axis. The bias should be close to 1, while the proportion correct should be as high as possible. For the RH threshold, an optimized value of 71% is found, while the delta q model has an optimum value of 1.9 g kg⁻¹. The optimization curve of the delta q model is systematically higher than the one of the RH threshold model, which means that this model systematically gives better results. This is the result of the surface temperature that is included in the delta q approximation. The model of Wichink Kruit et al. (2004) and Gleason et al. (1994) are more difficult to optimize. Therefore only the RH thresholds in these two models are adapted to the optimized RH threshold of Figure 4.6.

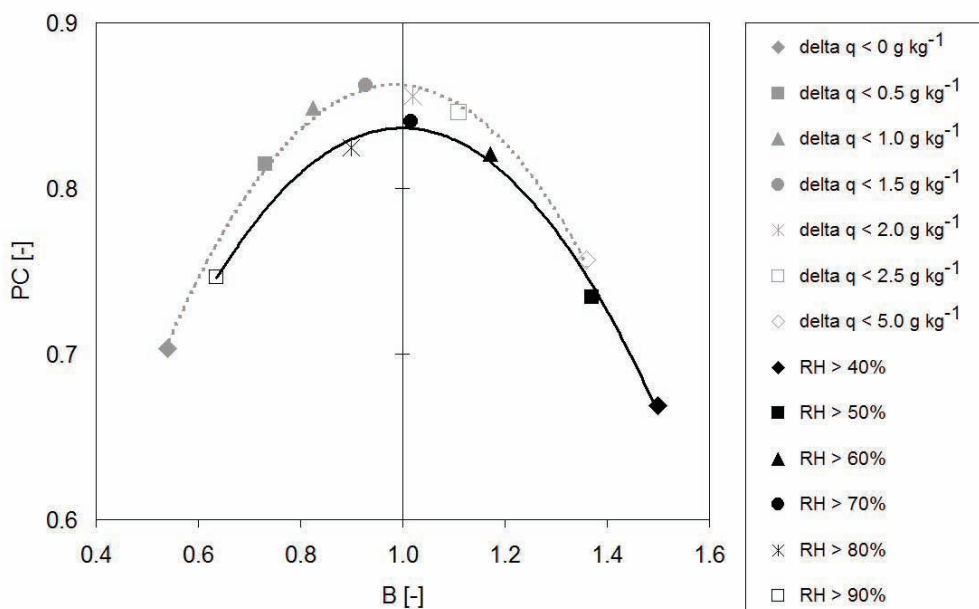


Figure 4.6. Statistical scores 'proportion correct' (y-axis) and 'bias' (x-axis) for different RH thresholds (black symbols and black solid line) and different thresholds for delta q (gray symbols and gray dotted line).

In Table 4.2 the statistical scores are shown for the different measurement devices as well as for the different physical and empirical models. Both the original and the optimized thresholds are shown. The scores are calculated relative to the grid sensor at 0.1 m, which is used as a reference.

Leaf wetness is observed 64 % of the time (Po/n) with the grid sensor at 0.1 m. With the grid sensor at 1.0 m this is only 38 % of the time, while the clip sensors measure wetness 65 % of the time. Clip sensors measure leaf wetness for a longer time period than the grid sensor at 0.1 m, because the clips are attached on individual grass leaves within the vegetation layer, where it remains wet for a longer time. The clips 'overestimate' leaf wetness in 8% of the cases, but they also 'underestimate' leaf wetness in 7% of the cases, which finally results in a small positive bias ($B = 1.02$). The grid sensor at 1.0 m systematically underestimates leaf wetness (26 % of the time), while it never overestimates leaf wetness, which finally results in a bias much smaller than 1 ($B = 0.59$).

The model of Garratt and Segal (1988) and the model of Pedro and Gillespie (1982a,b) estimate leaf wetness 43% and 39% of the time (Pm/n) respectively. They never estimate leaf wetness when it did not occur, but they also fail to estimate leaf wetness in 21% and 25% of the cases, which results in bias values of 0.67 and 0.61, respectively. The potential dew model of Monteith (1981) estimates leaf wetness 67% of the time. Leaf wetness does not occur in 9% of the predicted cases, but the model also fails to estimate leaf wetness in 6% of the cases, which finally results in a small positive bias.

The empirical leaf wetness models all underestimate leaf wetness. There are hardly any situations in which these models predict leaf wetness wrongly, but the models also fail to

estimate leaf wetness in 19 - 30% of the cases. This results in biases in the range between 0.54 and 0.74.

The modeled frequency (P_m/n) is equal to the observed frequency (P_o/n) with the optimized RH threshold model and the optimized delta q model, 64%. However, there is an overestimation of leaf wetness with both models (8 and 7% respectively), but this overestimation is equal to the underestimation of leaf wetness. Since the models were optimized, the bias is equal to 1 for both models, which is expected. Using the optimized RH value in Wichink Kruit et al. (2004), a small overestimation (65%) is observed, while using the optimized RH value in Gleason et al. (1994), a relatively large underestimation of leaf wetness is still obtained (46%).

In Figure 4.7 the bias (B) of all models is plotted on the x-axis and the proportion correct (PC) is plotted on the y-axis. The statistical scores for the physical models are represented by crosses, the empirical models by open symbols and the optimized empirical models by closed symbols. As B should be close to 1 and PC should be as high as possible (also close to 1), this figure shows that the optimized delta q model (closed circle) is the best way to model leaf wetness. This model has a B value of 1 and the highest PC value of all models, i.e., 0.86. The optimized RH threshold of 71% (closed square) also gives very good results (PC = 0.84), like the model of Wichink Kruit et al. (2004) using the optimized RH threshold (PC = 0.84). From the models that were not optimized, the model from Monteith (1981) gives the best results; it has a B value of slightly larger than 1 and it also gives a very high PC score of 0.85. The other two physical models underestimate leaf wetness and give considerably lower PC scores, i.e., 0.75 for the Pedro and Gillespie (1982a,b) model and 0.78 for the Garratt and Segal (1988) model. Also the empirical leaf wetness models before optimization give a large underestimation of leaf wetness duration and lower PC scores (0.70 - 0.79).

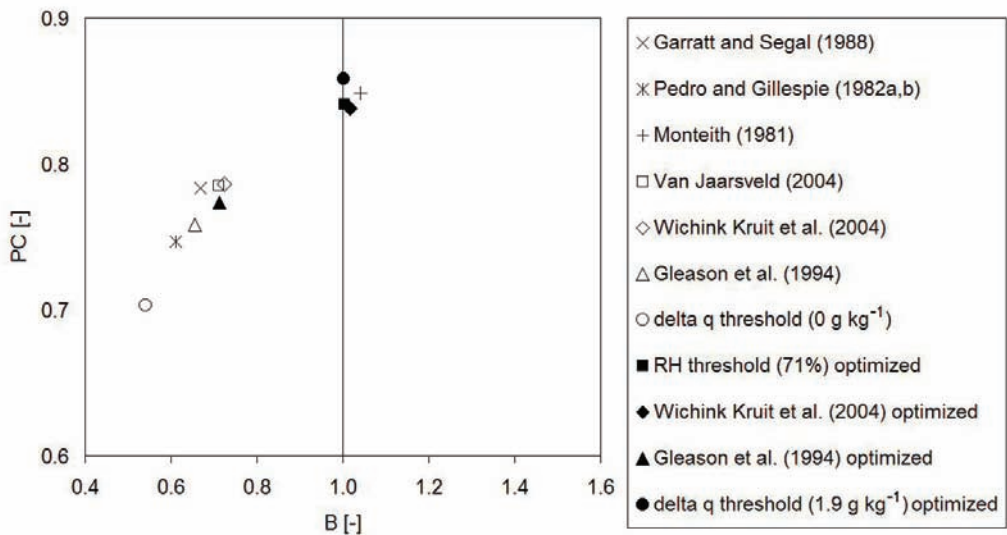


Figure 4.7. Statistical scores 'proportion correct' (y-axis) and 'bias' (x-axis) for the different leaf wetness models.

Table 4.2. Derived statistical scores from contingency tables.

score	measurement devices			physical leaf wetness models				empirical leaf wetness models				optimized empirical leaf wetness models			
	grid sensor 0.1 m = Reference	grid sensor 1.0 m	wetness clips	Garratt and Segal (1988)	Pedro and Gillespie (1982,a,b)	Monteith (1981)	RH threshold (87%) Van Jaarsveld (2004)	Wichink Kruit et al. (2004)	Gleason et al. (1994)	delta q threshold (0 g kg ⁻¹)	RH threshold (71%) optimized	Wichink Kruit et al. (2004) optimized	Gleason et al. (1994) optimized	delta q threshold (1.9 g kg ⁻¹) optimized	
hit	64%	38%	57%	43%	39%	58%	44%	45%	41%	35%	57%	44%	57%		
false alarm	0%	0%	8%	0%	0%	9%	1%	1%	1%	0%	9%	2%	7%		
miss	0%	26%	7%	21%	25%	6%	20%	20%	23%	30%	8%	21%	7%		
correct rejection	36%	36%	28%	36%	36%	27%	34%	34%	35%	36%	27%	34%	29%		
observed wetness	64%	38%	65%	-	-	-	-	-	-	-	-	-	-		
modeled wetness	-	-	-	43%	39%	67%	46%	46%	42%	35%	65%	46%	64%		
B	1.00	0.59	1.02	0.67	0.61	1.04	0.71	0.72	0.66	0.54	1.02	0.71	1.00		
PC ¹	-	-	-	0.78	0.75	0.85	0.79	0.79	0.76	0.70	0.84	0.77	0.86		
POD ²	-	-	-	0.67	0.61	0.90	0.69	0.70	0.64	0.54	0.88	0.68	0.89		
FAR ³	-	-	-	0.00	0.00	0.13	0.03	0.04	0.02	0.00	0.13	0.05	0.11		
ETS ⁴	-	-	-	0.41	0.35	0.50	0.41	0.41	0.37	0.29	0.48	0.39	0.53		
HSS ⁵	-	-	-	0.58	0.52	0.66	0.58	0.58	0.54	0.45	0.65	0.56	0.69		

¹ proportion correct

² probability of detection

³ false alarm ratio

⁴ equitable threat score

⁵ Heidke skill score.

Figure 4.8 shows two other statistical scores, the probability of detection (POD) on the y-axis and the false alarm ratio (FAR) on the x-axis. As the POD should be as high as possible and the FAR should be as small as possible, the models should be in the upper left corner of Figure 4.8. Again, the optimized delta q model gives best results, followed by the model of Monteith (1981), the optimized RH threshold and the optimized model of Wichink Kruit et al. (2004). The models of Garratt and Segal (1988), Pedro and Gillespie (1982a,b) and the other empirical models have lower POD scores, but they also have a very low FAR. This means that if these models predict leaf wetness, it will very likely also occur in reality. However, leaf wetness occurs more than these models predict, which leads to a large underestimation ($POD < 1$).

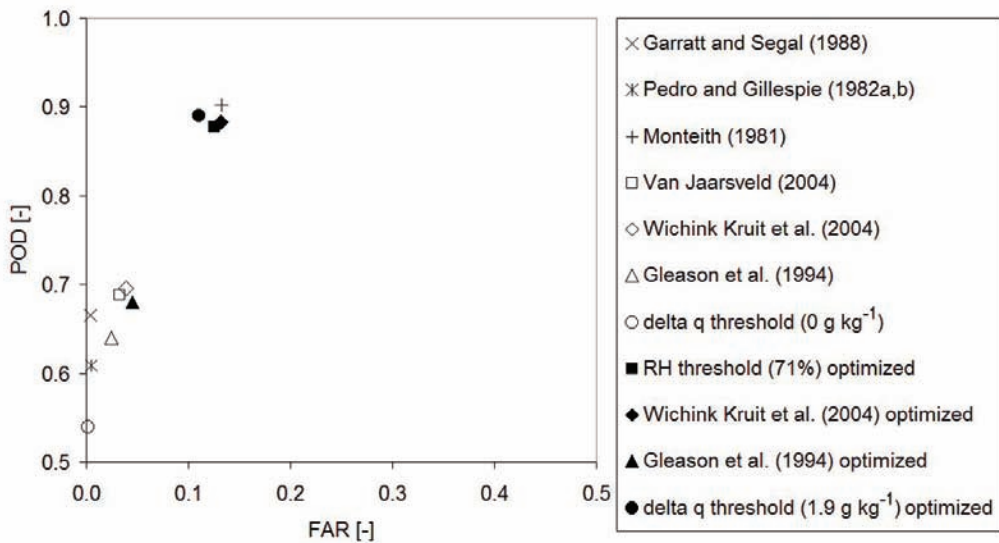


Figure 4.8. Statistical scores 'probability of detection' (y-axis) and 'false alarm ratio' (x-axis) for the different leaf wetness models.

Figure 4.9 shows two other important statistical scores, the equitable threat score (ETS) on the x-axis and the Heidke skill score (HSS) on the y-axis. This figure gives some kind of a ranking on the basis of two important statistical scores, which both need to be as high as possible. This figure confirms that the optimized delta q model gives the highest HSS (0.69) as well as the highest ETS (0.53). The potential dew model of Monteith (1981) also gives very good results, like the optimized RH threshold of 71% and the optimized model of Wichink Kruit et al. (2004).

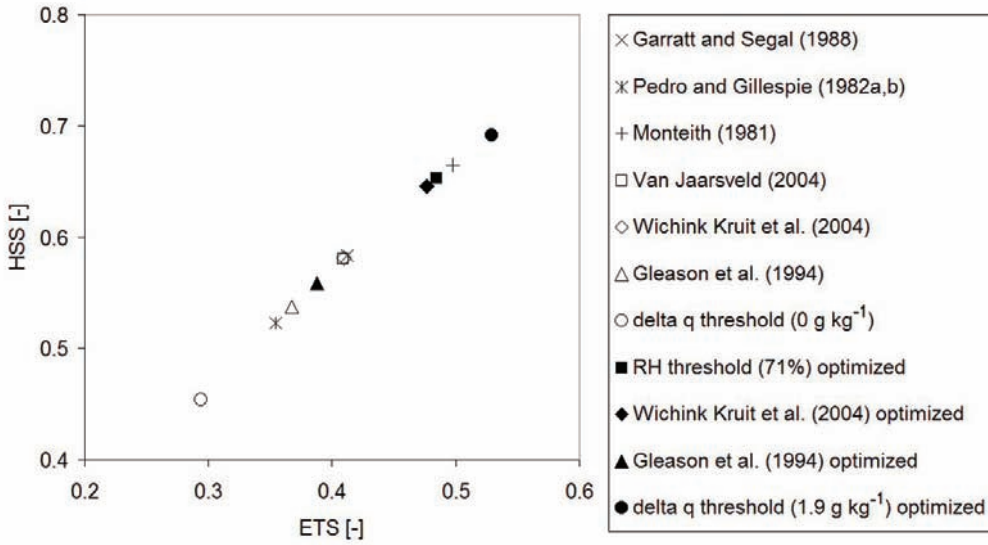


Figure 4.9. Statistical scores 'Heidke skill score' (y-axis) and 'equitable threat score' (x-axis) for the different leaf wetness models.

4.4 Discussion and conclusions

From the comparison between the different leaf wetness sensors follows that the grid sensor (at 0.1 m) is preferred. The signal of the grid sensors is rather continuous, while the clip sensors sometimes generate more noise and need to be averaged to get a representative signal for the whole vegetation. The strength of the signal of the clip sensors strongly depends on the contact area between the clips with the leaves and the place where they are attached to the leaves. Besides, the clips need to be moved from time to time as the grass grows quickly in spring and summer, which makes them rather labor-intensive. As the clip sensors measure electrical conductance, they provide information about leaf wetness, but also about the stomatal opening of leaves. The latter is not considered in this paper, but clips may still be very useful in other research areas.

The measurement height and angle of the grid sensor are of great importance for the leaf wetness duration (Lau et al., 2000; Sentelhas et al., 2004a). One of the reasons for this is that turbulence plays an important role in the drying process and at 1.0 m height there is more turbulence than closer to the surface. As the sun rises in the morning, turbulence increases and the drying process quickly starts at 1.0 m height. After some time, the grid sensor at 0.1 m also starts to dry up followed by the clip sensors that are attached in the vegetation. The equal slopes of the signals indicate that the drying speed is equal for all the sensors. The dew formation process (onset of leaf wetness) seems to be observed best by the grid sensor at 0.1 m with a strong increase of the signal. Similar results were also found by Sentelhas et al. (2004a) for turfgrass and corn.

Concerning the model prediction of leaf wetness, the physical models from Garratt and Segal (1988) and Pedro and Gillespie (1982a,b) both underestimate leaf wetness. The potential dew model of Monteith (1981) slightly overestimates leaf wetness, but the

statistical bias and proportion correct scores are much closer to 1. The empirical models all underestimated leaf wetness at the grass surface, as they were originally not derived for this kind of surface. However, after optimization with the statistical proportion correct and bias scores, the optimized delta q threshold (1.9 g kg^{-1}) model and the optimized RH threshold (71%) model gave very good results. Because only the optimized RH threshold was adapted in the empirical models from Wichink Kruit et al. (2004) and Gleason et al. (1994), these two models produced less good results than the simple optimized RH and delta q threshold models.

For application in atmospheric transport models, the availability of variables determines which model can be used. From the non-optimized models, which might be applied universally, the potential dew model from Monteith (1981) gives remarkable good results. However, the model needs the surface energy budget (net radiation and soil heat flux) as an input variable, which is not generally available in atmospheric transport models. If RH, pressure and temperature at reference height and surface temperature are known, this study showed that the delta q model, when optimized locally, gives the best estimations of leaf wetness. Usually, atmospheric transport models only have RH available and they can therefore only use the RH threshold model.

For good leaf wetness estimations, it appears to be essential to optimize the RH threshold and the delta q threshold to the local conditions. The RH threshold might be dependent on vegetation type, as the RH threshold of 87% from Van Jaarsveld (2004) was derived for pine forest, while the optimized RH threshold of 71% from this study is derived for agricultural grassland. More research is recommended to derive and optimize RH and delta q thresholds for different vegetation types.

5 Modeling the surface-atmosphere exchange of ammonia

This chapter has been published as Wichink Kruit R.J., Van Pul W.A.J., Sauter F.J., Van den Broek M., Nemitz E., Sutton M.A., Krol M.C., Holtslag A.A.M., 2010. Modeling the surface-atmosphere exchange of ammonia. Atmospheric Environment 44, 945-957.

Abstract

New parameterizations for surface-atmosphere exchange of ammonia are presented for application in atmospheric transport models and compared with parameterizations of the literature. The new parameterizations are based on a combination of the results of three years of ammonia flux measurements over a grassland canopy (dominated by *Lolium perenne* and *Poa trivialis*) near Wageningen, the Netherlands and existing parameterizations from literature. First, a model for the surface-atmosphere exchange of ammonia that includes the concentration at the external leaf surface is derived and validated. Second, a parameterization for the stomatal compensation point (expressed as Γ_s , the ratio of $[\text{NH}_4^+]/[\text{H}^+]$ in the leaf apoplast) that accounts for the observed seasonal variation is derived from the measurements. The new, temperature-dependent Γ_s describes the observed seasonal behavior very well. It is noted, however, that senescence of plants and field management practices will also influence the seasonal variation of Γ_s on a shorter timescale. Finally, a relation that links Γ_s to the atmospheric pollution level of the location through the 'long-term' NH_3 concentration in the air is proposed.

5.1 Introduction

Quantifying the magnitude of ammonia fluxes between vegetation and the atmosphere is of great interest in assessing the effects of regional atmospheric pollution. In areas with intensive agriculture, such as Europe and eastern North America, atmospheric inputs of reduced nitrogen (NH_x) (the sum of gaseous ammonia, NH_3 , and ammonium aerosol, NH_4^+) by dry and wet deposition may substantially contribute to acidification and nitrogen eutrophication of semi-natural ecosystems (Fowler et al., 1989; Bobbink et al., 1998; Pitcairn et al., 1998).

Estimates of NH_3 dry deposition fluxes to semi-natural plant communities are therefore directly relevant as a component in comparing pollutant inputs with 'critical loads' for vegetation and soils (Pitcairn et al., 1998). Thus, to quantify regional atmospheric budgets of NH_3 , it is important to quantify the net NH_3 flux for all major vegetation types. While semi-natural vegetation usually provides an efficient sink for atmospheric NH_3 , limited dry deposition, or even emission, of NH_3 is often observed above agricultural surfaces such as arable croplands and managed grassland (Dabney and Bouldin, 1990; Sutton et al., 1993a,b; Schjoerring et al., 1993).

The net NH_3 exchange between vegetation and the atmosphere can be calculated with different types of atmospheric resistance models. Canopy resistance (R_c) deposition models (e.g., Erisman et al., 1994) assume zero concentration at the surface and therefore treat plant surfaces exclusively as sinks for atmospheric NH_3 . By contrast, canopy compensation point (χ_c) models (e.g., Sutton et al., 1995a; Nemitz et al., 2001) allow bi-directional NH_3 fluxes by considering non-zero NH_3 concentrations within or at the surface of the canopy.

In both types of models the flux towards the external leaf surface or cuticles is very important. This pathway is parameterized by the external leaf surface, or cuticular resistance, R_w . Many studies have shown that R_w depends mainly on relative humidity (or vapor pressure deficit) (Sutton and Fowler, 1993; Nemitz et al., 2001), atmospheric ammonia concentration (Fowler et al., 1998; Jones et al., 2007a,b), temperature (Smith et al., 2000; Neiryneck et al., 2005) and leaf surface chemistry, for example due to the presence of SO_2 , HNO_3 or base cations (Erisman and Wyers, 1993; Flechard et al., 1999; Nemitz et al., 2001; Neiryneck et al., 2005; Burkhardt et al., 2009). In the Unified EMEP model, a preliminary parameterization that incorporates the effects of T , RH and SO_2 co-deposition, by combining response curves from different sources is currently included (Simpson et al., 2003), but not many measurements were available for the validation of this parameterization. In addition, this earlier parameterization did not respond to the atmospheric NH_3 concentration itself. It should be noted that ammonia models have included concentrations at the external leaf surface previously, using a time varying dynamic approach (χ_d) for adsorption/desorption (Sutton et al., 1998; Flechard et al., 1999; Neiryneck and Ceulemans, 2008). The approach for χ_w tested here contrasts with this in providing a simplified steady-state parameterization.

Another important parameter in the canopy compensation point models is the stomatal compensation point (χ_s). This is particularly true for arable crops and grasslands with a high nitrogen status. These crops have been shown to be net sources of ammonia during the growing season as well as during senescence (Farquhar et al. 1980; Sutton et al. 1995a; Nemitz et al., 2000; Wichink Kruit et al., 2007). The stomatal compensation point is defined as the ammonia concentration within the stomata, which forms in response to the temperature dependent Henry and solubility equilibrium with the concentration of NH_4^+

and H^+ (i.e., pH) in the apoplastic fluid. If stomatal exchange is the only exchange pathway (e.g., under very dry conditions, when external leaf surfaces provide inefficient sinks) no net exchange with the atmosphere takes place if the atmospheric concentration equals the compensation point (Farquhar et al., 1980). Some studies have shown that the apoplastic ammonium/hydrogen ratio ($\Gamma_s = [NH_4^+]/[H^+]$) depends on the nutrient (mainly NH_4^+ and NO_3^-) availability (Schjoerring et al., 2000; Mattsson and Schjoerring, 2002). Other studies showed that Γ_s also depends on the local management practice (Milford et al., 2001a) and that Γ_s has a seasonal variability linked to plant phenology (Husted and Schjoerring, 1995; Van Hove et al., 2002; Wichink Kruit et al., 2007; Neiryneck and Ceulemans, 2008).

In this paper, a model for surface-atmosphere exchange of ammonia is derived that includes the concentration at the external leaf surface, χ_w . The model is validated with flux measurements made on a non-fertilized grassland site in the Netherlands described in Wichink Kruit et al. (2007). The flux measurements are also used to explore the seasonal cycle in Γ_s and to derive a parameterization as a function of temperature. The complete model in which the new R_w , χ_w and Γ_s parameterizations are included is tested versus measurement data. Subsequently, the model is compared with two other model parameterizations of R_w currently used (keeping the parameterizations of χ_s and R_s the same for all models), i.e., the parameterization of R_w used in the DEPAC module in OPS (Operational Priority Substances model) at RIVM (Van Jaarsveld, 2004) and the parameterization of R_w used in the Unified EMEP model (Simpson et al., 2003).

Finally, a first attempt is made to link Γ_s to the pollution level of a location through the 'long-term' ammonia concentration from reported Γ_s values and concentrations in literature. A generally applicable parameterization is proposed that includes both the seasonal trend in Γ_s (through a temperature function) as well as the pollution level of the location (through a 'long-term' ammonia concentration).

5.2 Observations

Long-term ammonia concentration profiles were measured using the GRAdient Ammonia-High Accuracy- Monitor (GRAHAM; Wichink Kruit et al., 2007), a more advanced version of the AMANDA (a continuous rotating wet denuder analyzer; Wyers et al., 1993). The measurements were made between June 2004 and December 2006 at the 'Haarweg' meteorological observatory west of Wageningen in The Netherlands (51° 58' 18" N; 5° 38' 30" E; 6.8 m above mean sea level). The measurement site and its homogeneous surrounding are located on a heavy clay soil. Neither mineral nor organic fertilizers were applied at the measurement site for at least 10 years. The vegetation predominantly consists of temperate humid perennial ryegrass (*Lolium perenne* L.) and rough bluegrass (*Poa trivialis*). Continuous measurements of air and soil temperature, pressure, air humidity, radiation, wind direction and wind speed are available at the meteorological observatory (webpage of the meteorological observatory: www.maq.wur.nl). Leaf surface temperature, T_s , is derived from the outgoing long-wave radiation measured by a pyrgeometer (type Kipp en Zonen CG1). SO_2 concentrations were not directly measured in Wageningen, but are derived from nearby SO_2 concentration measurements at 2 locations in the Dutch air quality monitoring network by linear interpolation. Because SO_2 concentrations are generally low in the Netherlands and there are no significant nearby sources, we consider the derived SO_2 concentration appropriate for our purpose.

The ammonia fluxes are calculated using the aerodynamic flux-gradient method. This method requires the measurement of ammonia concentrations at several heights in the surface layer to provide vertical gradients. These vertical gradients combined with turbulence parameters then provide turbulent fluxes. The ammonia flux, F_{NH_3} , ($\mu\text{g m}^{-3}$) is calculated here as:

$$F_{NH_3} = -ku_* \frac{[\chi_2 - \chi_1]}{\left[\ln \left(\frac{z_2 - d}{z_1 - d} \right) - \Psi_{H_2} + \Psi_{H_1} \right]} \quad (5.1)$$

where k ($=0.4$) is the Von Karman constant, u_* (m s^{-1}) is the friction velocity, z_2 and z_1 (m) are the heights at which the atmospheric ammonia concentrations χ_2 and χ_1 ($\mu\text{g m}^{-3}$) are measured, d (m) is the zero plane displacement height, and ψ_H is the integrated stability correction function for sensible heat at each height, which is assumed to be equal to the integrated stability correction function for ammonia. Stability corrections were calculated according to functions proposed by Beljaars and Holtslag (1991) using the parameter $(z-d)/L$, where L (m) is the Monin-Obukhov length. Turbulence parameters (u_* and L) were measured with a Campbell Scientific 3-D sonic anemometer (type CSAT3) mounted at 3.3 m height. Note that the flux-gradient theory assumes horizontal homogeneous conditions and no flux divergence (e.g. by chemical reactions).

The analysis of Wichink Kruit et al. (2007) focused on two contrasting example periods in 2004: a warm and sunny summer period (between 18 July and 15 August 2004) and a cool and cloudy autumn period (between 23 September and 23 October 2004). However, the overall data coverage over the three years was rather scattered due to technical problems (Van Pul et al., 2008; Wichink Kruit et al., 2009), which made it impossible to compare full budgets for the three individual years. Nevertheless, the data are considered appropriate to study the exchange processes between the vegetation and the atmosphere. Furthermore, the randomly scattered data still gives us the opportunity to study the seasonal behavior of the stomatal compensation point (χ_s) and gamma (Γ_s).

5.3 Model parameterizations for NH_3 exchange with vegetation

Resistance models applied to the plant/atmosphere exchange of NH_3 have been reviewed by Sutton et al. (1998) and Nemitz et al. (2001). For this reason, only a brief overview is presented here. For short dense vegetation, like the grassland canopy in this study, the single-layer or 'big-leaf' approach can be applied. There is no pathway for NH_3 exchange with soil in this model approach, because the canopy is assumed to cover the soil surface completely. These single-layer models can be divided into two categories (see Figure 5.1):

1. Canopy resistance models (Figure 5.1a and 5.1b) assume zero surface concentrations, often applied to model dry deposition of NH_3 over natural and semi-natural ecosystems (Erisman and Wyers, 1993; Sutton et al., 1993a; Duyzer et al., 1994).
2. Canopy compensation point models (Figure 5.1c, 5.1d, and 5.1e) allow for bi-directional fluxes and are generally required to model plant/atmosphere exchange of NH_3 over agricultural crops and intensively managed grasslands (Sutton et al., 1995a; Sutton et al., 1998; Nemitz et al., 2001).

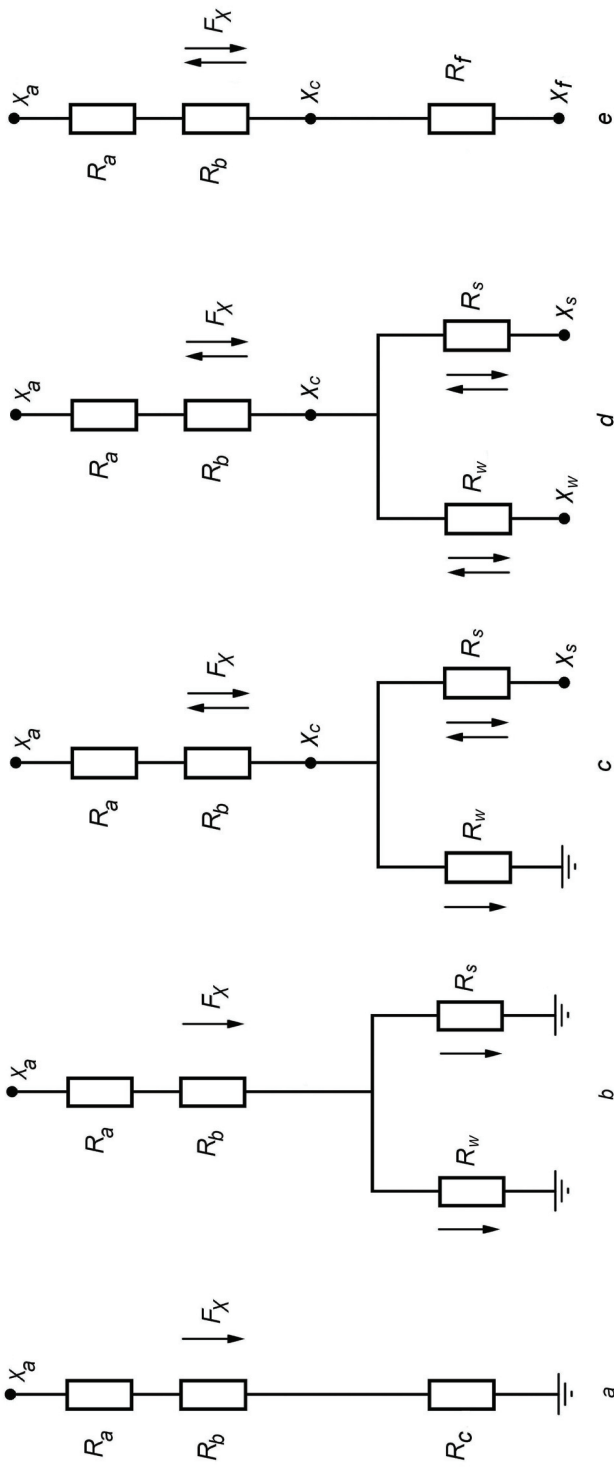


Figure 5.1. Examples of current single-layer models of plant-atmosphere exchange of NH_3 . (a) simple canopy resistance (R_c) model with the canopy resistance subdivided into a stomatal and a non-stomatal (or external leaf surface) pathway. (b) simple canopy resistance (R_c) model with the canopy resistance subdivided into a stomatal and a non-stomatal (or external leaf surface) pathway. (c) 'traditional' canopy compensation point (x_s - R_w) model, with a bi-directional pathway to the stomata and a deposition pathway towards the external leaf surface (or cuticle). (d) 'modified' canopy compensation point model (x_s - x_w) with two bi-directional pathways (to both stomata and cuticles). (e) 'effective' canopy compensation point model. The variables in the different models are explained in the text.

Canopy resistance models of dry deposition of ammonia tend to describe R_c (Figure 5.1a) as equivalent to a network of parallel resistances, with the main pathways described by the stomatal and external leaf surface resistances to gaseous uptake (Figure 5.1b). Such models fail when the surface concentrations differ from zero and gases can be emitted by plant canopies through physiological processes, as is the case for NH_3 . In such situations, the use of canopy compensation points (Figure 5.1c and 5.1d) provides an alternative to canopy resistance models. In Figure 5.1c the 'traditional' canopy compensation point model (χ_s - R_w model) is shown as introduced by Sutton et al. (1995a), with a bi-directional pathway to the stomata. (Note that the canopy resistance model shown in Figure 5.1b is a special case of the model that is shown in Figure 5.1c, with the stomatal compensation point (χ_s) set to zero). Figure 5.1d shows a 'modified' canopy compensation point model with an additional bi-directional pathway to the external leaf surface labeled as χ_s - χ_w model, as tested here. This model approach is similar to the canopy compensation point - cuticular capacitance model (χ_c - C_d model) introduced by Sutton et al. (1998), but the χ_s - χ_w model does not treat the water layer as a dynamically changing capacitor. Instead, empirical relations are derived here to estimate the atmospheric ammonia concentration that would be in Henry equilibrium with the concentration of the dissolved ammonia concentration at the external leaf surface, χ_w . This parameter will be called "the atmospheric ammonia concentration at the external leaf surface" hereafter.

In the χ_s - χ_w model, the ammonia flux, F_{NH_3} (in $\mu\text{g m}^{-2} \text{s}^{-1}$), can be calculated in analogy with the simplified representation of the χ_s - χ_w model shown in Figure 5.1e, which is only used in mass balance calculations:

$$F_{\text{NH}_3} = \frac{\chi_f - \chi_a(z-d)}{R_{\text{total}}} \quad (5.2)$$

$$R_{\text{total}} = R_a(z-d) + R_{b,\text{NH}_3} + R_f \quad (5.3)$$

$$\frac{1}{R_f} = \frac{1}{R_w} + \frac{1}{R_s} \quad (5.4)$$

$$\frac{(\chi_f - \chi_c)}{R_f} = \frac{(\chi_w - \chi_c)}{R_w} + \frac{(\chi_s - \chi_c)}{R_s} \quad (5.5a)$$

Eq. 5.5a can be simplified (using Eq.5.4) as:

$$\frac{\chi_f}{R_f} = \frac{\chi_w}{R_w} + \frac{\chi_s}{R_s} \quad (5.5b)$$

where:

- $\chi_a(z-d)$ is the atmospheric ammonia concentration at a specified height above displacement height (in our case $z-d = 1$ m) in $\mu\text{g m}^{-3}$,
- χ_s is the atmospheric ammonia concentration within the stomata or the stomatal compensation point in $\mu\text{g m}^{-3}$,
- χ_w is the atmospheric ammonia concentration at the external leaf surface in $\mu\text{g m}^{-3}$,

- χ_f is the effective atmospheric ammonia concentration of the foliage (weighted average of separate concentrations) in $\mu\text{g m}^{-3}$,
- R_{total} is the total resistance in s m^{-1} ,
- $R_a(z-d)$ is the aerodynamic resistance at the specified height above displacement height in s m^{-1} ,
- R_{b,NH_3} the quasi-laminar boundary-layer resistance for ammonia in s m^{-1} ,
- R_s is the stomatal resistance in s m^{-1} ,
- R_w is the external leaf surface (or cuticular) resistance in s m^{-1} , and
- R_f is the effective total foliage resistance in s m^{-1} .

5.3.1 Derivation of new model parameterizations of R_w and χ_w

The deposition of NH_3 on leaf surfaces appears to be closely related to the presence of water on the cuticle because of the large solubility of ammonia in water, which has been shown in both laboratory and field measurements (Sutton and Fowler, 1993; Erisman and Wyers, 1993; Duyzer et al., 1994). There is, however, also evidence that the presence of micro-scale water in or on 'dry' leaf cuticles may affect the rate of deposition. By comparing laboratory results from Van Hove et al. (1989) and Benner et al. (1992) with micrometeorological measurements, Sutton and Fowler (1993) estimated R_w , at 100% relative humidity as 2 s m^{-1} , with the following simplified humidity response:

$$R_{w,model} = \alpha \cdot \exp\left(\frac{100 - RH}{\beta}\right) \quad (5.6)$$

with $\alpha = 2$ and $\beta = 12$ based on the available laboratory measurements. The study of Sutton and Fowler (1993) was carried out over a wheat crop with high SO_2 concentrations. Milford et al. (2001b) found an $\alpha = 0.5$ and $\beta = 12$ for a moorland site in Scotland with low NH_3 concentrations (of about $0.25 \mu\text{g m}^{-3}$) and low SO_2 concentrations, while Milford et al. (2001a) found an $\alpha = 30$ and $\beta = 7$ for a fertilized intensively-managed grassland site, with low SO_2 concentrations. Nemitz et al. (2001) summarized the relative humidity responses of R_w for nine different studies in different pollution climates. They showed a dependence of R_w on the molar ratio between ammonia and sulfur dioxide at the measurement sites, which is consistent with the concept of NH_3 - SO_2 co-deposition (e.g., Erisman and Wyers, 1993). Similarly, Fowler et al. (1998) and Jones et al. (2007a) presented evidence that R_w is directly affected by the NH_3 concentration in the air, probably due to saturation or effects on leaf water pH. The observed dependency of R_w on the molar ratio between ammonia and sulfur dioxide by Nemitz et al. (2001) might, therefore, be partly caused by the difference in NH_3 concentrations at the different locations, or vice versa.

These results suggest, however, that leaf surface concentration/chemistry plays an important role in the magnitude of the flux with the external leaf surface, represented by R_w in Figure 5.1c and by R_w and χ_w in Figure 5.1d. In this study, we will use both the 'traditional' χ_s - R_w model with an optimized R_w parameterization presented in Figure 5.1c as well as the χ_s - χ_w model presented in Figure 5.1d.

During nighttime, when R_s is large due to stomatal closure, R_w may be approximated from the measured atmospheric ammonia concentration in the air, $\chi_a(z-d)$, the atmospheric ammonia concentration at the external leaf surface, χ_w , the ammonia flux, F_{NH_3} , and the atmospheric resistances, $R_a(z-d)$ and R_{b,NH_3} , according to:

$$R_w \approx \frac{\chi_w - \chi_a(z-d)}{F_{NH_3}} - (R_a(z-d) + R_{b,NH_3}) \quad (5.7)$$

R_w values are selected from 'turbulent' nighttime periods, i.e., nighttime periods with small atmospheric resistance (global radiation $\sim 0 \text{ W m}^{-2}$ and $R_a(z-d) + R_{b,NH_3} < 500 \text{ s m}^{-1}$), similar to the filtering by other authors (e.g., Nemitz et al., 2004).

As there are two unknowns in Eq. 5.7, i.e., R_w and χ_w , in a first approximation, we assume that the atmospheric ammonia concentration at the external leaf surface is zero ($\chi_w = 0$) as a means to derive R_w , as done by other authors (e.g., Sutton and Fowler, 1993; Nemitz et al., 2004). We derive optimized values for α in Eq. 5.6 (assuming that $\beta = 12$), resulting in an optimized external leaf surface resistance parameterization, $R_{w,opt}$, which will later be applied in the 'traditional' χ_s - R_w model approach (called the χ_s - $R_{w,opt}$ model hereafter).

In a second approximation, in the χ_s - χ_w model, we assume that the parameterization for R_w of Sutton and Fowler (1993), i.e., Eq. 5.6 with $\alpha = 2$ and $\beta = 12$, is valid for clean conditions (as supported by the findings of Milford et al., 2001b) and represents the minimum external leaf surface resistance, $R_{w,min}$, that only accounts for the relative humidity response. The higher R_w values found in literature (of which nine are summarized in Nemitz et al., 2001) reflect different air pollution climates, as well as potential variation in NH_3 supply from the canopy itself, which will be accounted for in χ_w .

Using the parameterization of $R_{w,min}$ (Eq. 5.6 with $\alpha = 2$ and $\beta = 12$), we are able to derive the remaining unknown, χ_w , from Eq. 5.7 according to:

$$\chi_w \approx \chi_a(z-d) + F_{NH_3} \cdot (R_a(z-d) + R_{b,NH_3} + R_{w,min}) \quad (5.8)$$

It should be noted that in following this approach, we are transferring uncertainty of the pollution climate, and ecosystem dependency of the cuticular exchange to a large extent from R_w to χ_w . While the exact partitioning between the two terms remains uncertain, this has the advantage of accounting for the bi-directional and concentration dependent exchange with the leaf cuticle, while avoiding the requirement to use more complex time-dependent dynamic modeling solutions.

At the external leaf surface water interface, the gaseous NH_3 concentration, χ_w , may be considered as being in equilibrium with the dissolved NH_4^+ concentration. The theoretical relationship between the gaseous ammonia concentration, leaf surface temperature (T_s), ammonium concentration and pH, can be derived from the temperature response of the Henry equilibrium for ammonia, $NH_3(g) \leftrightarrow NH_3(aq)$, and the ammonium-ammonia dissociation equilibrium, $NH_3(aq) + H^+(aq) \leftrightarrow NH_4^+(aq)$. The theoretical atmospheric NH_3 concentration at the leaf surface water interface, χ_w , can be calculated analogous to the stomatal compensation point (following the formulation of Nemitz et al., 2001, and Wichink Kruit et al., 2007):

$$\chi_w = \frac{2.75 \cdot 10^{15}}{T_s + 273.15} \exp\left(\frac{-1.04 \cdot 10^4}{T_s + 273.15}\right) \cdot \Gamma_w \quad (5.9)$$

where χ_w is the gaseous NH_3 concentration at the external leaf surface (in $\mu\text{g m}^{-3}$), T_s is the leaf surface temperature (in $^{\circ}\text{C}$) and Γ_w is the dimensionless molar ratio between the NH_4^+ and H^+ concentrations in the external leaf surface water.

From the derived atmospheric ammonia concentrations at the external leaf surface (χ_w ; Eq. 5.8) and the theoretical temperature relation (Eq. 5.9), a value for Γ_w can be derived as the ratio of χ_w to the temperature function.

5.3.2 Existing model parameterizations of R_w

The parameterization of R_w that is used in the Unified EMEP Model (Simpson et al., 2003) includes the effects of relative humidity, surface temperature and co-deposition on R_w :

$$R_{w,EMEP} = \gamma \cdot F_1(T_s, RH) \cdot F_2(\alpha_{SN}) \quad (5.10)$$

where:

$$F_1(T_s, RH) = 10^{10} \log(T_s + 2) \cdot \exp\left(\frac{100 - RH}{7}\right), \text{ and}$$

$$F_2(\alpha_{SN}) = 10^{(-1.1099 \cdot \alpha_{SN} + 1.6769)} \text{ with } \alpha_{SN} = 0.6 \cdot \frac{[\text{NH}_3]}{[\text{SO}_2]}.$$

γ is a normalizing factor (= 0.0455); T_s is surface temperature (in °C); RH is relative humidity (in %); α_{SN} is the molar 'acidity ratio'. The factor 0.6 is used to allow for the fact that the ratio of these gasses at the surface should be higher than predicted by the EMEP model, due to the large vertical gradients of NH_3 above source areas. $[\text{NH}_3]$ and $[\text{SO}_2]$ represent the modeled molar concentrations in the lowest model layer of the EMEP model. In this study, we have the molar $[\text{NH}_3]$ and $[\text{SO}_2]$ concentrations available at 4m height and will therefore not apply this factor of 0.6, but directly use the measured concentrations at the same height.

The DEPAC module developed at RIVM (Erisman et al., 1994; Van Jaarsveld, 2004) uses a simple relative humidity switch function for R_w for grassland, arable land and other grassy areas summarized in Table 5.1 (Van Jaarsveld, 2004). The dry/wet switch in this module is at 87% relative humidity, originally derived for a forest canopy in The Netherlands (Van Jaarsveld, personal communication). Wichink Kruit et al. (2008) showed that this switch is much lower for grassland: at 71% relative humidity. In this study, we therefore calculate the fluxes with the DEPAC module with the new switch value of 71% relative humidity for reference.

Table 5.1. $R_{w,DEPAC}$ parameterization (in s m^{-1}) for grassland, arable land and other grassy areas (Van Jaarsveld, 2004).

	Day		Night	
	Wet (RH \geq 71%)	Dry (RH < 71%)	Wet (RH \geq 71%)	Dry (RH < 71%)
Spring	20	100	20	50
Summer	20	100	20	50
Autumn	20	50	20	100
Winter	20	50	20	100

5.3.3 Derivation of new model parameterizations of χ_s and Γ_s

During daytime, the exchange of ammonia can occur through both the external leaf surface pathway and the stomatal pathway (see Figure 5.1c). During these hours the leaf surface may still be wet, which means that deposition towards the external leaf surface is still possible. However, exchange of ammonia to and from the stomata is also possible.

The stomatal compensation point can be derived from Eqs. 5.2-5.5 as:

$$\chi_s = \left(\frac{\chi_f}{R_f} - \frac{\chi_w}{R_w} \right) \cdot R_s \quad (5.11)$$

where $\chi_f = \chi_a(z-d) + F_{NH_3} \cdot R_{total}$ is derived from the measured flux, F_{NH_3} , the measured atmospheric ammonia concentration, $\chi_a(z-d)$, and the modeled total resistance, R_{total} .

To minimize the uncertainties in the external leaf surface exchange, χ_s is calculated from Eq. 5.11 during daytime with relative humidity < 71% (Wichink Kruit et al., 2008) and modeled $R_w > 2 R_s$. The stomatal resistance is parameterized according to Emberson et al. (2000a,b). The concentration at the external leaf surface, χ_w , is modeled according to Eq. 5.9 together with the new model parameterization for Γ_w (Eq. 5.13; see Results section). R_w is modeled according to Eq. 5.6 (with $\alpha = 2$ and $\beta = 12$).

Within the stomata, NH_3 is assumed to be in equilibrium with the apoplastic (intercellular leaf tissue) ammonium concentration as presented earlier for the atmospheric ammonia concentration at the external leaf surface. The theoretical stomatal compensation point, χ_s , is calculated following Nemitz et al. (2001) and Wichink Kruit et al. (2007) (equivalent to Eq. 5.9):

$$\chi_s = \frac{2.75 \cdot 10^{15}}{T_s + 273.15} \exp\left(\frac{-1.04 \cdot 10^4}{T_s + 273.15}\right) \cdot \Gamma_s \quad (5.12)$$

where χ_s is the stomatal compensation point (in $\mu g m^{-3}$), T_s is the leaf surface temperature (in °C) and Γ_s is the dimensionless ratio between the apoplastic molar NH_4^+ and H^+ concentration.

From the derived stomatal compensation points (χ_s) from Eq. 5.11 and the theoretical temperature relation (Eq. 5.12), a value for Γ_s can be derived.

In this study, the stomatal pathways in the DEPAC and EMEP model are parameterized like in the χ_s - $R_{w,opt}$ model and our new χ_s - χ_w model, i.e., the same parameterizations for χ_s and R_s are used for all parameterization schemes.

The parameterizations used in the comparison between the different parameterization schemes are summarized in Table 5.2.

Table 5.2. Parameterization schemes used for comparison.

parameterization scheme	R_w	χ_w	R_s	χ_s
χ_s - $R_{w,opt}$ model (with optimized R_w)	$R_{w,opt}$ = Eq. 5.6 with $\alpha = 31$ and $\beta = 12$	-	Emberson et al. (2000a,b)	Eq. 5.12 and Eq. 5.14
χ_s - χ_w model	$R_{w,min}$ = Eq. 5.6 with $\alpha = 2$ and $\beta = 12$	Eq. 5.9 and Eq. 5.13	Emberson et al. (2000a,b)	Eq. 5.12 and Eq. 5.14
χ_s - $R_{w,DEPAC}$ model	Table 5.1	-	Emberson et al. (2000a,b)	Eq. 5.12 and Eq. 5.14
χ_s - $R_{w,EMEP}$ model	Eq. 5.10	-	Emberson et al. (2000a,b)	Eq. 5.12 and Eq. 5.14

5.4 Results

5.4.1 New model parameterizations of R_w and χ_w

Figure 5.2 shows the derived cuticular resistances (R_w) from Eq. 5.7 in the upper panel, calculated on the assumption that $\chi_w = 0$ and that stomata are closed, i.e., for nocturnal conditions. In these conditions, the flux is dominated by exchange with the external leaf surface. The figure also shows the relation for $R_{w,min}$ (solid black line; Eq. 5.6 with $\alpha = 2$ and $\beta = 12$), and the optimized R_w parameterization ($R_{w,opt}$) for our data (dashed black line; Eq. 5.6 with $\alpha = 31$ and $\beta = 12$). The lower panel of Figure 5.2 shows the reciprocal of the derived cuticular resistances, referred to here as the cuticular conductances (g_w). In both cases the data are shown as a function of the relative humidity for 4 different ammonia air concentration classes (grayscale). There is large scatter in the data, but in general the cuticular resistance is small when the relative humidity is high and vice versa. The $R_{w,min}$ parameterization fits reasonably well to the minimum values of R_w and the maximum values of g_w derived from our measurement data. The correlation between the derived values and the parameterizations is low ($R = 0.16$), but significant ($p < 0.05$). Therefore, the use of this parameterization to describe the minimum value of the deposition limitation represented by R_w in response to relative humidity seems to be justified. The scatter in the data is caused by the assumption that the external leaf surface concentration is zero ($\chi_w = 0$ in Eq. 5.7). In the interpretation followed here, it is considered that the larger values of R_w (and smaller values of cuticular conductance, g_w) represent an additional limitation to deposition due to non-zero values of χ_w . In Figure 5.2, this surface limitation is simply represented as a resistance rather than concentration (cf. Sutton et al., 1993a). The figure also shows negative R_w values, which are caused by positive fluxes in Eq. 5.7, i.e., nighttime emission events. As negative resistances do not exist by definition, this seems to be an extra argument to introduce an external leaf surface concentration, χ_w , in our modeling.

Since Figure 5.2 shows that the parameterization of Sutton and Fowler (1993) provides a good description of the minimum values of R_w , we can now derive estimates for the concentration at the external leaf surface, χ_w , and the ratio between $[\text{NH}_4^+]$ and $[\text{H}^+]$ in the external leaf surface water, Γ_w , for our data from Eq. 5.8 and Eq. 5.9 respectively.

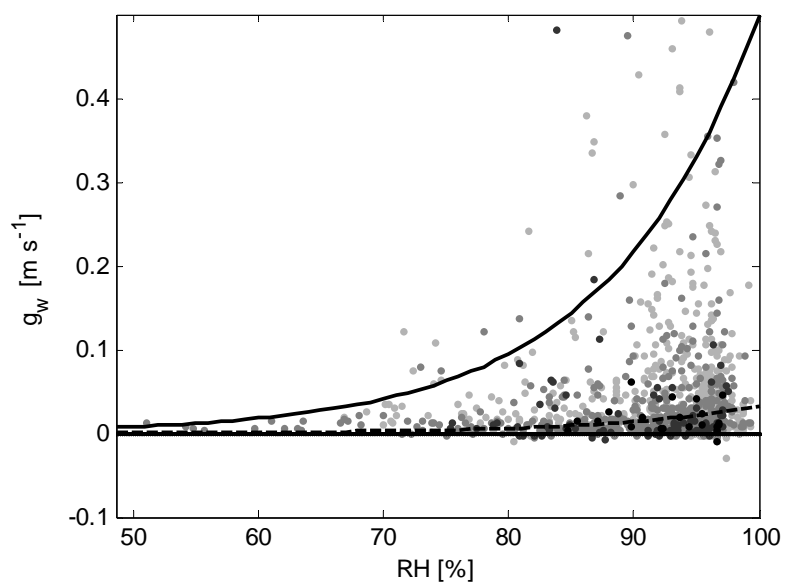
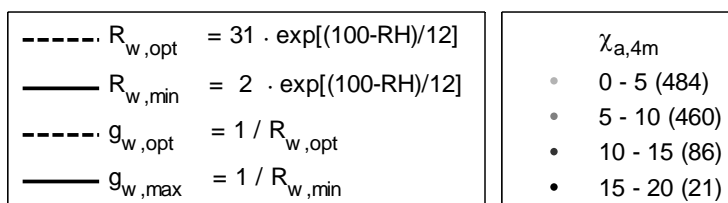
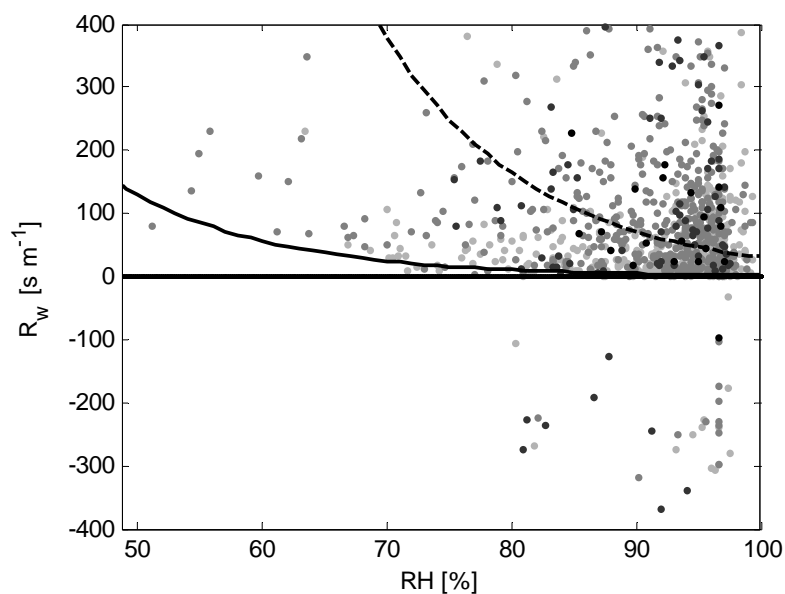


Figure 5.2. Cuticular resistance R_w ($s m^{-1}$) (upper panel) and cuticular conductance g_w ($m s^{-1}$) (lower panel) as a function of the relative humidity (RH) for different atmospheric ammonia concentration classes (grayscale). Between parentheses is the number of points in each concentration class.

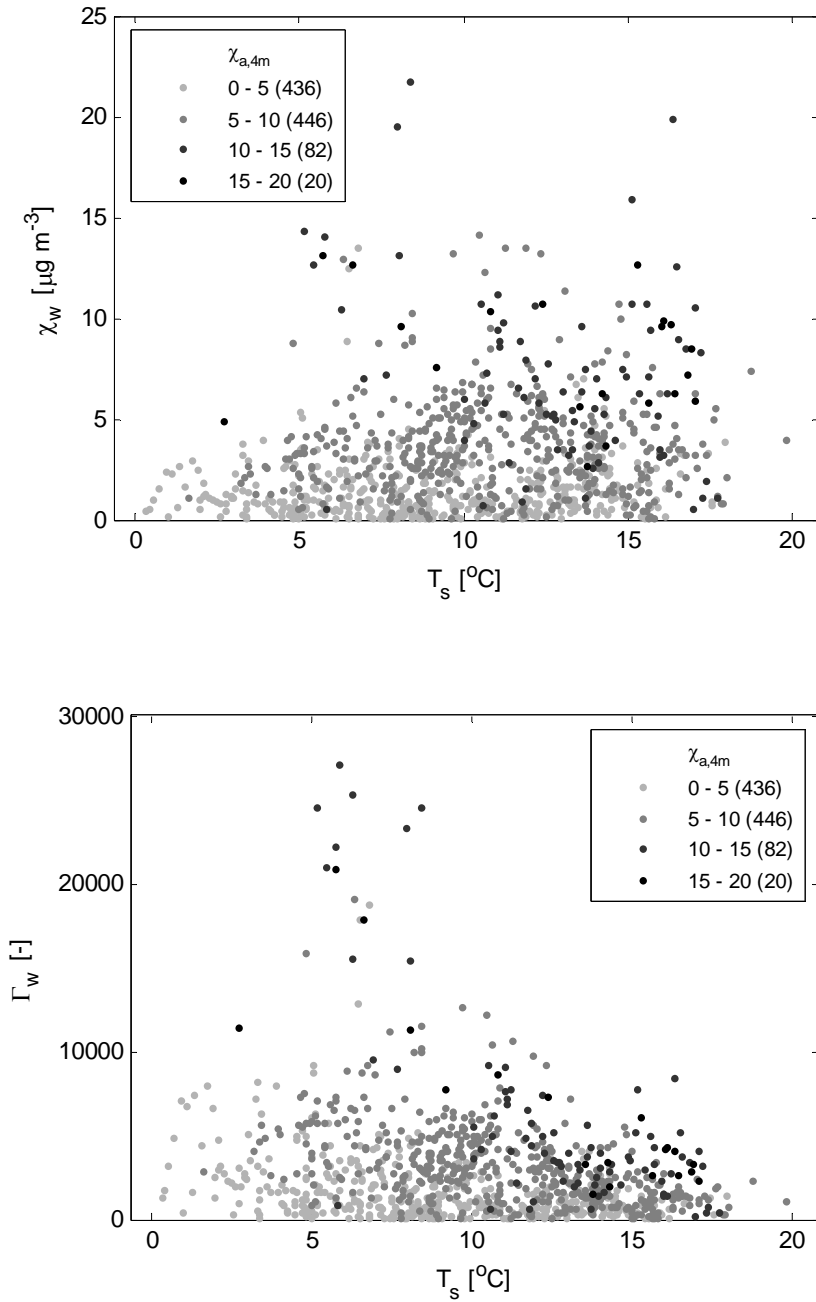


Figure 5.3. Derived ammonia concentrations at the external leaf surface, χ_w (upper panel), and derived Γ_w values (lower panel) as a function of canopy surface temperature, T_s ($^{\circ}\text{C}$), for different concentration classes (grayscale) derived from Eq. 5.8 and Eq. 5.9. Between parentheses is the number of points in each concentration class.

The upper panel of Figure 5.3 shows the derived χ_w versus the leaf surface temperature, T_s , grouped by different concentration classes (grayscale). The figure shows that most of the derived concentrations at the external leaf surface are in the range between 0 and $10 \mu\text{g m}^{-3}$ and higher temperatures give higher χ_w values. The lower panel of Figure 5.3 shows the derived Γ_w versus T_s grouped by different concentration classes (grayscale). Most of the derived Γ_w values are in the range between 0 and 10000. The figure shows that derived Γ_w decreases with increasing leaf surface temperature, but increases with increasing ambient air concentration.

An empirical relation is derived by applying least square fitting using multiple variance analysis between the derived Γ_w values and the variables T_s and $\chi_{a,4m}$, which both appeared to be significant ($p < 0.001$). The equation that is obtained by using this method is:

$$\Gamma_{w,model} = 1.84 \cdot 10^3 \cdot \chi_{a,4m} \cdot \exp(-0.11 \cdot T_s) - 850 \quad (5.13)$$

where $\chi_{a,4m}$ is in $\mu\text{g m}^{-3}$ and T_s is in $^{\circ}\text{C}$.

Figure 5.4 shows the modeled Γ_w values (Eq. 5.13) versus the derived Γ_w values from the measurements. The correlation coefficient R is 0.67.

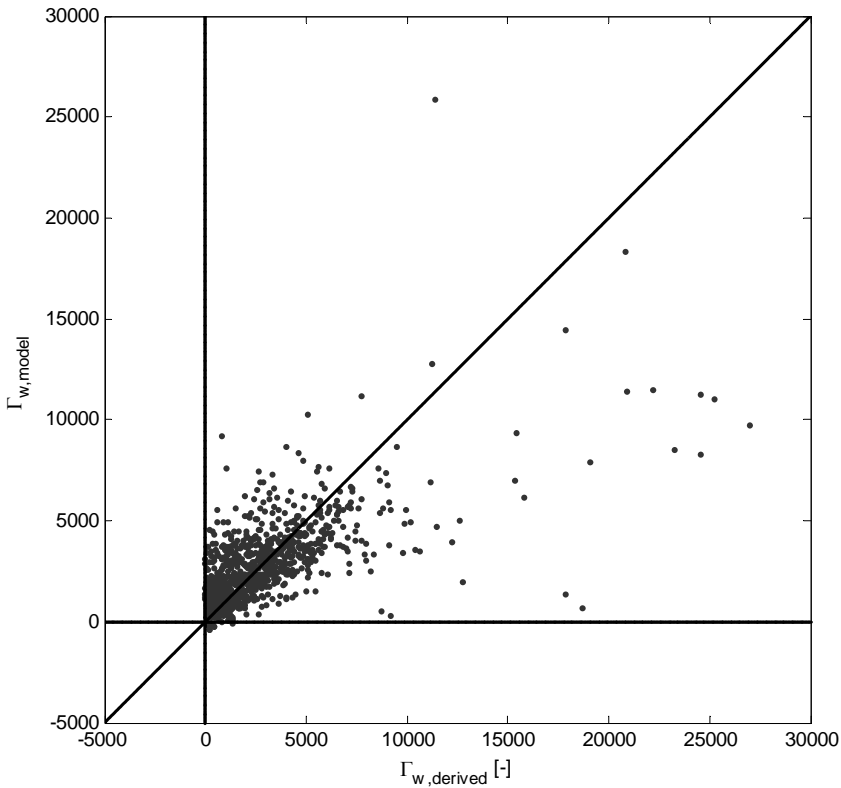


Figure 5.4. The model parameterization of Γ_w (Eq. 5.13) versus derived Γ_w values ($\Gamma_{w,derived}$). Equation 5.13 is an empirical relation between the variables T_s and $\chi_{a,4m}$ and the derived Γ_w values by applying least square fitting using multiple variance analysis. Only nighttime data (both deposition and emission fluxes) are considered to exclude possible effects of the stomatal pathway.

Nighttime fluxes (both nighttime deposition and emission) can now be modeled by combining Eqs. 5.2-5.6, 5.9 and 5.13. Figure 5.5 shows the model results for the χ_s - $R_{w,opt}$ model (Figure 5.5a), the new χ_s - χ_w model (Figure 5.5b), the χ_s - $R_{w,DEPAC}$ model (Figure 5.5c) and the χ_s - $R_{w,EMEP}$ model (Figure 5.5d), which are summarized in Table 5.3. The figure shows that the χ_s - $R_{w,opt}$ model, the χ_s - χ_w model and the χ_s - $R_{w,DEPAC}$ model have the highest correlation coefficients ($R = 0.49$, 0.48 and 0.51 respectively). However, the χ_s - $R_{w,DEPAC}$ model seems to overestimate deposition systematically with almost 60%, resulting in too low mean and median flux estimates. The χ_s - $R_{w,opt}$ model, the χ_s - χ_w model and the χ_s - $R_{w,EMEP}$ model all give good estimates of the mean and median values of the nighttime fluxes. The χ_s - $R_{w,EMEP}$ model, however, has a slightly lower correlation coefficient ($R = 0.43$). When looking at the root mean square deviations (RMSD), the χ_s - $R_{w,opt}$ model and the χ_s - χ_w model show the smallest deviations from the measured fluxes, while the χ_s - $R_{w,EMEP}$ model has a slightly higher deviation and the $R_{w,DEPAC}$ model has the largest deviation from the measured fluxes. This is more or less what we would expect, because the parameterizations in the χ_s - $R_{w,opt}$ model and the χ_s - χ_w model are derived from the nighttime flux measurements. To check whether the model is also valid during daytime, first, the stomatal pathway needs to be modeled.

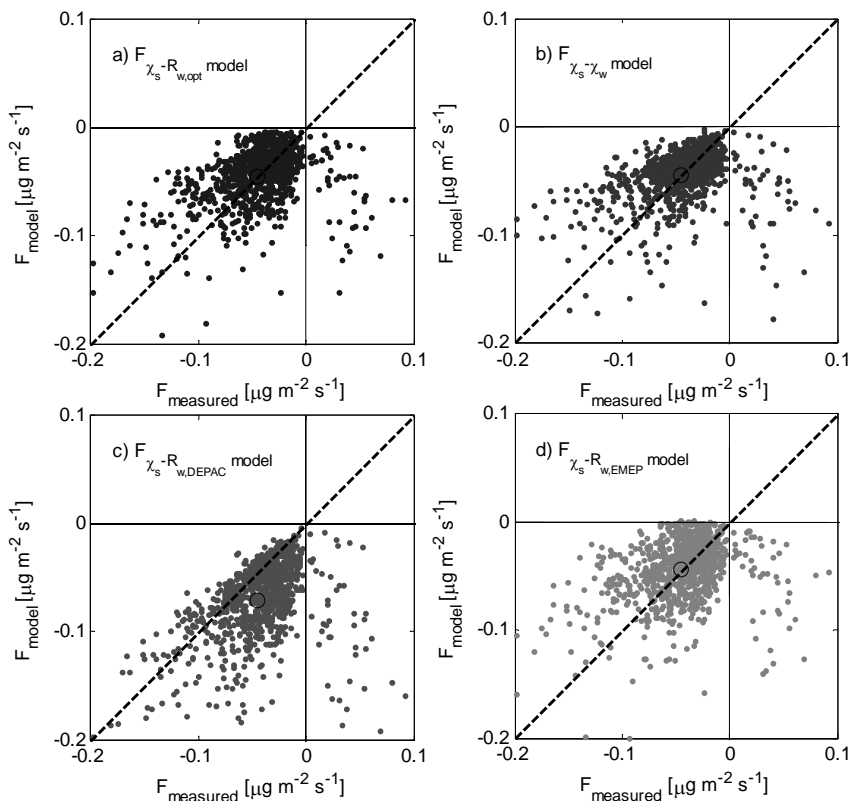


Figure 5.5. Modeled versus measured nighttime fluxes (both deposition and emission fluxes). The model results that are plotted versus the measurements are from the: a) χ_s - $R_{w,opt}$ model., b) χ_s - χ_w model, c) χ_s - $R_{w,DEPAC}$ model, d) χ_s - $R_{w,EMEP}$ model. A description of the model parameterizations used in this figure and the data statistics can be found in Table 5.3. The dashed black line is the 1:1 line. The open circle in each plot is the mean of the modeled flux versus the mean of the measured flux.

Table 5.3. Results of the different model parameterizations for all nighttime data.

parameterization scheme	R_w	χ_w	mean	median	R	RMSD
measured flux	-	-	-0.045	-0.039	-	-
χ_s - $R_{w,opt}$ model (with optimized R_w)	$R_{w,opt}$ = Eq. 5.6 with $\alpha = 31$ and $\beta = 12$	-	-0.045	-0.039	0.49	0.036
χ_s - χ_w model	$R_{w,min}$ = Eq. 5.6 with $\alpha = 2$ and $\beta = 12$	Eq. 5.9 and Eq. 5.13	-0.045	-0.039	0.48	0.036
χ_s - $R_{w,DEPAC}$ model	Table 5.1	-	-0.071	-0.063	0.51	0.048
χ_s - $R_{w,EMEP}$ model	Eq. 5.10	-	-0.044	-0.038	0.43	0.038

5.4.2 Seasonal variability of Γ_s

Figure 5.6 shows the seasonal variation of the derived Γ_s values using Eqs. 5.11-5.12. It is obvious that the estimated values of Γ_s are not constant during the year; in spring as well as in autumn Γ_s values are higher than in summer. This seasonal variability cannot be ascribed to the management practice (cutting) on the field and is likely due to plant physiological variables.

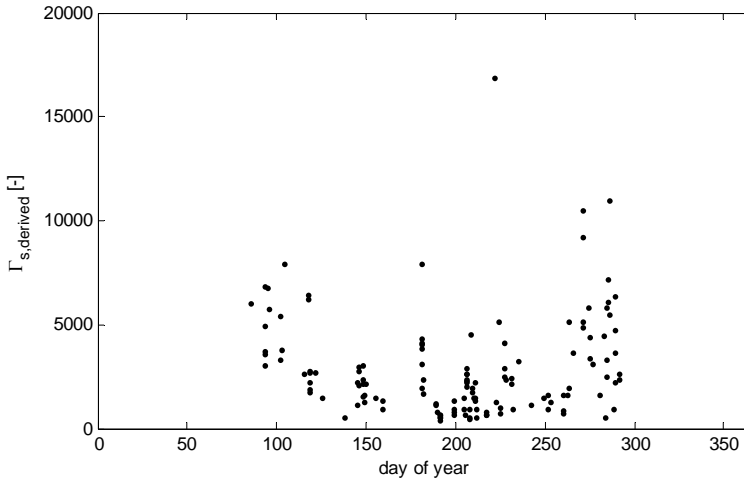


Figure 5.6. Seasonal variation of the derived Γ_s from Eqs. 5.11 and 5.12 providing that $R_w > 2 R_s$.

In Figure 5.7, the derived Γ_s values are plotted versus the leaf surface temperature, because Van Hove et al. (2002) suggest that temperature not only has an effect on the equilibrium between χ_s and NH_3 dissolved in the apoplast but also on the physiological processes responsible for the NH_4^+ concentration in the apoplast.

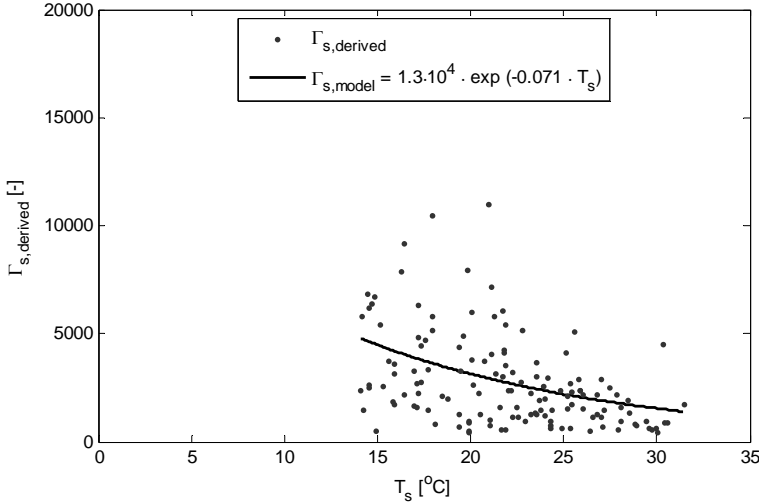


Figure 5.7. Leaf surface temperature (T_s) versus derived Γ_s from Eqs. 5.11 and 5.12 providing that $\underline{R_w} > 2 R_s$.

Although, there is a lot of scatter in the derived Γ_s values, a weak exponential dependence of Γ_s on leaf surface temperature exists. The least square exponential fit of these data ($R = 0.39$; $p < 0.001$) is:

$$\Gamma_s = 1.3 \cdot 10^4 \cdot \exp(-0.071 \cdot T_s) \quad (5.14)$$

5.4.3 Comparison of the new method with the DEPAC and EMEP schemes

Now we have defined the parameterizations of the stomatal pathway, we can compare the complete model parameterizations as defined in Table 5.2 for all available data in the period between June 2004 and December 2006 (both nighttime and daytime data). The upper panel in Figure 5.8 shows the median diurnal cycle of the measured and modeled ammonia fluxes. The lower panel in Figure 5.8 shows a histogram of the differences between the measured and the modeled fluxes. Table 5.4 summarizes the overall model performance.

Table 5.4. Results of the different model parameterizations for all data in the period between June 2004 and December 2006 (both nighttime and daytime data).

parameterization scheme	mean	median	R	RMSD
measured flux	-0.037	-0.036	-	-
χ_s - $R_{w,opt}$ model	-0.029	-0.029	0.35	0.056
χ_s - χ_w model	-0.042	-0.038	0.36	0.053
χ_s - $R_{w,DEPAC}$ model	-0.065	-0.059	0.36	0.065
χ_s - $R_{w,EMEP}$ model	-0.025	-0.026	0.32	0.059

The median diurnal cycles of the measured and modeled ammonia fluxes (Figure 5.8; upper panel) show that the $\chi_s-R_{w,opt}$ and the $\chi_s-R_{w,EMEP}$ model especially underestimates the daytime deposition fluxes (or overestimates the daytime emission), while the $\chi_s-R_{w,DEPAC}$ model especially overestimates the nighttime deposition fluxes. The $\chi_s-\chi_w$ model has a median diurnal cycle that is closest to the median diurnal cycle of the measured fluxes.

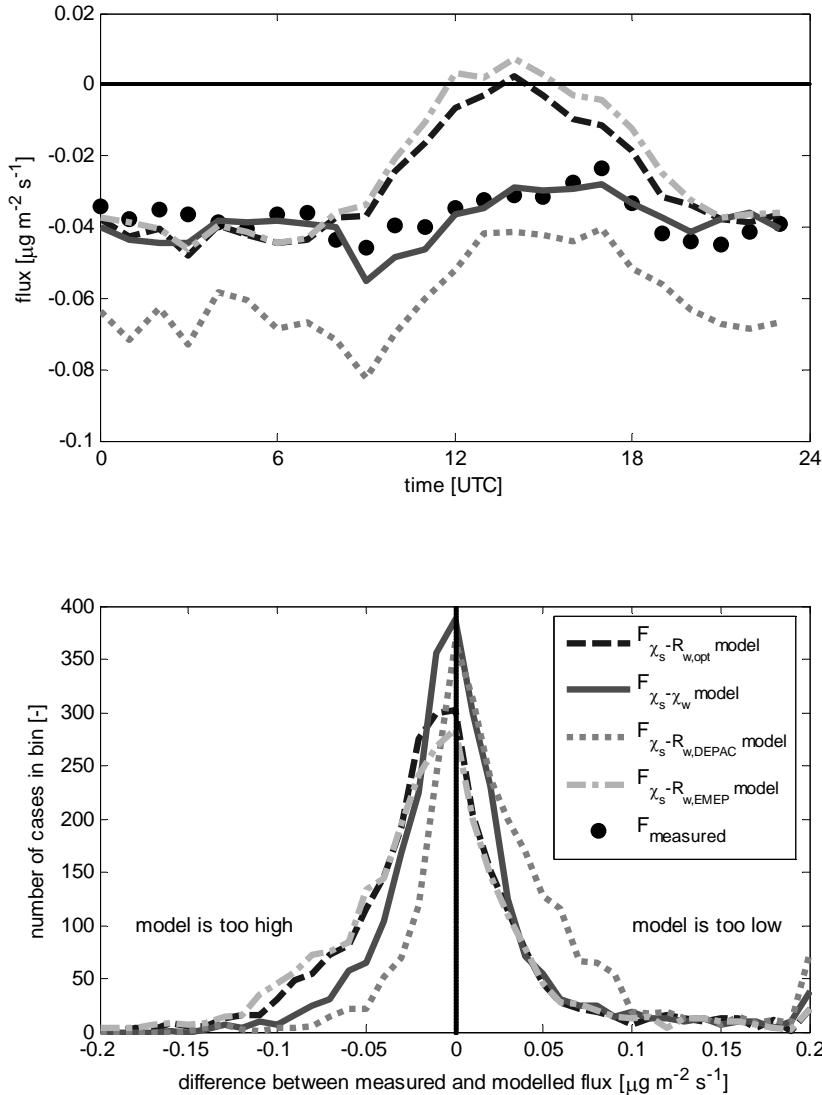


Figure 5.8. The median diurnal cycle of the measured (black dots) and modeled (lines) ammonia fluxes (upper panel) and a histogram of the differences between the measured and the modeled ammonia fluxes (lower panel) for all available data in the period between June 2004 and December 2006. The lines represent the different parameterization schemes described in Table 5.2.

This is confirmed by the data statistics. The mean ($-0.042 \mu\text{g m}^{-2} \text{s}^{-1}$) and median ($-0.038 \mu\text{g m}^{-2} \text{s}^{-1}$) values calculated by the χ_s - χ_w model are closest to the mean ($-0.037 \mu\text{g m}^{-2} \text{s}^{-1}$) and median ($-0.036 \mu\text{g m}^{-2} \text{s}^{-1}$) values of the measured flux. The χ_s - $R_{w,\text{opt}}$ model and the χ_s - $R_{w,\text{EMEP}}$ model underestimate the flux with a mean and median value of about $-0.029 \mu\text{g m}^{-2} \text{s}^{-1}$ for the χ_s - $R_{w,\text{opt}}$ model and about $-0.026 \mu\text{g m}^{-2} \text{s}^{-1}$ for the χ_s - $R_{w,\text{EMEP}}$ model. This underestimation is mainly caused by the underestimation of the deposition during daytime, while both models perform quite acceptable during nighttime. The χ_s - $R_{w,\text{DEPAC}}$ model systematically overestimates the deposition with a mean value of $-0.065 \mu\text{g m}^{-2} \text{s}^{-1}$ and median value of $-0.059 \mu\text{g m}^{-2} \text{s}^{-1}$. From the RMSD values the χ_s - χ_w model is most favorable (RMSD= $0.053 \mu\text{g m}^{-2} \text{s}^{-1}$), followed by the χ_s - $R_{w,\text{opt}}$ model (RMSD= $0.056 \mu\text{g m}^{-2} \text{s}^{-1}$), the χ_s - $R_{w,\text{EMEP}}$ model (RMSD= $0.059 \mu\text{g m}^{-2} \text{s}^{-1}$) and finally the χ_s - $R_{w,\text{DEPAC}}$ model (RMSD= $0.065 \mu\text{g m}^{-2} \text{s}^{-1}$).

The lower panel of Figure 5.8 shows a histogram of the differences between the measured and the modeled fluxes for all available data in the period between June 2004 and December 2006. Ideally, we would have no difference between the measured and the modeled fluxes and consequently a peak at zero difference. From the four models compared, the χ_s - χ_w model best agrees with this ideal situation, with a nice equal distribution on both sides of the y-axis and a high peak around zero. Although the χ_s - $R_{w,\text{DEPAC}}$ model also has a high peak around zero, the distribution is not equal on both sides of the y-axis, but is shifted toward the positive side (model estimates are too low). The χ_s - $R_{w,\text{opt}}$ model and the χ_s - $R_{w,\text{EMEP}}$ model both have a lower peak and a distribution that is slightly shifted towards the negative side (model estimates are too high).

5.5 Discussion

The new χ_s - χ_w model with a bi-directional pathway to the stomata and the external leaf surface shows good performance. Although the parameterization of the external leaf surface pathway (Eq. 5.9 and Eq. 5.13) is not effectively bi-directional (i.e., χ_w is approximately parameterized as a fraction of the ambient air concentration and will consequently never exceed the ambient air concentration), it accounts for saturation effects at high air concentrations and it is therefore also applicable to other pollution climates. The new parameterization for the pathway to the external leaf surface can explain the differences between many of the formerly derived dependencies on relative humidity found in literature of which nine are summarized in Nemitz et al. (2001). The derived parameterization for Γ_w is dependent on the ambient air concentration and the surface temperature. Higher ambient air concentrations will lead to higher concentrations at the external leaf surface and consequently to reduced deposition rates. In the χ_s - R_w model, the concentration at the external leaf surface is assumed to be zero, and a reduced deposition can only be obtained by using higher R_w values. That is why parameterizations with high values for R_w at 100% relative humidity are especially found in polluted areas. Spindler et al. (2001) found a value for α in Eq. 5.6 of 20 for a semi-natural grassland with an annual-mean ammonia concentration of $3.1 \mu\text{g m}^{-3}$. Nemitz et al. (2004) found a value for α of 21.0 for a Dutch heathland with an annual-median ammonia concentration of about $4.2 \mu\text{g m}^{-3}$. In Table 5.1 of Nemitz et al. (2001), we also find the highest values of α at 30 s m^{-1} (at 100% relative humidity) in agricultural and 10 to 20 s m^{-1} in the more polluted natural areas in the Netherlands (heathland in Elspeet and coniferous forest in Speuld). In a fumigation study, Jones et al. (2007a) found a linear dependency of R_w on concentration for a mixed

moorland canopy of about 1.1 times the concentration plus 4 s m^{-1} (Figure 5.10 in Jones et al., 2007a). In our model approach, the concentration dependency is incorporated in the concentration at the external leaf surface, χ_w , which is physically more realistic (as in the dynamic χ_c - C_d model; Sutton et al., 1998).

In this study, the dependency of χ_w on SO_2 concentration was also explored, but no dependency could be found for the timescales considered here. This is most likely due to the rather constant and low SO_2 concentrations measured in the Netherlands nowadays at our experimental site (mean and median SO_2 concentrations are 1.7 and $1.0 \mu\text{g m}^{-3}$, respectively). Although, SO_2 co-deposition not seemed to significantly influence our flux estimates, it might still be important for locations with relatively high ambient SO_2 concentrations.

The observed seasonal variation in Γ_s (Figure 5.6) is likely due to plant physiological effects. In spring and autumn the plant metabolism is small and therefore ammonium concentrations may be large, as the plants hardly use ammonium for their growth in these periods. When temperature rises and global radiation increases, photosynthetic activity increases and ammonium is effectively used for plant metabolism and ammonium concentration in the apoplastic fluid decreases (cf. Riedo et al., 2002). At senescence, plants build up their ammonium concentrations again, resulting in higher Γ_s values (Mattsson et al., 2009). It is likely that part of the scatter in Γ_s values in Figure 5.6 is caused by senescence of the grass. As no fertilizer (neither mineral nor organic) was applied at this field, no effects of (or no scatter caused by) fertilizer application are expected. Because the photosynthetic activity is mainly driven by global radiation and temperature (there is rarely water limitation at our experimental site), the dependencies of Γ_s on global radiation and temperature were investigated. In this study, the dependency of Γ_s on temperature appeared to be strongest (Figure 5.7; Eq. 5.14). The response suggests that at high temperatures ammonium is effectively used in plant metabolism and that the concentration in the apoplastic fluid is consequently low, which is in agreement with earlier findings by Van Hove et al. (2002) and Riedo et al. (2002). The obtained temperature response (Eq. 5.14) is useful in modeling the annual trend in Γ_s as we will show further on.

Furthermore, several studies have shown that Γ_s is dependent on the availability of NH_4^+ and NO_3^- in the soil (Sutton et al., 1993c; Sutton et al., 1995b; Mattsson and Schjoerring, 2002) and is varying between plant species (Mattsson et al., 2009). The availability of NH_4^+ and NO_3^- in the soil is dependent on fertilizer application and historical nitrogen deposition (both dry and wet deposition of all kind of nitrogen compounds). Both fertilizer application and historical nitrogen deposition are affecting/affected by the ammonia concentration in the air.

In this study, we collected Γ_s values of 21 literature studies (of which the most important details are summarized in Table 5.5) and plotted them against the 'long-term' ammonia concentration (Figure 5.9). 'Long-term' is quoted, because in most of the studies the long-term ammonia concentrations are the mean or median values for the duration of the measurement campaign. If several Γ_s values are given in a study (e.g., for different management practices), all values are included in Table 5.5, but only the Γ_s values representing the background situation are plotted in Figure 5.9.

Table 5.5. Characteristics of the studies providing estimates of L_s plotted in Figure 5.9.

nr	study	derived L_s	air concentration (in $\mu\text{g m}^{-3}$)	vegetation and management	nitrogen inputs	location	method
1	Husted et al. (1996)	830	11 (~ 15 nmol mol ⁻¹ air)	Brassica napus (oilseed rape)	high-N plants exposed to air with 15 nmol NH ₃ mol ⁻¹ air	laboratory	bioassay
2	Mattsson et al. (1997)	540	7.6 (~ 10 nmol mol ⁻¹ air)	Barley; wild-type	wild type Barley plants exposed to 10 nmol NH ₃ mol ⁻¹ air	laboratory	bioassay
3	Mattsson et al. (1997)	894	7.6 (~ 10 nmol mol ⁻¹ air)	Barley mutant with 47% of the GS activity of wild type Barley	Barley mutant 66% GS exposed to 10 nmol NH ₃ mol ⁻¹ air	laboratory	bioassay
4	Mattsson et al. (1997)	1270	7.6 (~ 10 nmol mol ⁻¹ air)	Barley mutant with 66% of the GS activity of wild type Barley	Barley mutant 66% GS exposed to 10 nmol NH ₃ mol ⁻¹ air	laboratory	bioassay
5	Husted et al. (2000)	390	0.75	Brassica napus (oilseed rape)	285 kg N ha ⁻¹ yr ⁻¹	North Berwick, UK	bioassay
6	Van Hove et al. (2002)	655	4.7	Lolium perenne (ryegrass) agricultural grassland	170 kg N ha ⁻¹ yr ⁻¹	Wageningen, NL	bioassay
7	Loubet et al. (2002)	20	0.2	Lolium perenne (ryegrass) intensively managed grassland	270 kg N ha ⁻¹ yr ⁻¹	Bush Estate, UK	bioassay
8	Burkhardt et al. (2009)	305 (green leaves) 5193 (senescent leaves)	2.2	Lolium perenne (ryegrass) agricultural grassland	250-350 kg N ha ⁻¹ yr ⁻¹	Braunschweig, DE	bioassay
9	Flechard and Fowler (1998)	132	0.4	lowland moorland	non-fertilized; dry deposition ~ 2.5 kg N ha ⁻¹ yr ⁻¹	Auchenoroth, UK	micrometeorological
10	Plantaz (1998)	4800	11	Lolium perenne (ryegrass) intensively managed grassland	300 kg N ha ⁻¹ yr ⁻¹	Zegveld, NL	micrometeorological
11	Milford et al. (2001a)	630 (precu) 6000 (postcu) 40000 (post fertilizing)	1.4	Lolium perenne (ryegrass) intensively managed grassland	270 kg N ha ⁻¹ yr ⁻¹	Easter Bush, UK	micrometeorological
12	Milford et al. (2001b)	50	0.26	upland moorland	non-fertilized; dry deposition ~ 1.5 kg N ha ⁻¹ yr ⁻¹	Dorback Estate, UK	micrometeorological
13	Spindler et al. (2001)	1000	3.1	Lolium perenne (ryegrass) semi-natural grassland	70 kg N ha ⁻¹ yr ⁻¹ ; dry deposition ~ 10 kg N ha ⁻¹ yr ⁻¹	Melpitz, DE	micrometeorological
14	Nemitz et al. (2004)	1200	5.2	Calluna vulgaris (heathland)	non-fertilized; dry deposition ~ 13 kg N ha ⁻¹ yr ⁻¹	Elspeet, NL	micrometeorological
15	Nemitz et al. (2004) (derived from Erisman and Wyers, 1993)	2500	5.2	Calluna vulgaris (heathland)	non-fertilized; dry deposition ~ 13 kg N ha ⁻¹ yr ⁻¹	Elspeet, NL	micrometeorological
16	Horvath et al. (2005)	200	2.2	Lolium perenne (ryegrass) semi-natural grassland	non-fertilized; one application of 100 kg N ha ⁻¹	Great Plain, HU	micrometeorological
17	Walker et al. (2006)	955	5.5	Soybean	65 kg N ha ⁻¹	North Carolina, US	micrometeorological
18	Wichink Knit et al. (2007)	2200	7	Lolium perenne (ryegrass) agricultural grassland	non-fertilized; dry deposition ~ 10 kg N ha ⁻¹ yr ⁻¹	Wageningen, NL	micrometeorological
19	Neirynck and Ceulemans (2008)	3300	7.8*	mixed coniferous forest spring	non-fertilized; depositions ~ 30 kg N ha ⁻¹ yr ⁻¹	near Antwerp, BE	micrometeorological
20	Neirynck and Ceulemans (2008)	1375	2.6*	mixed coniferous forest summer/autumn	non-fertilized; depositions ~ 30 kg N ha ⁻¹ yr ⁻¹	near Antwerp, BE	micrometeorological
21	Wichink Knit et al. (2009)	2500	7.6	Lolium perenne (ryegrass) agricultural grassland	non-fertilized; dry deposition ~ 10 kg N ha ⁻¹ yr ⁻¹	Wageningen, NL	micrometeorological

* weighted average derived from Table 1 in Neirynck and Ceulemans (2008)

- In Figure 5.9, we tried to further segregate the studies into different classes for:
- derivation method of Γ_s (i.e., black and gray symbols; black symbol represents micrometeorological estimate; gray symbol represents bioassay estimate),
 - vegetation type (i.e., different symbols for different vegetation types; \blacktriangle represents fertilized agricultural grassland; \bullet represents semi-natural grassland; \blacksquare represents mixed coniferous forest; $*$ represents heather/moorland; \blacklozenge represents agricultural crop), and
 - fertilization level (i.e., encircled symbols; encircled symbol represents fertilized plot).

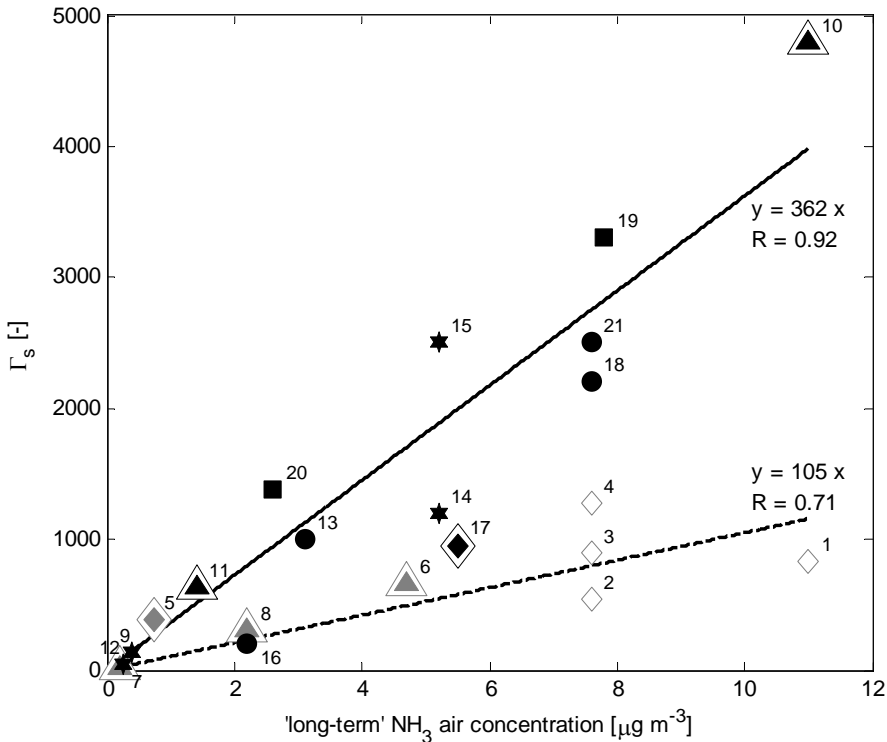


Figure 5.9. Γ_s versus 'long-term' NH_3 air concentration for reported Γ_s values in literature for different vegetation types represented by the different symbols. \blacktriangle represents fertilized agricultural grassland; \bullet represents semi-natural grassland; \blacksquare represents mixed coniferous forest; $*$ represents heather/moorland; \blacklozenge represents agricultural crops. The black symbols are micrometeorological estimates of Γ_s ; gray symbols are bioassay (closed symbols = laboratory; open symbols = field) estimates of Γ_s . The encircled symbols represent fertilized plots, while the other symbols represent non-fertilized plots. The solid line is the regression line through the micrometeorological estimates of Γ_s . The dashed line is the regression line through the bioassay estimates of Γ_s . The numbers correspond to the literature references in Table 5.5.

No clear dependencies of Γ_s on different vegetation types or fertilization levels can be distinguished, which does not mean that these dependencies do not exist. Due to a lack of Γ_s values in literature, these dependencies can probably just not be distinguished yet. However, rather clear different dependencies of Γ_s on the 'long-term' ammonia concentrations are found for the different derivation methods. The dependency of Γ_s on 'long-term' ammonia concentration can be represented by the following simple linear

relations for the micrometeorological estimates (solid black line in Figure 5.9; Eq. 5.15a) and the bioassay estimates (dashed black line in Figure 5.9; Eq. 5.15b):

$$\Gamma_{s,micromet} = 362 \cdot \chi_{a,4m('long-term')} \quad (5.15a)$$

$$\Gamma_{s,bioassay} = 105 \cdot \chi_{a,4m('long-term')} \quad (5.15b)$$

where $\chi_{a,4m('long-term')}$ is the 'long-term' NH₃ concentration (in $\mu\text{g m}^{-3}$).

Γ_s (both $\Gamma_{s,micromet}$ and $\Gamma_{s,bioassay}$) is linearly increasing with the 'long-term' NH₃ concentration, which means that on average, Γ_s is higher in more polluted areas, which is in agreement with our expectations.

However, it is clear that the Γ_s values from bioassay measurements, $\Gamma_{s,bioassay}$, are about a factor of 3 smaller than the Γ_s values from micrometeorological measurements, $\Gamma_{s,micromet}$. A possible reason for this difference is that the $\Gamma_{s,micromet}$ values also include possible other pathways, like the soil and/or the leaf litter pathway through Γ_{soil} and Γ_{litter} , as showed to be important by Sutton et al. (2009). This suggests that Eq. 5.15a should be used in a single-layer canopy compensation point model ($\chi_s\text{-R}_w$ or $\chi_s\text{-}\chi_w$ model) that does not include the soil and/or leaf litter pathways explicitly, because insufficient soil/leaf litter information is generally available.

Equation 5.15b can be used in a two-layer canopy compensation point model, which includes separate pathways for the leaves (stomata and cuticles), the soil and/or the leaf litter. This two-layer model approach needs more specific information which is generally unavailable for atmospheric transport models.

Therefore, for practical application in atmospheric transport models, we recommend the one-layer canopy compensation point model with Eq. 5.15a to be used for Γ_s .

To account for the annual trend in Γ_s , Eq. 5.14 and Eq. 5.15a can be combined. The generalized equation that describes the annual trend in Γ_s as a function of the 'long-term' NH₃ concentration and the leaf surface temperature is:

$$\Gamma_s(T_s) = \Gamma_{s,method} \cdot 4.7 \cdot \exp(-0.071 \cdot T_s) \quad (5.16)$$

where $\Gamma_{s,method}$ is Eq. 5.15a for the single-layer canopy compensation point model or Eq. 5.15b for the two-layer canopy compensation point model, with $\chi_{a,4m('long-term')}$ being the 'long-term' NH₃ concentration at 4 meters height. With the measured 'long-term' NH₃ concentration at our measurement site ($\sim 7.6 \mu\text{g m}^{-3}$) and Eq. 5.15a, $\Gamma_{s,micromet}$ becomes about 2750 and Eq. 5.16 is approximately equal to Eq. 5.14.

By using Eq. 5.16 with Eq. 5.15b, we are able to simulate the annual trend in Γ_s for the independent data set used by Van Hove et al. (2002), which are bioassay estimates of Γ_s . For this purpose, we estimated the 'long-term' ammonia concentration of $4.7 \mu\text{g m}^{-3}$ from the figures in the paper of Van Hove et al. (2002) and used the leaf surface temperatures from our weather station for the years 2004 till 2006 to simulate the range in which the Γ_s values are to be expected. The model results (small gray dots) and the observations (large black dots) of Γ_s by Van Hove et al. (2002), derived from the NH₄⁺ concentrations and pH in their figures, are shown in Figure 5.10 (upper panel). By using Eq. 5.16 in Eq. 5.12, we can calculate the annual trend in χ_s as shown in the lower panel of Figure 5.10. The figure shows that both the annual trend of Γ_s and the annual trend of χ_s are rather well described by the equations provided above. We have to remind that these equations do not explicitly

account for management practices, like cutting and fertilizing, which are known to significantly affect the value of Γ_s . Therefore, part of the scatter in the observed Γ_s and χ_s is likely caused by the management practice (cutting and fertilizing) at the measurement site as pointed out by Van Hove et al.(2002).

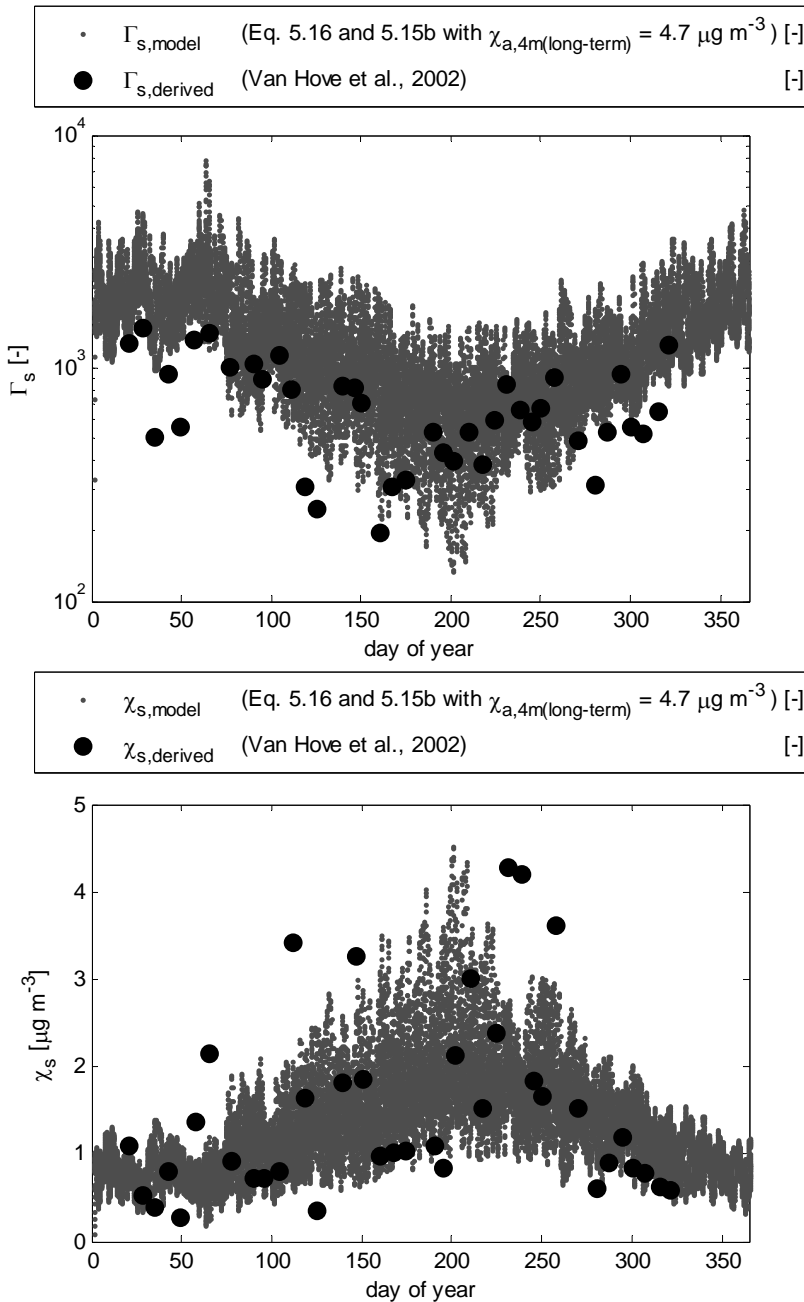


Figure 5.10. Modeled Γ_s (upper panel; Eq. 5.16 with Eq. 5.15b) and χ_s (lower panel; Eq. 5.11 with Eq. 5.16 and Eq. 5.15b) for a 'long-term' NH_3 air concentration of $4.7 \mu\text{g m}^{-3}$ (small gray dots) and derived from the bioassay estimates (large black dots) from Van Hove et al. (2002).

5.6 Conclusion

In this paper, a new model for the surface-atmosphere exchange of ammonia is presented with bi-directional pathways to both the stomata and the external leaf surface. For this purpose, new parameterizations have been derived from long-term ammonia flux measurements over non-fertilized grassland and literature.

- The external leaf surface pathway is described by an external leaf surface resistance, R_w (Eq. 5.6 with $\alpha = 2$ and $\beta = 12$), and a concentration at the external leaf surface, χ_w (Eq. 5.9 with Γ_w from Eq. 5.13). Note that the parameterization of R_w is only accounting for the relative humidity response and that possible effects of the pollution climate and ecosystem on the cuticular exchange are included in χ_w .
- The stomatal pathway is described by a stomatal resistance, R_s (using Emberson et al., 2000a,b), and a stomatal compensation point, χ_s (Eq. 5.12 with Γ_s from Eq. 5.16 with $\Gamma_{s,method}$ from Eq. 5.15).

The generalized equation for Γ_s (Eq. 5.16 with Eq. 5.15a or Eq. 5.15b) accounts for the seasonal variation through the leaf surface temperature and the pollution climate through the 'long-term' NH_3 concentration. This equation is based on 21 literature studies, including this work. The choice for Eq. 5.15a or 5.15b critically depends on the model approach chosen:

- Eq. 5.15a should be used in a single-layer canopy compensation point model (χ_s - R_w or the new χ_s - χ_w model) that does not include the soil and/or leaf litter pathways explicitly, because insufficient soil/leaf litter information is generally available.
- Eq. 5.15b should be used if the stomatal/leaf litter/soil pathways are modeled explicitly.

Although some of the parameterizations are derived from measurements over non-fertilized grassland, we expect that the parameterizations are also valid for other vegetation types and pollution climates. Hence, the new χ_s - χ_w model might be useful for regional and large scale modeling. However, validation of the parameterization scheme with independent data is desirable.

6 Summary and Recommendations

6.1 Summary

In this thesis the surface-atmosphere exchange of ammonia over agricultural grassland in the Netherlands is studied. The main objectives of this thesis are to achieve a better understanding of the surface-atmosphere exchange process of ammonia, especially over agricultural grassland in the Netherlands, and to improve the model description of the surface-atmosphere exchange process of ammonia.

To achieve these objectives, long-term flux measurements of ammonia over agricultural grassland at a micrometeorological weather station in Wageningen have been carried out by the National Institute for Public Health and the Environment (RIVM) in cooperation with the department of Meteorology and Air Quality of Wageningen University. Especially for this project, a new measurement device was designed by the Energy research Centre of the Netherlands (ECN), i.e., the Gradient Ammonia – High Accuracy – Monitor (GRAHAM). The GRAHAM is an improved version of the AMANDA rotating wet denuder system that was developed in the 90s to measure the surface-atmosphere exchange of ammonia.

With the GRAHAM, ammonia concentrations at three heights are measured once every 10 minutes. By using the aerodynamic gradient or flux-profile technique, the vertical concentration gradients are combined with micrometeorological turbulence measurements to obtain ammonia fluxes. This technique can only be applied under certain conditions, e.g. sufficient upwind fetch (homogeneous horizontal conditions), stationarity, no advection, no chemical reactions. If these conditions are not met this will lead to serious errors in the estimated flux. Therefore, only data were selected for data analysis when these conditions were likely to be met. The ammonia flux measurements were performed from June 2004 till December 2006.

An uncertainty analysis revealed that the relative random error in the GRAHAM concentration measurements is about 1.9% under field conditions. The relative random errors in the concentration measurements are propagated in the flux calculation. The relative random error in the ammonia flux is found to be about 52% on average (with a median value of 31%).

Two contrasting periods in 2004 are highlighted in Chapter 3 to illustrate the important mechanisms in the surface-atmosphere exchange process, i.e., a dry and warm summer period and a wet and cool autumn period. In the summer period, (downward) deposition fluxes are observed in the evening, night and early morning, while in the afternoon, (upward) emission fluxes are observed. The autumn period is mainly characterized by deposition fluxes. Frequency distributions of the measured NH_3 -concentrations and fluxes show that despite higher average ambient NH_3 -concentrations ($13.3 \mu\text{g m}^{-3}$ in the summer period vs. $6.4 \mu\text{g m}^{-3}$ in the autumn period) there are more emission events in the summer period than in the autumn period (about 50% in summer vs. 20% in autumn).

The leaf surface wetness appears to be of great importance for the surface-atmosphere exchange of ammonia. In wet condition, mainly deposition occurs. This is due to the high solubility of ammonia in water. However, in dry circumstances, the dissolved ammonia may evaporate from the surface again. Besides, high temperatures can lead to high internal plant concentrations, which may also cause emissions. Note that emission of ammonia from the surface can only be explained if the concentration at the surface is larger than the ambient air concentration. The equilibrium concentration at the vegetated surface for which the net ammonia flux is zero is generally called canopy compensation point. We derived canopy compensation points from flux direction changes during non-stable dry daytime conditions. In these conditions, the canopy compensation point is equal to the air

concentration. For the non-fertilized agricultural grassland site, the derived canopy compensation points range from 0.5 to 29.7 $\mu\text{g m}^{-3}$ with associated leaf temperatures between 7 and 29°C. The average canopy compensation point was $7.0 \pm 5.1 \mu\text{g m}^{-3}$. This is quite high for non-fertilized conditions and is probably caused by high nitrogen input in the past.

As presented in Chapter 3, the surface wetness is an important variable in the surface-atmosphere exchange process of ammonia. Therefore, a comparison between three physical and four empirical leaf wetness models was made in Chapter 4. For this purpose, two different techniques to measure leaf wetness were compared; namely a painted flat-plate grid sensor and a system of four clip sensors. Although both techniques gave comparable results, the flat-plate grid sensor was preferred, because of its stable signal and its ease of use. In this technique, the measurement height turned out to be of great importance for the leaf wetness duration (LWD); the flat-plate sensor at 1.0 m systematically underestimated LWD, while the flat-plate sensor at 0.1 m better represented the actual LWD. To obtain a representative signal, leaf wetness should therefore be measured close to the surface.

Using the available leaf wetness measurements, a comparison was made between the three physical and four empirical leaf wetness models. Without any optimization, the physical model that calculates the potential condensation at the leaf surface gave the best results. However, after optimizing the humidity thresholds in the empirical leaf wetness models, the optimized model based on the difference between the actual and saturated specific humidity at the surface gave best results. For practical application in atmospheric transport models, the relative humidity (RH) threshold model might be easiest to implement. In this study, an optimized RH threshold of 71% was derived for the agricultural grassland site, which is much lower than the threshold of 87% that was previously derived for coniferous forest.

To model the surface-atmosphere exchange of ammonia, different modeling approaches of varying complexity are used. These models are all based on the same concept: resistance modeling using electrical circuit analogue. The different deposition pathways are represented by resistances that may act in series and/or in parallel.

In the canopy resistance modeling approach, the surface resistance is essential in model parameterizations that describe the deposition process of ammonia to the surface. This modeling approach assumes that the surface is a perfect sink, i.e. the ammonia concentration at the surface is zero. However, this assumption is not correct. This can be concluded from the many observed emission events over non-fertilized grassland in Chapter 3, which can only be explained if the concentration at the surface is larger than the ambient air concentration. However, if we would neglect this and apply this canopy resistance model to our data, the derived surface resistances become very large or even negative in emission cases. This is conceptually wrong, as resistances can not be negative by definition.

The canopy compensation point modeling approach does account for a non-zero surface concentration. However, most of these kinds of models only allow for bi-directional exchange through the stomata of plants. In nighttime conditions, there is no stomatal exchange and a zero surface concentration is generally assumed again. In these conditions, we are able to derive the external leaf surface resistance that controls the ammonia exchange at night. In Chapter 2, we have shown that the relatively high background concentrations in this study lead to relatively high external leaf surface resistances. Many studies in literature report similar findings and there are also a few studies that directly relate the external leaf surface resistance to the ambient air concentration.

A close look at the data presented in Chapter 3, learns that emission does not only occur during daytime, but also during nighttime. This means that the exchange with the external

leaf surface should also be bi-directional. Therefore, in Chapter 5, we derived a new model description of the surface-atmosphere exchange of ammonia that accounts for bi-directional exchange with both the stomata and the external leaf surface. This model approach, labeled as χ_s - χ_w model, is similar to the canopy compensation point - cuticular capacitance model (χ_s - C_d model) that is used to model the absorption and desorption of ammonia in a dynamically changing water layer. However, the χ_s - χ_w model does not consider the water layer as a dynamically changing capacitor, but uses empirical relations to estimate the external leaf surface concentration. The external leaf surface concentration appeared to be higher in more polluted conditions and therefore accounts for the pollution climate, but it does not effectively make the exchange with the surface bi-directional. This is because the external leaf surface concentration is approximately parameterized as a fraction of the ambient air concentration and will consequently never exceed the ambient air concentration. Therefore, dynamic processes like desorption of ammonia in the morning due to dew evaporation will not be modeled explicitly by the χ_s - χ_w model.

An important driver in the stomatal exchange of ammonia and thus possible daytime emission fluxes is the stomatal compensation point. The stomatal compensation point is mainly determined by the leaf temperature and the molar ratio between NH_4^+ and H^+ concentration in the intercellular or apoplastic fluid, Γ_s . Reported values for Γ_s in literature range between 20 and 5000. The lower values are found in areas with low ambient ammonia concentrations/low pollution levels, while the higher values are mostly found in agricultural areas/high pollution levels. For non-fertilized grassland, we found a value of 2200 ± 1600 for the summer and autumn data in 2004 and 2500 ± 1700 for all data in 2004-2006.

In this thesis, a seasonal variation in Γ_s is observed. A new, temperature-dependent Γ_s parameterization is therefore developed that accounts for this seasonal variation. It is noted, however, that senescence of plants and field management practices are also expected to influence the seasonal variation of Γ_s on a shorter timescale.

An inventory of 21 literature studies yielded a relation that links Γ_s to the atmospheric pollution level of the location through the 'long-term' NH_3 concentration in the air. Γ_s is linearly increasing with the 'long-term' NH_3 concentration, which means that on average, Γ_s is higher in more polluted areas. Clearly different dependencies of Γ_s on the 'long-term' ammonia concentrations are found for the different derivation methods of Γ_s , i.e., micrometeorological estimates and bioassay estimates. It is clear that the Γ_s values from bioassay estimates, $\Gamma_{s,\text{bioassay}}$, are about a factor of 3 smaller than the Γ_s values from micrometeorological estimates, $\Gamma_{s,\text{micromet}}$. A possible explanation for this difference is that the $\Gamma_{s,\text{micromet}}$ values also include possible other pathways, like the soil and/or the leaf litter pathway. When the soil pathway is not explicitly modeled, the micrometeorological estimates of Γ_s are recommended. In this thesis, the linear relation that accounts for the pollution level is combined with the relation that accounts for the seasonal variation to obtain a more universal relation for Γ_s .

All together, this thesis resulted in a better understanding of the surface-atmosphere exchange process of ammonia over agricultural grassland in the Netherlands and over vegetated surfaces in general. The new insights resulted in a new model description of the surface-atmosphere exchange process of ammonia that is expected to be generally applicable in atmospheric transport models.

6.2 Recommendations

6.2.1 Improving the measurement device

Essential in the research on surface-atmosphere exchange of ammonia are accurate flux measurements. Although the GRAHAM can be considered as state-of-the-art as an improved version of the AMANDA system with many extra data and quality control options, it appeared that the instrument still needs intensive maintenance. Besides, the many moving parts and the long tubes are less favorable.

Recent studies have shown the potential of fast response Tunable Diode Laser Absorption Spectroscopy (TDLAS) and Quantum Cascade Laser Absorption Spectroscopy (QCLAS) for measuring ammonia fluxes by eddy covariance (Famulari et al., 2004; Whitehead et al., 2008). These instruments, however, still use tubes that potentially absorb ammonia on their walls, which may disturb the measurements. However, reasonable good results are presented, especially for periods of large ammonia fluxes, e.g., after manure spreading.

Another instrument that has been developed in the last few years is the Differential Optical Absorption Spectroscopy (DOAS) gradient system at RIVM. This instrument uses two paths (50 meters length) at two different heights over which the concentrations are measured once in about every 2 seconds by absorption spectroscopy. These concentrations are averaged over a certain time interval and are combined with turbulence measurements to obtain the ammonia flux by using the aerodynamic gradient method. Preliminary results over the agricultural grassland site in Wageningen and a maize field in the Netherlands look very promising. Because of its high accuracy, high uptime, low maintenance and its open path, i.e., no wall disturbances, the DOAS gradient system shows a good potential for flux measurements.

6.2.2 Application of the χ_s - χ_w model

Recommended model

Based on the work in this thesis, the following equations (Table 6.1) are recommended in an atmospheric transport model using the single-layer canopy compensation point modeling approach:

Table 6.1. Recommended equations for the new single-layer canopy compensation point model, i.e., the χ_s - χ_w model (derived in this thesis), to be applied in atmospheric transport models.

R_a	Equation 1.7 with Equation 1.8a for unstable ($L < 0$) and with Equation 1.8b for stable conditions ($L > 0$)
R_b	Equation 1.9
R_w	Equation 1.10 with $\alpha=2$ and $\beta=12$
χ_w	Equation 5.9 with Equation 5.13
R_s	Equation 1.11
χ_s	Equation 5.12 with Equation 5.16 with Equation 5.15a

The new description of the surface-atmosphere exchange process of ammonia is expected to be applicable for several vegetation types and is intended to be useful for regional and global atmospheric transport models.

The parameterization for the external (leaf) surface concentration can be considered as vegetation independent, as Van Hove et al. (1987) showed that the transfer of ammonia through the cuticle is very slow and can be neglected. The external (leaf) surface exchange mainly depends on the amount of ammonia dissolved in the external (leaf) surface water layer, parameterized as a function of the ambient air concentration and the surface temperature. The surface concentration is used in combination with the often used relative humidity function that is assumed to account for the wetness of the surface, i.e., the external leaf surface resistance (Equation 1.10 or 5.6). Many studies over different vegetation types use the same formulation of the external leaf surface resistance with different values for the minimum external leaf surface resistance, but generally the same value for the relative humidity response. The constant value for the relative humidity response suggests that the leaf surface wetness is independent on the vegetation, which confirms the general applicability of this function.

The applicability of the parameterization of the stomatal compensation point is more uncertain, as many studies in literature have shown different dependencies. In our literature survey, we could not distinguish a clear vegetation dependent Γ_s , as sometimes is suggested in literature. Instead, the pollution/fertilization level of a site seemed to be more important. In our approach, we used the long-term ammonia concentration at a site as an indicator of the pollution/fertilization level of a site and derived a Γ_s parameterization that is independent on the vegetation.

In the present work and analysis, different dependencies on long-term ammonia concentration for the two methods to derive the compensation points are found, i.e., the bioassay estimates and the micrometeorological estimates. Sutton et al. (2009a) showed that this difference is possibly caused by influences of the soil and/or leaf litter in the micrometeorological estimates. Therefore, the parameterization based on the micrometeorological estimates can be used straightforwardly in a single-layer canopy compensation point model (χ_s - R_w model or the χ_s - χ_w model, derived in this thesis) that does not include the soil and/or leaf litter pathways explicitly, but parameterizes it as a bulk. The parameterization based on the bioassay estimates is suitable for more detailed two-layer canopy compensation point models that include separate pathways for the leaves (stomata and cuticles), the soil and/or the leaf litter. This two-layer model approach needs more specific information about the soil and leaf litter, which is generally unavailable in atmospheric transport models.

Using the χ_s - χ_w model in OPS

A preliminary version of this χ_s - χ_w model was tested with an experimental version of the OPS model at RIVM on independent ammonia measurements from the 'Measuring Ammonia in Nature areas network' (Stolk et al., 2009). The model simulation with the preliminary new model parameterizations is called "OPS new" here, while the model simulation with the old model parameterizations (causing the "ammonia gap") is called "OPS old" here. "OPS old" does not include the stomatal compensation point (χ_s) neither the external leaf surface concentration (χ_w).

Figure 6.1 shows a comparison of the model performances of "OPS new" (closed symbols) and "OPS old" (open symbols) with 117 passive samplers located in nature areas around the country. The modeled concentrations are calculated with the emissions of 2005 and the meteorology of the years 2005-2007, and they are corrected for the difference between the modeling and measurement height. Modeled and measured concentrations are averaged over the whole period 2005-2007. A distinction is made between inland measurement sites (diamonds) and coastal measurement sites (triangles).

The modeled air concentrations with "OPS new" compare very well with the measured air concentrations at inland measuring sites (solid line in Figure 6.1). This seems to confirm that the applied changes in the model description of the surface-atmosphere exchange process explain the former difference between the modeled ("OPS old") and the measured concentrations (dashed line in Figure 6.1), i.e., the ammonia gap. Besides a slope that is closer to 1, the correlation coefficient also increases significantly from 0.75 to 0.84. A part of the improvements, however, are attributed to changes in the description of dispersion in the new version of the experimental OPS model (personal communication Van Jaarsveld). For the coastal measuring sites, however, the systematic underestimation of the modeled concentrations is still observed with "OPS new". A possible explanation is that the ambient air concentration is not accurately modeled at these sites, because the deposition over sea is overestimated and emission from the sea is still underestimated (Stolk et al., 2009). Besides, the measurement technique is less accurate in this concentration range.

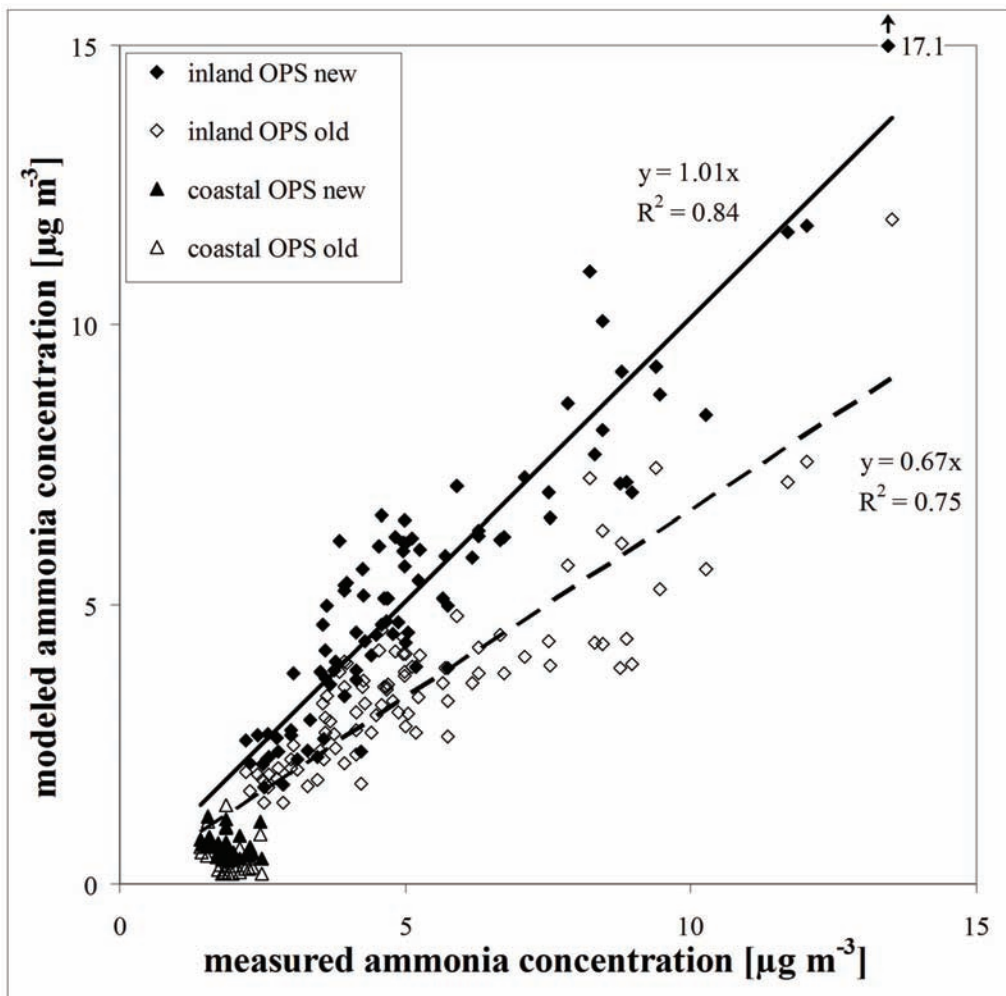


Figure 6.1. Modeled versus measured ammonia concentrations from 2005-2007 in the 'Measuring Ammonia in Nature areas network'. (Source: Stolk et al., 2009; Courtesy to H. Noordijk (PBL) for providing data)

In their report, Stolk et al. (2009) also show the performance of the model simulations as a function of the distance from the edge of the nature area (Figure 6.2). They present this as the fraction between the measured and the modeled concentration (ideally being 1) against the distance from the edge of the nature area.

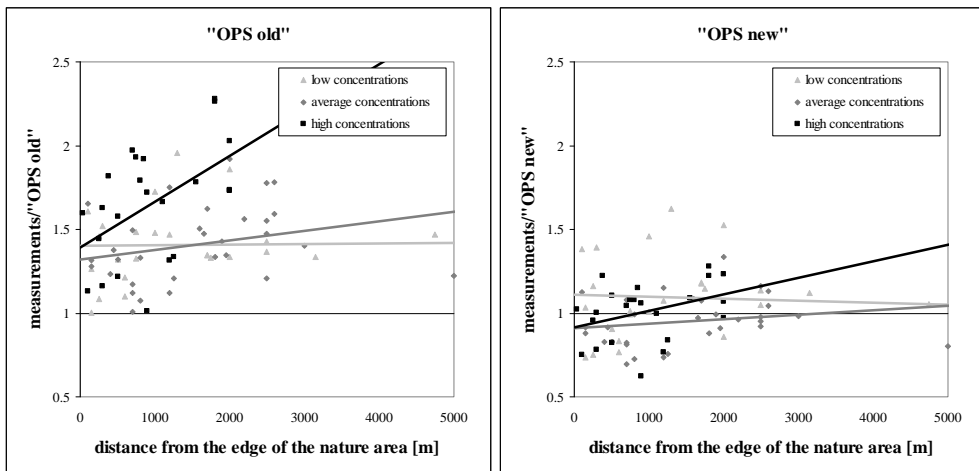


Figure 6.2. Ratio between the measured concentrations and the OPS model simulations versus the distance from the edge of the nature area. Source: Stolk et al. (2009).

It appears that the fraction increases with the distance from the edge for "OPS old", or in other words, deeper into the nature area, the underestimation of "OPS old" becomes larger. This suggests that the deposition onto nature areas used to be too large. This effect is larger for nature areas in more polluted areas. In "OPS new", the fraction is rather constant and closer to 1, in rather clean as well as in more polluted areas. These results support the introduction of the new model description of the surface-atmosphere exchange process also for the (semi-)natural vegetation types. The χ_s - χ_w model can be considered as 'state of the art' in ammonia modeling.

References

- Asman W.A.H., Harrison R.M., Ottley C.J., 1994. Estimation of the net air-sea flux of ammonia over the southern bight of the North Sea. *Atmospheric Environment* 28, 3647-3654.
- Aylor D.E., 1986. A framework for examining inter-regional aerial transport of fungal spores. *Agricultural and Forest Meteorology* 38, 263-288.
- Baldocchi D.D., Hicks B.B., Camara P., 1987. A canopy stomatal resistance model for gaseous deposition to vegetated surfaces. *Atmospheric Environment* 21, 91-101.
- Bass B., Savdie I., Gillespie T.J., 1991. Simulation of leaf wetness duration for field corn. *Agricultural and Forest Meteorology* 57, 69-84.
- Bates R.G., Pinching G.D., 1950. Dissociation constant of aqueous ammonia at 0 to 50° from E. m. f. studies of the ammonium salt of a weak acid. *American Chemical Journal* 72, 1393-1396.
- Beljaars A.C.M., Holtslag A.A.M., 1991. Flux parameterization over land surface for atmospheric models. *Journal of Applied Meteorology* 30, 327-341.
- Benner W.H., Ogorevc B., Novakov T., 1992. Oxidation of SO₂ in thin water films containing NH₃. *Atmospheric Environment* 26, 1713-1723.
- Berkhout A.J.C., van der Hoff G.R., Bergwerff J.B., Swart D.P.J., Hensen A., Kraai A., Bleeker A., Huijsmans J.F.M., Mosquera J., van Pul W.A.J., 2008. Measuring ammonia emissions from manured fields. RIVM Report 6801500003/2008, Bilthoven, the Netherlands. 80pp.
- Bobbink R., Hornung M., Roelofs J.G.M., 1998. The effects of air-borne nitrogen pollutants on species diversity in natural and semi-natural European vegetation. *Journal of Ecology* 86, 717-738.
- Bouwman A.F., Lee D.S., Asman W.A.H., Dentener F.J., Van der Hoek K.W., Olivier J.G.J., 1997. A global high-resolution emission inventory for ammonia. *Global Biogeochemical Cycles* 11, 561-587.
- Buijsman E., Beck J.P., van Bree L., Cassee F.R., Koelemeijer R.B.A., Matthijssen J., Thomas R., Wieringa K., 2005. Fijn stof nader bekeken. MNP Rapport 500037008, Bilthoven, the Netherlands. 58 pp.
- Burkhardt J., Eiden R., 1994. Thin water films on coniferous needles (with an appendix "A new device for the study of water vapor condensation and gaseous deposition to plant surfaces and particle samples", by Burkhardt J. and J. Gerchau). *Atmospheric Environment* 28, 2001-2017.
- Burkhardt J., Flechard C.R., Gresens F., Mattsson M., Jongejan P.A.C., Erisman J.W., Weidinger T., Meszaros R., Nemitz E., Sutton M.A., 2009. Modelling the dynamic chemical interactions of atmospheric ammonia with leaf surface wetness in a managed grassland canopy. *Biogeosciences* 6, 67-84.
- Businger J.A., Wyngaard J.C., Izumi Y., Bradley E.F., 1971. Flux-profile relationships in the atmospheric surface layer. *Journal of the Atmospheric Sciences* 28, 181-189.
- Bussink D.W., Harper L.A., Corre W.J., 1996. Ammonia transport in a temperate grassland: II. Diurnal fluctuations in response to weather and management conditions. *Agronomy Journal* 88, 621-626.
- Cleveland C.C., Townsend A.R., Schimel D.S., Fisher H., Howarth R.W., Hedin L.O., Perakis S.S., Latty E.F., Von Fischer J.C., Elseroad A., Wasson M.F., 1999. Global patterns of terrestrial nitrogen (N₂) fixation in natural ecosystems. *Global Biogeochemical Cycles* 13, 623-645.
- Dabney S.M., Bouldin D.R., 1990. Apparent deposition velocity and compensation point of ammonia inferred from gradient measurements above and through alfalfa. *Atmospheric Environment* 24, 2655-2666.
- Dasgupta P.K., Dong S., 1986. Solubility of ammonia in liquid water and generation of trace levels of standard gaseous ammonia. *Atmospheric Environment* 20, 565-570.

- David M., Loubet B., Cellier P., Mattsson M., Schjoerring J.K., Nemitz E., Roche R., Riedo M., Sutton M., 2009. Ammonia sources and sinks in an intensively managed grassland using dynamic chambers. *Biogeosciences Discussion* 6, 1625-1655.
- Davis D.R., Hughes J.E., 1970. A new approach to recording the wetting parameter by the use of electrical resistance sensors. *Plant Disease Reporter* 54, 474-479.
- Dentener F.J., Crutzen P.J., 1994. A three-dimensional model of the global ammonia cycle. *Journal of Atmospheric Chemistry* 19, 331-369.
- Denmead O.T., Freney J.R., Simpson J.R., 1976. A closed ammonia cycle within a plant canopy. *Soil Biology and Biochemistry* 8, 161-164.
- Derwent R.G., Dollard G.J., Metcalfe S.E., 1988. On the nitrogen budget for the United Kingdom and north-west Europe. *Quarterly Journal of the Royal Meteorological Society* 114, 1127-1152.
- Driscoll C. T., Whittall D., Aber J., Boyer E., Castro M., Cronan C., Goodale C., Groffman P., Hopkinson C., Lambert K., Lawrence G., Ollinger S., 2003. Nitrogen pollution: From the sources to the sea. Hubbard Brook Research Foundation, Science Links Publication 1, 1-24.
- Duyzer J.H., Verhagen H.L.M., Weststrate J.H., Bosveld F.C., Vermetten A.W.M., 1994. The dry deposition of ammonia onto a Douglas fir forest in the Netherlands. *Atmospheric Environment* 28, 1241-1253.
- Duyzer J.H., 1994. Dry deposition of ammonia and ammonium aerosols over heathland. *Journal of Geophysical Research* 99, 18757-18763.
- Dyer A.J., Hicks B.B., 1970. Flux gradient relationships in the constant flux layer. *Quarterly Journal of the Royal Meteorological Society* 96, 715-721.
- Dyer A.J., 1974. A review of flux-profile relationships. *Boundary-Layer Meteorology* 7, 363-372.
- Emberson L.D., Ashmore M.R., Simpson D., Tuovinen J.-P., Cambridge H.M., 2000a. Towards a model of ozone deposition and stomatal uptake over Europe. EMEP/MSC-W 6/2000, Norwegian Meteorological Institute, Oslo, Norway, 57 pp.
- Emberson L.D., Ashmore M.R., Simpson D., Tuovinen J.-P., Cambridge H.M., 2000b. Modelling stomatal ozone flux across Europe. *Water, Air and Soil Pollution* 109, 403-413.
- Erisman J.W., Wyers P., 1993. Continuous measurements of surface exchange of SO₂ and NH₃; Implications for their possible interaction in the deposition process. *Atmospheric Environment* 27, 1937-1949.
- Erisman, J.W., Van Elzakker B.G., Mennen M.G., Hogenkamp J., Zwart E., Vandenbeld L., Romer F.G., Bobbink R., Heil G., Raessen M., Duyzer J.H., Verhage H., Wyers G.P., Otjes R.P., Mols J.J., 1994a. The Elspeetsche Veld Experiment on Surface Exchange of Trace Gases – Summary of Results, *Atmospheric Environment* 28, 487-496.
- Erisman J.W., Van Pul W.A.J., Wyers P., 1994b. Parameterization of surface resistance for the quantification of atmospheric deposition of acidifying compounds and ozone. *Atmospheric Environment* 28, 2595-2607.
- Erisman J.W., Bleeker A., Hensen A., Vermeulen A., 2008. Agricultural air quality in Europe and the future perspectives. *Atmospheric Environment* 42, 3209-3217.
- EU, 2001. Directive 2001/81/EC of the European Parliament and of the Council of 23 October 2001 on national emission ceilings for certain atmospheric pollutants. *Official Journal of the European Communities* L 309/22.
- Famulari D., Fowler D., Hargreaves K., Milford C., Nemitz E., Sutton M.A., Weston K., 2004. Measuring eddy covariance fluxes of ammonia using tunable diode laser absorption spectroscopy. *Water, Air, Soil Pollution* 4, 151-158.
- Fangmeier A., Hadwiger-Fangmeier A., van der Eerden L., Jaeger H.J., 1994. Effects of atmospheric ammonia on vegetation – a review. *Environmental Pollution* 86, 43-82.

- Farquhar G.D., Firth P.M., Wetselaar R., Weir B., 1980. On the gaseous exchange of ammonia between leaves and the environment: Determination of the ammonia compensation point. *Plant Physiology* 66, 710-714.
- Flechard C.R., 1998. Turbulent exchange of ammonia above vegetation. PhD thesis. University of Nottingham. 236 pp.
- Flechard C.R., Fowler D., 1998. Atmospheric ammonia at a moorland site. II: Long-term surface-atmosphere micrometeorological flux measurements. *Quarterly Journal of the Royal Meteorological Society* 124, 759-791.
- Flechard C.R., Fowler D., Sutton M.A., Cape J.N., 1999. A dynamic chemical model of bi-directional ammonia exchange between semi-natural vegetation and the atmosphere. *Quarterly Journal of the Royal Meteorological Society* 125, 2611-2641.
- Fowler D., Cape J.N., Unsworth M.H., 1989. Deposition of atmospheric pollutants on forests. *Phil. Trans. R. Soc. Lond. B* 324, 247-265.
- Fowler D., Pitcairn C.E.R., Sutton M.A., Flechard C., Loubet B., Coyle M., Munro R.C., 1998a. The mass budget of atmospheric ammonia in woodland within 1 km of livestock buildings. *Environmental Pollution* 102, 343-348.
- Fowler D., Flechard C.R., Sutton M.A., Storeton-West R.L., 1998b. Long term measurements of the land-atmosphere exchange of ammonia over moorland. *Atmospheric Environment* 32, 453-459.
- Galloway J.N., Cowling E.B., 2002. Reactive nitrogen in the world: 200 years of change. *Ambio* 31, 64-71.
- Galloway J.N., Aber J.D., Erisman J.W., Seitzinger S.R., Howarth R.W., Cowling E.B., Cosby, B.J., 2003. The Nitrogen Cascade. *BioScience* 53, 341-356.
- Galloway J.N., Dentener F.J., Capone D.G., Boyer E.W., Howarth R.W., Seitzinger S.P., Asner G.P., Cleveland C.C., Green P.A., Holland E.A., Karl D.M., Michaels A.F., Porter J.H., Townsend A.R., Vorosmarty C.J., 2004. Nitrogen cycles: past, present, and future. *Biogeochemistry* 70, 153-226.
- Garland J.A., 1977. The dry deposition of sulphur dioxide to land and water surfaces. *Proceedings of the Royal Society of London A* 354, 245-268.
- Garland J.A., 1978. Dry and wet removal of sulphur from the atmosphere. *Atmospheric Environment* 12, 349-362.
- Garratt J.R., Segal M., 1988. On the contribution of atmospheric moisture to dew formation. *Boundary-Layer Meteorology* 45, 209-236.
- Garratt J.R., 1992. *The atmospheric boundary layer*. Cambridge University Press, Cambridge. 316 pp.
- Gash J.H.C., 1986. A note on estimating the effect of a limited fetch on micrometeorological evaporation measurements. *Boundary-Layer Meteorology* 35, 409-413.
- Gillespie T.J., Kidd G.E., 1978. Sensing duration of leaf moisture retention using electrical impedance grids. *Canadian Journal of Plant Science* 58, 179-187.
- Gleason M.L., Taylor S.E., Loughin T.M., Koehler K.J., 1994. Development of validation of an empirical model to estimate the duration of dew periods. *Plant Disease* 78, 1011-1016.
- Grennfelt P., Hov Ø., Derwent R.G., 1994. Second generation abatement strategies for NO_x, NH₃, SO₂ and VOC. *Ambio* 23, 425-433.
- Heusinkveld B.G., Berkowicz S.M., Jacobs A.F.G., Hillen W., Holtslag A.A.M., 2008. A new remote optical wetness sensor and its applications. *Agricultural and Forest Meteorology* 148, 580-591.
- Hicks B.B., Baldocchi D.D., Meyers T.P., Hosker R.P., Matt D.R., 1987. A preliminary multiple resistance routine for deriving dry deposition velocities from measured quantities. *Water, Air and Soil Pollution* 36, 311-330.

- Hill P.W., Raven J.A., Loubet B., Fowler D., Sutton M.A., 2001. Comparison of gas exchange and bioassay determinations of the ammonia compensation point in *Luzula sylvatica* (Huds.) Gaud. *Plant Physiology* 125, 476-487.
- Holtslag A.A.M., Van Ulden A.P., 1983. A simple scheme for daytime estimates of the surface fluxes from routine weather data. *Journal of Climate and Applied Meteorology* 22, 517-529.
- Holtslag A.A.M., de Bruin H.A.R., 1988. Applied modeling of the nighttime surface energy balance over land. *Journal of Applied Meteorology* 27, 689-704.
- Horvath L., Asztalos M., Fuhrer E., Meszaros R., Weidinger T., 2005. Measurement of ammonia exchange over grassland in the Hungarian Great Plain. *Agricultural and Forest Meteorology* 130, 282-298.
- Huber L., Itier B., 1990. Leaf wetness duration in a field bean canopy. *Agricultural and Forest Meteorology* 51, 281-292.
- Huber L., Gillespie T.J., 1992. Modeling leaf wetness in relation to plant disease epidemiology. *Annual Reviews of Phytopathology* 30, 553-577.
- Husted S., Mattsson M., Schjoerring J.K., 1996. NH₃ compensation points in 2 cultivars of *Hordeum vulgare* L. during vegetative and generative growth. *Plant, Cell and Environment* 19, 1299-1306.
- Husted S., Schjoerring J.K., 1995. A computer-controlled system for studying ammonia exchange, photosynthesis and transpiration of plant canopies growing under controlled environmental conditions. *Plant Cell Environment* 18, 1070-1077.
- Husted S., Schjoerring J.K., 1995. Apoplastic pH and ammonium concentration in leaves of *Brassica napus* L.. *Plant Physiology* 109, 1453-1460.
- Husted S., Schjoerring J.K., 1996. Ammonia flux between oilseed rape plants and the atmosphere in response to changes in leaf temperature, light intensity, and air humidity: interactions with leaf conductance and apoplastic NH₄⁺ and H⁺ concentrations. *Plant Physiology* 112, 67-74.
- Husted S., Schjoerring J.K., Nielsen K.H., Nemitz E., Sutton M.A., 2000. Stomatal compensation points for ammonia in oilseed rape plants under field conditions. *Agricultural and Forest Meteorology* 105, 371-383.
- IPCC, 2007. *Climate Change 2007: The Physical Science Basis. Contribution of Working Group I to the Fourth Assessment Report of the Intergovernmental Panel on Climate Change.* Editors: S. Solomon, D. Qin, M. Manning, Z. Chen, M. Marquis, K.B. Averyt, M. Tignor and H.L. Miller. Cambridge University Press, Cambridge, United Kingdom and New York, NY, USA, 996 pp.
- Jacob D.J., 1999. *Introduction to atmospheric chemistry.* Princeton University Press, Princeton, New Jersey. 266 pp.
- Jacobs A.F.G. Nieveen J.P., 1995. Formation of dew and the drying process within crop canopies. *Meteorological Applications* 2, 249-256.
- Jacobs A.F.G., Heusinkveld B.G., Kessel G.J.T., 2005. Simulating of leaf wetness duration within a potato canopy. *Netherlands Journal of Agricultural Science* 53, 151-166.
- Jacobs A.F.G., Heusinkveld B.G., Wichink Kruit R.J., Berkowicz S.M., 2006. Contribution of dew to the water budget of a grassland area in the Netherlands. *Water Resources Research* 42, W03415, doi:10.1029/2005WR004055. 8pp.
- Jakobsen H.A., Jonson J.E., Berge E., 1997. The multi-layer Eulerian model: Model description and evaluation of transboundary fluxes of sulphur and nitrogen for one year, EMEP/MS-CW Report 2/97, EMEP/Meteorological Synthesizing Centre - West, The Norwegian Meteorological Institute, Oslo, 1997.
- Jolliffe I.T., Stephenson D.B., 2003. *Forecast verification: A practitioner's guide in atmospheric science.* J. Wiley, Chichester, England, 240pp.

- Jones A.L., 1986. Role of wet periods in predicting foliar diseases. In: K.J. Leonard & W.E. Fry (Eds), *Plant Disease Epidemiology*. Vol. 1. Population Dynamics and Management. MacMillan, New York, pp. 87–100.
- Jones M.R., Leith I.D., Fowler D., Raven J.A., Sutton M.A., Nemitz E., Cape J.N., Sheppard L.J., Smith R.I., Theobald M.R., 2007a. Concentration-dependent NH₃ deposition processes for mixed moorland semi-natural vegetation. *Atmospheric Environment* 41, 2049-2060.
- Jones M.R., Leith I.D., Raven J.A., Fowler D., Sutton M.A., Nemitz E., Cape J.N., Sheppard L.J., Smith R.I., 2007b. Concentration-dependent NH₃ deposition processes for moorland plant species with and without stomata. *Atmospheric Environment* 41, 8980-8994.
- Kaimal J.C. and Finnigan J.J., 1994. *Atmospheric Boundary Layer Flows. Their Structure and Measurement*. Oxford University Press, New York, Oxford. 289 pp.
- Kim K.S., Gleason M.L., Taylor S.E., 2006. Forecasting site-specific leaf wetness duration for input to disease-warning systems. *Plant Disease* 90, 650-656.
- Kim K.S., Taylor S.E., Gleason M.L., Koehler K.J., 2002. Model to enhance site-specific estimation of leaf wetness duration. *Plant Disease* 86, 179-185.
- Klemm O., Milford C., Sutton M.A., Spindler G., van Putten E., 2002. A climatology of leaf surface wetness. *Theoretical and Applied Climatology* 71, 107-117.
- Lau Y.F., Gleason M.L., Zriba N., Taylor S.E., Hinz P.N., 2000. Effects of coating, deployment angle, and compass orientation on performance of electronic wetness sensors during dew periods. *Plant Disease* 84, 192–197.
- Lelieveld J. and Dentener F., 2000. What controls tropospheric ozone? *Journal of Geophysical Research* 105, 3531–3551.
- Long I.F., 1955. Dew and guttation. *Weather* 10, 128.
- Loubet B., Milford C., Hill P.W., Tang Y.S., Cellier P., Sutton M.A., 2002. Seasonal variability of apoplastic NH₄⁺ and pH in an intensively managed grassland. *Plant and Soil* 238, 97-110.
- Luo W.H., Goudriaan J., 2000. Dew formation on rice under varying durations of nocturnal radiative loss. *Agricultural and Forest Meteorology* 104, 303–313.
- Madeira A.C., Kim K.S., Taylor S.E., Gleason M.L., 2002. A simple cloud-based energy balance model to estimate dew. *Agricultural and Forest Meteorology* 111, 55-63.
- Mattsson M., Hausler R.E., Leegood R.C., Lea P.J., Schjoerring J.K., 1997. Leaf-atmosphere NH₃ exchange in Barley mutants with reduced activities of glutamine synthetase. *Plant Physiology* 114, 1307-1312.
- Mattsson M., Schjoerring J.K., 2002. Dynamic and steady-state responses of inorganic nitrogen pools and NH₃ exchange in leaves of *Lolium Perenne* and *Bromus erectus* to changes in root nitrogen supply. *Plant Physiology* 128, 742-750.
- Mattsson M., Schjoerring J.K., 2003. Senescence-induced changes in apoplastic and bulk tissue ammonia concentrations of ryegrass leaves. *New Phytologist* 160, 489-499.
- Mattsson M., Herrmann B., Jones S., Neftel A., Sutton M.A., Schjoerring J.K., 2009. Contribution of different grass species to plant-atmosphere ammonia exchange in intensively managed grassland. *Biogeosciences* 6, 59-66.
- Meixner F.X., Wyers G.P., Neftel A., 1996. Bi-directional exchange of ammonia over cereals. In: Borrell P.M., Borrell P., Kelly K., Cavitas T., Seiler W. (Eds.). *Proceedings of EUROTRAC '96*. Computer Mechanics Publications, Southampton, UK. pp 129-135.
- Mennen M.G., Van Elzakker B.G., Van Putten E.M., Uiterwijk J.W., Regts T.A., Van Hellemond J., Wyers G.P., Otjes R.P., Verhage A.J.L., Wouters L.W., Heffels C.J.G., Römer F.G., Van den Beld L., Tetteroo J.E.H., 1996. Evaluation of automatic ammonia monitors for application in an air quality monitoring network. *Atmospheric Environment* 30, 3239-3256.

- Milford C., Theobald M.R., Nemitz E., Sutton M.A., 2001a. Dynamics of ammonia exchange in response to cutting and fertilising in an intensively-managed grassland. *Water, Air, and Soil Pollution: Focus* 1, 167-176.
- Milford C., Hargreaves K.J., Sutton M.A., 2001b. Fluxes of NH₃ and CO₂ over upland moorland in the vicinity of agricultural land. *Journal of Geophysical Research* 106, 24169-24181.
- Milieubalans, 2008. PBL Report 500081007, Planbureau voor de Leefomgeving, Bilthoven, the Netherlands, 232 pp.
- Milieu- en Natuurcompendium, 2008. Ammoniakemissie door de land- en tuinbouw, 1990-2007. MNP, Bilthoven, CBS, Voorburg, and WUR, Wageningen, PBL/MNC/jul08/0101.
- Monin A.S., Obukhov A.M., 1954. Basic laws of turbulent mixing in the ground layer of the atmosphere. *Trans. Geophys. Inst. Akad. Nauk USSR* 151, 163-187.
- Monteith J.L., 1957. Dew. *Quarterly Journal of the Royal Meteorological Society* 83, 322-341.
- Monteith J.L., 1981. Evaporation and surface temperature, *Quarterly Journal of the Royal Meteorological Society* 107, 1-27.
- Monteith J.L., Unsworth M.H., 1990. *Principles of environmental physics* 2nd edn. Edward Arnold, London, 291 pp.
- Mosquera J., Hensen A., Van den Bulk W.C.M., Vermeulen A.T., Erisman J.W., 2001. Long term NH₃-flux measurements above grasslands in the Netherlands. *Water, Air and Soil Pollution* 1, 203-212.
- Murphy A.H., 1993. What is a good forecast? An essay on the nature of goodness in weather forecasting.
- Neirynek J., Kowalski A.S., Carrara A., Ceulemans R., 2005. Driving forces for ammonia fluxes over mixed forest subjected to high deposition loads. *Atmospheric Environment* 39, 5013-5024.
- Neirynek J., Ceulemans R., 2008. Bidirectional ammonia exchange above a mixed coniferous forest. *Environmental Pollution* 154, 424-438.
- Nemitz E., Sutton M.A., Gut A., San Jose R., Husted S., Schjoerring J.K., 2000a. Sources and sinks of ammonia within an oilseed rape canopy. *Agricultural and Forest Meteorology* 105, 385-404.
- Nemitz E., Sutton M.A., Schjoerring J.K., Husted S., Wyers G.P., 2000b. Resistance modelling of ammonia exchange over oilseed rape. *Agricultural and Forest Meteorology* 105, 405-425.
- Nemitz E., Milford C., Sutton M.A., 2001. A two-layer canopy compensation point model for describing bi-directional biosphere-atmosphere exchange of ammonia. *Quarterly Journal of the Royal Meteorological Society* 127, 815-833.
- Nemitz E., Sutton M.A., Wyers G.P., Jongejan P.A.C., 2004. Gas-particle interactions above a Dutch heathland: I. Surface exchange fluxes of NH₃, SO₂, HNO₃ and HCl. *Atmospheric Chemistry and Physics* 4, 989-1005.
- Nemitz E., Flechard C., Famulari D., Sutton M.A., 2008. Towards a generalised parameterisation of bi-directional ammonia exchange. Presentation at the NitroEurope IP Open Science conference: Reactive nitrogen and the European greenhouse gas balance. Ghent, Belgium.
- Nieuwstadt F., 1978. The computation of the friction velocity u_* and the temperature scale T_* from temperature and wind velocity profiles by least-square methods. *Boundary-Layer Meteorology* 14, 235-246.
- Norman J.M., Campbell G., 1983. Application of a plant environment model to problems in the environment. *Advanced Irrigation* 2, 155-188.
- Nurmi P., 2003. Recommendations on the verification of local weather forecasts. ECMWF, Reading, UK, Technical Memorandum No. 430, 19 pp.

- Paulson C.A., 1970. The mathematical representation of wind speed and temperature profiles in the unstable atmospheric surface layer. *Journal of Applied Meteorology* 9, 857-861.
- Pedro M.J., 1980. Relation of leaf surface wetness duration to meteorological parameters. PhD Dissertation. University of Guelph, Guelph, ON, Canada. 200 pp.
- Pedro M.J., Gillespie T.J., 1982a. Estimating dew duration. I. Utilizing micrometeorological data. *Agricultural Meteorology* 25, 283-296.
- Pedro M.J., Gillespie T.J., 1982b. Estimating dew duration. II. Utilizing standard weather station data. *Agricultural Meteorology* 25, 297-310.
- Personne E., Loubet B., Herrmann B., Mattsson M., Schjoerring J.K., Nemitz E., Sutton M.A., Cellier P., 2009. SURFATM-NH3: a model combining the surface energy balance and bi-directional exchanges of ammonia applied at the field scale. *Biogeosciences* 6, 1371-1388.
- Pitcairn C.E.R., Leith I.D., Sheppard L.J., Sutton M.A., Fowler D., Munro R.C., Tang S., Wilson D., 1998. The relationship between nitrogen deposition, species composition and foliar nitrogen concentrations in woodland flora in the vicinity of livestock farms. *Environmental Pollution* 102, 41-48.
- Plantaz M.A.H.G., 1998. Surface/atmosphere exchange of ammonia over grazed pasture. PhD thesis, Wageningen Universiteit, the Netherlands, 199 pp.
- Postgate J, 1998. Nitrogen Fixation. Cambridge University Press, Cambridge UK. 196 pp.
- Rao P.S., Gillespie T.J., Schaafsma A.W., 1998. Estimating wetness on maize ears from meteorological observations. *Canadian Journal of Soil Science* 78, 149-154.
- Riedo M., Milford C., Schmid M., Sutton M., 2002. Coupling soil-plant-atmosphere exchange of ammonia with ecosystem functioning in grasslands. *Ecological Modelling* 158, 83-110.
- Schjoerring J.K., Kyllingsbaek A, Mortensen J.V., Byskov-Nielsen S., 1993. Field investigations of ammonia exchange between barley plants and the atmosphere. I. Concentration profiles and flux densities of ammonia. *Plant Cell Environment* 16, 161-167.
- Schjoerring J.K., Husted S., Mattsson M., 1998. Physiological parameters controlling plant-atmosphere ammonia exchange. *Atmospheric Environment* 32, 491-498.
- Schjoerring J.K., Husted S., Mack G., Nielsen K.H., Finnemann J., Mattsson M., 2000. Physiological regulation of plant-atmosphere ammonia exchange. *Plant and Soil* 221, 95-102.
- Schlesinger R.B., Cassee F., 2003. Atmospheric secondary inorganic particulate matter: the toxicological perspective as a basis for health effects risk assessment. *Inhalation toxicology* 15, 197-235.
- Schuepp P.H., Leclerc M.Y., Macpherson J.I., Desjardins R.L., 1990. Footprint prediction of scalar fluxes from analytical solutions of the diffusion equation. *Boundary-layer Met.*, 50, 353-373.
- Seinfeld J.H., Pandis S.N., 2006. Atmospheric chemistry and physics. From air pollution to climate change. John Wiley and Sons, New Jersey. 1203 pp.
- Sentelhas P.C., Gillespie T.J., Gleason M.L., Monteiro J.E., Helland S.T., 2004a. Operational exposure of leaf wetness sensors. *Agricultural and Forest Meteorology* 126, 59-72.
- Sentelhas P.C., Monteiro J.E., Gillespie T.J., 2004b. Electronic leaf wetness duration sensor: why it should be painted. *International Journal of Biometeorology* 48, 202-205.
- Sentelhas P.C., Gillespie T.J., Batzer J.C., Gleason M.L., Monteiro J.E., Pezzopane J.R., Pedro M.J., 2005. Spatial variability of leaf wetness duration in different crop canopies. *International Journal of Biometeorology* 49, 363-370.

Simpson D., Fagerli H., Jonson J.E., Tsyro S., Wind P., Tuovinen J-P., 2003. Transboundary Acidification, Eutrophication and Ground Level Ozone in Europe. Part 1. Unified EMEP Model Description. EMEP Report 1/2003, EMEP/MS-CHEM, 74 pp.

Smil V., 1999a. Nitrogen in crop production: An account of global flows. *Global Biogeochemical Cycles* 13, 647-662.

Smil V., 1999b. Detonator of the population explosion. *Nature* 440, 415.

Smith R.I., Fowler D., Sutton M.A., Flechard C., Coyle M., 2000. Regional estimation of pollutant gas dry deposition in the UK: model description, sensitivity analyses and outputs. *Atmospheric Environment* 34, 3757-3777.

Spindler G., Teichmann U., Sutton M.A., 2001. Ammonia dry deposition over grassland - micrometeorological flux-gradient measurements and bidirectional flux calculations using an inferential model. *Quarterly Journal of the Royal Meteorological Society* 127, 795-814.

Steenvoorden J.H.A.M., Bruins W.J., van Eerd M.M., Hoogeveen M.W., Hoogervorst N., Huijsmans J.F.M., Lenemann H., van der Meer H.G., Monteny G.J., de Ruijter F.J., 1999. Monitoring van nationale ammoniakemissies uit de landbouw. Op weg naar een verbeterde rekenmethodiek. Reeks Milieuplanbureau 6, DLO-Staring Centrum.

Stolk A.P., van Zanten M.C., Noordijk H., van Jaarsveld J.A., van Pul W.A.J., 2009. Meetnet Ammoniak in Natuurgebieden. Meetresultaten 2005-2007. RIVM Rapport 680710001, Bilthoven, the Netherlands, 140 pp.

Stull R.B., 1988. An introduction to Boundary Layer Meteorology. Kluwer Academic Publishers, Dordrecht, the Netherlands. 670 pp.

Sutton M.A., Moncrieff J.B., Fowler D., 1992. Deposition of atmospheric ammonia to moorlands. *Environmental Pollution* 75, 15-24.

Sutton M.A., Fowler D., 1993. A model for inferring bidirectional fluxes of ammonia over plant canopies. *Proceedings of the WMO Conference on the Measurement and Modelling of Atmospheric Composition Changes Including Pollution Transport. WMO/GAW-91, WMO Geneva, 179-182.*

Sutton M.A., Fowler D., Moncrieff J.B., 1993a. The exchange of atmospheric ammonia with vegetated surfaces. I: Unfertilized vegetation. *Quarterly Journal of the Royal Meteorological Society* 119, 1023-1045.

Sutton M.A., Fowler D., Moncrieff J.B., Storeton-West R.L., 1993b. The exchange of atmospheric ammonia with vegetated surfaces. II. Fertilized vegetation. *Quarterly Journal of the Royal Meteorological Society* 119, 1047-1070.

Sutton M.A., Pitcairn C.E.R., Fowler D., 1993c. The exchange of ammonia between the atmosphere and plant communities. *Advances in Ecological Research* 24, 301-389.

Sutton M.A., Schjoerring J.K., Wyers G.P., 1995a. Plant-atmosphere exchange of ammonia [and discussion]. *Philosophical Transactions of the Royal Society London A* 351, 261-278.

Sutton M.A., Fowler D., Burkhardt J.K., Milford C., 1995b. Vegetation atmosphere exchange of ammonia: canopy cycling and the impacts of elevated nitrogen inputs. *Water, Air and Soil Pollution* 85, 2057-2063.

Sutton M.A., Milford C., Dragosits U., Singles R., Fowler D., Ross C., Hill R., Jarvis S.C., Pain B.F., Harrison R., Moss D., Webb J., Espenhahn S., Halliwell C., Lee D.S., Wyers G.P., Hill J., ApSimon H.M., 1997. Gradients of atmospheric ammonia concentrations and deposition downwind of ammonia emissions: First results of the ADEPT Burrington Moor Experiment. Pp. 131-139 in *Gaseous nitrogen emissions from grasslands*. Eds S.C. Jarvis and B.F. Pain. CAB International, Oxford, UK.

Sutton M.A., Burkhardt J.K., Guerin D., Nemitz E. and Fowler D., 1998. Development of resistance models to describe measurements of bi-directional ammonia surface-atmosphere exchange. *Atmospheric Environment* 32, 473-480.

- Sutton M.A., Nemitz E., Fowler D., Wyers G.P., Otjes R.P., Schjoerring J.K., Husted S., Nielsen K.H., San José R., Moreno J., Gallagher M.W., Gut A., 2000. Fluxes of ammonia over oilseed rape - Overview of the EXAMINE experiment. *Agricultural and Forest Meteorology* 105, 327-349.
- Sutton M.A., Milford C., Nemitz E., Theobald M.R., Hill P.W., Fowler D., Schjoerring J.K., Mattsson M.E., Nielsen K.H., Husted S., Erisman J.W., Otjes R., Hensen A., Mosquera J., Cellier P., Loubet B., David M., Genermont S., Neftel A., Blatter A., Herrmann B., Jones S.K., Horvath L., Führer E.C., Mantzanas K., Koukoura Z., Gallagher M., Williams P., Flynn M. and Riedo M., 2001. Biosphere-atmosphere interactions of ammonia with grasslands: Experimental strategy and results from a new European initiative. *Plant and Soil* 228, 131-145.
- Sutton M.A., Nemitz E., Milford C., Campbell C., Erisman J.W., Hensen A., Cellier P., David M., Loubet B., Personne E., Schjoerring J.K., Mattsson M., Dorsey J.R., Gallagher M.W., Horvath L., Weidinger T., Meszaros R., Dammgen U., Neftel A., Herrmann B., Lehman B.E., Flechard C., Burkhardt J., 2009a. Dynamics of ammonia exchange with cut grassland: strategy and implementation of the GRAMINAE Integrated Experiment. *Biogeosciences* 6, 309-331.
- Sutton M.A., Reis S., Baker S.M.H., 2009b. *Atmospheric Ammonia. Detecting emission changes and environmental impacts.* Springer, 464 pp.
- Thom A.S., Stewart J.B., Oliver H.R., Gash J.H.C., 1975. Comparison of aerodynamic and energy budget estimates of fluxes over a pine forest. *Quarterly Journal of the Royal Meteorological Society* 101, 93-105.
- UNEP, WHRC, 2007. *Reactive Nitrogen in the Environment: Too much or too little of a good thing.* United Nations Programme, Paris, 56 pp.
- Van Breemen N., Burrough P.A., Velthorst E.J., Van Dobben H.F., De Wit T., Ridder T.B., Reijnders H.F.R., 1982. Soil acidification from atmospheric ammonium sulphate in forest canopy throughfall. *Nature* 299, 548-550.
- Van den Ende J.E., Pennock-Vos M.G., Bastiaansen C., Koster A.Th.J., Van der Meer L.J., 2000. BoWaS: a weather-based warning system for the control of Botrytis blight in lily. *Acta Horticulturae* 519, 215-220.
- Van Dijk A., Moene A.F., De Bruin H.A.R., 2004. *The principles of surface physics: theory, practice and description of the ECPACK library.* Internal Report 2004/1, Meteorology and Air Quality Group, Wageningen University, Wageningen, the Netherlands. 99 pp.
- Van Gijlswijk R., Coenen P., Pulles T., Van der Sluijs J., 2004. Uncertainty assessment of NO_x, SO₂ and NH₃ emissions in the Netherlands. Rapport R 2004/100, TNO Environment, Energy and Process Innovation, Apeldoorn.
- Van Hove L.W.A., Koops A.J., Adema E.H., Vredenberg W.J., Pieters G.A., 1987. Analysis of the uptake of atmospheric ammonia by leaves of *Phaseolus vulgaris* l. *Atmospheric Environment* 21, 1759-1763.
- Van Hove L.W.A., Tonk W.J.M., Pieters G.A., Adema E.H., Vredenberg W.J., 1988. A leaf chamber for measuring the uptake of pollutant gases at low concentrations by leaves, transpiration and carbon dioxide assimilation. *Atmospheric Environment* 22, 2515-2523.
- Van Hove L.W.A., Adema E.H., Vredenberg W.J., Pieters G.A., 1989. A study of the adsorption of NH₃ and SO₂ on leaf surfaces. *Atmospheric Environment* 23, 1479-1486.
- Van Hove L.W.A., Adema E.H., 1996. The effective thickness of water films on leaves. *Atmospheric Environment* 30, 2933-2936.
- Van Hove L.W.A., Heeres P., Bossen M.E., 2002. The annual variation in stomatal ammonia compensation point of rye grass (*Lolium perenne* L.) leaves in an intensively managed grassland. *Atmospheric Environment* 36, 2965-2977.
- Van Jaarsveld J.A., Bleeker A., Hoogervorst N.J.P., 2000. Evaluatie ammoniak emissiereducties met behulp van metingen en modelberekeningen. RIVM rapport 722108025, Bilthoven, the Netherlands. 62 pp.
- Van Jaarsveld J.A., Van Pul W.A.J., 2002. Berekenende ammoniakconcentraties in Nederland vergeleken met de intensiveringsmetingen met passieve samplers. RIVM Report 725501006/2002, Bilthoven, the Netherlands. 36 pp.

- Van Jaarsveld J.A., 2004. The Operational Priority Substances model: Description and validation of OPS-Pro 4.1. RIVM report 500045001, Bilthoven, the Netherlands, 156 pp.
- Van Pul W.A.J., Jacobs A.F.G., 1994. The conductance of a maize crop and the underlying soil to ozone under various environmental conditions. *Boundary-Layer Meteorology* 69, 83-99.
- Van Pul W.A.J., De Haan B.J., Van Dam J.D., Van Eerd M.M., De Ruiten J.F., Van Hinsberg A., Westhoek H.J., 2004. (Kosten-) Effectiviteit Generiek en Gebiedsgericht ammoniakbeleid. RIVM Report 500033001/2004, Bilthoven, the Netherlands, 58 pp.
- Van Pul W.A.J., Van den Broek M.M.P., Volten H., Van der Meulen A., Berkhout S., Van der Hoek K.W., Wichink Kruit R., Huijsmans J.F.M., Van Jaarsveld J.A., De Haan B., Koelemeijer R., 2008. Het ammoniakgat: onderzoek en duiding. RIVM Report 680150002, Bilthoven, the Netherlands, 97 pp.
- Velthof G.L., van Bruggen C., Groenestein C.M., de Haan B.J., Hoogeveen M.W., Huijsmans J.F.M., 2009. Methodology to calculate ammonia emissions by Dutch agriculture. Wageningen, Statutory Research Tasks Unit for Nature and the Environment, WOt Report No. 70. 180 pp.
- Walker J.T., Whitall D.R., Robarge W., Paerl H.W., 2004. Ambient ammonia and ammonium aerosol across a region of variable ammonia emission density. *Atmospheric Environment* 38, 1235-1246.
- Walker J.T., Robarge W.P., Wu Y., Meyers T.P., 2006. Measurement of bi-directional ammonia fluxes over soybean using the modified Bowen-ratio technique. *Agricultural and Forest Meteorology* 138, 54-68.
- Warneck P., 2000. Chemistry of the natural atmosphere. International Geophysics Series 71. Academic Press, San Diego. 927 pp.
- Webb E.K., Pearman G.I., Leuning R., 1980. Correction of flux measurements for density effects due to heat and water vapour transfer. *Quarterly Journal of the Royal Meteorological Society* 106, 85-100.
- Wei Y.Q., Bailey B.J., Stenning B.C., 1995. A wetness sensor for detecting condensation on tomato plants in greenhouses. *Journal of Agricultural Engineering Research* 61, 197-204.
- Wesely M.L., 1989. Parameterization of surface resistances to gaseous dry deposition in regional-scale numerical models. *Atmospheric Environment* 23, 1293-1304.
- Whitehead D.C., Lockyer D.R., Raistrick N., 1988. The volatilization of ammonia from perennial ryegrass during decomposition, drying and induced senescence. *Annals of Botany* 61, 567-571.
- Whitehead D.C., Lockyer D.R., 1989. Decomposing grass herbage as a source of ammonia in the atmosphere. *Atmospheric Environment* 23, 1867-1869.
- Whitehead J.D., Twigg M., Famulari D., Nemitz E., Sutton M.A., Gallagher M.W., Fowler D., 2008. Evaluation of laser absorption spectroscopic techniques for eddy covariance flux measurements of ammonia. *Environmental Science and Technology* 42, 2041-2046.
- Wichink Kruit R.J., Van Pul W.A.J., Jacobs A.F.G., Heusinkveld B.G., 2004. Comparison between four methods to estimate leaf wetness duration caused by dew on grassland. 26th Conference on Agricultural and Forest Meteorology. Proceedings, 4 pp.
- Wichink Kruit R.J., Van Pul W.A.J., Otjes R.P., Hofschreuder P., Jacobs A.F.G., Holtslag A.A.M., 2007. Ammonia fluxes and derived canopy compensation points over non-fertilized agricultural grassland in the Netherlands using the new gradient ammonia - high accuracy - monitor (GRAHAM). *Atmospheric Environment* 41, 1275-1287.
- Wichink Kruit R.J., Jacobs A.F.G., Holtslag A.A.M., 2008. Measurements and estimates of leaf wetness over agricultural grassland for dry deposition modeling of trace gases. *Atmospheric Environment* 42, 5304-5316.
- Wichink Kruit R.J., Stolk A., Van Pul W.A.J., 2009. NH₃ flux estimates at the micrometeorological weather station in Wageningen, the Netherlands. RIVM Letter Report 680150004, Bilthoven, the Netherlands, 56pp.

Wichink Kruit R.J., Van Pul W.A.J., Sauter F.J., Van den Broek M., Nemitz E., Sutton M.A., Krol M., Holtslag A.A.M., 2010. Modeling the surface-atmosphere exchange of ammonia. *Atmospheric Environment* 44, 945-957.

Wilks D.S., 1995. *Statistical methods in the atmospheric sciences: An introduction*. International Geophysics Series, Vol. 59, Academic Press, San Diego, 464 pp.

Wyers G.P., Otjes R.P., Slanina J., 1993. A continuous flow denuder for the measurement of ambient concentrations and surface fluxes of ammonia. *Atmospheric Environment* 27, 2085-2090.

Wyers G.P., Erisman J.W., 1998. Ammonia Exchange over coniferous forest. *Atmospheric Environment* 32, 441-451.

Appendix A. Ammonium-ammonia equilibrium

A general relationship between the gaseous ammonia concentration and the NH_4^+ concentration and pH in a solution, can be derived from the temperature response of the Henry equilibrium and the ammonium-ammonia dissociation equilibrium. Ammonia is well soluble in water, although the solubility decreases with increasing temperature (T) according to the Henry equilibrium:



where H_{NH_3} ($\text{mol l}^{-1} \text{Pa}^{-1}$) is the Henry equilibrium constant (Dasgupta and Dong, 1986):

$$H_{\text{NH}_3} = \frac{[\text{NH}_3(\text{aq})]}{[\text{NH}_3(\text{g})]} = 5.527 \cdot 10^{-4} \exp\left[4092\left(\frac{1}{T} - \frac{1}{298.15}\right)\right] \quad (\text{A1.1b})$$

In the presence of water, ammonia is readily protonated to ammonium, the degree of dissociation depends on the pH and temperature:



where $K_{\text{NH}_4^+}$ (mol l^{-1}) is the ammonium-ammonia dissociation equilibrium constant (Bates and Pinching, 1950):

$$K_{\text{NH}_4^+} = \frac{[\text{NH}_3(\text{aq})] \cdot [\text{H}^+]}{[\text{NH}_4^+]} = 5.67 \cdot 10^{-10} \exp\left[-6286\left(\frac{1}{T} - \frac{1}{298.15}\right)\right] \quad (\text{A1.2b})$$

Both these processes are reversible and in this way, NH_3 can be volatilized from NH_4^+ in solution. The partial pressure of gaseous NH_3 , p_{NH_3} (Pa), can then be calculated from these two equilibriums:

$$p_{\text{NH}_3} = \frac{K_{\text{NH}_4^+} [\text{NH}_4^+]}{H_{\text{NH}_3} [\text{H}^+]} = \frac{5.67 \cdot 10^{-10} \exp\left[-6286\left(\frac{1}{T} - \frac{1}{298.15}\right)\right] [\text{NH}_4^+]}{5.527 \cdot 10^{-4} \exp\left[4092\left(\frac{1}{T} - \frac{1}{298.15}\right)\right] [\text{H}^+]} \quad (\text{A1.3})$$

p_{NH_3} (Pa) is only a function of temperature, T (K), and the molar ratio between the NH_4^+ and H^+ concentration (dimensionless), which is often reduced to a single variable, Γ .

Using the ideal gas law, the NH_3 concentration in air can be calculated as:

$$\text{NH}_3(\text{g}) = \frac{p_{\text{NH}_3} \cdot M_{\text{NH}_3}}{R^* \cdot T} = \frac{2.75 \times 10^6}{T} \exp\left(\frac{-1.04 \times 10^4}{T}\right) \cdot \Gamma \quad (\text{A1.4})$$

where $\text{NH}_3(\text{g})$ is the gaseous ammonia concentration (kg m^{-3}), p_{NH_3} is the partial pressure of ammonia (Pa), M_{NH_3} is the molecular mass of ammonia ($\sim 0.017 \text{ kg mol}^{-1}$), R^* is the universal gas constant ($8.314 \text{ J mol}^{-1} \text{ K}^{-1}$ or $\text{kg m}^2 \text{ s}^{-2} \text{ mol}^{-1} \text{ K}^{-1}$), T is the temperature (K) and Γ is the molar ratio between the NH_4^+ and H^+ concentration in the solution (dimensionless).

Appendix B. Micrometeorological variables and instrumentation at the micro meteorological observatory 'Haarweg' in Wageningen, the Netherlands

Meteorological variable	Units	Instruments	Type & Specifications
dry (T_d) and wet bulb (T_w) temperature	$^{\circ}\text{C}$	aspirated psychrometer	Home made
vapor pressure	Pa	derived from T_d and T_w	-
saturation vapor pressure	Pa	derived from T_d and T_w	-
relative humidity	%	derived from T_d and T_w	-
relative humidity	%	hair hygrometer	
temperature and relative humidity	$^{\circ}\text{C}$ %	thermo-Hygrometer	Vaisala
air pressure	kPa	air pressure sensor	
precipitation amount	mm	rain gauge	Mierij Meteo
precipitation duration	minutes	rain gauge	Thies
wind speed at 4 levels	m s^{-1}	cup anemometer	KNMI
wind direction	deg	wind vane	Wieringa type
short wave radiation	W m^{-2}	pyranometer	Kipp en Zonen CM11
long wave radiation	W m^{-2}	pyrgeometer	Kipp en Zonen CG1
net radiation	W m^{-2}	derived from short and long wave radiation	
sun shine duration	minutes	sunshine Sensor	Heany (Austria)
soil temperatures under: bare soil:-5,-10,-20 cm grass:-5,-10,-20,-50,-100 cm	$^{\circ}\text{C}$	Pt 100	Pico Technology
soil heat flux	W m^{-2}	heat flux plates	TNO type: Wp 51
$\text{CO}_2/\text{H}_2\text{O}$ -concentration	mol m^{-3}	$\text{CO}_2/\text{H}_2\text{O}$ Gas Analyzer	Licor-7500
wind speed (orthogonal)	m s^{-1}	sonic anemometer	CSAT3
(virtual) temperature T_v	$^{\circ}\text{C}$	sonic anemometer	CSAT3
leaf wetness	-	leaf wetness sensor	Campbell Scientific model 237

Appendix C. Cuticular resistance (R_w) parameterization in the DEPAC module

This appendix is adapted from Appendix I in Van Jaarsveld (2004).

In the parameterization of R_w for NH_3 , there is a distinction made in pollution climates represented by NH_3/SO_2 ratios classified as low, high and very low. The corresponding NH_3/SO_2 ratios are, however, not defined. In the present implementation of the OPS model the 'high' definition is applicable under all circumstances. Only this part of the parameterization is described here.

- For temperatures below 0 °C: $R_w = 200$
- For the land-use classes, water, urban and desert: $R_w = 5 + 19257 \exp(-0.094 \text{ RH})$
- For coniferous and deciduous forests:
 - dry conditions: $R_w = 25 + 19257 \exp(-0.094 \text{ RH})$
 - global radiation > 300 W m⁻²: $R_w = -500\#$
 - wet conditions: $R_w = 20$
- For grassland, arable land and other grassy areas:
 - Daytime:
 - Spring and summer (dry): $R_w = 100$
 - Spring and summer (wet): $R_w = 20$
 - Autumn and winter (dry): $R_w = 50$
 - Autumn and winter (wet): $R_w = 20$
 - Nighttime:
 - Spring and summer (dry): $R_w = 50$
 - Spring and summer (wet): $R_w = 20$
 - Autumn and winter (dry): $R_w = 100$
 - Autumn and winter (wet): $R_w = 20$

wet = relative humidity $\geq 87\%$

dry = relative humidity < 87%

This condition suggests that there is an upward (emission) flux.

Samenvatting

In dit proefschrift wordt de oppervlakte-atmosfeer uitwisseling van ammoniak boven agrarisch grasland in Nederland bestudeerd. De belangrijkste doelstellingen van dit proefschrift zijn om een beter begrip van het oppervlakte-atmosfeer uitwisselingsproces van ammoniak te krijgen, vooral boven agrarische grasland in Nederland, en om de modelbeschrijving van het oppervlakte-atmosfeer uitwisselingsproces van ammoniak te verbeteren.

Om deze doelstellingen te bereiken zijn lange termijn flux metingen van ammoniak boven agrarisch grasland op een micrometeorologisch weerstation in Wageningen uitgevoerd door het Rijksinstituut voor Volksgezondheid en Milieu (RIVM) in samenwerking met de leerstoelgroep Meteorologie en Luchtkwaliteit van Wageningen Universiteit. Speciaal voor dit project is een nieuw meetinstrument ontwikkeld door het Energieonderzoek Centrum Nederland (ECN), de Gradient Ammonia - High Accuracy - Monitor (GRAHAM). De GRAHAM is een verbeterde versie van het AMANDA roterende natte denuder systeem dat is ontwikkeld in de jaren '90 om de oppervlakte-atmosfeer uitwisseling van ammoniak te meten.

Met de GRAHAM worden één keer per 10 minuten ammoniakconcentraties op drie hoogtes gemeten. Met behulp van de aerodynamische gradiënt of flux-profiel methode worden de verticale concentratiegradiënten gecombineerd met micro-meteorologische turbulentie-metingen om ammoniakfluxen te verkrijgen. Deze techniek kan alleen worden toegepast onder bepaalde voorwaarden, bijvoorbeeld voldoende aanstroming (horizontaal homogene omstandigheden), stationariteit, geen advection, geen chemische reacties. Indien aan deze voorwaarden niet wordt voldaan zal dit leiden tot ernstige fouten in de geschatte flux. Daarom zijn voor de gegevensanalyse alleen de gegevens geselecteerd als aan deze voorwaarden wordt voldaan. De ammoniakfluxmetingen zijn uitgevoerd van juni 2004 tot december 2006.

Uit een onzekerheidsanalyse is gebleken dat de relatieve toevallige fout in de GRAHAM concentratiemetingen ongeveer 1,9% is onder veldomstandigheden. De relatieve toevallige fouten in de concentratiemetingen planten zich voort in de fluxberekening. De relatieve toevallige fout in de ammoniakflux is gemiddeld ongeveer 52% (met een mediane waarde van 31%).

Twee contrasterende periodes in 2004 zijn in hoofdstuk 3 gemarkeerd om de belangrijkste mechanismen in het oppervlakte-atmosfeer uitwisselingsproces te illustreren, een droge en warme zomerperiode en een natte en koele herfstperiode. In de zomerperiode worden (neerwaartse) depositiefluxen waargenomen in de avond, nacht en vroege ochtend, terwijl in de middag, (opwaartse) emissiefluxen worden waargenomen. De herfstperiode wordt vooral gekenmerkt door depositiefluxen. Frequentieverdelingen van de gemeten ammoniakconcentraties en -fluxen tonen aan dat er ondanks de hogere gemiddelde achtergrondconcentraties ($13,3 \mu\text{g m}^{-3}$ in de zomerperiode tegen $6,4 \mu\text{g m}^{-3}$ in het najaar periode) meer emissiegevallen in de zomerperiode zijn dan in de herfstperiode (ongeveer 50% in de zomer tegen 20% in de herfst).

De natheid van het bladoppervlak blijkt van groot belang te zijn voor de oppervlakte-atmosfeer uitwisseling van ammoniak. In natte omstandigheden treedt voornamelijk depositie op. Dit is te wijten aan de hoge oplosbaarheid van ammoniak in water. In droge omstandigheden kan de opgeloste ammoniak echter weer van het oppervlak verdampen. Bovendien kunnen hoge temperaturen leiden tot hoge interne plant concentraties, die ook

uitstoot van ammoniak kunnen veroorzaken. Emissie van ammoniak van een oppervlak kan alleen worden verklaard als de concentratie aan het oppervlak groter is dan de concentratie in de omgevingslucht. De evenwichtsconcentratie van een begroeid oppervlak, waarvoor de netto ammoniakflux nul is, wordt meestal gewascompensatiepunt genoemd. Wij hebben gewascompensatiepunten afgeleid uit veranderingen van de fluxrichting tijdens niet-stabiele droge omstandigheden overdag. In deze omstandigheden is het gewascompensatiepunt gelijk is aan de concentratie in de omgevingslucht. Voor onbemest agrarisch grasland waren de afgeleide gewascompensatiepunten in het bereik van 0,5 tot 29,7 $\mu\text{g m}^{-3}$ met bijbehorende bladtemperaturen tussen de 7 en 29 °C. Het gemiddelde gewascompensatiepunt was $7,0 \pm 5,1 \mu\text{g m}^{-3}$. Dit is vrij hoog voor onbemeste omstandigheden en wordt waarschijnlijk veroorzaakt door een hoge stikstofgift in het verleden.

Zoals gepresenteerd is in hoofdstuk 3, is bladnatheid een belangrijke variabele in het oppervlakte-atmosfeer uitwisselingsproces van ammoniak. Daarom is in hoofdstuk 4 een vergelijking tussen drie fysische en vier empirische bladnatheidsmodellen gemaakt. Voor dit doel zijn twee verschillende technieken om bladnatheid te meten met elkaar vergeleken; namelijk een geschilderde vlakke-plaat gridsensor en een systeem van vier clipsensoren.

Ondanks dat beide technieken vergelijkbare resultaten gaven, heeft de vlakke-plaat gridsensor de voorkeur vanwege het stabiele signaal en het gebruiksgemak. In deze techniek is de meethoogte van groot belang voor de bladnatheidsduur (LWD); de vlakke-plaat gridsensor op 1.0 m onderschat de LWD systematisch, terwijl de vlakke-plaat gridsensor op 0.1 m de werkelijke LWD beter representeert. Om een representatief signaal te krijgen moet er daarom dicht op het oppervlak worden gemeten.

Gebruikmakend van de beschikbare bladnatheidsmetingen is een vergelijking gemaakt tussen de drie fysische en de vier empirische bladnatheidsmodellen. Zonder enige optimalisatie gaf het fysische model dat de potentiële condensatie aan het bladoppervlak berekent de beste resultaten. Echter, na optimalisatie van de relatieve vochtigheidsdrempels in de empirische bladnatheidsmodellen, gaf het model gebaseerd op het verschil tussen de actuele en de verzadigde specifieke vochtigheid aan het oppervlak de beste resultaten. Voor praktisch gebruik in atmosferische transport modellen is het model dat gebruik maakt van een relatieve vochtigheidsdrempel het eenvoudigst te implementeren. In deze studie hebben we een geoptimaliseerde relatieve vochtigheidsdrempel van 71% afgeleid voor grasland, wat veel lager is dan de drempel van 87% die voorheen is afgeleid voor naaldbos.

Om de oppervlakte-atmosfeer uitwisseling van ammoniak te modelleren worden verschillende modelbenaderingen van verschillende complexiteit gebuikt. Deze modellen zijn allemaal gebaseerd op hetzelfde concept: weerstandsmodellering gebruikmakend van de analogie met elektrische stroomcircuits. De verschillende depositiepaden worden voorgesteld door weerstanden die in serie en/of in parallel met elkaar kunnen staan.

In het gewasweerstandsmodel is de oppervlakteweerstand essentieel in de modelparametrisaties die het depositieproces van ammoniak naar het oppervlak beschrijven. Deze modelbenadering neemt aan dat het oppervlak een perfecte put voor ammoniak is, d.w.z. de ammoniakconcentratie aan het oppervlak is nul. Deze aanname is echter niet correct. Dit kan worden geconcludeerd uit de vele waargenomen emissies boven onbemest grasland in hoofdstuk 3, die alleen kunnen worden verklaard als de concentratie aan het oppervlak groter is dan de achtergrondconcentratie. Als we dit echter zouden negeren en toch dit model zouden toepassen op onze data, dan vinden we oppervlakteweerstanden die heel hoog kunnen zijn of zelfs negatief bij de emissiegevallen. Dit is conceptueel onjuist, omdat weerstanden per definitie niet negatief kunnen zijn.

De gewascompensatiepuntmodellering houdt wel rekening met een oppervlakteconcentratie die niet gelijk is aan nul. De meeste van dit soort modellen staan echter alleen bidirectionele uitwisseling met de huidmondjes van planten toe. 's Nachts is er geen uitwisseling met de huidmondjes en wordt de oppervlakteconcentratie alsnog nul verondersteld. In deze omstandigheden zijn we in staat om de externe bladoppervlakteweerstand af te leiden, die 's nachts de uitwisseling van ammoniak met het oppervlak bepaalt. In hoofdstuk 2 hebben we laten zien dat de relatief hoge achtergrond concentraties in deze studie leiden tot relatief hoge externe bladoppervlakteweerstanden. Er zijn veel studies in de literatuur die soortgelijke bevindingen rapporteren en er zijn ook een aantal studies die de externe bladoppervlakteweerstand rechtstreeks relateren aan de achtergrondconcentratie.

Een nauwkeuriger blik op de data die gepresenteerd is in hoofdstuk 3 leert dat emissie niet alleen overdag voorkomt maar ook 's nachts. Dit betekent dat de uitwisseling met het externe bladoppervlak ook bidirectioneel moet zijn. Daarom hebben we in hoofdstuk 5 een nieuwe modelbeschrijving voor de oppervlakte-atmosfeer uitwisseling van ammoniak afgeleid die rekening houdt met bidirectionele uitwisseling met zowel de huidmondjes als met het externe bladoppervlak. Deze modelbenadering, genaamd χ_s - χ_w model, is vergelijkbaar met het gewascompensatiepunt - cuticulaire capaciteitsmodel (χ_s - C_d model) dat wordt gebruikt om de absorptie en desorptie van ammoniak in een dynamisch veranderend waterlaagje te modelleren. Het χ_s - χ_w model beschouwt het waterlaagje echter niet als een dynamisch veranderende condensator, maar gebruikt empirische relaties om de concentratie aan het externe bladoppervlak te schatten. De concentratie aan het externe bladoppervlak blijkt hoger te zijn in meer vervuilde omstandigheden en houdt daarom rekening met het vervuilingssklimaat, maar het maakt de uitwisseling met het oppervlak niet effectief bidirectioneel. Dit komt doordat de concentratie aan het externe bladoppervlak bij benadering wordt gemodelleerd als een fractie van de omgevingsconcentratie en daarom nooit groter wordt dan de omgevingsconcentratie. Daarom zullen dynamische processen zoals de desorptie van ammoniak als gevolg van verdamping van dauw niet expliciet worden gemodelleerd in het χ_s - χ_w model.

Een belangrijke parameter in de uitwisseling van ammoniak met de huidmondjes van planten en dus mogelijke emissiefluxen overdag, is het stomatale compensatiepunt. Het stomatale compensatiepunt wordt vooral bepaald door de bladtemperatuur en de molaire verhouding tussen de NH_4^+ and H^+ concentratie in de intercellulaire of apoplastvloeistof, Γ_s . Gerapporteerde waarden voor Γ_s in de literatuur liggen tussen de 20 en 5000. De lagere waarden worden gevonden in gebieden met lage achtergrondconcentraties/lage vervuilingsniveaus, terwijl de hogere waarden vooral worden gevonden in agrarische gebieden/hoge vervuilingsniveaus. Voor onbemest grasland hebben we een waarde van 2200 ± 1600 gevonden voor de zomer- en herfstdata in 2004 en 2500 ± 1700 voor alle data in 2004-2006.

In dit proefschrift is een seizoensvariatie in Γ_s waargenomen. Daarom is een nieuwe, temperatuursafhankelijke parametrisatie van Γ_s ontwikkeld die rekening houdt met deze seizoensvariatie. Het moet worden opgemerkt dat het verouderingsproces van planten (afrijping) en landgebruik waarschijnlijk ook invloed op de seizoensvariatie van Γ_s zullen hebben op een kortere tijdschaal.

Een inventarisatie van 21 literatuurstudies heeft een relatie opgeleverd, die Γ_s koppelt aan het vervuilingsniveau van de locatie, door middel van de 'lange termijn' ammoniakconcentratie in de lucht. Γ_s neemt lineair toe met de 'lange termijn' ammoniakconcentratie, wat betekent dat Γ_s gemiddeld gesproken hoger is in meer vervuilde gebieden. Duidelijk verschillende relaties kunnen worden onderscheiden voor de

verschillende afleidingsmethoden voor Γ_s , zoals daar zijn de micrometeorologische afleidingsmethode en de bioassay afleidingsmethode. Het is duidelijk dat de Γ_s waarden van de bioassay afleidingsmethode, $\Gamma_{s,bioassay}$, ongeveer een factor 3 kleiner zijn dan de Γ_s waarden van de micrometeorologische afleidingsmethode, $\Gamma_{s,micromet}$. Een mogelijke verklaring voor dit verschil is dat de $\Gamma_{s,micromet}$ waarden mogelijk ook de effecten van andere uitwisselingspaden bevat, zoals effecten van de bodem of van bladafval. Als het bodempad niet expliciet wordt gemodelleerd, dan worden de waarden van de micrometeorologische afleiding, $\Gamma_{s,micromet}$, aanbevolen. In dit proefschrift is de lineaire relatie die rekening houdt met het vervuilingsniveau gecombineerd met de relatie die rekening houdt met de seizoensvariatie, om zodoende een meer universele relatie voor Γ_s te verkrijgen.

Alles tezamen heeft dit proefschrift geresulteerd in een beter begrip van het oppervlakte-atmosfeer uitwisselingsproces van ammoniak boven agrarisch grasland in Nederland en boven begroeide oppervlakken in het algemeen. De nieuwe inzichten hebben geresulteerd in een nieuwe modelbeschrijving van het oppervlakte-atmosfeer uitwisselingsproces van ammoniak die waarschijnlijk algemeen toepasbaar is in atmosferische transport modellen.

Curriculum vitae

Roy Wichink Kruit is geboren op 28 december 1977 te Schalkhaar. Hier heeft hij eveneens zijn lagere school doorlopen. In juni 1995 behaalde hij het VWO diploma aan het Geert Groote College in Deventer. In 1996 heeft hij een jaar Meteorologie en Fysische Oceanografie gestudeerd in Utrecht. In 1997 is hij begonnen met de opleiding Bodem, Water en Atmosfeer in Wageningen en heeft deze studie in 2003 afgerond met de MSc thesis 'Sea Breeze Scaling in the Netherlands', uiteindelijk resulterend in de publicatie van zijn eerste artikel in een internationaal wetenschappelijk tijdschrift (Boundary Layer Meteorology). Zijn stage vond plaats bij het KNMI in De Bilt, waar hij twee verschillende convectieschema's in het HiRLAM model met elkaar heeft vergeleken. In 2000 heeft hij een half jaar onderzoek verricht voor Alterra in Wageningen op het gebied van CO₂ vastlegging in natuurlijke ecosystemen ter voorbereiding van de Conference of the Parties 6 van het UNFCCC. Dit onderzoek was gericht op het doorrekenen van scenario's ter ondersteuning van de onderhandelingen tijdens de klimaatconferentie in november 2000 in Den Haag. Vanaf 2003 tot en met februari 2007 voerde hij het promotiewerk uit aan Wageningen Universiteit, waarvan hier verslag gedaan is. Vanaf maart 2007 is hij werkzaam bij het RIVM in Bilthoven als wetenschappelijk onderzoeker bij de afdeling Verkennende Metingen van het Centrum voor MilieuMonitoring.

Scientific publications and contributions

Wichink Kruit R.J., Van Pul W.A.J., Sauter F.J., Van den Broek M., Nemitz E., Sutton M.A., Krol M.C., Holtslag A.A.M., 2010. Modeling the surface-atmosphere exchange of ammonia. Submitted to Atmospheric Environment.

Wichink Kruit R.J., Stolk A.P., Volten H., Van Pul W.A.J., 2009. Flux measurements of ammonia at the micrometeorological weather station in Wageningen, the Netherlands. Bilthoven, RIVM Letter report 680150004/2009, 56 pp.

Wichink Kruit R.J., Jacobs A.F.G., Holtslag A.A.M., 2008. Measurements and estimates of leaf wetness over agricultural grassland for dry deposition modelling of trace gases. Atmospheric Environment 42, 5304-5316.

Wichink Kruit R.J., Van Pul W.A.J., Otjes R.P., Hofschreuder P., Jacobs A.F.G., Holtslag A.A.M., 2007. Ammonia fluxes and derived canopy compensation points over non-fertilized agricultural grassland in the Netherlands using the new gradient ammonia-high accuracy-monitor (GRAHAM). Atmospheric Environment 41, 1275-1287.

Wichink Kruit R.J., Van Pul W.A.J., Jacobs A.F.G., Heusinkveld B.G., 2004. Comparison between four Methods to estimate Leaf Wetness Duration caused by Dew on Grassland. In Proceedings of the 26th Conference on Agricultural and Forest Meteorology of the AMS, 23-28 August 2004, Vancouver, Canada, 10.1.

Wichink Kruit R.J., Holtslag A.A.M., Tijn A.B.C., 2004. Scaling of the Sea-Breeze Strength with Observations in the Netherlands. Boundary Layer Meteorology, 112, 369-380.

Wichink Kruit R.J., Tijn A.B.C., 2002. Evaluation of two convection schemes in the High Resolution Limited Area Model (HIRLAM). In proceedings of 24th EWGLAM and 9th SRNWP meetings, 7-10 October 2002, De Bilt, p.191-195.

Fowler D., Pilegaard K., Sutton M.A., Ambus P., Raivonen M., Duyzer J., Simpson D., Fagerli H., Fuzzi S., Schjoerring J.K., Granier C., Nefel A., Isaksen I.S.A., Laj P., Maione M., Monks P.S., Burkhardt J., Daemngen U., Neiryck J., Personne E., Wichink-Kruit R., Butterbach-Bahl K., Flechard C., Tuovinen J.P., Coyle M., Gerosa G., Loubet B., Altimir N., Gruenhage L., Ammann C., Cieslik S., Paoletti E., Mikkelsen T.N., Ro-Poulsen H., Cellier P., Cape J.N., Horváth L., Loreto F., Niinemets Ü., Palmer P.I., Rinne J., Misztal P., Nemitz E., Nilsson D., Pryor S., Gallagher M.W., Vesala T., Skiba U., Brüggemann N., Zechmeister-Boltenstern S., Williams J., O'Dowd C., Facchini M.C., de Leeuw G., Flossman A., Chaumerliac N., Erismann J.W., 2009. Atmospheric Composition Change: Ecosystems - Atmosphere interactions. Atmospheric Environment 43, 5193-5267.

Sutton M.A., Reis S., Baker S.M.H., 2009. Atmospheric Ammonia. Detecting emission changes and environmental impacts. Springer, 464 pp.

Van Pul W.A.J., Van den Broek M.M.P., Volten H., Van der Meulen A., Berkhout A.J.C., Van der Hoek K.W., Wichink Kruit R.J., Huijsmans J.F.M., Van Jaarsveld J.A., De Haan B.J., Koelemeijer R.B.A., 2008. Het ammoniakgat: onderzoek en duiding. Bilthoven, RIVM Report 680150002/2008. 97 pp.

Jacobs A.F.G., Heusinkveld B.G., Wichink Kruit R.J., Berkowicz S.M., 2006. Contribution of dew to the water budget of a grassland area in the Netherlands. Water Resources Research 42, W03415, doi:10.1029/2005WR004055.

Jacobs A.F.G., Heusinkveld B.G., Wichink Kruit R.J., 2004. Leaf Wetness within a Lily Canopy. In Proceedings of the 26th Conference on Agricultural and Forest Meteorology of the AMS, 23-28 August 2004, Vancouver, Canada, 5.1.

Waterloo M.J., Spiertz P.H., Diemont H., Emmer I., Aalders E., Wichink-Kruit R., Kabat P., 2003. Criteria, potentials and costs of forestry activities to sequester carbon within the framework of the clean development mechanism. Wageningen, Alterra report 777, 136 pp.

Brinkman S., Kuikman P.J., Wichink Kruit R.J., Nabuurs G.J., Dolman A.J., 2001. National submission by the Netherlands to the UNFCCC - credits through article 3.3 and 3.4 activities under the Kyoto Protocol. Wageningen, Alterra report 162.1, 44 p.

Waterloo M.J., Wichink Kruit R.J., Spiertz P.H., 2001. CDM Forest Sink model. Version 2.01. A user guideline. Wageningen, Alterra, 27 p.

PE&RC PhD Education Certificate



With the educational activities listed below the PhD candidate has complied with the educational requirements set by the C.T. de Wit Graduate School for Production Ecology and Resource Conservation (PE&RC) which comprises of a minimum total of 32 ECTS (= 22 weeks of activities)

Review of Literature (4.2 ECTS)

- General aspects of sources, sinks and transport characteristics of ammonia in a grassland area (2003)

Writing of Project Proposal (4.2 ECTS)

- Dry deposition of ammonia (2003)

Laboratory Training and Working Visits (2.8 ECTS)

- Modelling of dry deposition of ammonia; CEH Edinburgh (2005)

Post-Graduate Courses (2.8 ECTS)

- Summer school: surface emissions and prediction of atmospheric composition changes; ESF-ACCENT-CNRS-GEIA (2007)

Competence Strengthening / Skills Courses (3.7 ECTS)

- PhD Competence assessment; WGS (2006)
- Professional communication strategies; WGS (2006)
- Scientific writing; CENTA (2003)
- Professional communication strategies for PhD students; Education and Competence Studies Group (2006)

Discussion Groups / Local Seminars and Other Scientific Meetings (5.6 ECTS)

- Meteorology and air quality (internal) discussion group (2003/2007)

PE&RC Annual Meetings, Seminars and the PE&RC Weekend (1.8 ECTS)

- Yearly Buys Ballot meeting for PhD students (2 days) (2004/2005)
- PE&RC Day (2004/2005)

International Symposia, Workshops and Conferences (7.4 ECTS)

- American Meteorological Society conference; Vancouver, Canada (2004)
- ILEAPS Conference; Boulder, USA (2006)
- NEU Workshop; Edinburgh, UK (2006)

Courses in which the PhD candidate has worked as a teacher (40 days)

- Inleiding Atmosfeer; MAQ (2003/2004/2005/2006)